



**BNL-95030-2011**

***Seismic Fragility Analysis of a Condensate Storage  
Tank with Age-Related Degradations***

Jinsuo Nie, Joseph Braverman, Charles Hofmayer, BNL  
Young-Sun Choun, Min Kyu Kim, In-Kil Choi, KAERI

April 2011

**Nuclear Science and Technology Department**

**Brookhaven National Laboratory**

**U.S. Department of Energy  
Korea Atomic Energy Research Institute**

Notice: This manuscript has been authored by employees of Brookhaven Science Associates, LLC under Contract No. DE-AC02-98CH10886 with the U.S. Department of Energy. The publisher by accepting the manuscript for publication acknowledges that the United States Government retains a non-exclusive, paid-up, irrevocable, world-wide license to publish or reproduce the published form of this manuscript, or allow others to do so, for United States Government purposes.

## **DISCLAIMER**

This report was prepared as an account of work sponsored by an agency of the United States Government. Neither the United States Government nor any agency thereof, nor any of their employees, nor any of their contractors, subcontractors, or their employees, makes any warranty, express or implied, or assumes any legal liability or responsibility for the accuracy, completeness, or any third party's use or the results of such use of any information, apparatus, product, or process disclosed, or represents that its use would not infringe privately owned rights. Reference herein to any specific commercial product, process, or service by trade name, trademark, manufacturer, or otherwise, does not necessarily constitute or imply its endorsement, recommendation, or favoring by the United States Government or any agency thereof or its contractors or subcontractors. The views and opinions of authors expressed herein do not necessarily state or reflect those of the United States Government or any agency thereof.

**Joint Development of  
Seismic Capability Evaluation Technology  
for Degraded Structures and Components**

**Annual Report for Year 4 Task**

**Seismic Fragility Analysis of a Condensate Storage  
Tank with Age-Related Degradations**

March 2011

Jinsuo Nie, Joseph Braverman, and Charles Hofmayer  
Brookhaven National Laboratory  
Upton, NY 11973, USA

Young-Sun Choun, Min Kyu Kim, and In-Kil Choi  
Korea Atomic Energy Research Institute  
Daejeon, 305-353, Korea



**Korea Atomic Energy  
Research Institute**

**BROOKHAVEN**  
NATIONAL LABORATORY

## **NOTICE/DISCLAIMER**

This manuscript has been authored by employees of Brookhaven Science Associates, LLC under Contract No. DE-AC02-98CH10886 with the U.S. Department of Energy. The United States Government retains a non-exclusive, paid-up, irrevocable, world-wide license to publish or reproduce the published form of this manuscript, or allow others to do so, for United States Government purposes.

Neither the United States Government nor any agency thereof, nor any of their employees, nor any of their contractors, subcontractors, or their employees, makes any warranty, express or implied, or assumes any legal liability or responsibility for the accuracy, completeness, or any third party's use or the results of such use of any information, apparatus, product, or process disclosed, or represents that its use would not infringe privately owned rights. Reference herein to any specific commercial product, process, or service by trade name, trademark, manufacturer, or otherwise, does not necessarily constitute or imply its endorsement, recommendation, or favoring by the United States Government or any agency thereof or its contractors or subcontractors. The views and opinions of authors expressed herein do not necessarily state or reflect those of the United States Government or any agency thereof.

## ABSTRACT

The Korea Atomic Energy Research Institute (KAERI) is conducting a five-year research project to develop a realistic seismic risk evaluation system which includes the consideration of aging of structures and components in nuclear power plants (NPPs). The KAERI research project includes three specific areas that are essential to seismic probabilistic risk assessment (PRA): (1) probabilistic seismic hazard analysis, (2) seismic fragility analysis including the effects of aging, and (3) a plant seismic risk analysis. Since 2007, Brookhaven National Laboratory (BNL) has entered into a collaboration agreement with KAERI to support its development of seismic capability evaluation technology for degraded structures and components. The collaborative research effort is intended to continue over a five year period. The goal of this collaboration endeavor is to assist KAERI to develop seismic fragility analysis methods that consider the potential effects of age-related degradation of structures, systems, and components (SSCs). The research results of this multi-year collaboration will be utilized as input to seismic PRAs.

In the Year 1 scope of work, BNL collected and reviewed degradation occurrences in US NPPs and identified important aging characteristics needed for the seismic capability evaluations. This information is presented in the Annual Report for the Year 1 Task, identified as BNL Report-81741-2008 and also designated as KAERI/RR-2931/2008. The report presents results of the statistical and trending analysis of this data and compares the results to prior aging studies. In addition, the report provides a description of U.S. current regulatory requirements, regulatory guidance documents, generic communications, industry standards and guidance, and past research related to aging degradation of SSCs.

In the Year 2 scope of work, BNL carried out a research effort to identify and assess degradation models for the long-term behavior of dominant materials that are determined to be risk significant to NPPs. Multiple models have been identified for concrete, carbon and low-alloy steel, and stainless steel. These models are documented in the Annual Report for the Year 2 Task, identified as BNL Report-82249-2009 and also designated as KAERI/TR-3757/2009.

In the Year 3 scope of work, BNL developed the seismic fragility capacities for a condensate storage tank with various degradation scenarios. The conservative deterministic failure margin (CDFM) method was utilized for the undegraded case and was modified to accommodate the degraded cases. A total of five seismic fragility analysis cases were considered: (1) undegraded case, (2) degraded stainless tank shell, (3) degraded anchor bolts, (4) anchorage concrete cracking, and (5) a perfect correlation of the three degradation scenarios. The design water level was used in these studies. The results and insights from these fragility analyses were described in the Annual Report for the Year 3 Task, identified as BNL-93771-2010 and also designated as KAERI/TR-4068/2010.

This report describes the research effort performed by BNL for the Year 4 scope of work. This report was developed as an update to the Year 3 report by incorporating a major supplement to the Year 3 fragility analysis. In the Year 4 research scope, an additional study was carried out to consider an additional degradation scenario, in which the three basic degradation scenarios, i.e., degraded tank shell, degraded anchor bolts, and cracked anchorage concrete, are combined in a non-perfect correlation manner. A representative operational water level is used for this effort. Building on the same CDFM procedure implemented for the Year 3 Tasks, a simulation method was applied using optimum Latin Hypercube samples to characterize the deterioration behavior of the fragility capacity as a function of age-related degradations. The results are summarized in Section 5 and Appendices G through I.



## TABLE OF CONTENTS

ABSTRACT .....	iii
LIST OF TABLES .....	vi
LIST OF FIGURES .....	vi
1 INTRODUCTION .....	1
1.1 Background .....	1
1.2 Objectives .....	2
1.3 Organization of Report .....	3
2 METHODOLOGIES FOR FRAGILITY ANALYSIS OF DEGRADED STRUCTURES AND PASSIVE COMPONENTS .....	5
2.1 Overview of Seismic Fragility Analysis .....	5
2.2 Seismic Fragility Analysis of Degraded SPCs .....	8
3 FRAGILITY ANALYSIS OF UNDEGRADED CONDENSATE STORAGE TANK ...	11
3.1 The Conservative Deterministic Failure Margin Method .....	11
3.2 Information of Condensate Storage Tank .....	11
3.3 Fragility Analysis of the Undegraded CST .....	15
3.3.1 Seismic Response Evaluation .....	16
3.3.2 Seismic Capacity Assessment .....	19
3.3.3 Summary of the CST Seismic Fragility .....	26
4 FRAGILITY ANALYSIS OF DEGRADED CONDENSATE STORAGE TANK .....	29
4.1 Fragility Analysis for (A) Degraded Tank Shell .....	29
4.1.1 Degradation Model for Stainless Steel Tank Shell .....	29
4.1.2 Assessment of the Tank Shell Degradation .....	30
4.1.3 Fragility Assessment of CST with Degraded Tank Shell .....	31
4.2 Fragility Analysis for (B) Degraded Anchor Bolts .....	34
4.2.1 Degradation Model for Anchor Bolts .....	34
4.2.2 Fragility Assessment of CST with Degraded Anchor Bolts .....	35
4.3 Fragility Analysis for (C) Cracked Anchorage Concrete .....	38
4.3.1 Degradation Model for Cracked Anchorage Concrete .....	38
4.3.2 Fragility Assessment of CST with Cracked Anchorage Concrete .....	42
4.4 Fragility Analysis for Multiple Degradations .....	47
5 ADDITIONAL FRAGILITY ANALYSES IN THE YEAR 4 TASK .....	51
5.1 Fragility Analysis of Undegraded CST Considering the Operational Water Level .....	51
5.2 Fragility Analysis with Realistic Correlations between the Degradation Cases .....	52
5.2.1 Development of Sample Degradation Scenarios .....	53
5.2.2 Simulation-based Seismic Fragility Analyses .....	54
6 CONCLUSIONS AND RECOMMENDATIONS .....	59
6.1 The Year 3 Cases .....	59
6.2 The Year 4 Cases .....	62

6.3	Additional Remarks.....	63
7	REFERENCES.....	65
Appendix A	FRAGILITY ANALYSIS OF UNDEGRADED CONDENSATE STORAGE TANK	
Appendix B	FRAGILITY ANALYSIS OF THE CST WITH DEGRADED STAINLESS TANK SHELL	
Appendix C	FRAGILITY ANALYSIS OF THE CST WITH DEGRADED ANCHOR BOLTS	
Appendix D	FRAGILITY ANALYSIS OF THE CST WITH FOUNDATION CONCRETE CRACKING – APPLICATION OF MODEL C-1	
Appendix E	FRAGILITY ANALYSIS OF THE CST WITH FOUNDATION CONCRETE CRACKING – APPLICATION OF MODEL C-2	
Appendix F	FRAGILITY ANALYSIS OF THE CST WITH MULTIPLE DEGRADATIONS	
Appendix G	FRAGILITY ANALYSIS OF UNDEGRADED CST WITH OPERATIONAL WATER LEVEL	
Appendix H	GENERATION OF OPTIMUM LATIN HYPER CUBE SAMPLES	
Appendix I	A SAMPLE RUN FOR FRAGILITY ANALYSIS OF THE CONDENSATE STORAGE TANK WITH REALISTIC DEGRADATION COMBINATION	

**LIST OF TABLES**

Table 3-1	Key Dimensions of the Condensate Storage Tank.....	13
Table 3-2	Summary of Weights and the Centers of Gravity .....	16
Table 4-1	Average Values for Corrosion Parameters $C$ and $\alpha$ [Albrecht and Naemi, 1984]. ....	35
Table 5-1	Sample Rate Factors.....	54
Table 5-2	Standard Deviation in Years .....	57

**LIST OF FIGURES**

Figure 2-1	Illustration of Fragility Curves .....	7
Figure 2-2	Fragility as A Function of Time .....	9
Figure 2-3	Fragility as a Function of Degradation Levels [Braverman, et al, 2005].....	10
Figure 3-1	Photo of the Condensate Storage Tanks [KAERI Email Communication to BNL, 09/29/2009] .....	12
Figure 3-2	Elevation View of the Condensate Storage Tank [KEPC Ulchin NPP Unit 3 & 4, Drawing No. M262-DG-A03-01, Rev. 6] .....	12
Figure 3-3	Anchor Bolt Orientation [KEPC Ulchin NPP Unit 3 & 4, Drawing No. M262-DG-A03-01, Rev. 6].....	13
Figure 3-4	Anchor Bolt Chair [KEPC Ulchin NPP Unit 3 & 4, Drawing No. M262-DG-A03-01, Rev. 6].....	13

Figure 3-5 Anchor Bolt Embedment [KAERI Email Communication to BNL, 09/29/2009, Document No. 9-251-C118-002] .....	14
Figure 3-6 Illustration of Tank Bottom Behavior near Tensile Region of Tank Shell [from NUREG/CR-5270] .....	21
Figure 3-7 Relation of Fluid Hold-down Force and Uplift Displacement.....	21
Figure 3-8 Vertical Loading on Tank Shell at Base [from NUREG/CR-5270] .....	22
Figure 3-9 Plan View of CST/Auxiliary Building at Roof Level [KAERI Email Communication to BNL, 09/29/2009, Document No. 9-251-C118-002].....	25
Figure 3-10 Detailing of CST/Roof of Auxiliary Building [KAERI Email Communication to BNL, 09/29/2009, Document No. 9-251-C118-002] .....	26
Figure 3-11 Fragility Curves of the CST.....	27
Figure 3-12 A 3D View of the CST Fragility as a Function of PGA and Confidence Level Q...	27
Figure 4-1 Change of Tank Shell Thickness/SCC Depth with Time .....	31
Figure 4-2 Mean Fragility Capacity of the CST with Degraded Tank Shell.....	32
Figure 4-3 HCLPF Capacity of the CST with Degraded Tank Shell .....	33
Figure 4-4 Median Capacity of the CST with Degraded Tank Shell .....	34
Figure 4-5 The Depth of Corrosion of the Anchor Bolts .....	35
Figure 4-6 Mean Fragility Capacity of the CST with Degraded Anchor Bolts.....	36
Figure 4-7 HCLPF Capacity of the CST with Degraded Anchor Bolts .....	37
Figure 4-8 Median Capacity of the CST with Degraded Anchor Bolts .....	38
Figure 4-9 Crack Depth Models Based on Measurements in Korean NPPs (Courtesy of KAERI) .....	39
Figure 4-10 Crack Width Models Based on Measurements in Korean NPPs (Courtesy of KAERI) .....	40
Figure 4-11 New Crack Width Model Based on Measurements in Korean NPPs .....	40
Figure 4-12 Mean Fragility Capacity of the CST with Cracked Anchorage Concrete (C-1).....	42
Figure 4-13 HCLPF Capacity of the CST with Cracked Anchorage Concrete (C-1) .....	43
Figure 4-14 Median Capacity of the CST with Cracked Anchorage Concrete (C-1).....	43
Figure 4-15 Mean Fragility Capacity of the CST with Cracked Anchorage Concrete (C-2).....	44
Figure 4-16 HCLPF Capacity of the CST with Cracked Anchorage Concrete (C-2) .....	45
Figure 4-17 Median Capacity of the CST with Cracked Anchorage Concrete (C-2).....	46
Figure 4-18 Mean Fragility Capacity of the CST with Combined Degradations.....	48
Figure 4-19 HCLPF Capacity of the CST with Combined Degradations .....	48
Figure 4-20 Median Capacity of the CST with Combined Degradations .....	49
Figure 4-21 Comparison of HCLPF Capacities among All Degradation Scenarios .....	49
Figure 5-1 Fragility Curves of The CST with the Operational Water Level.....	52
Figure 5-2 Simulated CST HCLPF Capacity vs Time .....	55
Figure 5-3 Standard Deviation in Years to Reach a HCLPF Level.....	58
Figure 5-4 Standard Deviation in HCLPF .....	58



# 1 INTRODUCTION

## 1.1 Background

The Korea Atomic Energy Research Institute (KAERI) is conducting a five-year research project to develop a realistic seismic risk evaluation system which includes the consideration of aging of structures and components in nuclear power plants (NPPs). The KAERI research project includes three specific areas that are essential to seismic probabilistic risk assessment (PRA): (1) probabilistic seismic hazard analysis, (2) seismic fragility analysis including the effects of aging, and (3) a plant seismic risk analysis. Since 2007, Brookhaven National Laboratory (BNL) has entered into a collaboration agreement with KAERI to support its development of seismic capability evaluation technology for degraded structures and components. The collaborative research effort is intended to continue over a five year period. The goal of this collaboration endeavor is to assist KAERI to develop seismic fragility analysis methods that consider the potential effects of age-related degradation of selected structures, systems, and components (SSCs). The research results of this multi-year collaboration will be utilized as input to seismic PRAs, and ultimately to support periodic safety reviews, license renewal applications, and upgrade of the seismic safety of NPPs in Korea.

The essential part of this collaboration is to achieve a better understanding of the effects of aging on the performance of SSCs and ultimately on the safety of NPPs. Based on data collected from the Licensee Event Reports of the U.S. NPPs, the Year 1 research showed that the rate of aging-related degradation in NPPs was not significantly large but increasing as the plants get older [Nie, et al. 2008]. The slow but increasing rate of degradation of structures and passive components (SPCs) can potentially affect the safety of the older plants and become an important factor in decision making in the current trend of extending the licensed operating period of the plants from 40 years to 60 years, and even potentially to 80 years, which can be seen in the recent keen interest in life-beyond-60 discussions and explorations. The condition and performance of major aged NPP structures such as containment contributes to the life span of a plant. A frequent misconception of such low degradation rate of SPCs, in contrast to the high degradation rate for active components, is that such degradation may not pose significant risk to plant safety. However, under low probability high consequence initiating events, such as large earthquakes, SPCs that have slowly degraded over many years may not be able to maintain its intended function and can potentially cause significant failures and consequently put the public health and the environment into risk.

Although the age-related degradation of SPCs is fundamentally important to the safety of NPPs, research results that can lead to good prediction of long-term performance of the SPCs are rare [Nie, et al., 2009]. Through a recent revisit to references generated in the NRC structural aging (SAG) program [e.g., Naus, et al., 1991, 1996, Oland, et al., 1993, among others], it was confirmed that very limited data were available for long-term environment-dependent material properties at the time of this large scale research project. One exception is the change in compressive strength of concrete over time, which is well known and is available through public resources. Therefore, the Year 2 task of this collaboration focused on an extensive search and review of publically available information on time-dependent material models, which may not be necessarily developed for the environment of nuclear power plants. Several models have been identified for three dominant materials: concrete, carbon and low alloy steels, and stainless steel, which were determined to be common materials for safety significant SPCs. These models were judged to be suitable for application in fragility analysis of degraded SPCs [Nie, et al., 2009].

Following the assessment of degradation occurrences in U.S. NPPs and the identification of time-dependent degradation models for dominant materials, the goal of the Year 3 task was to utilize

these results for fragility analysis of a selected safety significant SPC under various degradation situations. Fragility of a degraded SPC best describes its seismic capacity given the level of prescribed degradation. Choun, et al, [2008] showed that the failure of a particular condensate storage tank (CST) has a 17.7% contribution to the seismic core damage frequency for a Korean nuclear power plant, ranking it as the 3<sup>rd</sup> among all considered components (diesel generator and offsite power ranked the first two) and ranking it the 1<sup>st</sup> among all SPCs. Therefore, KAERI and BNL agreed to choose a typical CST in Korean NPPs as a representative SPC for seismic fragility analysis with various postulated degradation scenarios. The intent of this example is to demonstrate the seismic fragility calculation methodology considering various time-dependent degradations that are envisioned to be most probable for an SPC.

As part of the Year 4 task, the scope of the seismic fragility analysis of the CST is further expanded to consider a non-perfect correlation between the various degradation cases as outlined in the following.

## **1.2 Objectives**

The fragility analysis of the CST reported herein aims at understanding how various degradation scenarios can affect the seismic fragility capacity. The seismic fragility capacities of the CST in the Year 3 Scope of Work were developed for five cases: (1) a baseline analysis where the design condition (undegraded) are assumed, (2) a scenario with degraded stainless tank shell, (3) a scenario with degraded anchor bolts, (4) a scenario with anchorage concrete cracking, and (5) a perfect correlation of the above three degradation scenarios. Integration of time-dependent age-related degradation models in the fragility analysis is the key aspect of this study. A design water level was assumed for these cases. For the Year 4 Scope of Work, as the operational water level recently became available, the calculation procedures are updated to utilize the operational water level for the additional cases. An undegraded case with the operational water level is first analyzed and the resultant seismic fragility capacities are compared to those obtained using the design water level. The most important effort in the Year 4 Scope of Work is to develop an approach for seismic fragility analysis considering non-perfect correlation between the three degradation scenarios.

The degradation models applied in this study are directly taken from the Year 2 study or developed specifically for this study by incorporating concrete cracking data recorded in Korean NPPs. The goal is to determine the significance of the postulated degradation scenarios in the deterioration of the CST seismic fragility and to demonstrate the approaches to perform fragility analysis of degraded SPCs.

The conservative deterministic failure margin (CDFM) method, a well known procedure for fragility analysis of flat bottom tanks as presented in Appendix A of NUREG/CR-5270 [Kennedy, et al, 1989], is selected as the basic procedure for the fragility analysis of the CST. Various degradation models are then incorporated into this basic procedure in fragility analysis of the degraded CST. The CDFM method is a closed form solution; therefore, it can serve well for the purpose of demonstration.

The analyses in this report were based on assumed degradation types and rates and are presented to demonstrate the process of characterizing the deterioration of fragility capacity as a function of age-dependent degradations. These analyses do not take into account the inspection/maintenance programs that are normally established in nuclear power plants. However, the results of these analyses can be utilized for the planning of inspection/maintenance.

### **1.3 Organization of Report**

Section 2 presents an overview of the methods for seismic fragility analysis and generic approaches to incorporate time-dependent degradation models into a fragility analysis. Fundamental concepts of seismic fragility analysis are summarized to facilitate discussions in later sections.

Section 3 describes the seismic fragility analysis of the undegraded CST, which is assumed to have all of its components in design condition. The subject CST was located in an operating Korean NPP. The purpose of this section is to obtain the baseline fragility capacity of the CST and to establish the basic procedure of seismic fragility analysis, which will be updated in the next section to incorporate degradation models.

Section 4 presents the results and insights of the seismic fragility analysis of the CST under various postulated degradation scenarios. The undegraded case described in Section 3 and the degraded cases in this section assume the water level as specified in the design drawing.

Section 5 presents the seismic fragility analysis of the undegraded CST using the operational water level, and the results and insights obtained from a simulation-based approach for consideration of non-perfect correlations between the degradation scenarios.

Section 6 presents the conclusions and recommendations related to the seismic fragility analysis of the degraded CST, including discussions regarding consideration of realistic correlations between multiple simultaneous degradations.



## 2 METHODOLOGIES FOR FRAGILITY ANALYSIS OF DEGRADED STRUCTURES AND PASSIVE COMPONENTS

### 2.1 Overview of Seismic Fragility Analysis

Seismic fragility of a structure or passive component (SPC) is a measure of its capacity to resist earthquake motions. It is expressed as the conditional limit state probability for a given level of seismic excitation, such as peak ground acceleration (PGA) or spectral acceleration (SA). A key requirement of a seismic fragility analysis is the definition/selection of appropriate limit states, which are very often represented by dominant failure modes. As failure modes are component- and loading- dependent, a seismic fragility analysis of a particular SPC requires a sufficient knowledge of the static and dynamic behaviors of that particular SPC, even though the fundamental procedure for fragility analysis is the same. In addition to failure modes, the limit states can also be represented with major performance measurements, such as an allowable maximum inter-story drift of a structure or the mid-span deflection of a beam. Using performance measures as limit state functions is often a convenient choice in simulation based fragility analysis, in which the structural responses are obtained by finite element analyses and the failure modes are embedded in the modeling.

The seismic fragility capacity is often in practice represented by a capacity value, e.g., a median capacity or a high confidence low failure probability (HCLFP) capacity, and the associated epistemic and aleatory uncertainties. Epistemic uncertainty is knowledge/model-based and can be reduced by obtaining more data or choosing more accurate models. The aleatory uncertainty refers to the inherent randomness in a property that is irreducible. The epistemic uncertainty and the aleatory uncertainty have been traditionally referred to as uncertainty ( $\beta_U$ ) and randomness ( $\beta_R$ ), respectively.

The seismic fragility of an SPC can be obtained by closed form solution, simulation based finite element analysis, or testing. Direct development of a seismic fragility by testing is prohibitively costly, because this method requires too many specimens to obtain a good assessment of the uncertainties. A viable simplified testing approach is to determine the seismic capacity of just one specimen and use it as the median fragility value; the associated uncertainties have to be estimated appropriately through other ways. Even with this simplified approach, development of seismic fragility through testing is still very costly since (1) there are many types of SPCs in a NPP, (2) each type may have quite a number of different construction configurations, and (3) high-excitation-level full-scale testing is a necessity for high quality seismic fragilities. Therefore, test-based fragility curves are rare and closed form solution and simulation based fragility analysis are the most common approaches to obtain fragility capacity for SPCs.

A very classical and generic closed form solution can be developed based on the double lognormal model using the median PGA capacity  $A_m$  and the two logarithmic standard deviations  $\beta_U$  and  $\beta_R$  (epistemic and aleatory uncertainties):

$$A = A_m \epsilon_R \epsilon_U, \quad (2-1)$$

where  $A$  is a random variable representing the fragility capacity as PGA, and  $\epsilon_R$  and  $\epsilon_U$  are two lognormal random variables with unit median and lognormal standard deviations  $\beta_R$  and  $\beta_U$  [Kennedy and Ravindra, 1984]. A lognormal standard deviation  $\beta$  refers to the standard deviation of a normal random variable which is the log of the lognormal random variable, i.e.,  $\beta = \sqrt{\ln(1 + \text{COV}^2)}$ , where COV stands for the coefficient of variation. For  $\text{COV} \leq 0.3$ ,  $\beta \approx \text{COV}$ . The random variables  $\epsilon_R$  and  $\epsilon_U$  represent the inherent randomness and the uncertainty in the

median capacity. This representation of the seismic fragility facilitates the development of an entire series of fragility curves for various levels of uncertainties. The seismic fragility analysis method based on this double lognormal model has been well studied and documented in the literature [e.g., Ellingwood, 1994, Ellingwood and Song, 1996, Kaplan, et al, 1989, Kennedy, et al, 1980, Kennedy and Ravindra, 1984].

The fragility  $F$  (conditional failure probability) of an SPC for a given level of uncertainty  $Q$  and a given level of ground acceleration  $a$  can be conveniently expressed as:

$$F(a, Q) = \Phi \left[ \frac{\ln\left(\frac{a}{A_m}\right) + \beta_U \Phi^{-1}(Q)}{\beta_R} \right], \quad (2-2)$$

in which  $\Phi$  is the standard normal cumulative distribution function and  $\Phi^{-1}$  is its inverse. The uncertainty  $Q$  is the probability that the true failure probability is less than or equal to  $F$  for a given PGA  $a$ . A simpler form of Equation 2-2 can be derived for the case with perfect knowledge, i.e.,  $\beta_U = 0$ .

Figure 2-1 illustrates the fragility curves for confidence levels of 0.95, 0.5, and 0.05 and a mean (composite) fragility curve, which is defined as:

$$F_{mean}(a) = \Phi \left[ \frac{\ln\left(\frac{a}{A_m}\right)}{\beta_C} \right] \quad (2-3)$$

$$\beta_C = \sqrt{\beta_R^2 + \beta_U^2}$$

where  $\beta_C$  is the composite lognormal standard deviation.

Figure 2-1 also shows the HCLPF capacity, which is the PGA value at which the failure probability is 5% (low probability of failure) and the associate confidence level is 95% (high confidence). The mean fragility curve does not explicitly separate the epistemic uncertainty and the aleatory uncertainty, and is often used for convenience in simulation-based fragility analysis.

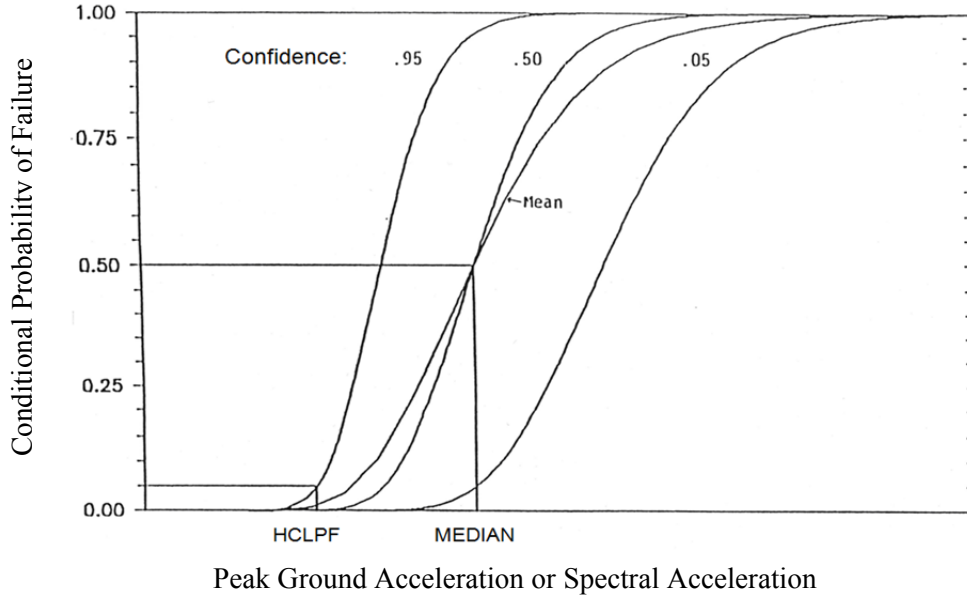


Figure 2-1 Illustration of Fragility Curves

Following the definition in Equation 2-1, the HCLPF capacity can be expressed as:

$$HCLPF = A_m \exp(-1.645(\beta_R + \beta_U)), \quad (2-4)$$

which corresponds to about a 1% probability of failure on the mean curve.

The fragility of an SPC can be developed based on a product of a series of factors, which are often assumed statistically independent. Accordingly, the median capacity  $A_m$  can be typically expressed as a product of a median safety factor and the reference ground acceleration, the former of which can be further decomposed into multiplication of a median strength factor, an inelastic energy absorption factor, and a median response factor. Some other presentations may also include other factors, depending on the specific situation of a given SPC. The corresponding logarithmic standard deviation can be expressed as:

$$\begin{aligned} \beta_R &= \sqrt{\beta_{R1}^2 + \beta_{R2}^2 + \dots + \beta_{Rn}^2} \\ \beta_U &= \sqrt{\beta_{U1}^2 + \beta_{U2}^2 + \dots + \beta_{Un}^2} \end{aligned} \quad (2-5)$$

where  $n$  is the number of factors in the product representation of the fragility.

A fragility curve can also be developed based on computerized simulation, in which finite element analysis is used to obtain the structural responses. In this approach, a complete set of random variables need to be determined for the governing limit state(s), and the statistical parameters for the random variables are defined subsequently. Information required to fully define the random variables may include the marginal/joint probability distribution, mean, coefficient of variation, and correlation. Simulation-based seismic fragility analysis also requires the determination of proper simulation techniques, depending on the accuracy requirement, how efficiently the structural responses can be obtained, target failure probability, etc. The common

techniques include the brute-force Monte Carlo simulation, Latin Hypercube sampling, importance sampling, and Fekete Point sampling [Nie, et al, 2007]. The uncertainties in this approach are usually provided in a composite sense, i.e., no distinction between the epistemic uncertainty and the aleatory uncertainty. Consequently, there is only one resultant fragility curve, which can be considered as the best estimate (composite or mean) fragility curve, in contrast to the family of fragility curves as described above for the typical closed form solution.

## 2.2 Seismic Fragility Analysis of Degraded SPCs

The effect of age-related degradation on the seismic fragility of an SPC is twofold: on the median capacity and on the uncertainties, with the former being potentially more significant. Degradation of an SPC, often observed as loss of cross section or cracking, reduces the strength of the SPC and consequently causes the median fragility to decrease. However, the level of degradation may not affect the median fragility in a linear fashion, due to the dynamic nature of the seismic responses and also possibly the nonlinear behaviors of the SPC [Ellingwood and Song, 1996]. Since the degradation phenomena of SPCs have a significant amount of uncertainty and the knowledge for the development of the degradation models is not perfect, the uncertainty measures  $\beta_R$  and  $\beta_U$  increase as the SPCs age.

The seismic fragility of a degraded SPC is a function of time. Using the classical double lognormal model as an example, the seismic fragility of a degraded SPC can be expressed as the following general form,

$$F(a, Q, t) = \Phi \left[ \frac{\ln\left(\frac{a}{A_m(t)}\right) + \beta_U(t)\Phi^{-1}(Q)}{\beta_R(t)} \right], \quad (2-6)$$

in which  $t$  represents time and the fragility parameters  $A_m$ ,  $\beta_R$ , and  $\beta_U$  become time-dependent to represent their instant values at time  $t$ . Equation 2-6 is conceptually clear; however, except for very simple cases, the time-dependent fragility is usually very difficult to be further developed by analytically determining the time-dependent fragility parameters. In most realistic situations, these fragility parameters are complex functions of time and may often be defined implicitly. Therefore,  $F(a, Q, t)$  is more suitable to be developed numerically either at some discrete time points or at postulated levels of degradations.

When there is a reliable age-related degradation model for the subject SPC, the fragility capacity can be developed for a prescribed period of time, e.g., 80 years (a potentially extended life expectation of a nuclear power plant in the U.S.). Figure 2-2 illustrates a series of mean fragility curves that correspond to a series of specified time points (years). This representation of the time-dependent fragility can assist a fragility analyst to assess how the deteriorating fragility capacity progresses with time as the subject SPC degrades and to make better decision on inspection/maintenance scheduling. Of course, the quality of such a decision depends on how well the age-related degradation model represents the real degradation environment of the subject SPC.

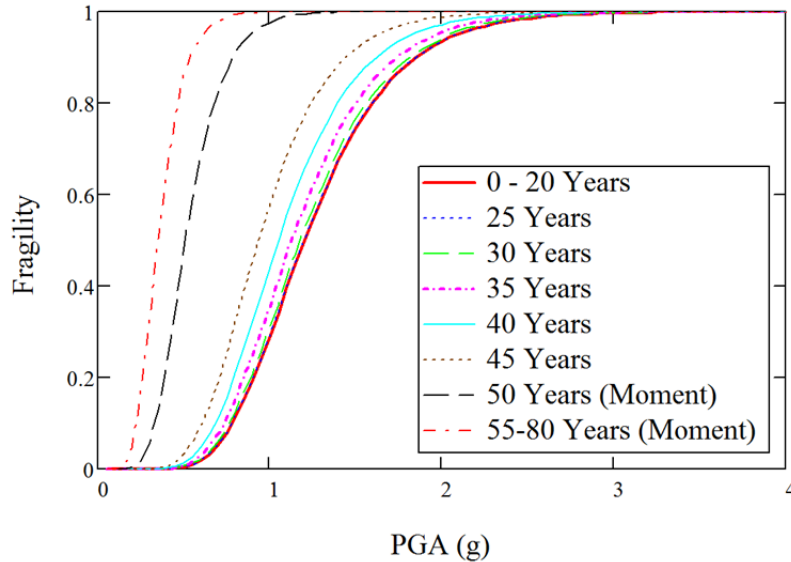


Figure 2-2 Fragility as A Function of Time

In cases where no reliable degradation models are available, the fragility capacity can be developed for various levels of degradation. This approach is very useful when degradation data can be obtained from in-service inspections or maintenance programs. The seismic fragility of an SPC with an observed level of degradation can be used to update the plant PRA to determine whether the change of core damage frequency (CDF) due to the decreased fragility is significant enough to warrant a further action. In addition, once a degradation model can be developed using the observed data, the series of fragility curves developed for various levels of degradation can be interpolated to predict the performance of the SPC at different times. This approach lends the analyst the flexibility in changing the time-dependent degradation model (e.g. for the purpose of sensitivity study) without repeating the fragility analysis, provided that the initial series of fragility curves adequately cover the range of degradation for the specified period of time. Figure 2-3 shows an example of some fragility curves for specified levels of degradation.

From a computational point of view, these two approaches do not differ as significantly as they appear. Both approaches share a common requirement that the structural strengths need to be physically reduced, e.g. through reducing the area of a cross section or enlarging a crack. The first approach that directly integrates time-dependent degradation models usually uses constant time intervals to determine the levels of cross section loss or the degrees of a crack growth, while the second approach in general uses a constant spacing to change the same physical parameters. It should be pointed out that both approaches do not inherently require such constant spacing in time or in physical parameters; the use of constant spacing is only for better presentation of the relevant relationships between fragility and time or a physical parameter.

In this report, since the time-dependent degradation models have been selected or developed, the first approach will be used for the four degradation cases: (A) degraded stainless tank shell, (B) degraded anchor bolts, (C) anchorage concrete cracking, (D) a perfect correlation between the three degradation scenarios, and (E) a non-perfect correlation between the degradation scenarios.

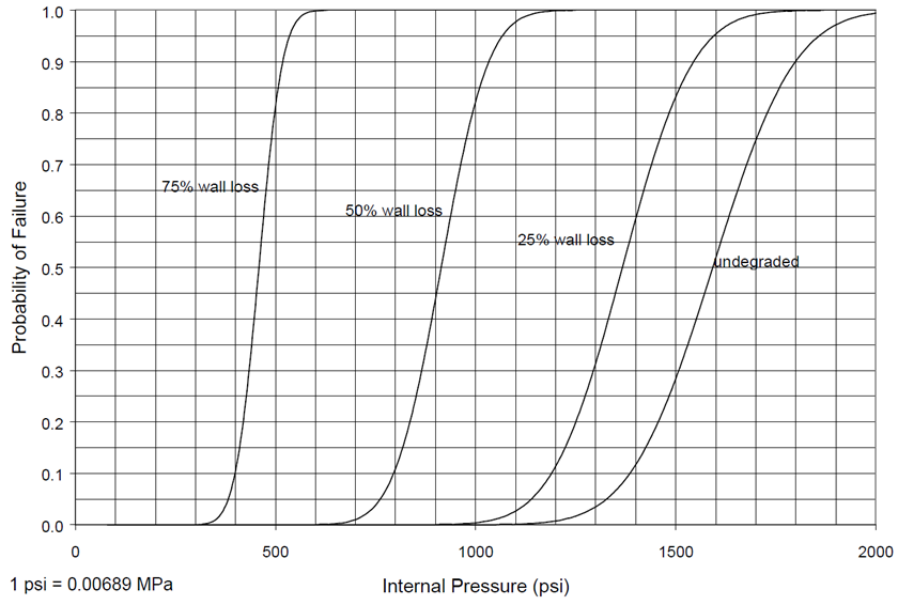


Figure 2-3 Fragility as a Function of Degradation Levels [Braverman, et al, 2005]

### 3 FRAGILITY ANALYSIS OF UNDEGRADED CONDENSATE STORAGE TANK

#### 3.1 The Conservative Deterministic Failure Margin Method

Two methods, namely the conservative deterministic failure margin (CDFM) method and Fragility Analysis (FA) method were introduced in NUREG/CR-5270 [Kennedy, et al, 1989] to estimate the seismic margins of structures, systems, and components (SSCs) in nuclear power plants (NPPs). The seismic margin of a component is defined in these methods as the high confidence low probability of failure (HCLPF) capacity. The procedure to obtain the HCLPF capacity of a component requires the estimation of its seismic response as a function of the seismic margin earthquake (SME) and its seismic capacity. The CDFM method conservatively prescribes values for the parameters and requires some level of subjective decisions in formulating the procedures; it produces a deterministic HCLPF capacity. On the other hand, the FA method requires the determination of the median and the associated uncertainties ( $\beta_R$  and  $\beta_U$ ), which are under substantial subjective judgment; this method yields an HCLPF capacity as well as the overall randomness  $\beta_R$  and uncertainty  $\beta_U$ . The CDFM method was developed for simplicity based on the FA analysis method, such that the HCLPF capacity can be calculated deterministically without specifying many subjective parameters. The FA method is based on the double lognormal model, which is described in Section 2.

In the CDFM method, a set of deterministic guidelines are specified to prescribe the selection of strength, damping, ductility, load combination, structural model, soil-structural interaction, in-structural response spectra, etc, in the fragility calculation. This method follows the design procedures commonly used by the industry, except that some parameters are chosen differently. It is therefore easy to be implemented and accepted by fragility analysts. The selection of the parameters is somewhat judgmental to account for the margins and uncertainties. The goal of this method is to obtain conservative but somewhat realistic HCLPF capacities.

More details on the CDFM method and the FA method can be found in NUREG/CR-5270. Very similar introduction of the same methods were also included in EPRI NP-6041-SL [Reed, et al, 1991].

#### 3.2 Information of Condensate Storage Tank

The condensate storage tank (CST) to be analyzed in this study was provided by KAERI, in light of the high contribution of the CST to the core damage frequency. This CST is located in the Ulchin nuclear power plant, which is located on the east side of Korea on the coast of the Pacific Ocean. Two CSTs are built close to each other, with a center-to-center separation of 89' (27.13 m). There is an auxiliary building between the two CSTs, with the roof about 13 feet above the tank foundation. Figure 3-1 shows a photo of the CSTs and the auxiliary building. The shell plate, bottom plate, and the roof plate of the tank are SA240-304 stainless steel.



Figure 3-1 Photo of the Condensate Storage Tanks [KAERI Email Communication to BNL, 09/29/2009]

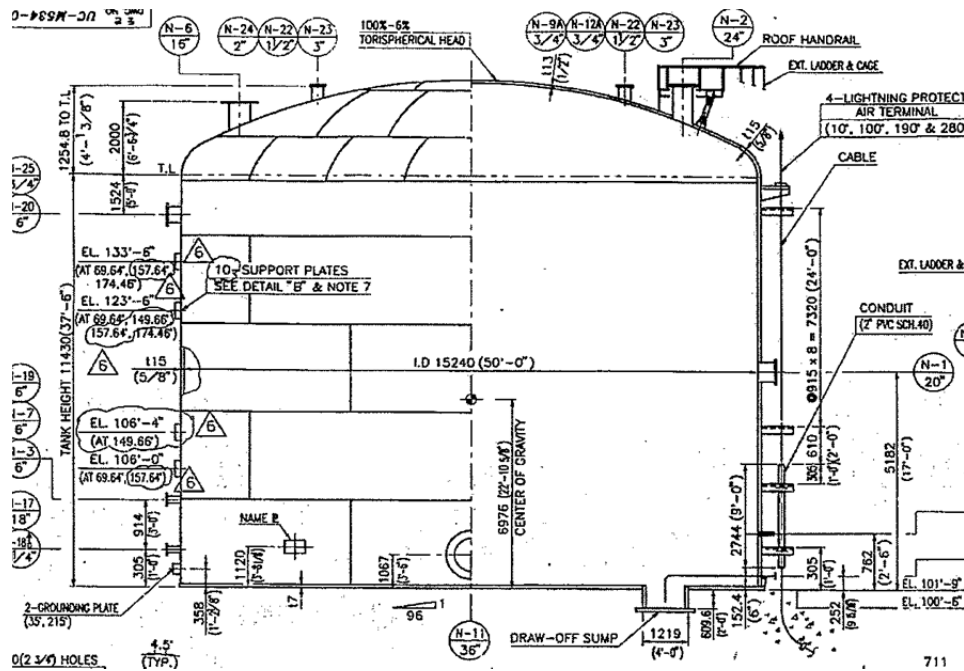


Figure 3-2 Elevation View of the Condensate Storage Tank [KEPC Ulchin NPP Unit 3 & 4, Drawing No. M262-DG-A03-01, Rev. 6]

Table 3-1 Key Dimensions of the Condensate Storage Tank

Inner Diameter	50' (15.24 m)
Tank Height (to water level)	37'-6" (11.43 m)
Shell Thickness	5/8" (15.875 mm)
Torispherical Head Thickness	1/2" (12.7 mm)
Bottom Plate Thickness	1/4"~5/16" (7 mm)

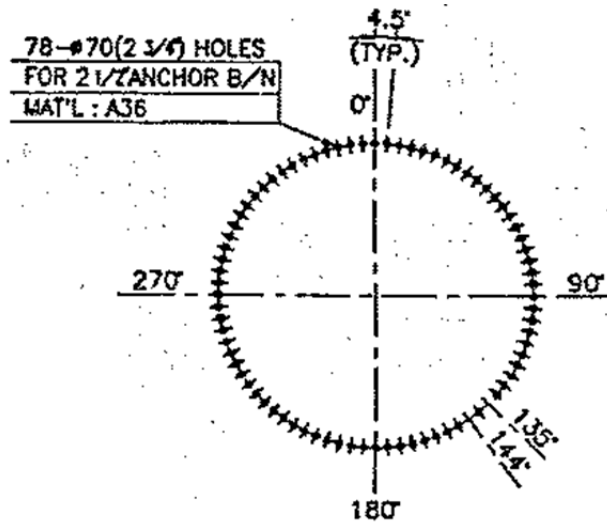


Figure 3-3 Anchor Bolt Orientation [KEPC Ulchin NPP Unit 3 & 4, Drawing No. M262-DG-A03-01, Rev. 6]

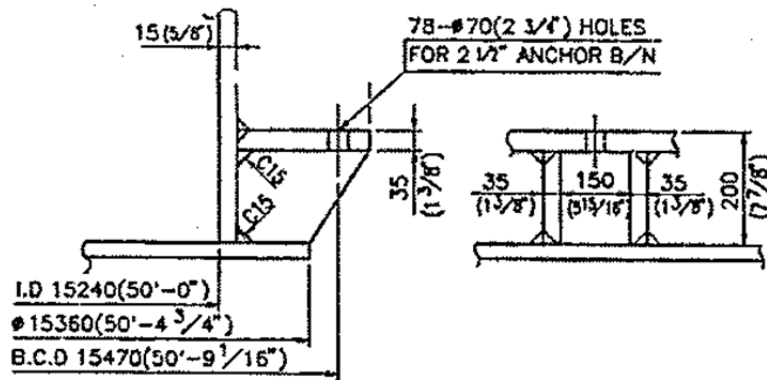


Figure 3-4 Anchor Bolt Chair [KEPC Ulchin NPP Unit 3 & 4, Drawing No. M262-DG-A03-01, Rev. 6]

Figure 3-2 shows an elevation view of the CST. The CST is a flat-bottom cylindrical tank filled with water and under atmospheric pressure. The key dimensions of the tank are summarized in Table 3-1. The inner diameter of the tank is 50' and the height of tank (up to the water level) is 37'-6". The thickness of the tank shell is 5/8". Unlike other dimensions in Figure 3-2 that are shown in both the metric unit and the U.S. customary unit, the thickness of the bottom plate is only shown in metric unit (7 mm). A corresponding conversion to the U.S. customary unit could be between 1/4" and 5/16". Therefore, a thickness of 7 mm will be used in the calculation because the software that was used in this study can handle mixed units simultaneously. The radius of the torispherical head is not readily available and neither is its height. Since the elevation view is provided as part of a scaled design drawing, the missing dimensions of the torisphere were estimated using measurements of the CST elevation view.

The CST is heavily anchored to the reinforced concrete foundation through 78 anchor bolts. The anchor bolts have a diameter of 2-1/2" and are A36 steel. Figure 3-3 and Figure 3-4 show a plan view of the anchor bolt layout and the anchor bolt chair, respectively. The length of the anchor bolts is 3'-6", with an embedment of about 2'-1". The anchor bolts were post-installed in the pre-formed holes in the concrete foundation with non-shrinking grout. No information about the strength of the reinforcement concrete and the non-shrinking grout can be found in the drawings provided by KAERI. However, in an experimental study of the tensile strength of anchor bolts used for very similar CSTs in another Korean NPP, the compressive strength of the concrete foundation of the CSTs was specified as 4,500 psi. Therefore, a compressive strength of 4,500 psi was assumed in the fragility analysis of the subject CST. In the test, the actual 7 day and 28 day compressive strengths of the concrete were measured to be 5,419 psi and 7,180 psi, respectively. The actual compressive strength of the non-shrinking grout was reported to be 7,550 psi and 111,000 psi, respectively, at 7 days and 21 days [Lee, et al, 2001].

KAERI indicated that the tank is founded on a rock site. Therefore, soil-structure interaction (SSI) is not relevant to the subject CST.

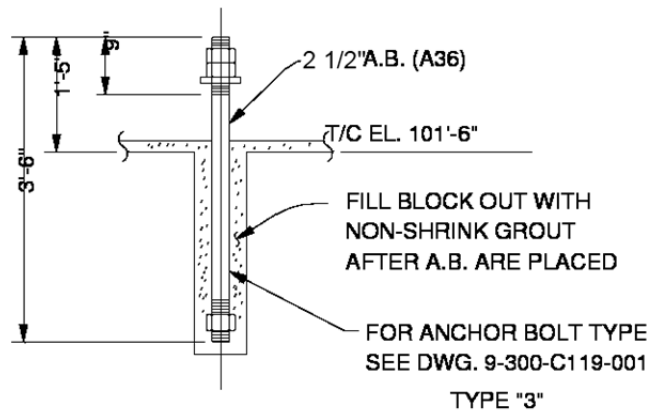


Figure 3-5 Anchor Bolt Embedment [KAERI Email Communication to BNL, 09/29/2009, Document No. 9-251-C118-002]

### 3.3 Fragility Analysis of the Undegraded CST

A sophisticated procedure to calculate the HCLPF capacity of flat bottom tanks using the CDFM method is introduced in Appendix A of NUREG/CR-5270 [Kennedy, et al, 1989]. This procedure involves an extensive set of equations to calculate the seismic responses and seismic margin capacities. Within the scope of Year 3 work, fragility analysis of the undegraded case (baseline) as well as a few other cases involving multiple degradation scenarios will be performed. Each of the degraded cases is further divided into a series of fragility analyses for various levels of degradation. To accomplish such a large computational effort with the given resources, an efficient and robust method is necessary. To this end, the mathematical software Mathcad [2007] was chosen because of: (1) its capability in explicitly expressing mathematical equations in a fashion that a common engineer is familiar with, (2) its advanced functions in performing interpolation and root finding without significant programming, (3) its capability in mixing documentation and calculation so that the necessary technical background and explanations can be documented, and (4) its instant numerical calculation and plot rendering when any parameters are varied. The utilization of this tool saved considerable time that would be used in developing a spreadsheet or in-house code, because the clear presentation of equations avoided much unnecessary debugging time.

The calculation of the HCLPF capacity using the CDFM method follows mostly the recommendations in NUREG/CR-5270, supplemented with BNL 52361 [Bandyopadhyay, et al, 1995], ASCE 4-98 [1998], NASA SP-8007 [1968], and other references. This section presents a summary of the analysis and the results; more details can be found in Appendix A of this report.

The CDFM method is an iterative process: (1) a seismic response evaluation is performed for a given level of estimated seismic margin earthquake  $SME_e$ ; (2) a seismic capacity assessment is performed considering the current level of seismic loading to obtain the actual seismic margin earthquake SME based on the following equation:

$$SME = \frac{CAPACITY - STATIC}{k_{\mu} \times SEISMIC_e} \times SME_e \quad (3-1)$$

in which CAPACITY is the HCLPF capacity of the tank, STATIC is the portion of this capacity used to resist static loads,  $k_{\mu}$  is the inelastic energy absorption effective seismic stress correction factor, and SEISMIC<sub>e</sub> is the seismic response; and (3) steps (1) and (2) are repeated using an updated  $SME_e$  until SME is close to  $SME_e$ .

KAERI indicated that the design basis earthquake (DBE) used for the design of the subject CST was based on NRC Regulatory Guide (RG) 1.60 [1973] design spectrum anchored to a PGA level of 0.20 g. Therefore, the NRC RG. 1.60 spectrum shapes for the horizontal ground motion and the vertical ground motion were used for the HCLPF capacity evaluation reported herein. The median response spectra from NUREG/CR-0098 [Newmark and Hall, 1978] were utilized in the example reported in Appendix A of NUREG/CR-5270. The RG 1.60 spectra differ from the median spectra in NUREG/CR-0098 in that the vertical response spectrum is 2/3 of the horizontal response spectrum not for the entire frequency domain but only for frequencies less than 0.25 Hz. The RG 1.60 spectrum shapes were implemented in Mathcad using its interpolation function to automatically determine the spectral acceleration for any given frequency. In addition, the initial SME estimate is set to  $1.67 \times 0.2 \text{ g} = 0.334 \text{ g}$ , in which the factor 1.67 comes from the SRM/SECY 93-087 [1993] requirement that the HCLPF capacity shall be greater than or equal to 1.67 times the safe shutdown earthquake (SSE) in a margin assessment of seismic events. After several iterations by trial-and-error, the SME capacity converges to 0.426g, which is used for discussion

in the following. Since only the converged SME capacity is used, the repetitive nature of the CDFM method is effectively omitted in the following discussion.

### 3.3.1 Seismic Response Evaluation

The weight and the center of gravity (CG) of various parts of the tank were first estimated based on the dimensions either as shown in Figure 3-2 or as estimated from the same figure. The center of gravity is defined as its height above the tank bottom plate. As summarized in Table 3-2, the torispherical head, tank shell, bottom plate, and water weigh 54.5 kips, 157.8 kips, 22.3 kips, 4604.2 kips, respectively. The total weight of the tank including water is 4,839 kips (2195 metric ton), and the center of gravity is 19.0' (5.8 m). The water dominates the total weight and the calculation of the center of gravity. The calculated center of gravity including the tank and water does not agree with that shown in Figure 3-2 (22'-10 5/8"). However, this CG in the drawing is close to the center of gravity of the tank only (23.1'). The minor difference may arise from the estimation of the dimensions of the torispherical tank head.

Table 3-2 Summary of Weights and the Centers of Gravity

Parts	Weight (kips/kN)	Center of Gravity (ft/m)
Torispherical Tank Head	54.5 / 242.4	42.7 / 13.0
Tank Shell	157.8 / 702.0	19.6 / 6.0
Bottom Plate	22.3 / 99.0	0.0 / 0.0
Water	4604.2 / 20,480.0	18.8 / 5.7

Seismic response evaluation includes the calculation of hydrostatic and hydrodynamic loads on the tank that is subjected to the earthquake motions at the base of the tank. These responses are then combined to provide six demand estimates for the HCLPF capacity assessment. These combined responses are described in the following based on Appendix A of NUREG/CR-5270:

*The overturning moment in the tank shell immediately above the base plate of the tank:* this moment is then compared to the base moment capacity, which is governed by a combination of shell buckling and anchor bolt yielding or failure and often governs the SME capacity of the tank.

*The overturning moment applied to the tank foundation through the tank shell and the base plate:* this moment is only required for tanks founded on soil sites and is generally determined as part of the SSI analysis. For soil sites, a foundation failure mode should be investigated. This mode as reported in NUREG/CR-5270 seldom governs the SME capacity. Since the subject CST is founded on a rock site, the calculation of this moment and the related capacity is not necessary in this study.

*The base shear beneath the tank base plate:* this base shear is compared with the horizontal sliding capacity of the tank. NUREG/CR-5270 reported that for atmospheric tanks with a radius greater than 15' (4.6 m), the sliding capacity rarely governs the SME capacity. However, as will be demonstrated later, the sliding capacity controls the SME capacity of the subject CST in this study.

*The combination of the hydrostatic and hydrodynamic pressures on the tank side wall:* The common design practice is to compare the combined pressures with the membrane hoop

capacity of the tank shell at one-foot above the base and each wall thickness change. Since there is no thickness change in the shell of the subject CST, only one location will be compared. The combined pressures usually do not control the SME capacity if the tank is properly designed. However, when degradation of the tank shell is considered, the combined pressures can govern the SME capacity of the degraded CST.

*The average hydrostatic minus hydrodynamic pressure on the base plate of the tank:* this pressure is used to calculate the sliding capacity of the tank. In addition, if fluid hold-down forces on the base plate are included in the assessment of the overturning moment capacity, the minimum value of this pressure near the tank side wall is needed.

*The fluid slosh height:* the slosh height is compared to the freeboard above the water level to assess the possibility of roof damage. It is noted in NUREG/CR-5270 that roof damage usually does not affect the safety function of the tank immediately after an earthquake and is seldom a concern in seismic margin assessment.

Important specifics in the calculation of the HCLPF capacity of the subject CST are described in the following to facilitate the understanding of Appendix A of this report, where more detailed calculations can be found.

### **3.3.1.1 Horizontal Impulsive Mode Response**

The natural frequency of the horizontal impulsive mode is a function of the water level height, tank radius, tank shell thickness, and tank shell material properties. The ratio of the water level to the tank radius is 1.498, slightly less than the threshold value (1.5) for determination of how the effective impulsive weight and its center of gravity are calculated. The ratio of the tank shell thickness to the tank radius is 0.0021. Using Table 7.4 in reference “Seismic Response and Design of Liquid Storage Tanks,” [Veletos, 1984] and Equation 4.18 in BNL-52631 [Bandyopadhyay, et al, 1995], the horizontal impulsive mode natural frequency was estimated to be 9.3 Hz.

A 5% of critical damping was recommended in Appendix A of NUREG/CR-5270 as a conservative estimate of the median damping for the horizontal impulsive mode response. Based on the RG 1.60 response spectrum anchored to 0.426 g (the converged SME capacity), the spectral acceleration for the impulsive mode was found to be 1.1 g, equivalent to an amplification factor of 2.6.

The effective impulsive weight of water and its effective center of gravity (above the bottom plate of the tank) are calculated to be 3264 kips (14,520 kN) and 14.0' (4.3 m), respectively. For determining the effective fluid weight, the tank shell is assumed to be rigid, as recommended per ASCE 4-98. Accordingly, the impulsive base shear and the moment at the base of the tank shell were estimated to be 3,838 kips (17,070 kN) and 56,600 kips-ft (76,730 kN-m), respectively. In addition to the effective impulsive water weight, these impulsive shear and moment also include the effect of dead weights for the torispherical tank head and the tank shell.

The impulsive hydrodynamic pressure is estimated to be 7.3 psi (50.6 kPa) for a depth (downward from the water surface) greater than 0.15H (1.7 m). For a depth less than 0.15H, the impulsive pressure varies linearly from 0 psi to 7.3 psi.

### 3.3.1.2 Horizontal Convective (Sloshing) Mode Response

The natural frequency of the horizontal sloshing mode is a function of the water level height and the tank radius, and was estimated to be 0.2 Hz. The convective mode is very lightly damped and the same damping ratio of 0.5% as recommended in NUREG/CR-5270 will be used herein for the subject CST. Using the sloshing natural frequency 0.2 Hz and a 0.5% damped RG 1.60 horizontal response spectrum anchored at 0.426 g, the spectral acceleration  $SA_C$  was determined to be 0.3 g. Since the sloshing natural frequency is smaller than the lowest corner frequency (point D in RG 1.60 horizontal spectrum), the RG 1.60 spectrum was defined using data point at 0.1 Hz and point D which were obtained from the spectrum shape.

The effective convective mode water weight and its effective application height were estimated to be 1,402 kips (6,236 kN) and 25.5' (7.8 m), respectively. Using a spectral acceleration 0.3 g, the convective base shear and moment are then determined to be 407.8 kips (1,814 kN) and 10,400 kips-ft (14,100 kN-m), respectively.

The hydrodynamic convective pressure, which is a function of depth (downward from the water surface), was estimated to be 2.6 psi (18.2 kPa) at the water surface and 0.3 psi (2.3 kPa) at the base of the tank. The hydrodynamic convective pressure is generally smaller at greater depths. In general, it is negligible compared to either the hydrodynamic impulsive pressure or the hydrostatic pressure at the base of tank.

The fundamental mode fluid slosh height was estimated to be 6.1 ft (1.9 m), corresponding to a SME capacity of 0.426 g.

### 3.3.1.3 Vertical Fluid Mode Response

The alternative method reported in Appendix A of NUREG/CR-5270 and also available in ASCE 4-98 was used to estimate the fundamental frequency of the vertical fluid mode, because the equations in NUREG/CR-5270 are not applicable to the shell-thickness/radius ratio of the CST (0.0021). Using Equation C3.5-13 of ASCE 4-98, the fundamental frequency of the vertical fluid mode of the CST was estimated to be 9.5 Hz, which is slightly greater than the fundamental frequency of the horizontal impulsive mode. A similar observation was also reached in NUREG/CR-5270.

A 5% of critical damping was assumed for the evaluation of the vertical spectral acceleration, as recommended in NUREG/CR-5270. This damping recommendation partially accounted for the foundation flexibility. Using the RG 1.60 vertical response spectrum anchored to 0.426 g (note: RG 1.60 horizontal and vertical spectra anchor to the same horizontal PGA), the spectral acceleration for the vertical mode was determined to be 1.1 g.

The hydrodynamic pressure for the vertical fluid response mode is a function of depth, and is zero at the water surface. It was estimated to be 14.3 psi at the tank base plate, which is greater than those due to the horizontal impulsive mode and the horizontal convective mode.

### 3.3.1.4 Combined Responses

The horizontal responses due to the horizontal impulsive mode and the horizontal convective mode can be combined using the squared root of sum of squares (SRSS) method.

For the purpose of the membrane hoop stress capacity check, the maximum seismic hydrodynamic pressures can be obtained by SRSS of the horizontal seismic pressures and the

vertical fluid response hydrodynamic pressure. The maximum seismic hydrodynamic pressure was found to be 16.0 psi at the tank base plate.

For the purpose of estimating the buckling capacity of the tank shell, it is necessary to estimate the expected maximum and minimum of the fluid pressures acting against the tank shell near its base at the location of the maximum axial compression during the time of maximum base moment. The expected maximum and minimum compression zone pressures  $P_{C+}$  and  $P_{C-}$ , were estimated to be 29.2 psi and 17.9 psi, respectively. These estimates include hydrostatic pressure, hydrodynamic pressure due to the horizontal fluid response modes, and 40% (see Appendix A) of the hydrodynamic pressure due to the vertical fluid response mode.

For the purpose of estimating the expected minimum fluid hold-down forces in the zone of maximum tank wall axial tension, it is required to estimate the minimum tension zone fluid pressure  $P_T$  at the time of maximum moment.  $P_T$  was estimated to be 3.2 psi, in a similar way to the pressures at the compression zone.

For the evaluation of the sliding capacity, the expected minimum average fluid pressure  $P_a$  on the base plate, at the time of the maximum base shear, can be estimated to be 10.5 psi. This pressure was determined as the hydrostatic pressure less 40% of the hydrodynamic pressure due to the vertical fluid response mode.

The expected minimum total effective weight  $W_{Te}$  of the tank shell acting on the base, at the time of maximum moment and base shear, can be estimated to be 188.2 kips.

### **3.3.2 Seismic Capacity Assessment**

The seismic capacity assessment requires the determinations of three basic capacities of the tank: (1) compressive buckling capacity of the tank shell, (2) the tensile hold down capacity of the anchorage, and (3) the hold-down capacity of the fluid pressure acting on the base plate. Each of these basic capacities will be discussed below, followed by the discussion of the overturning moment capacity, sliding capacity, fluid pressure capacity of the tank shell, and other capacities. In general, the seismic capacity evaluation is more complicated than the seismic response evaluation.

#### **3.3.2.1 Compressive Buckling Capacity of the Tank Shell**

The most likely buckling for tanks is the "elephant-foot" buckling near the base of the tank shell. The "elephant-foot" buckling is a combined effect of hoop tension, axial (vertical) compression, and restriction of radial deformation of the tank shell by the base plate. "Elephant-foot" buckling does not necessarily lead to failure of a tank (e.g. leakage). However, no simple capability evaluation method exists to predict tank performance after the development of "elephant-foot" buckling. Therefore, for the evaluation of the SME capacity of tanks, the onset of "elephant-foot" buckling will be judged to represent the limit to the compressive buckling capacity of the tank shell. The onset of "elephant-foot" buckling can be estimated using elastic-plastic collapse theory.

The CST shell is SA 204-type 304 stainless steel. This material does not have a flat yield plateau and as strain increases its stress can grow to a minimum ultimate stress capacity of 75 ksi. In the CDFM method, an effective yield stress  $\sigma_{ye}$  is set to  $2.4S_M$  or 45 ksi, in line with the ASME seismic design limit for primary local membrane plus primary bending [ASME 1983, "ASME Boiler & Pressure Vessel Code"]. The potential uncertainty range for  $\sigma_{ye}$  was reported to be between 30 ksi and 60 ksi, according to the original CDFM method description in Appendix A of NUREG/CR-5270. In this calculation, the effective yield stress took the median value of 45 ksi.

The "elephant-foot" buckling axial stress of the tank shell can be accurately predicted to be 21.4 ksi. The compressive buckling capacity for HCLPF capacity computations utilizes a recommended 0.9 reduction of the buckling stress and was estimated to be 12.1 kips/in.

A check of the buckling capacity of the supported cylindrical shells under combined axial bending and internal pressure showed that it did not govern the buckling capacity of the CST shell. This check required the reference NASA SP-8007 [1968] to define parameters and procedures to compute the buckling capacity under combined axial bending and internal pressure. Figure 6 of NASA SP-8007 will be digitalized in the next section to automatically determine a parameter that varies with the degradation state.

### **3.3.2.2 Bolt Hold-Down Capacity**

The bolt hold-down capacity should be determined as the smallest of the bolt tensile capacity, anchorage of bolt into the concrete foundation, capacity of the top plate of bolt chairs to transfer bolt loads to the vertical chair gussets, attachment of the top plate and vertical chair gussets to the tank shell, and the capacity of tank shell to withstand concentrated loads imposed on it by bolt chairs.

According to the drawing, the anchor bolt chairs form a circumferentially continuous construction. Based on the continuous chair construction and the sizing of the plates and weld, it is judged that the anchor bolt chair and its attachment to the tank shell are adequate to transfer the bolt capacity load for the CST. The tank shell is also considered to be adequate in withstanding the concentrated loads imposed on it by bolt chairs, especially because the "elephant-foot" buckling capacity is also checked.

The anchor bolt is A36 steel and has a diameter of 2 1/2". Based on the AISC code [9<sup>th</sup> edition, 1989], the tensile capacity of the anchor bolt was determined to be 159.4 kips.

The failure of the anchorage of the bolt into the concrete foundation can be bolt failure, plug pull-out, and concrete cone failure. The tensile capacity of the anchorage is difficult to analyze. Fortunately, Lee, et al [2001] performed an experimental study of very similar anchor bolts and anchorages. Based on the test results, the anchorage capacity was about 200 kips, which is about 26% higher than the tensile strength of the anchor bolt. It should be noted that in the test one specimen had abrasion in its thread, suggesting the anchor bolt capacity should be also close to 200 kips. However, since the embedment in the test was about 1-3/8 inch longer than the subject CST case, the spacing of anchor bolts in the test is twice as long as in the subject CST case, and the lab test condition usually have a higher quality control, the bolt hold-down capacity is assumed to be the bolt tensile capacity 159.4 kips.

### **3.3.2.3 Fluid Hold-Down Capacity**

Figure 3-6 shows a schematic depiction of the relationship among the hold-down tension  $T_e$ , the uplift  $\delta_e$ , the uplift distance  $l$ , the rotation  $\alpha_e$ , the moment  $M_e$ , and water pressure  $P$ , at the region of axial tension in tank shell. Based on a small displacement theory, a set of equations were developed in NUREG/CR-5270 to determine a relation between  $T_e$  and  $\delta_e$ . For unanchored tanks, it was showed that the fluid hold-down force  $T_e$  and the uplift  $\delta_e$  can be greatly increased if a large displacement membrane theory had been employed. Nevertheless, for anchored tanks like the subject CST, the uplift is not expected to be very large. For the small displacement theory to be applicable, the maximum  $\delta_e$  must be less than or equal to  $0.6 \times t_B = 0.165'$ , where  $t_B$  is the thickness of the tank bottom plate. Since the hold-down force  $T_e$  increases as the fluid pressure  $P$

increases, the fluid pressure  $P$  was conservatively assumed to take the minimum tension zone fluid pressure  $P_T = 3.2$  psi.

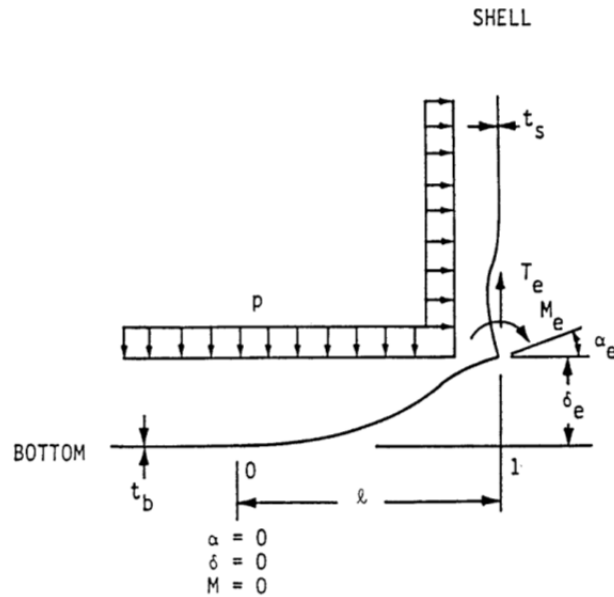


Figure 3-6 Illustration of Tank Bottom Behavior near Tensile Region of Tank Shell [from NUREG/CR-5270]

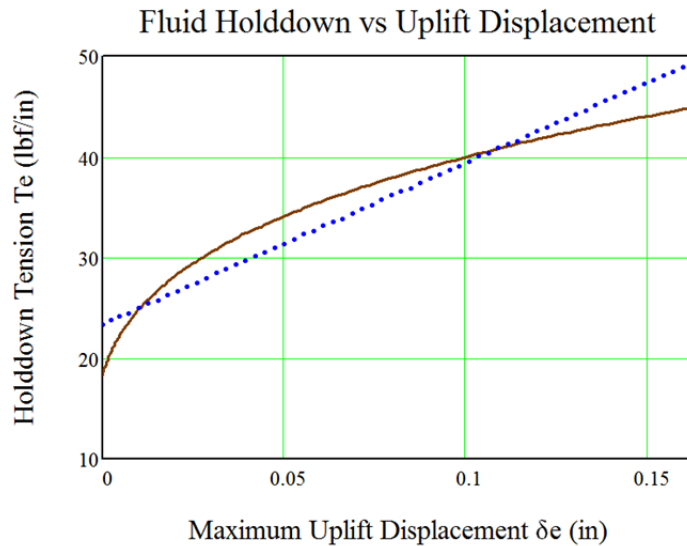


Figure 3-7 Relation of Fluid Hold-down Force and Uplift Displacement

Figure 3-7 shows a relationship between the fluid hold-down force and the uplift displacement in solid line. It should be noted that with no uplift, the fluid hold-down force was non zero (about 19 lbf/in). Beyond the limit of an uplift displacement of 0.165", the small displacement theory will be increasingly conservative. A linear approximation of this relationship is also shown in Figure 3-7, and will be used in the evaluation of overturning moment capacity. This linear

approximation was implemented in Mathcad in a highly automated fashion, so that no manual intervention is needed during the trial-and-error iteration process for the SME capacity evaluation.

An upper limit on the fluid hold-down capacity was assessed based on the assumption of two plastic hinges at both ends of the uplifted zone of the tank base plate. The upper limit of the fluid hold-down capacity indicates that the linear approximation of the  $T_e$ - $\delta_e$  relation shall not be used beyond  $\delta_e = 1.07''$ .

More detailed discussion can be found in Appendix A of NUREG/CR-5270 and Appendix A of this report.

### 3.3.2.4 Overturning Moment Capacity

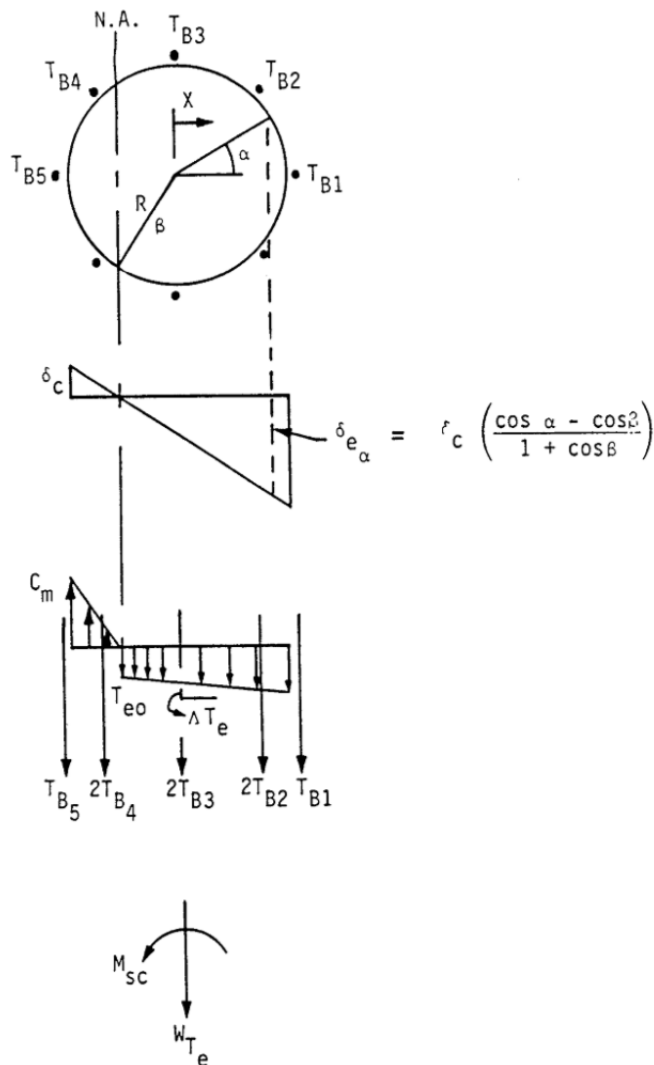


Figure 3-8 Vertical Loading on Tank Shell at Base [from NUREG/CR-5270]

The overturning moment capacity can be estimated using the compressive buckling capacity of the tank shell, the anchor bolt hold-down capacity, and the relationship between fluid hold-down force and uplift displacement. Several conservative but reasonable assumptions were also made: (1) the bottom of the tank shell is assumed to rigidly rotate vertically (plane sections remain plane); (2) the cross-section of the tank right above the top plate of the bolt chairs is assumed to remain horizontal so that all vertical tank distortions needed to result in base uplift and mobilization of the anchor bolts must be accommodated below this level; and (3) the compressive stress varies linearly from zero at the neutral axis ( $\alpha = \beta$  as in Figure 3-8) to its maximum value at  $\alpha = 180^\circ$ . Because the bolt pretension is unreliable after a number of years in service, it is conservatively assumed to be zero.

The neutral axis angle  $\beta$  was determined iteratively by trial-and-error in NUREG/CR-5270, so that the tank shell compressive buckling capacity was achieved. This study utilized the root finding function in Mathcad to automate the determination of  $\beta$ ; Appendix A of this report provides more details on the procedure and the technique to determine  $\beta$ . Corresponding to the converged SME 0.426 g,  $\beta$  was found to be  $131.3^\circ$ . The overturning moment was estimated, using  $\beta$  and the shell compressive capacity, to be 152,232 kips-ft.

The largest bolt elongation (at  $\alpha = 0$ ), at the time of the maximum overturning moment, was estimated to be 0.08%, much smaller than the 1% recommendation for the A307 bolt in Appendix A of NUREG/CR-5270. It is assumed that A36 bolts and the A307 bolts have a similar elongation capacity.

The corresponding maximum tank shell uplift distortion was found to be 0.03", which is much smaller than the linear limit of 0.165", and certainly much smaller than the applicability limit of 1.07".

The study of the example tank in Appendix A of NUREG/CR-5270 needed to consider  $\alpha = 0$  both at a bolt or in the midway between two adjacent bolts, because there were only 8 anchor bolts tied the tank to its foundation. On the other hand, the subject CST has 78 anchor bolts, therefore a case with  $\alpha = 0$  at a bolt is sufficient.

An inelastic energy absorption factor  $k$  of unity was conservatively applied in the analysis, because it is difficult to make an appropriate estimation of  $K$  for a hybrid failure mode that combines bolt yielding and tank shell buckling. At an SME earthquake of 0.426 g, the overturning moment SME was found to be at a value of 1.1 g, which is significantly higher than that of the sliding capacity.

### **3.3.2.5 Sliding Capacity**

The base shear and the base overturning moment are primarily due to the horizontal impulsive mode of fluid response, and their maxima coincide in time. The key in assessment of sliding capacity is the selection of the coefficient of friction (COF). For the example tank where several rough steps exist on the surface between the bottom plate and the sand cushion, NUREG/CR-5270 recommended a COF of 0.70. For flat-bottom steel tanks on concrete foundation, the COF is estimated to be 0.55 [Bandyopadhyay, et al, 1995]. A COF of 0.55 will be used in this study.

The sliding capacity of the tank cannot take advantage of the shear capacity of the anchor bolts because (a) there is a large space between the concrete foundation and the anchor bolt chair, and (b) there is 1/4" diametric clearance in the hole in the anchor bolt chair, and (c) the pretension in the anchor bolts, if any, are not reliable.

It is recommended in NUREG/CR-5270 that the inelastic energy absorption reduction factor to take a value of unity for the base shear sliding.

The calculated SME capacity for the sliding mode is 0.426 g, and governs the seismic margin capacity of this tank. This is different from the example tank in NUREG/CR-5270, in which the overturning moment capacity governs. Had a COF of 0.7 was used, the sliding SME capacity was calculated as 0.555 g.

### **3.3.2.6 Fluid Pressure Capacity**

The hoop membrane stress capacity was recommended in NUREG/CR-5270 to take the ASME seismic design limit of  $2 S_M$  for primary stress, which is 37.5 ksi for SA240-type 304 stainless steel. The inelastic energy absorption reduction factor was recommended to be 0.8.

At an SME earthquake of 0.426 g, the estimated HCLPF SME for the fluid pressure mode was found to be 2.1 g, which is significantly larger than the sliding HCLPF SME capacity.

### **3.3.2.7 Other Capacity Check**

There are a few other capacities that were recommended to check, although they usually do not govern the SME capacity. In particular for this study, the two CSTs can potentially interact with the auxiliary building between them, possibly resulting in a lower SME capacity. These checks are coded in the Mathcad worksheet so that any (unlikely) governing case from these capacities can be detected.

*Slosh height for roof damage:* with the HCLPF shear capacity of 0.426 g, the sloshing height can be about 6.1 ft, which is lower than the total height of the head (8.7', as approximated in the beginning part of this calculation). It was found during the iteration process that the increase of sloshing height was not significant as  $SME_e$  increased from 0.334 g to 0.426g. In addition, as pointed out in the NUREG/CR-5270, even if roof damage might occur, such damage usually does not impair the ability of the tank to contain fluid.

*Foundation failure:* as indicated by KAERI, the CST founded on a rock site, therefore soil-tank foundation interaction was not considered.

*Piping failure or failure of nozzles:* these failures may lead to loss of fluid in the tank, and more importantly, may impair the normal function of the condensation system. As reported in NUREG/CR-5270, a significant fraction of the cases of seismic induced loss of tank contents have been due to piping/nozzle failures because of poor detailing. It is recommended that an SME evaluation of piping/nozzle failures is necessary only when poor seismic detailing is found in the involved piping attached to the tank. In this study, the subject CST is assumed to be appropriately detailed, i.e. the piping and nozzles directly attached to the tank are properly designed and constructed so that sufficient piping flexibility can be achieved to accommodate large relative seismic anchor movements. KAERI also expressed a similar observation on the pipe/nozzle failure in an email communication.

*Interaction of tank-auxiliary building:* the influence of the auxiliary building in between the two CSTs on the SME capacity was assessed in the study. The 3" gap between the roof of the auxiliary building and the CSTs is filled with elastomeric sealant; there are no other contact points above the tank foundation (see Figure 3-9 and Figure 3-10).

A simplified check was performed by calculating the rotation angle at the tank base and the maximum horizontal displacement at the roof level. The maximum tank shell uplift distortion is found to be 0.026 in, which corresponds to a neutral axis angle  $\beta$  of  $131.2^\circ$ . Since the horizontal plane at the anchor bolt chair is assumed to remain plane and all distortion is assumed to occur below this level, the rotation angle around the neutral axis was estimated to be  $5.3 \times 10^{-5}$  ( $0.003^\circ$ ). The height of the auxiliary building between the top of the foundation and the top of the roof is about 13'. The maximum horizontal displacement at the roof level was estimated to be 0.008" (0.2 mm), which is only about 0.3% of the 3" gap. Based on this result, it is judged that influence of the auxiliary building on the SME capacity of the CST is minimal.

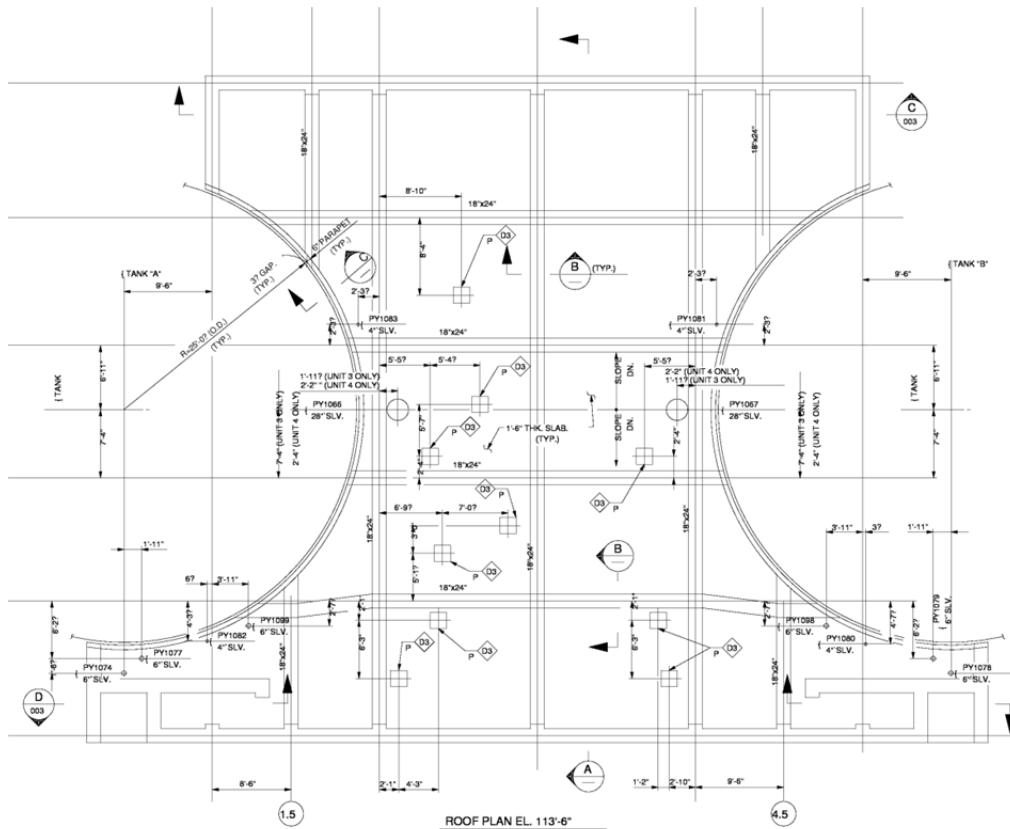


Figure 3-9 Plan View of CST/Auxiliary Building at Roof Level [KAERI Email Communication to BNL, 09/29/2009, Document No. 9-251-C118-002]

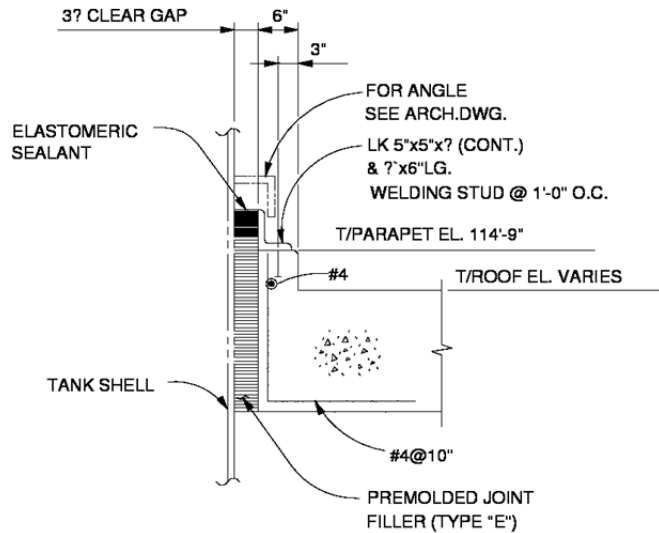


Figure 3-10 Detailing of CST/Roof of Auxiliary Building [KAERI Email Communication to BNL, 09/29/2009, Document No. 9-251-C118-002]

### 3.3.3 Summary of the CST Seismic Fragility

The HCLPF SME capacity of the CST was estimated to be 0.426 g, which is governed by the sliding capacity. At this capacity, the calculated SME's based on the overturning moment and the fluid pressure response modes were 1.1 g and 2.1 g, respectively. It should be noted that these calculated SME's are not the converged overturning moment SME capacity or the fluid pressure SME capacity, which require separate iterations to be determined. It is important to emphasize that the estimated HCLPF SME capacity is conditioned on the RG 1.60 response spectra anchored to 0.426 g.

This HCLPF SME capacity estimate is very close to the value reported by Choun, et al [2008], which is 0.41 g and also sliding capacity governs. This good agreement validates the accuracy of the calculation implemented in Mathcad and provides confidence in the results of the fragility analysis of the degraded CST, which will be introduced in the next section.

Uncertainties  $\beta_R$  and  $\beta_U$  are required to develop the full fragility of the CST. Since the CDFM method relies on deterministic but conservative parameters and only yields the HCLPF capacity, the uncertainties are not available in this analysis. As commonly understood, the uncertainties are very much subjective; therefore their determination depends on a significant level of expertise, which may not be readily available through one source or by one person. In this study, a full examination of the uncertainties associated with the CST was not performed because of the subjective nature of the uncertainty estimates. Instead, the uncertainties in various parameters, especially the resultant uncertainties associated with the median fragility of the example tank in NUREG/CR-5270, were used directly, because these two tanks are similar in size and materials. As reported in Appendix A of NUREG/CR-5270 in the FA method, the aleatory uncertainty  $\beta_R$  and the epistemic uncertainty  $\beta_U$  were 0.20 and 0.27, respectively. These uncertainty values are almost identical to those reported by Choun, et al [2008], where the only difference is that the aleatory uncertainty was 0.21. The composite uncertainty  $\beta_C$  can be calculated as 0.34.

Based on the HCLPF capacity and the uncertainties, the median fragility capacity can be estimated to be 0.923 g. Figure 3-11 shows the mean fragility curve and the median, 5%

percentile, and 95% percentile fragility curves. Figure 3-12 shows a 3-dimensional view of the fragility of the CST as a function of the controlling variable PGA and the confidence level Q.

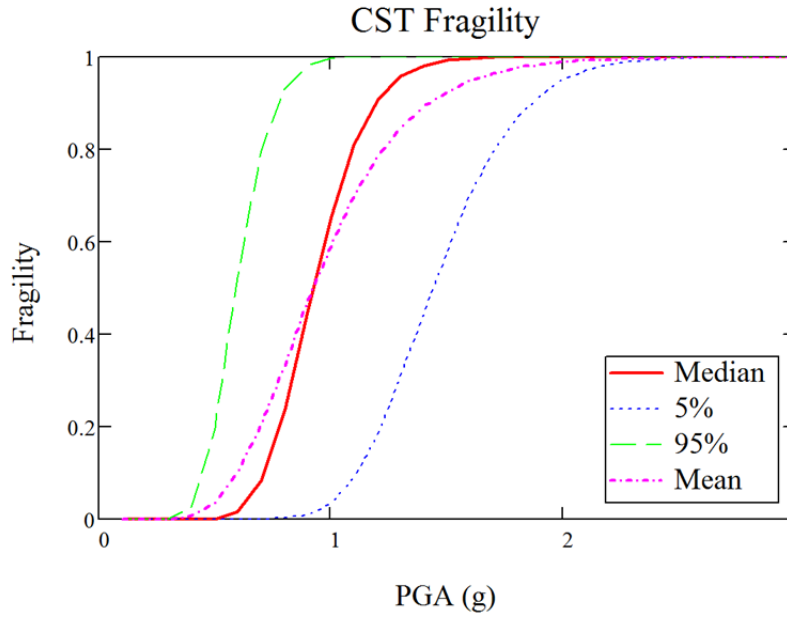


Figure 3-11 Fragility Curves of the CST

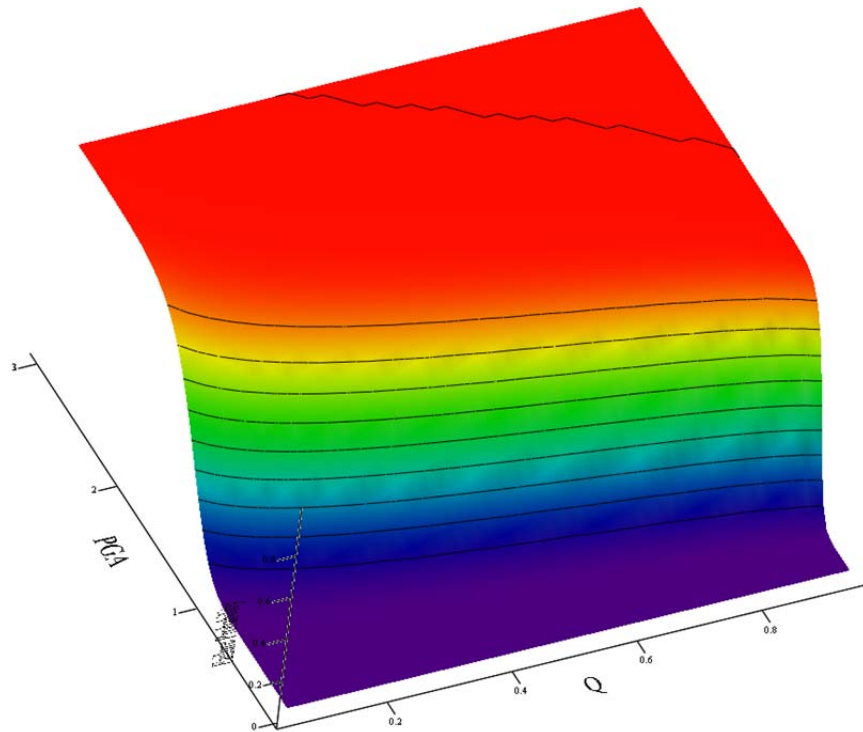


Figure 3-12 A 3D View of the CST Fragility as a Function of PGA and Confidence Level Q

The Mathcad worksheet for the fragility analysis of the undegraded CST was modified to incorporate various degradation scenarios and the results of these time-dependent fragility analyses will be documented in the next section.

## **4 FRAGILITY ANALYSIS OF DEGRADED CONDENSATE STORAGE TANK**

BNL performed a series of time-dependent fragility analyses of the CST by incorporating selected aging-related material degradation models into the fragility analysis. Three separate degradation scenarios and one combined degradation scenario were considered: (A) degraded stainless tank shell, (B) degraded anchor bolts, (C) anchorage concrete cracking, and (D) a perfect correlation of the three degradation scenarios. As agreed with KAERI, the degradation scenarios A and B will use degradation models from the Year 2 report for demonstration purposes, with a best effort in determining the required parameters. In degradation scenario C, a hybrid degradation model was developed based on available anchorage test results for cracked concrete and KAERI's recent regression model/data that utilized measurements from Korean NPPs. The recorded degradation data were very valuable because such data are not commonly available. The degradation scenario D considers all three degradation cases A, B, and C together, assuming a perfect correlation among them.

This section describes for each of the four cases the selected degradation model, determination of parameters, fragility analysis for the degraded CST, and the results from these analyses. More specifics can be found in Appendices B through E. It should be noted that these appendices were developed based on the undegraded case, and therefore some portion of the analysis that is not specifically important to the degraded cases, such as the weight and the frequency calculation, is omitted (hidden, in the Mathcad terms) for simplicity.

### **4.1 Fragility Analysis for (A) Degraded Tank Shell**

#### **4.1.1 Degradation Model for Stainless Steel Tank Shell**

The material degradation model for the stainless steel tank shell to be used in this study is the mechanochemical model for stress corrosion cracking (SCC), which is one of the three time-dependent material degradation models for stainless steel that are documented in the Year 2 annual report [Nie, et al, 2009]. It is noticed from Figure 3-1 that there are no signs of significant degradation in the CST shell, therefore, the consideration of tank shell degradation in fragility analysis in this section of the report is for the purpose of demonstration. SCC is assumed to be the degradation mechanism that will be considered for the subject CST.

The mechanochemical model [Saito and Kuniya, 2001] was developed to predict the SCC growth in stainless steel components submerged in 288 °C water. This model was judged to be relevant in the NPP environment because austenitic stainless steel (especially type 304) is widely used in light water reactors (LWRs) and in particular for the subject CST. The structural integrity of the involved components due to inter-granular stress corrosion cracking (IGSCC) is often a concern in NPPs. Since the water temperature in the CST is similar to the atmospheric temperature at the site, the use of this model will demonstrate its application even though the parameters were chosen to alleviate the effect of high temperatures (which do not exist in this case).

This SCC crack growth model for type 304 stainless steel is based on a hypothesis of the slip-formation/dissolution mechanism and is expressed as a function of material conditions, water chemistry, and stress related parameters. This model involves two major mechanisms: 1) slip step formation due to dislocation movement at the crack tip, and 2) anodic dissolution at the bare surface after the slip deformation. The derivation of this model was lengthy, highly theoretical, and cannot be easily summarized in this report. Interested readers are recommended to refer back to the original reference. Fortunately, based on the theoretical development, a relatively simple numerical model was also developed for type 304 stainless steel in 288 °C water, using a minimal number of parameters [Saito and Kuniya, 2001].

This relatively simple model of the SCC crack growth rate (m/s) is represented by the following simple power law of two parameters only,

$$\frac{da}{dt} = 1.1 \times 10^{-7} \left[ 2.5 \times 10^{10} \exp \left( -\frac{3 - 0.15(K - 9)^{1/3}}{0.0774} \right) \right]^n \quad (4-1)$$

In which  $a(t)$  is the crack size at a time instance  $t$ ,  $K$  is the applied stress intensity factor and  $K > 9 \text{ MPa}\sqrt{\text{m}}$ , and the numerical constant  $n$  can be expressed as,

$$n = -\frac{1}{3} \{ \ln[(1 + C_1 \text{EPR})(C_2\kappa + C_3)(C_4\phi_C + C_5)] + C_6\phi_C + C_7 \}, \quad (4-2)$$

where EPR is the electrochemical potential kinetic reactivation,  $\kappa$  the bulk water conductivity, and  $\phi_C$  the bulk corrosion potential,  $C_1$ - $C_7$  are numerical constants, which are determined from a database of test data using a wide range of stressing ( $11 \text{ MPa}\sqrt{\text{m}} \leq K \leq 60 \text{ MPa}\sqrt{\text{m}}$ ), material ( $1.4 \text{ C/m}^2 \leq \text{EPR} \leq 13 \text{ C/m}^2$ ), and water chemistry ( $0.1 \mu\text{S/cm} \leq \kappa \leq 1.5 \mu\text{S/cm}$ ,  $-280 \text{ mV} \leq \phi_C \leq 250 \text{ mV}$ ). The values of  $C_1$ - $C_7$  are given as,

$$\begin{aligned} C_1 &= 3.57 \times 10^{-2}, \\ C_2 &= 1.49 \times 10^{-8}, \\ C_3 &= 2.23 \times 10^{-8}, \\ C_4 &= 4.57 \times 10^{-3}, \\ C_5 &= 23.12, \\ C_6 &= 2.29 \times 10^{-3}, \\ C_7 &= 11.56. \end{aligned} \quad (4-3)$$

To summarize, the model of the SCC crack growth rate really only has four parameters:  $K$ , EPR,  $\kappa$ , and  $\phi_C$ . As for application to type 304 stainless steel in 288 °C water, Saito and Kuniya [2001] suggested the following ranges (or typical values) of these four parameters,

$$\begin{aligned} K &= 28 \text{ Mpa}\sqrt{\text{m}}, \text{ depends on loading} \\ \kappa &= 0.1 - 1.2 \mu\text{S/cm} \\ \text{EPR} &= 6 - 13 \text{ C/cm}^2 \\ \phi_C &= -200 - +250 \text{ mV}. \end{aligned} \quad (4-4)$$

#### 4.1.2 Assessment of the Tank Shell Degradation

To alleviate the effect of the high temperature that biases from the actual temperature of the CST, EPR was assigned to the lower bound value  $6 \text{ C/cm}^2$ ,  $\kappa$  to  $0.4 \mu\text{S/cm}$ , and  $\phi_C$  to  $-50 \text{ mV}$ . Using these values and Equation 4-2, the exponent  $n$  in Equation 4-1 was evaluated to 0.87.

The stress intensity factor  $K$  can be estimated based on the static water pressure, which is 16.3 psi as determined previously in Section 3. The stress intensity factor is also a function of the crack geometry; therefore  $K$  is time dependent due to crack growth and can be symbolically represented as  $K(a(t))$ . Since  $K(a(t))$  is not readily available and the purpose of the current study is for demonstration, a simplified approach was used. Assuming a through crack in the vertical direction at the bottom of the tank shell and of a length that is twice of the tank thickness,  $K$  can be estimated using the following simple formula [Tada, et al, 2000]:

$$\sigma_{hoop} = \frac{P_{ST} \times R}{t_S} = 7.8 \text{ ksi} \quad (4-5)$$

$$K = \sigma_{hoop} \times \sqrt{\pi \delta_S} = 12.018 \text{ MPa}\sqrt{m}$$

Based on Equation 4-1, a constant  $K$  leads to a constant crack growth rate of 0.0075 in/year. A list of crack depths can then be calculated for a period of 80 years, which is the current expectation of the longest operating life of NPPs. Figure 4-1 shows the change of SCC depth as a function of time (year) and the corresponding wall thinning of the tank shell. Since a few isolated cracks in the tank shell may not affect much the seismic capacity of the tank, it is further assumed that many cracks cluster at a small region at the base of the tank shell and the effect of the crack assembly is similar to loss of material in that location. The fragility analysis of CST with levels of tank shell degradations will follow this assumption.

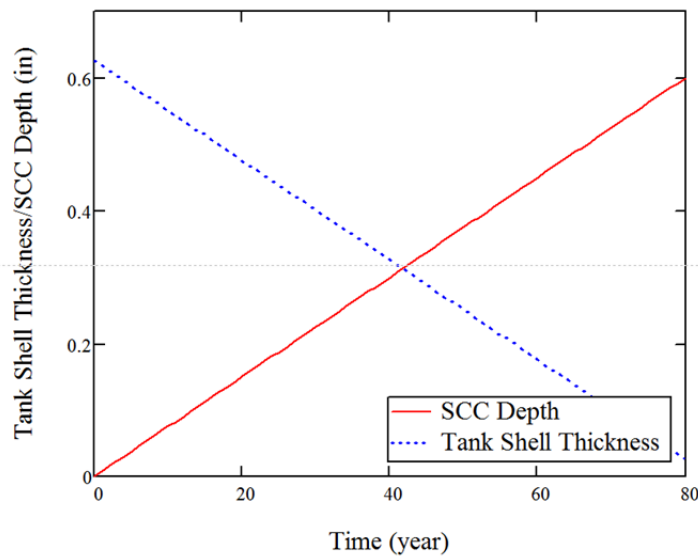


Figure 4-1 Change of Tank Shell Thickness/SCC Depth with Time

#### 4.1.3 Fragility Assessment of CST with Degraded Tank Shell

The Mathcad worksheet for the undegraded CST, also designated as the base case, was modified to incorporate the degradation model for the stainless tank shell. A new variable for the thickness of tank shell was created separately to track the degradation process. The smaller thickness due to loss of material is assumed to occur at local regions at the base of the tank shell, and therefore only the capacity calculation but not the frequency and the response calculation will be changed. Because of this change of thickness of the tank shell, the upper bound check of the compressive buckling capacity requires the digitalization of the Figure 6 of NASA SP-8007 and implementation of an automatic interpolation to determine the necessary parameters. More details on the update of Mathcad worksheet can be found in Appendix B of this report. It should be noted that some portion of the calculation and documentation was hidden in Appendix B because there is no change in that portion and some of the documentation may not be updated from the base case to minimize the calculation effort.

The direct impact of the degraded tank shell is on the compressive buckling capacity and the fluid hold down capacity, but obviously not on the bolt hold down capacity. All three major resultant capacities: the overturning moment capacity, sliding capacity, and the fluid pressure capacity are

affected. Both the slosh height and the horizontal displacement at the roof level of the auxiliary building become smaller as the SME becomes smaller due to degradation. These decreases are because of the decrease in the SME capacity of the CST. Given the same level of input earthquake the slosh height would be unchanged and the horizontal displacement at the roof level of the auxiliary building would increase as the level of degradation increases.

Only mean fragility curves will be presented in this report because it is difficult to present the family of median fragility curves in a plot for more than one degradation level unless utilizing 3D surfaces such as in Figure 3-12. Even with 3D surfaces, it will be difficult to interpret the 3D fragility data without an interactive tool because of surface overlapping.

Figure 4-2 shows the mean fragility capacity of the CST with degraded tank shell for a series of years, from 0 up to 60 years, after which the fragility calculation was not mathematically achievable. These mean fragility curves were calculated using unchanged uncertainties, i.e.,  $\beta_R = 0.2$  and  $\beta_U = 0.27$ , the same as utilized for the base case. In reality, since the degradation process is highly random and uncertain, both the epistemic and aleatory uncertainties should vary with time. However, reliable uncertainty data on the degradation model were not available to be utilized. Provided the uncertainty data are available, the updated uncertainties, as functions of time, can be updated based on Equation 2-5, and these mean fragility curves can be updated without any technical difficulty. Since the objective of this study is for demonstration purposes, the effect of the degradation on the uncertainties is not considered. In Figure 4-2, it is obvious that the spacing of the fragility curves suddenly increases significantly after 45 years, when the governing failure mode shifted from the sliding failure to the overturning moment failure.

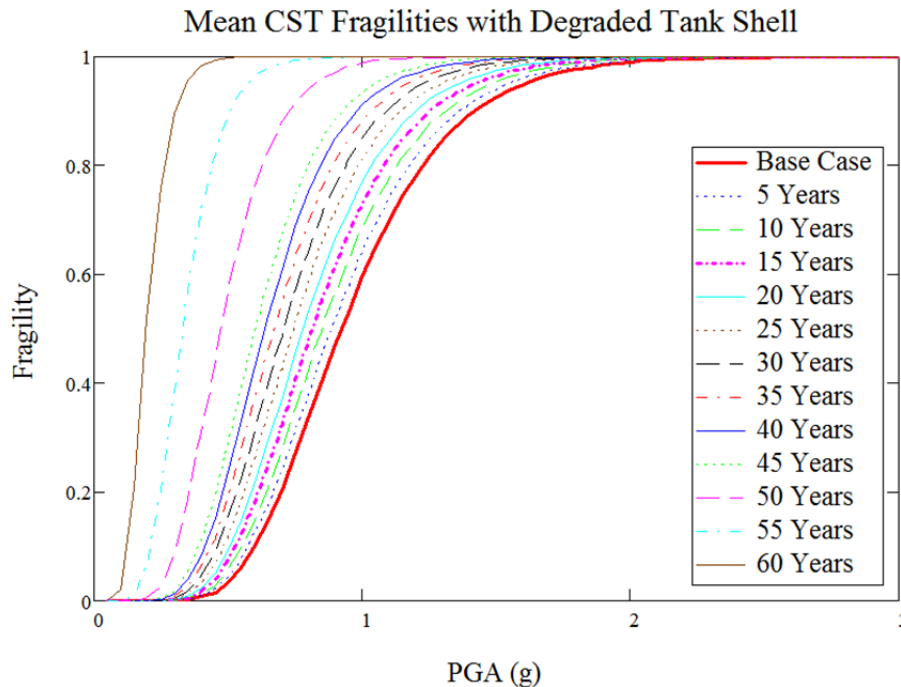


Figure 4-2 Mean Fragility Capacity of the CST with Degraded Tank Shell

It is easier to see the transition of failure mode by the relation of the HCLPF fragilities / the median capacities and time. Figure 4-3 and Figure 4-4 show in solid lines the HCLPF fragilities and the median capacities of the CST as a function of time, respectively. These figures also included the corresponding overturning moment capacities, sliding capacities, and the fluid pressure capacities, in dotted, dashed, and dash-dot lines, respectively. The fragility capacity is taken as the minimum of these three capacities. It should be noted that the non-governing capacities are higher than the corresponding real fragility capacities, which require separate iterations to be determined. From these figures, it is obvious that the tank shell degradation (wall thinning) has the most significant impact on fluid pressure capacity and the least impact on sliding capacity. The fragility capacity (either HCLPF capacity or the median capacity) is clearly dominated by the sliding mode until slightly after 45 years, and then by the overturning mode. Although the fluid pressure mode does not dominate the fragility capacity up to 60 years, it would be dominant shortly after 60 years had the calculation continued.

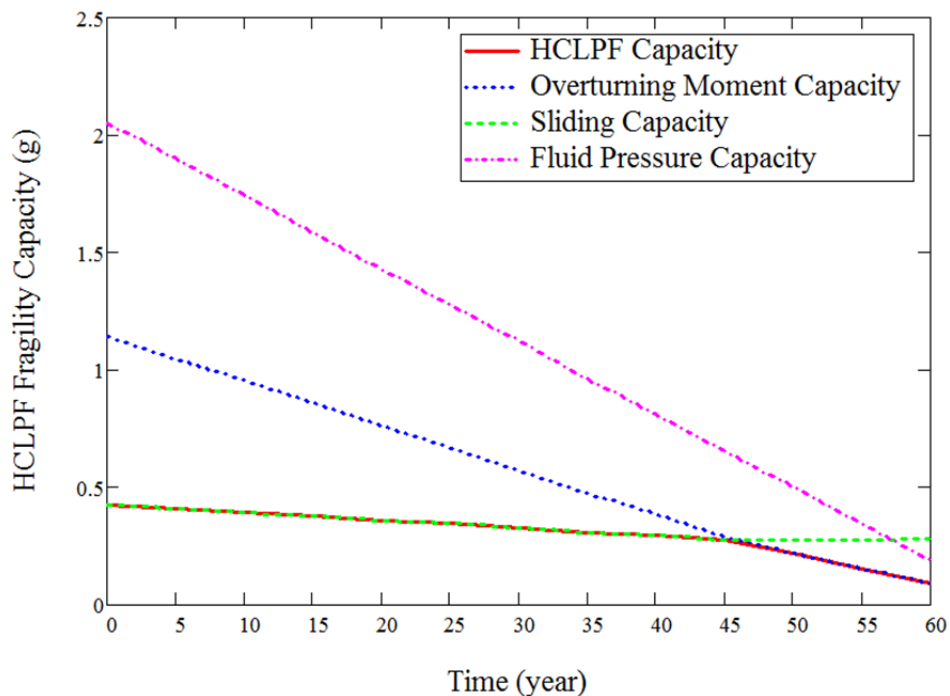


Figure 4-3 HCLPF Capacity of the CST with Degraded Tank Shell

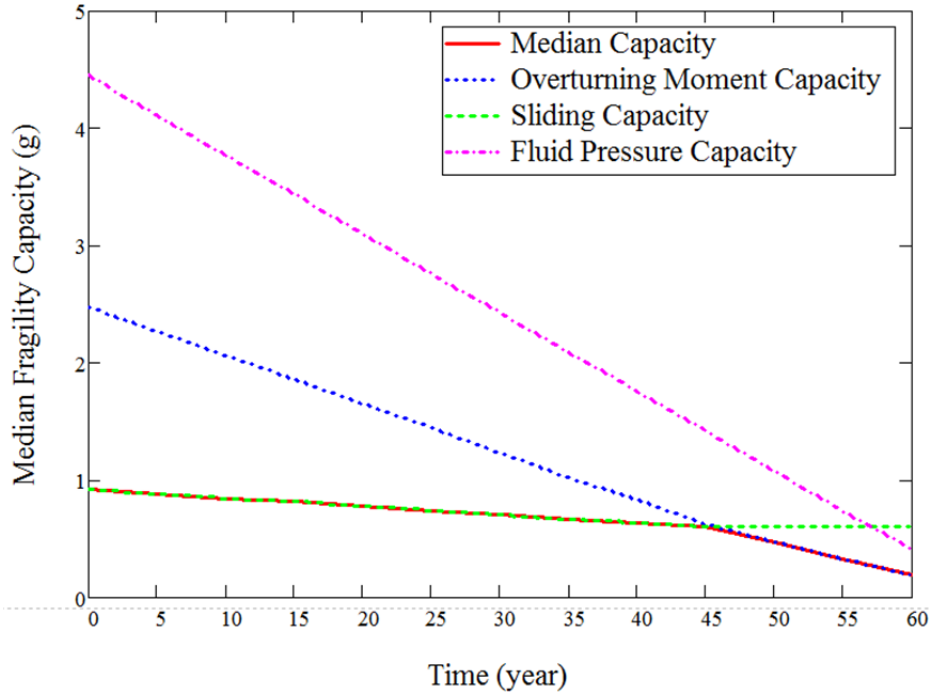


Figure 4-4 Median Capacity of the CST with Degraded Tank Shell

## 4.2 Fragility Analysis for (B) Degraded Anchor Bolts

### 4.2.1 Degradation Model for Anchor Bolts

Unlike the stainless steel tank shell of the CST, the anchor bolts made of A36 are prone to corrosion because of the salty moisture in a location close to the ocean. The protecting stainless steel cover as shown in Figure 3-1 is assumed not to be leak-tight. The power model for steel corrosion was chosen for modeling the degradation of the anchor bolts, from the Year 2 annual report [Nie, et al, 2009]. This model had been used by Mori [2005] in a study of reliability-based service life prediction, which provides a direct indication of its applicability in fragility analysis. The power model can be used for modeling of both concrete cracking/reinforcement corrosion and corrosion of carbon and low alloy steel. This model is briefly introduced in the following and the parameters in the model are then defined.

The depth of corrosion in the power model can be represented by,

$$X(t) = Ct^\alpha \tag{4-6}$$

in which  $t$  is the elapsed time in years,  $C$  the rate parameter, and  $\alpha$  the order of the power model that depends on the nature of the attack. The corrosion rate  $C$  is a function of material, ambient moisture, and temperature. The parameters  $C$  and  $\alpha$  can be estimated using experiments. Table 4-1 shows the average values for these parameters determined by Albrecht and Naeemi [1984]. The level of attack  $X(t)$  applicable to this table is in units of  $\mu\text{m}$ , and the time  $t$  is in years.

Since the Ulchin NPP, where the subject CST is installed, is located on the coast, the marine environment in Table 4-1 was assumed in the fragility analysis of the CST for degraded anchor bolts, i.e.,  $C = 70.6$  and  $\alpha = 0.79$ .

Table 4-1 Average Values for Corrosion Parameters  $C$  and  $\alpha$  [Albrecht and Naeemi, 1984].

Environment	Carbon Steel		Weathering Steel	
	$C$	$\alpha$	$C$	$\alpha$
Rural	34.0	0.65	33.3	0.50
Urban	80.2	0.59	50.7	0.57
Marine	70.6	0.79	40.2	0.56

Based on the power model and the selected parameters  $C$  and  $\alpha$ , the depth of corrosion of the anchor bolt is shown in Figure 4-5 as a function of the time in years. Albeit the nature of the model is nonlinear, the actual depth of the corrosion for this particular application is close to a linear relation with time.

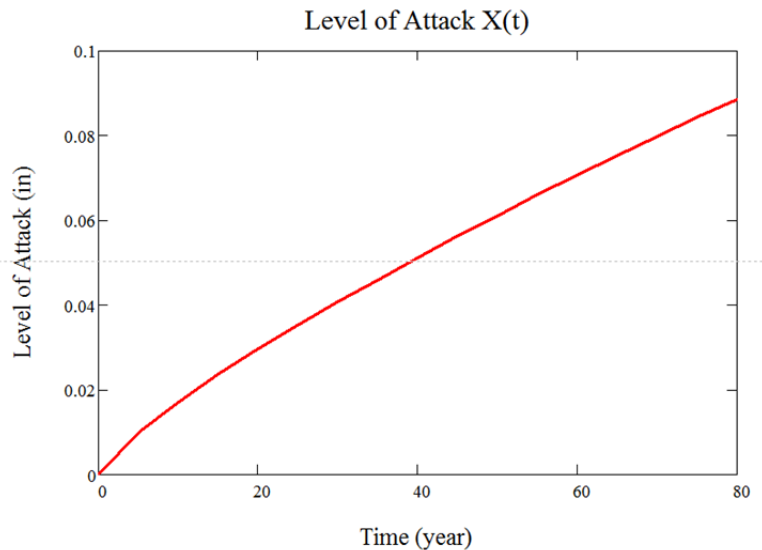


Figure 4-5 The Depth of Corrosion of the Anchor Bolts

#### 4.2.2 Fragility Assessment of CST with Degraded Anchor Bolts

Similar to degradation case A, the Mathcad worksheet for the base case fragility analysis was modified to incorporate the degradation model for the A36 anchor bolts. A new variable for the diameter of the anchor bolts was created separately to track the degradation process. A reduction of bolt diameter was assumed uniformly for all anchor bolts, as given by,

$$D_{bolt\_degraded} = D_0 - 2X(t). \quad (4-7)$$

The direct impact of degraded anchor bolts is simply on the bolt hold down capacity, and consequently on the overturning moment capacity and the sliding capacity. The degradation of anchor bolts does not affect the compressive buckling capacity, the fluid hold down capacity, and the fluid pressure capacity. More details on the update of Mathcad worksheet can be found in Appendix C of this report. It should be noted that some portion of the calculation and documentation was hidden in Appendix C because there is no change in that portion and some of the documentation may not be updated from the base case to minimize the calculation effort.

Both the slosh height and the horizontal displacement at the roof level of the auxiliary building become smaller as the SME becomes smaller due to degradation. These decreases are because of the decrease in the SME capacity of the CST. Given the same level of input earthquake the slosh height would be unchanged and the horizontal displacement at the roof level of the auxiliary building would increase as the level of degradation increases.

Only mean fragility curves will be presented in this report because it is difficult to present the family of median fragility curves in a plot for more than one degradation level unless utilizing 3D surfaces such as in Figure 3-12. Even with 3D surfaces, it will be difficult to interpret the 3D fragility data without an interactive tool because of surface overlapping.

Figure 4-6 shows the mean fragility capacity of the CST with corroded anchor bolts for a series of years, from 0 up to 80 years. For the same reason as in degradation case A, the effect of the degradation on the uncertainties is not considered. In a practical sense, it is obvious that the mean fragility is virtually unchanged for a period of 80 years. Even with a degradation level of half of the bolt diameter (approximate 950 years using the current power model), the HCLPF SME capacity was found to be still as high as 0.34 g, compared to 0.426 g in the base case. Sliding capacity dominates the HCLPF capacity for the same period. With the bolt diameter reduced to half, the overturning moment capacity reduced to about 0.582 g from 1.14 g in the base case (without iteration) and the fluid pressure capacity remains unchanged as expected. This high level of HCLPF capacity and the high reliability of the CST are believed to be attributed to the large number of bolts (78 in total).

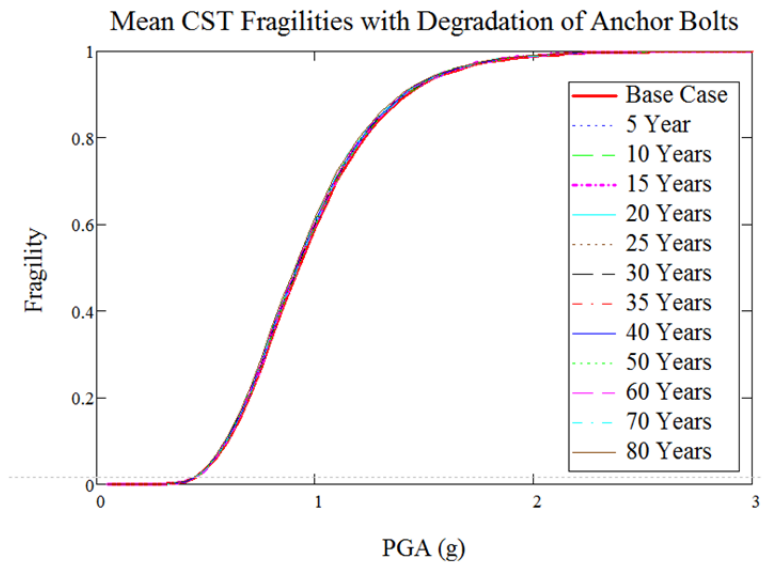


Figure 4-6 Mean Fragility Capacity of the CST with Degraded Anchor Bolts

Figure 4-7 and Figure 4-8 show in solid lines the HCLPF fragilities and the median capacities of the CST as a function of time, respectively. These figures also included the corresponding overturning moment capacities, sliding capacities, and the fluid pressure capacities, in dotted, dashed, and dash-dot lines, respectively. The fragility capacity is taken as the minimum of these three capacities. It should be noted that the non-governing capacities are higher than the corresponding real fragility capacities, which require separate iterations to be determined. From these figures, it is obvious that the anchor bolt corrosion has no or minimal impact on all three major capacities, with slightly noticeable effect on the overturning moment capacity. It is clear that the sliding capacity dominates.

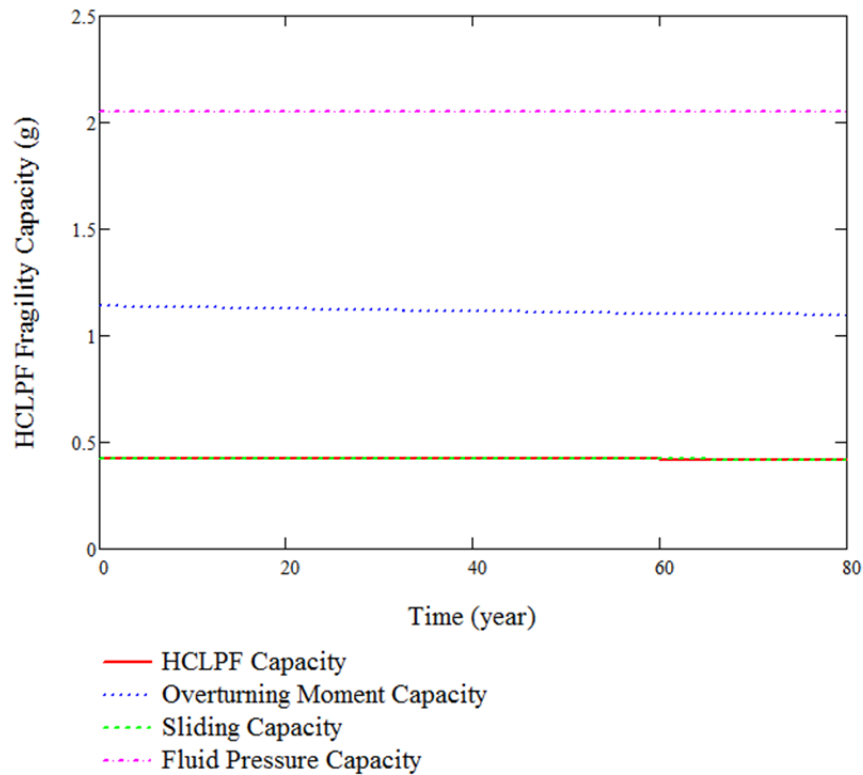


Figure 4-7 HCLPF Capacity of the CST with Degraded Anchor Bolts

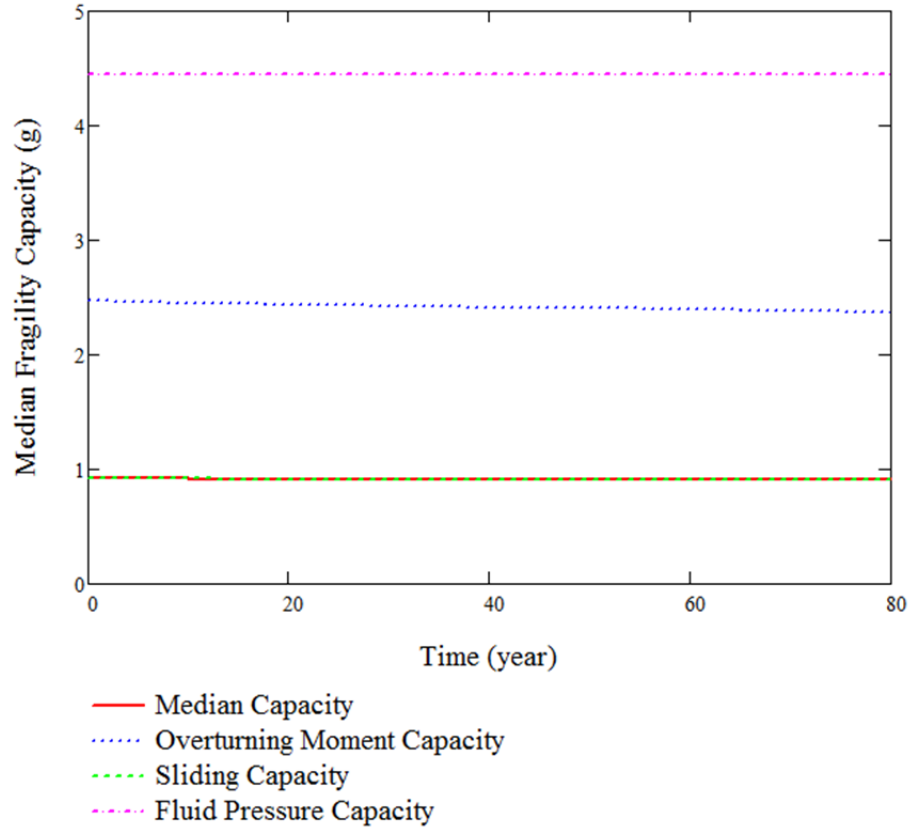


Figure 4-8 Median Capacity of the CST with Degraded Anchor Bolts

### 4.3 Fragility Analysis for (C) Cracked Anchorage Concrete

#### 4.3.1 Degradation Model for Cracked Anchorage Concrete

KAERI identified data regarding the crack width and depth of reinforced concrete that were in four Korean NPPs over a period of about 25 years. Time-dependent models based on regressions of these data were also provided by KAERI, as shown in Figure 4-9 and Figure 4-10. The linear crack width model, as reproduced in the following, was used for the fragility analysis of the CST with cracked anchorage concrete:

$$W(t) = 0.00119 t + 0.108, \quad (4-8)$$

In which  $W(t)$  is the crack width (mm) and time  $t$  is in years. Since the impact of this model on the fragility capacity of the CST with cracked anchorage concrete was found to be marginal, a revised version of this model was developed using the same measurements, by disallowing the intercept in the linear regression equation. The original version provided by KAERI is designated as C-1, while the new model is designated as C-2. As shown in Figure 4-11, the new model C-2 can be simply expressed as,

$$W(t) = 0.0078 t, \quad (4-9)$$

with the same units as in Equation 4-8. It should be pointed out that the measured crack widths have significant variation and the linear regression models do not necessarily represent true underlying relationships. The use of these curves in this study is for the purpose of demonstration; the applicability of these models in practice should be investigated with careful scrutiny.

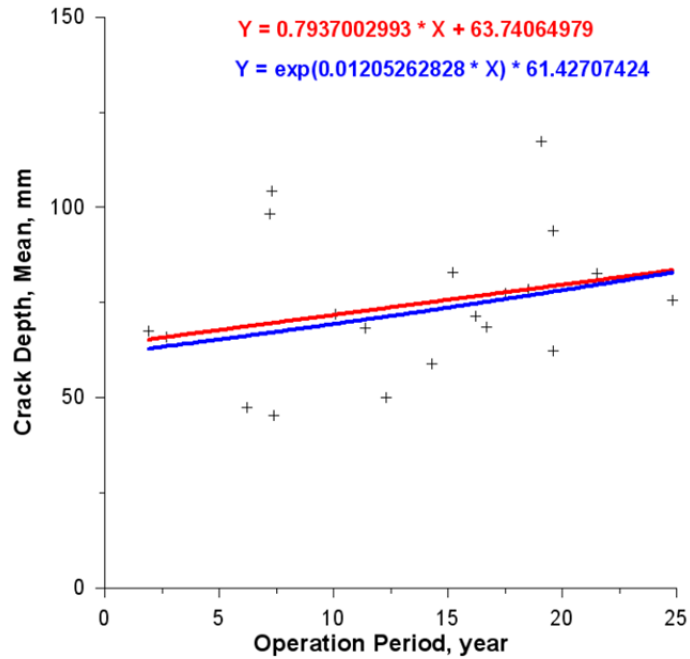


Figure 4-9 Crack Depth Models Based on Measurements in Korean NPPs (Courtesy of KAERI)

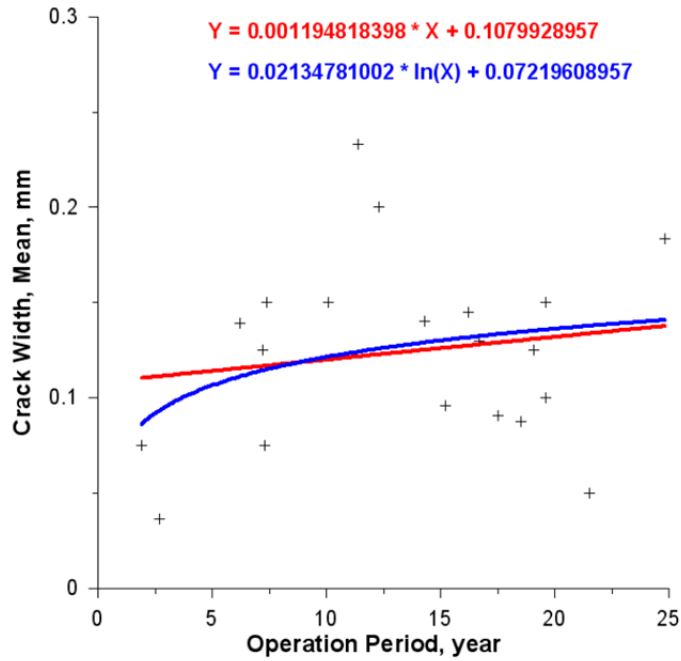


Figure 4-10 Crack Width Models Based on Measurements in Korean NPPs (Courtesy of KAERI)

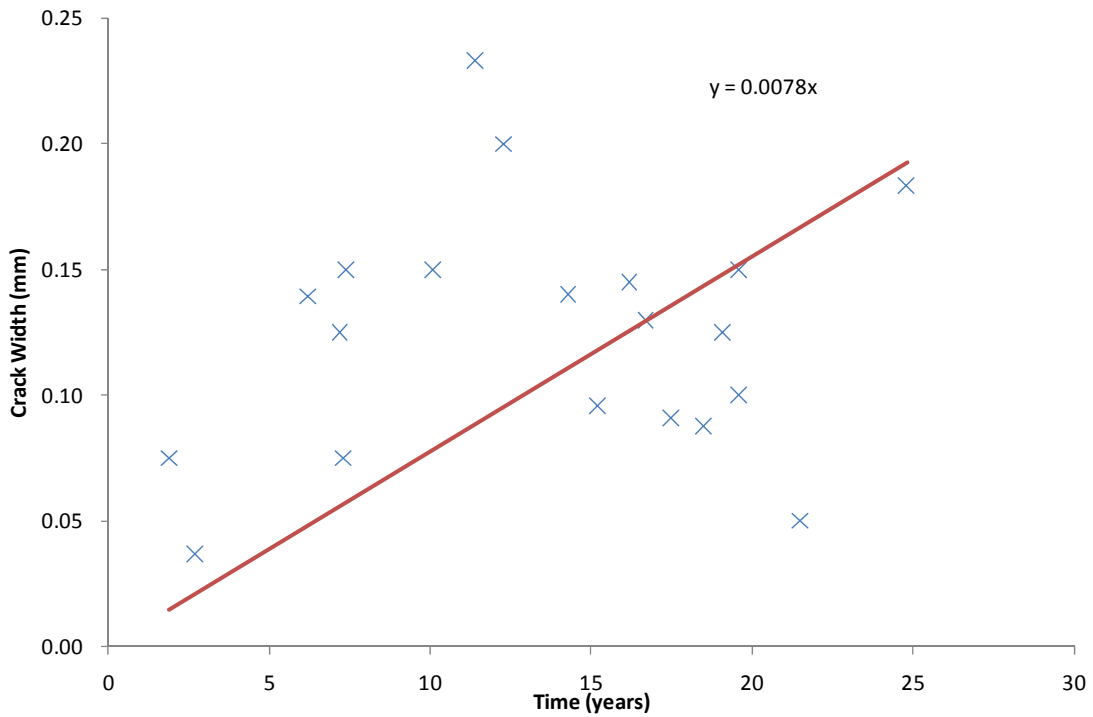


Figure 4-11 New Crack Width Model Based on Measurements in Korean NPPs

The crack width models must be mapped to the anchorage strength for its application to the fragility analysis of the CST with cracked anchorage concrete. Klingner, et al [1998] developed an empirical anchor strength – crack width relation for grouted anchors:

$$P = k h_{eff}^{1.5} \sqrt{f'_c}, \quad (4-10)$$

where  $k$  is a constant determined from test that represents the normalized tensile capacity,  $h_{eff}$  the effective embedment (in),  $P$  observed tensile capacity (lbf), and  $f'_c$  is the tested concrete compressive strength. The grouted anchors reported in NUREG/CR-5434 [Klingner, et al, 1998] had a diameter of  $\frac{3}{4}$ ", an embedment of 4", and an effective embedment of 4", which are much smaller than those of the anchor bolts for the subject CST. For the anchorage construction of the subject CST,  $h_{eff}$  was estimated to be 23" by subtracting 1" from the total embedment length to account for the nut. The concrete nominal compressive strength for the subject CST was unknown but was assumed to be 4,500 psi according to an experiment by Lee, et al [2001], which appeared to target at a CST very much similar to the subject CST. The measured concrete and grout compressive strength were much higher than 4,500 psi in the test; however, since the use of the nominal compressive strength had already led to a much higher anchor tensile strength, as to be shown later in this section, than the test results reported by Lee, et al [2001], these measured strengths were not utilized.

Grout plug pullout is the most dominant failure mode for the anchor bolts under tensile loads, therefore the friction between the concrete and the grout is crucial in determining the tensile capacity of the anchor bolts [Lee, et al, 2001, Klingner, et al, 1998]. As shown in Figure 5.20 of NUREG/CR-5434, the dynamic tensile capacity is higher than the static capacity for uncracked concrete/grout, while for cracked concrete/grout, the dynamic tensile capacity is lower than the static capacity. Comparing cracked to uncracked conditions, the reduction in dynamic tensile capacity was 73% while the reduction in static tensile capacity was 41%. The data for dynamic load capacity will be utilized for the seismic fragility assessment of the CST. The typical normalized tensile strength  $k$  is 57 for uncracked case and 12.5 for cracked case. The artificial crack in the test had a width of 0.3 mm (0.012").

The tensile strength of the anchorage for uncracked case was estimated to be 421.8 kips based on Equation 4-10, which is much higher than the capacity of 200 kips that was reported by Lee, et al. [2001]. The reason for this difference may be the substantial difference in the scales of the anchor bolts in the two test studies; smaller scale usually leads to higher strength as commonly observed. Therefore, the test data in NUREG/CR-5434 will be used as factors to scale the test data reported by Lee, et al. [2001]. For the subject CST, the tensile capacity of the anchorage for a crack width of 0.3 mm can be estimated as  $200 \text{ kips} \times 15.5 / 57 = 54.4 \text{ kips}$ . The tensile capacity of the anchorage for a crack width of  $w$  mm can be estimated based on the following linear interpolation/extrapolation:

$$T = 200 + \frac{w}{0.3} (54.4 - 200) \text{ kips.} \quad (4-11)$$

In the calculation,  $T$  is set to 0 kips as a lower bound value when Equation 4-11 results in an impractical negative tensile strength. Multiple cracks at one anchor bolt location were not considered in NUREG/CR-5434 and were not assumed in this study as well.

The smaller of the tensile strength of the anchorage determined using Equation 4-11 and the anchor bolt tensile capacity becomes the anchor bolt hold-down capacity.

The impact of the cracked concrete is directly on the bolt hold-down capacity but not the tank shell buckling capacity and the fluid pressure capacity; the overturning moment capacity and the

sliding capacity are affected as a consequence. More details on the implementation can be found in Appendices D and E, which differ only in the crack width model. The crack width model C-1 as provided by KAERI was used in the development of Appendix D, while the newly developed crack width model C-2 was used in Appendix E.

### 4.3.2 Fragility Assessment of CST with Cracked Anchorage Concrete

#### 4.3.2.1 Using C-1 Crack Growth Model

Figure 4-12 shows the mean fragility capacity of the CST with anchorage concrete cracking for a series of years, from 0 up to 80 years. For the same reason as in degradation case A, the effect of the degradation on the uncertainties is not considered. Figure 4-13 and Figure 4-14 shows the HCLPF SME capacity and the median SME capacity, respectively. In a practical sense, it is obvious that all fragility capacities are virtually unchanged for a period of 80 years. The fragility capacity starts to slightly decrease after 60 years and reaches a HCLPF SME capacity of 0.423 g at the end of 80 years, which is almost unchanged from the base case of a 0.426 g HCLPF capacity. Sliding capacity dominates the fragility capacity for the entire period of 80 years. The overturning moment capacity varied similarly to the sliding capacity, while the fluid pressure capacity remained unchanged.

At the end of 80 years, the bolt hold-down capacity reduced to 101.2 kips from 159.4 kips at the base case, representing a 37% reduction. Such a large reduction in the bolt hold-down capacity did not lead to a comparable level of reduction in fragility capacities because of the large number of anchor bolts (78). The detailed results can be found in Appendix D.

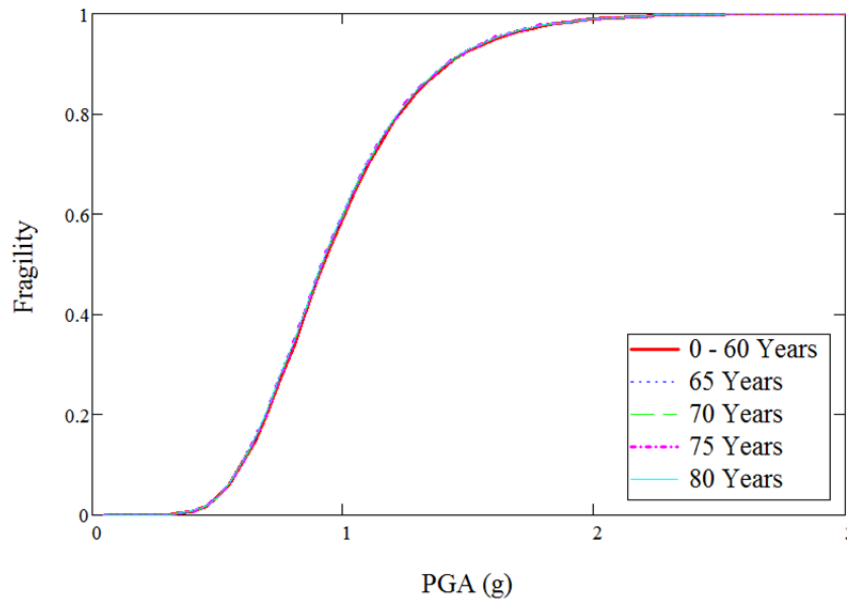


Figure 4-12 Mean Fragility Capacity of the CST with Cracked Anchorage Concrete (C-1)

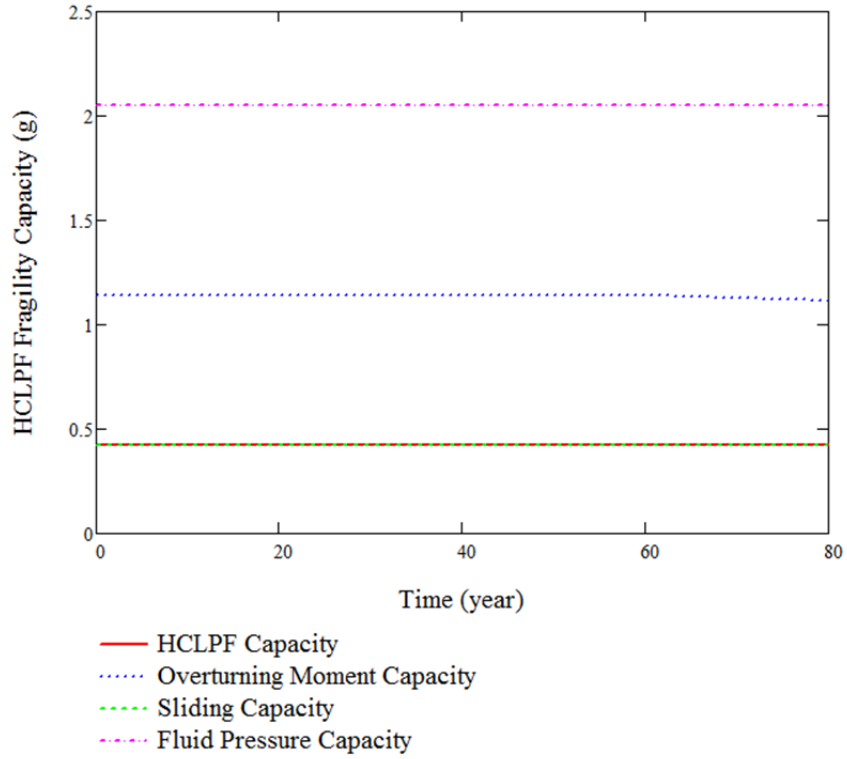


Figure 4-13 HCLPF Capacity of the CST with Cracked Anchorage Concrete (C-1)

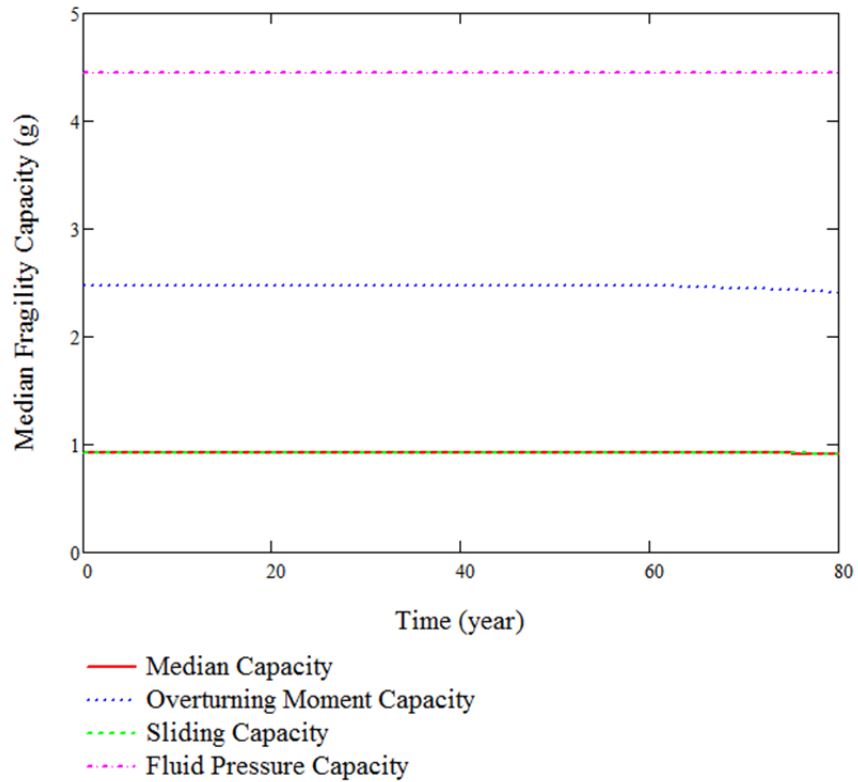


Figure 4-14 Median Capacity of the CST with Cracked Anchorage Concrete (C-1)

#### 4.3.2.2 Using C-2 Crack Growth Model

To investigate the sensitivity of the fragility capacities on the degradation model, the newly developed crack width model C-2 was employed in place of the C-1 model, as shown in Appendix E.

Figure 4-15 shows the mean fragility capacity of the CST with degraded tank shell for a series of years, from 0 up to 80 years. Similarly to the previous cases, these mean fragility curves were calculated using unchanged uncertainties, i.e.,  $\beta_R = 0.2$  and  $\beta_U = 0.27$ , and the effect of the degradation on the uncertainties is not considered. In Figure 4-15, the mean fragility does not change in the first 20 years and in the last 25 years, with an increasing rate of fragility capacity deterioration for the years in the middle. The governing failure changed from the sliding mode to overturning moment mode at 50 years.

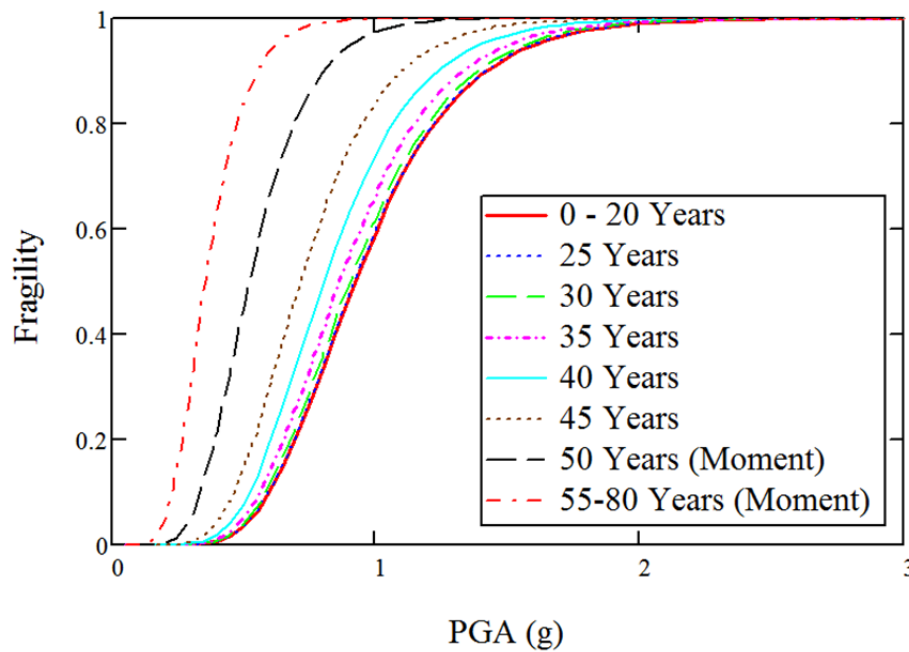


Figure 4-15 Mean Fragility Capacity of the CST with Cracked Anchorage Concrete (C-2)

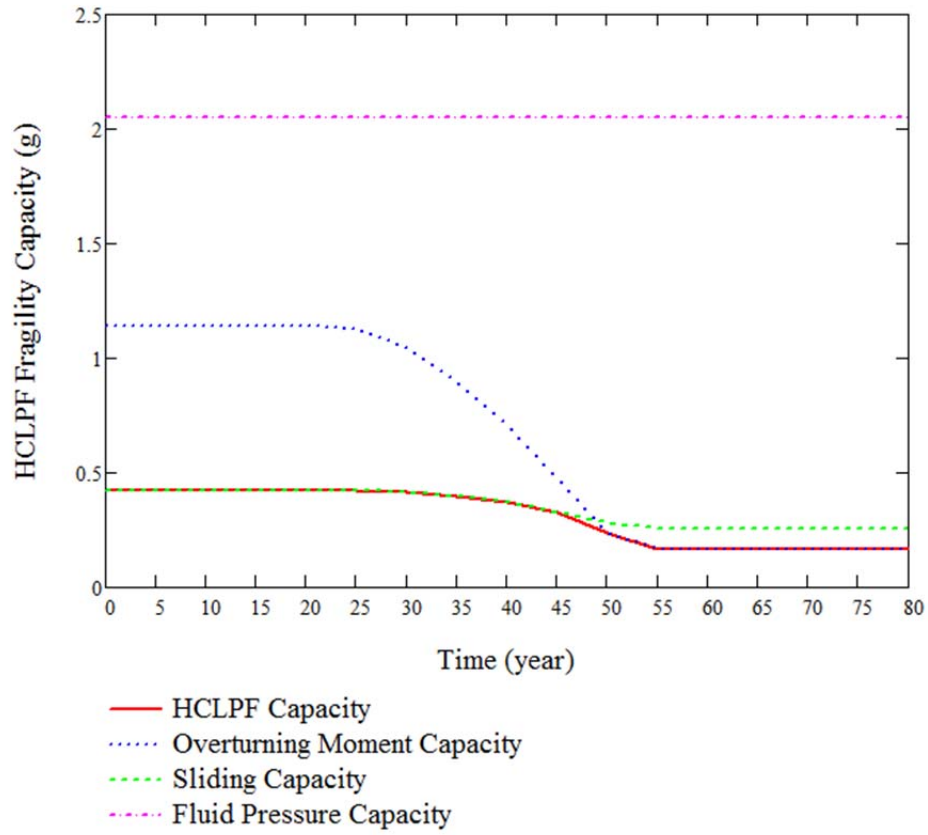


Figure 4-16 HCLPF Capacity of the CST with Cracked Anchorage Concrete (C-2)

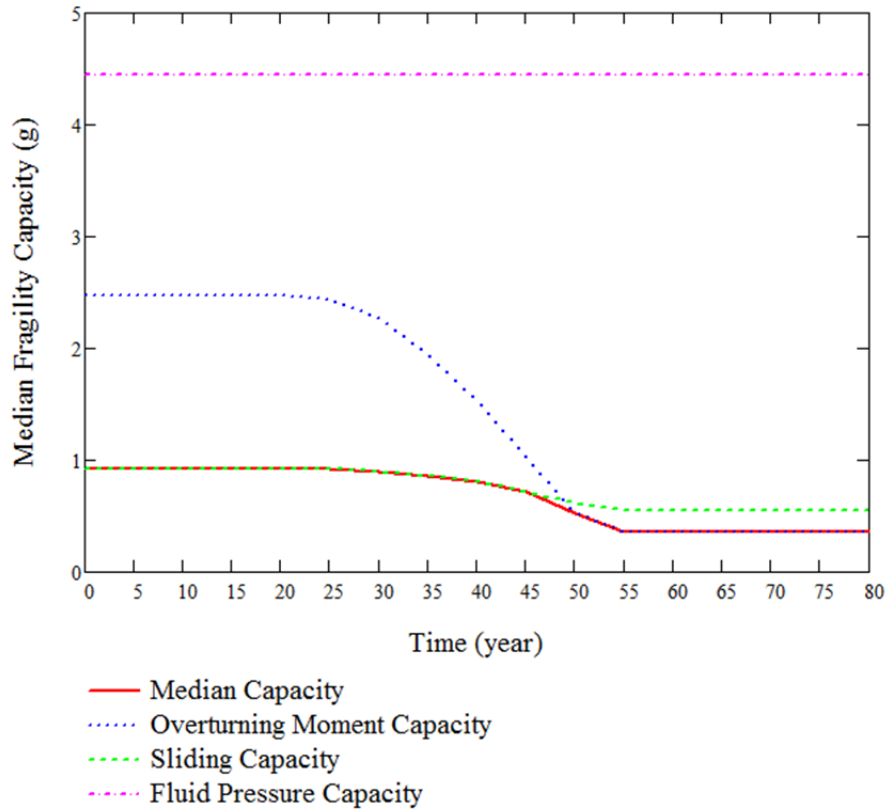


Figure 4-17 Median Capacity of the CST with Cracked Anchorage Concrete (C-2)

The deterioration of fragility capacities as a function of time can be easily observed in the HCLPF fragility and the medina fragility, as shown in Figure 4-16 and Figure 4-17. There are 4 regions in these figures: (1) during 0-20 years, with a maximum crack width of 0.156 mm (about half of the crack width in the test), the fragility capacities were unchanged because of the large number of bolts that have no or moderate reduction in their bolt hold-down capacity; (2) between 20 to about 48 years, the fragility capacities were dominated by the sliding mode; (3) before 55 years, the fragility capacities were dominated by the overturning moment mode and the reduction in the bolt hold-down capacity affect the overturning moment capacity; and (4) after 55 years, the fragility capacities continue to be dominated by the overturning moment capacity, the bolts in tension appeared to have been pulled out, and the CST effectively becomes an unanchored tank. The overturning moment capacity starts to be affected dramatically by the bolt hold-down capacity after 20 years until the bolts reach a zero capacity around 55 years. The bolt hold-down capacity does not have as great an impact on the sliding capacity as on the overturning moment capacity, and it does not have any impact on the fluid pressure capacity as expected.

The fragility capacity is taken as the minimum of these three capacities. It should be noted that the non-governing capacities are higher than the corresponding real fragility capacities, which require separate iterations to be determined.

The slosh height become smaller as the SME becomes smaller due to degradation. The horizontal displacement at the roof level of the auxiliary building becomes larger at the end of years (also some other years prior to 80 years) than the base case due to the pull out of the anchor bolts and the CST becomes unanchored. Even in such a case, the largest horizontal displacement at the

roof level of the auxiliary building was found to be 0.314", about 10% of the 3" gap. This could cause a complication of the failure mode of the CST, and will remain as a recommendation for future study.

From this sensitivity analysis, the crack growth model has a great impact on the fragility capacities of the CST. However, the model C-2 may not be accurate after about 40 years because the crack width becomes greater than 0.3 mm and the crack width estimate after 40 years is extrapolated. On the other hand, the model C-1 has a maximum crack width of 0.204 mm at the end of 80 years, which is still in the tested range. It is important to note that provided the linear inter/extrapolation relation in Equation 4-11 is reasonable, a crack width of 0.429 mm at the end of 55 years, based on the model C-2 prediction, indicates a pull-out failure of the anchor bolts and a 61% reduction in seismic fragility capacity, even with a very dense array of anchor bolts (78). This observation shows the importance of concrete cracking in the CST seismic safety, and certainly leads to a recommendation of regular inspection of the concrete foundation for cracking.

It is cautioned that the above observation is based on a greatly simplified conversion from the NUREG/CR-5434 test results to the large size anchor bolts, in which many uncertain factors were not considered, for example, how the crack depth in conjunction with the crack width affect the bolt hold-down capacity. As discussed in the Year 2 Annual Report, the surface crack may not always be a good indicator of the crack depth.

#### **4.4 Fragility Analysis for Multiple Degrations**

Degradation cases A, B, and C-2 were combined together to investigate the effect of multiple degradations on the seismic fragility capacities. The three degradation cases are assumed to be perfectly correlated, i.e., the severity of each of the degradation cases is a deterministic function of the common time variable. The detailed implementation is presented in Appendix F, which combines the updates in Appendices B, C, and E. Concrete cracking model C-2 was chosen instead of model C-1 in order to obtain more interesting fragility results.

Figure 4-18 shows the median fragility curves for the CST with combined degradations up to 65 years. The fragility curves before the end of 45 years show equal and fine spacing between them, indicating a steady but slow degradation process. Between 45 years and 55 years, a sudden increase of the degradation severity is shown by the large spacing between the corresponding fragility curves. The very small spacing between 55 and 60 years suggest a very small drop in the fragility capacity, followed by a slightly increased drop in fragility capacity. As shown in Figure 4-19, the fragility capacity diminishes at 65 years, after which the fragility calculation in Mathcad could not reach a plausible solution.

The trend of the fragility capacity change can be better characterized by the HCLPF fragility capacity and the median fragility capacity, as shown in Figure 4-19 and Figure 4-20. Before the end of 45 years, the fragility capacity is dominated by the slow deterioration of the sliding capacity. Between 45 years and 55 years, the dominating failure mode switches to the overturning moment mode and the resultant deterioration rate in the fragility becomes higher. Between 55 and 60, the fragility capacity is still dominated by the overturning moment capacity, which levels to a small constant because the CST effectively is an unanchored tank as previously shown in the degradation case C-2. At the end of 65 years, the overturning moment capacity and the fluid pressure capacity are very close, with the latter dominating the fragility capacity. This is the only occasion among all degradation scenarios that the fluid pressure capacity dominates the fragility calculation.

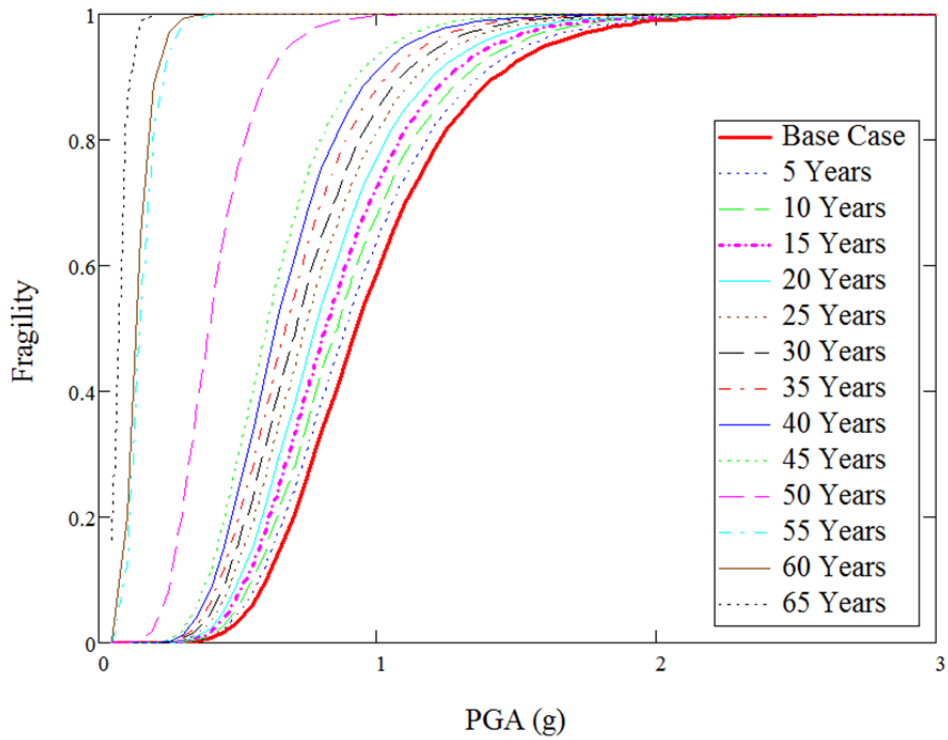


Figure 4-18 Mean Fragility Capacity of the CST with Combined Degrations

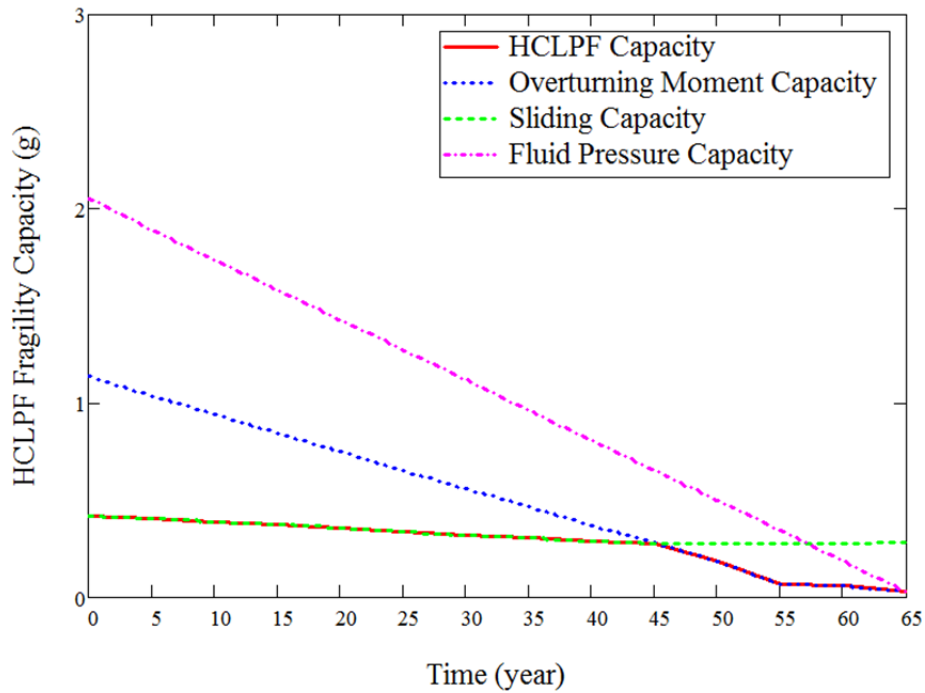


Figure 4-19 HCLPF Capacity of the CST with Combined Degrations

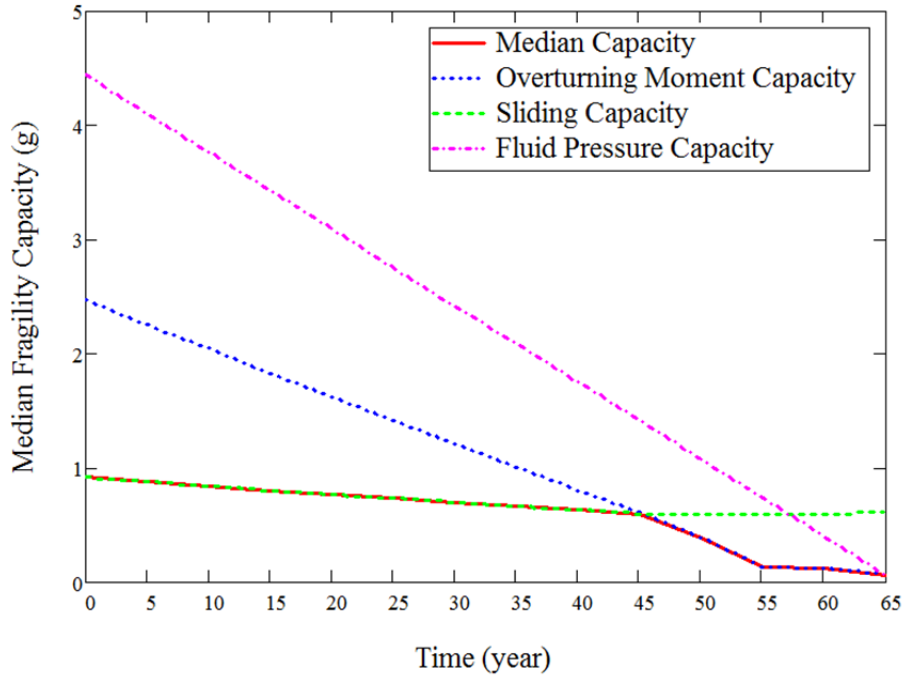


Figure 4-20 Median Capacity of the CST with Combined Degrations

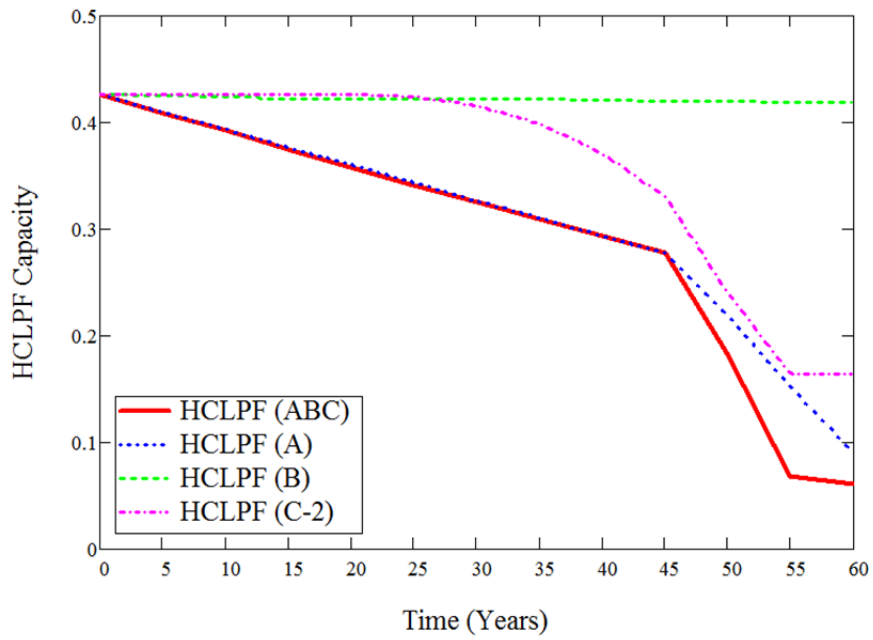


Figure 4-21 Comparison of HCLPF Capacities among All Degradation Scenarios

Figure 4-21 compares the HCLPF capacities among all 4 degradation cases, with the solid line for the combined degradations, the dotted line for the degraded tank shell, the dashed line for the degraded anchor bolt, and the dash-dotted line for the cracked anchorage concrete using model C-2. It is interesting to note that before 45 years, the HCLPF fragility for the combined degradation case is the same as that for the degradation of the tank shell, indicating the degradation of anchor

bolts and the anchorage concrete cracking have no effect on the fragility. After 45 years, it appears all three degradation scenarios contribute to the HCLPF fragility for the combined degradation case. Figure 4-21 also shows that the corrosion model for the anchor bolts, although appearing to be for the severest environment (marine) case, does not incur a significant amount of loss of cross section and the corresponding deterioration in fragility capacity is minimal.

## 5 ADDITIONAL FRAGILITY ANALYSES IN THE YEAR 4 TASK

This section presents the additional seismic analyses of the CST performed in the Year 4 Task. KAERI recently indicated that the range of the operational water level is lower than the design level, which may significantly affect the seismic demand and consequently the seismic fragility capacity. Therefore, the first task was to revisit the relevant Mathcad calculation sheet to reflect the operational water level and assess its impact on the seismic fragility capacity. Based on the revised calculation procedure, a simulation-based method is implemented to characterize relationship between the CST fragility capacity and non-perfectly correlated degradations.

This section describes the major changes to the analytical procedure and results from these analyses. Appendices G through I include the detailed Mathcad calculation sheets.

### 5.1 Fragility Analysis of Undegraded CST Considering the Operational Water Level

The elevation of operational water level in the CST is normally maintained by opening/closing the makeup valve. The normal range of the operational water level is between 131'-5" and 132'-3". An elevation of 132' was agreed to be used as a representative operational water level. The corresponding representative water head is then calculated to be  $132' - 101'-9" = 30'-3"$ . The baseline fragility analysis of undegraded CST, as described in Section 3 and Appendix A, was revised to reflect this change of water level. The updated calculation procedure is shown in Appendix G.

Using the representative operational water level, the water weight is calculated to be 3714.0 kips, equivalent to a 19.2% reduction of the original water weight of 4604.2 kips (using the design water level). The center of gravity for water was accordingly reduced to 15.1 ft from 18.8 ft. The hydro-static pressure profile is updated due to the change of water head as well.

The fundamental frequency of the horizontal impulsive mode was estimated to be 11.3 Hz, about 21.5% higher than 9.3 Hz as determined using the design water level. Based on the RG 1.60 horizontal spectrum shape, this change of fundamental frequency results in smaller spectral accelerations. The H/R (radius) ratio becomes 1.2. Because H/R is less than 1.5, a different set of equations from ASCE 4-98 had to be used for the calculation of the effective impulsive weight and its center of gravity. As a result, the effective impulsive weight and its center of gravity were determined to be 2313 kips and 11.3 ft, respectively. Compared to 3264 kips and 14.0 ft calculated using the design water level, these changes are about 29.1% and 19.3% , respectively.

The fundamental frequency of the horizontal convective (sloshing) mode was calculated to be 0.242 Hz, which is only slightly smaller than the original 0.244 Hz. The effective convective mode weight and its center of gravity were found to be 1380 kips and 19.3 ft, respectively. The change in the effective convective mode weight due to the change of water level is not significant (1402 kips when the design water level was used), but the change in the center of gravity of the convective mode weight is significant (originally 25.5 ft). This observation is expected because the effective convective mode weight is the surface portion of the water. The change of spectral acceleration due to the small frequency change is minimal.

The fundamental frequency of the vertical mode was determined to be 11.8 Hz, which is about 24.0% higher than the original fundamental frequency 9.5 Hz. Based on the RG 1.60 vertical spectrum shape, this change of fundamental frequency results in smaller spectral accelerations.

As the operational water level is lower than the design water level, the CST can reach a higher SME fragility capacity for the operation situation. In the calculation, to achieve this higher level

of SME, the fluid hold-down force becomes effectively 0. This can be seen in the linearization equation for  $T_e$ , as shown in Appendix G. Accordingly, the Mathcad sheet was revised to automatically prevent the artificially negative fluid hold-down force.

The HCLPF capacity was determined to be 0.549 g, representing a 28.9% increase over the original 0.426 g estimated using the design water level. The sliding mode of the CST still dominates. At an SME of 0.549 g, the corresponding overturning moment capacity and the fluid pressure capacity are 2.0 g and 2.8 g, respectively. The influence of the auxiliary building to the two CSTs was found to be negligible; the same observation was made in Section 3 when the design water level was considered.

The median seismic fragility capacity was determined to be 1.2 g, by assuming the overall aleatory and epistemic uncertainties to be 0.2 and 0.27, respectively. The same assumption regarding the uncertainties was made in Section 3. The relative change of the median seismic fragility capacity is about 30%, compared to using the design water level. Figure 5-1 shows the mean fragility curve; and the median, 5% percentile, and 95% percentile fragility curves.

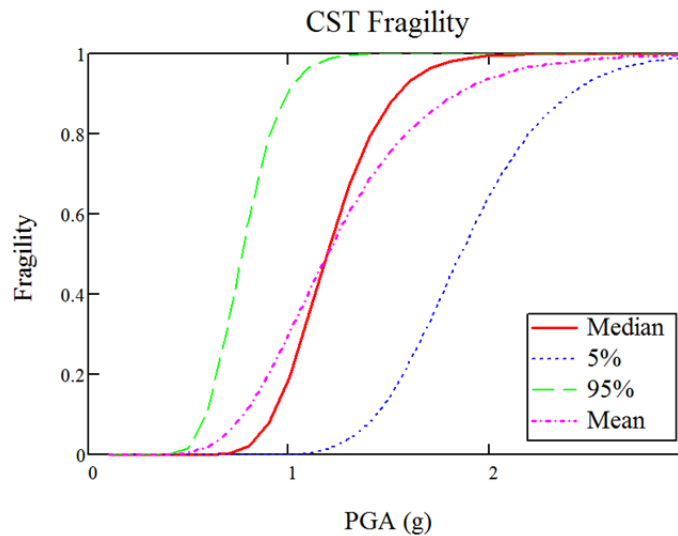


Figure 5-1 Fragility Curves of The CST with the Operational Water Level

## 5.2 Fragility Analysis with Realistic Correlations between the Degradation Cases

One of the analyses in Section 4 was to assess the seismic fragility deterioration behavior of the CST as a function of the three degradations, which were assumed to be perfectly correlated, i.e., the degradation rates were expressed as deterministic functions of time. In reality, large uncertainties exist in the physical degradation phenomena and there is no perfect knowledge in representing them. On the other hand, there is some degree of assurance in the correlations between the three degradation scenarios, namely in the tank shell, in the anchor bolts, and in the foundation concrete. For example, the degradations in the anchor bolts and the reinforce concrete foundation may have a higher correlation because of their similar local environment, degradation interaction, similar metallic behavior, etc. Therefore, these degradations could be better treated stochastically.

For degradation scenarios A, B, and C, let  $A_0(t)$ ,  $B_0(t)$ , and  $C_0(t)$  be the deterministic degradation models that are defined in Section 4, and the corresponding random models  $A(t)$ ,  $B(t)$ , and  $C(t)$  can be expressed as,

$$\begin{aligned} A(t) &= A_0(t) \times a \\ B(t) &= B_0(t) \times b \\ C(t) &= C_0(t) \times c \end{aligned} \tag{5-1}$$

where rate factors  $a$ ,  $b$ , and  $c$  are random variables with unit mean and covariance matrix  $\Sigma$ . These models are relatively simple because they represent the time-dependent degradation models as random variables instead of more realistic but complicated random processes. Should a random process approach be opted, the deterministic models  $A_0(t)$ ,  $B_0(t)$ , and  $C_0(t)$  can be treated as the mean, but time-dependent variance models would need to be defined. In addition, the use of random processes requires separate realization of the degradation rates at each time step to determine the HCLPF capacity and carries no extra benefit for the demonstration. The simple models as shown in Equation 5-1 require much less computation. Once a set of samples are identified for random variables  $a$ ,  $b$ , and  $c$ , a sample degradation case can be defined by Equation 5-1.

### 5.2.1 Development of Sample Degradation Scenarios

Each sample in the simulation requires a separate Mathcad calculation sheet because of the limitation of Mathcad in nesting multiple level loops. In addition, for each sample, the calculation of the SME HCLPF capacity must be repeated manually for a series of years to obtain the deterioration behavior of the seismic fragility as a function of time. To facilitate this involved computation process, an efficient simulation scheme is required to minimize the number of Mathcad sheets. To this end, Latin Hypercube samples (LHS) were selected for this study. LHS have been widely used as alternatives to samples randomly generated by the brute-force Monte Carlo (MC) method for their low variance.

There are a number of algorithms in the literature to generate LHS. Although they have been developed using different optimization goals, all emphasize on distributing the samples with high fidelity to the underlying distribution in the hyper cube and consequently improving the simulation efficiency. The particular algorithm used in this study is the so-called Optimum LHS, which is part of the “lhs” package for the R statistical environment [2010]. This algorithm generates an optimal set of samples with respect to the S-optimality criterion, which seeks to maximize the mean distance from each point to all the other points in the set and effectively to scatter the points as evenly as possible [Socki, 2005].

The generated optimum LHS, uniformly distributed in the Hypercube, need to be transformed to the correlated rate factors  $a$ ,  $b$ , and  $c$ . In this study, the three rate factor random variables are assumed to have lognormal marginal distributions with unit mean and standard deviations 0.2, 0.25, and 0.3, respectively. The correlation coefficients between  $(a,b)$ ,  $(a,c)$ , and  $(b,c)$  are specified as 0.4, 0.4, and 0.7, recognizing that degradations in the anchor bolts and the reinforced concrete foundation have stronger correlation than those involving the stainless steel tank shell. The procedure to transform the optimum LHS into correlated lognormal random vectors is described in detail in NUREG/CR-6922 [Nie, et al, 2007]. The implementation of this procedure in Mathcad is presented in Appendix H.

A total number of 11 samples were generated for the rate factors for this study. It should be noted that there is some level of correlation in the independent samples because the number of samples is finite. For the optimum LHS generated for this study, the correlation coefficients are estimated

to be 0.04, 0.09, and -0.10. As a comparison, the correlation coefficients for the resultant lognormal rate factor samples are 0.36, 0.43, and 0.7, respectively, which are very close to the specified values. The resultant correlated rate factors are listed below in Table 5-1:

Table 5-1 Sample Rate Factors

Sample Id	<i>a</i>	<i>b</i>	<i>c</i>
1	0.892	0.666	0.717
2	0.867	1.127	1.128
3	1.111	1.254	1.525
4	0.956	0.801	0.670
5	1.062	1.847	1.496
6	1.597	1.240	1.192
7	0.728	0.861	0.690
8	0.995	1.120	0.816
9	1.254	0.877	0.992
10	0.779	0.814	0.927
11	1.030	0.894	1.375

### 5.2.2 Simulation-based Seismic Fragility Analyses

For seismic fragility analyses of the CST considering non-perfect correlations between the three degradation scenarios, eleven Mathcad calculation sheets were developed, each of which corresponds to a row in Table 5-1. These Mathcad sheets were derived from Appendix F, and include revisions to utilize the operational water level and apply rate factors to the deterministic degradation models. Each Mathcad calculation sheet is a sample degradation case that is completely defined by the rate factors. Appendix I shows the Mathcad sheet that utilizes the first rate factor set:  $(a, b, c) = (0.892, 0.666, 0.717)$ . Calculation details are not shown in Appendix I for simplicity.

For each sample degradation case, the same manual procedure used in Section 3 is applied here to determine the HCLPF capacity of the CST at every 5 years. The total number of calculations of HCLPF is about 176 times. The results are exported from all Mathcad sheets and aggregated in Excel for post processing. Similar to previous sections, the uncertainties associated with the CDFM method are assumed invariant in time, so that the median fragilities and the HCLPF capacities carry similar information, as shown similarly in Section 4. Therefore, only HCLPF capacities are considered in the following statistical analysis.

Two approaches were implemented for determining the mean curve: (1) averaging HCLPF capacities at every 5 years and (2) averaging years to reach a HCLPF level.

Figure 5-2 shows various time-dependent HCLPF capacity curves: the 11 thin curves represent the 11 analyzed sample degradation cases, the thick dotted curve is the average HCLPF capacity at every 5 years, the thick dashed curve is the average year to reach a HCLPF level, and the thick solid curve represent an additional analysis which assumed a perfect correlation between the degradation scenarios A, B, and C (i.e., rate factors  $a = b = c = 1$ ) and used the operational water level.

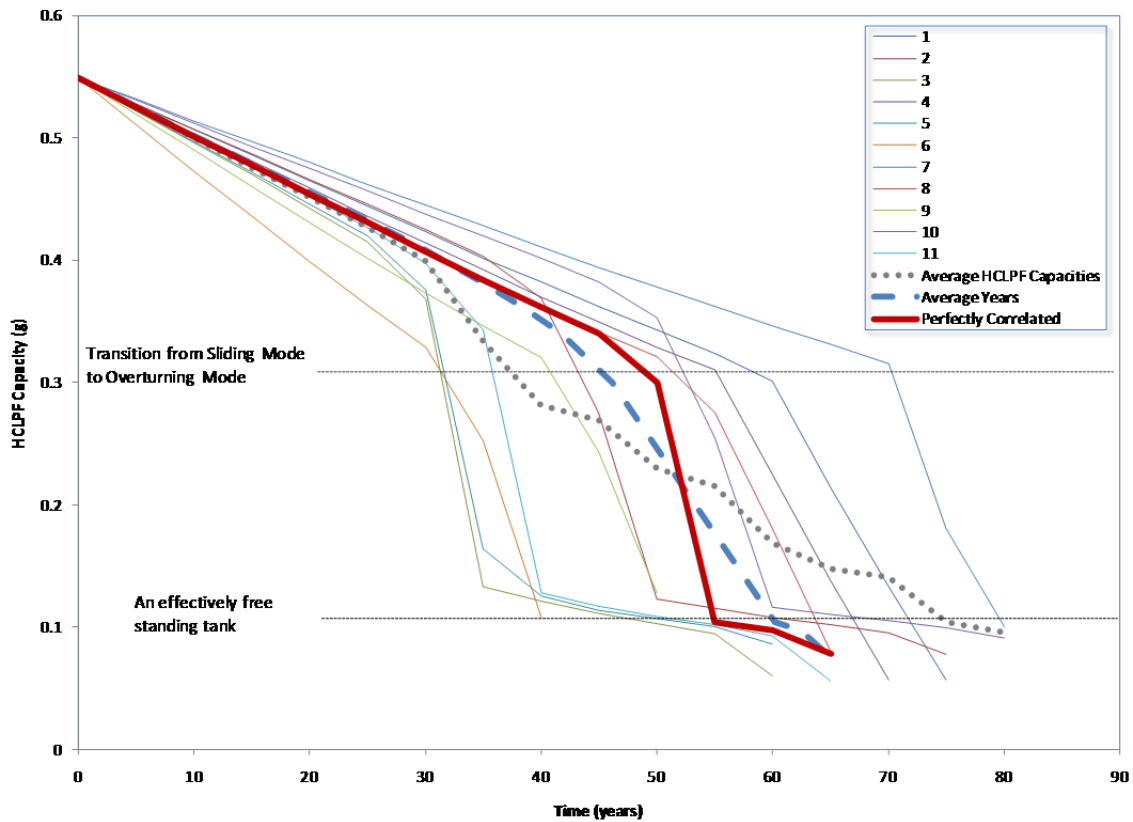


Figure 5-2 Simulated CST HCLPF Capacity vs Time

By examining the 11 simulated curves, it is clear that the deterioration characteristics of the HCLPF actually cannot be appropriately described in terms of time. Rather, there are two apparent sharp bends in the curves as indicated by the two horizontal dotted lines. The first bend occurs at a HCLPF level of about slightly higher than 0.3 g, where the controlling mode changes from the sliding mode to the overturning mode. The second bend occurs at slightly higher than a HCLPF level of 0.1 g, where the CST effectively becomes unanchored. The time for the CST to reach these two HCLPF levels varies significantly among the samples but generally lies in the range of about 30 to 40 years.

Based on Figure 5-2, the average HCLPF capacity can represent well the mean curve up to 30 years but not after 30 years. The apparent reason is that the samples at any time after 30 years can be dominated by either the sliding mode or the overturning mode, and that some even may have failed in producing a meaningful HCLPF capacity at that time. This averaging approach appears to be inappropriate in this case because of the limited number of samples. It is obvious in Figure 5-2 that averaging the years at which a given level of HCLPF capacity is achieved should lead to a much better mean curve (the thick dashed curve). Such an averaging required interpolation among data points because all HCLPF data were not produced at levels of HCLPF capacity, rather at each 5 years.

An additional degradation case was analyzed with all three degradation scenarios perfectly correlated. This analysis resulted in the thick solid curve in Figure 5-2, which matches very well the two averaging curves before 30 years and apparently maintains in the middle of the simulated

curves after that. It even seems to be a better mean curve than the average years curve, partly because the limited number of samples used. Therefore, this perfectly correlated case is considered as the mean curve in the following discussion.

Although determined using the operational water level, the mean curve appears to have a similar trend to that using the design water level, except for higher HCLPF capacities (see Figure 4-19 and Figure 4-21 for a comparison). Specifically, before the end of 45 years, the fragility capacity is dominated by the slow deterioration of the sliding capacity. At about 50 years, the dominating failure mode switches to the overturning moment mode and the HCLPF capacity deteriorates at a much higher rate. Between 55 and 65, the fragility capacity is still dominated by the overturning moment capacity and levels to a very small value because the CST effectively becomes an unanchored tank.

Table 5-2 shows the standard deviation in years to reach a HCLPF value, with respect the mean curve (the perfectly correlated case). Except for the last three data points where not all samples have a feasible HCLPF capacity, the standard deviation monotonically increases. It is worthwhile to note that this increasing standard deviation occurs while the uncertainties and the correlations in the rate factors are constant. In another words, even without considering the rate factor variation in time (through random processes), the uncertainty in years to reach a HCLPF level increases. The coefficient of variation (COV) also generally increases but not as significantly as that of the standard deviation. This effect has not been able to be observed through deterministic degradation analyses such as those described in Section 4. Figure 5-3 illustrates the trend of the standard deviation in years to reach a HCLPF level.

Figure 5-4 shows the trend of the standard deviation in HCLPF at every 5 years. Similar to the standard deviation in years to reach a HCLPF level, the standard deviation in HCLPF also increases in general. The smaller standard deviation close to 80 years is due to fewer samples having a feasible HCLPF value during that period. More importantly, since the mean HCLPF becomes smaller as time proceeds, the COV in HCLPF capacity increases at an even greater rate. For example, the COV is only about 0.05 at 20 years, and increases to 0.31 at 35 years. In contrast, the COV in years to reach a HCLPF level stays in a range of 0.2 to 0.26.

The above observation is also very important in quantifying the overall uncertainties in the seismic fragility of the CST. The additional time-dependent uncertainties should be properly taken into account. For example, at 20 years, the additional uncertainty  $\beta_A$  associated with a HCLPF capacity of 0.452 g (average HCLPF) can be estimated to be 0.05 (COV). Given the initial composite uncertainty  $\beta_C = 0.34$  (using  $\beta_R = 0.2$  and  $\beta_U = 0.27$ ), the composite uncertainty in the fragility barely change. However, at 35 years, the composite uncertainty in the fragility increases to 0.46. As stated previously, the statistics in HCLPF capacity and the confidence in the additional uncertainty can be improved by increasing the number of samples.

Table 5-2 Standard Deviation in Years

Years	Mean HCLPF (g)	Standard Deviation in Years With Respect to the Mean Curve	COV
0	0.549	0.000	
5	0.525	1.048	0.21
10	0.501	2.050	0.20
15	0.478	3.044	0.20
20	0.454	4.071	0.20
25	0.431	5.047	0.20
30	0.407	6.197	0.21
35	0.384	7.401	0.21
40	0.362	8.771	0.22
45	0.340	10.587	0.24
50	0.300	13.081	0.26
55	0.104	12.558	0.23
60	0.097	11.791	0.20
65	0.078	11.986	0.18
70	NA		
75	NA		
80	NA		

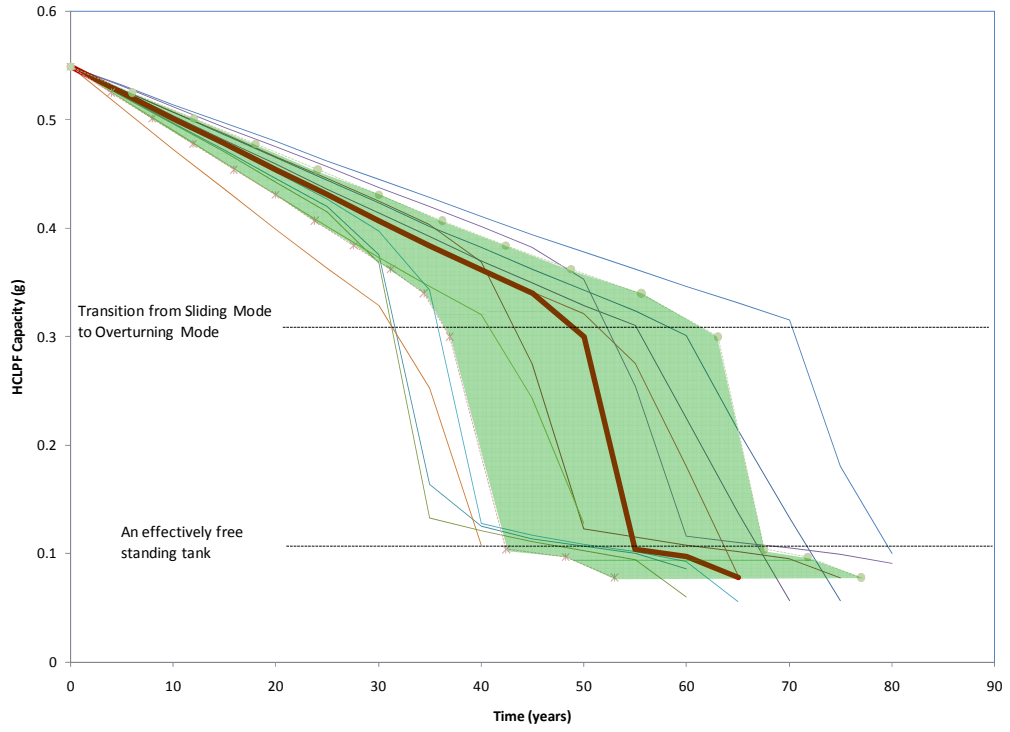


Figure 5-3 Standard Deviation in Years to Reach a HCLPF Level

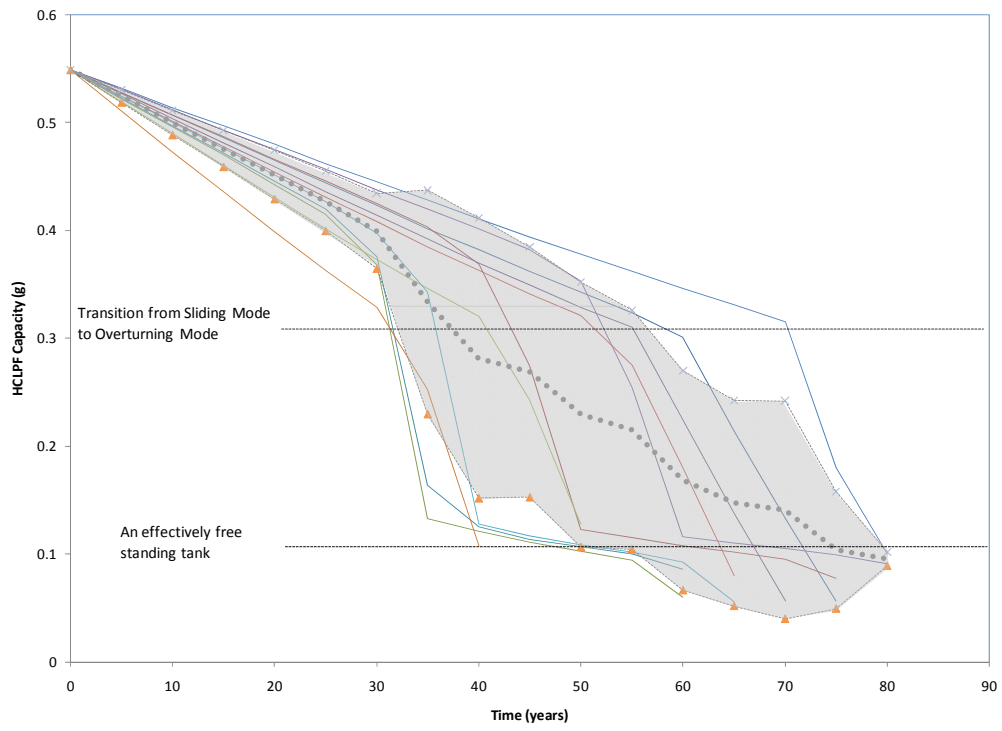


Figure 5-4 Standard Deviation in HCLPF

## 6 CONCLUSIONS AND RECOMMENDATIONS

This report presents a summary of BNL's seismic fragility analysis of a condensate storage tank (CST) considering various degradations. This is a major part of the five year BNL-KAERI collaboration program to support KAERI in its development of seismic capability evaluation technology for degraded structures and components in nuclear power plants (NPPs). The objective of the Year 3 and 4 research is for BNL to develop the seismic fragility capacity for a CST with various degradation scenarios. The conservative deterministic failure margin (CDFM) method was utilized for the undegraded case (base case) and was modified to accommodate the degraded cases. A total of eight seismic fragility analysis cases have been described for the Year 3 research and part of the Year 4 research. The study in Year 3 utilized the design water level and included five cases: (1) the base case, (2) degraded stainless tank shell, (3) degraded anchor bolts, (4) anchorage concrete cracking, and (5) a perfect correlation of the three degradation scenarios. The fragility analysis of the CST for anchorage concrete cracking involved a sensitivity study of the impact of the degradation model on the fragility capacity. The study in Year 4 utilized a representative operational water level and included three cases: (i) an undegraded case, (ii) a case with perfectly correlated degradations, and (iii) a case with non-perfectly correlated degradations. The last case required a simulation-based approach that utilizes 11 optimum Latin Hypercube samples.

A general discussion of the fragility analysis methods and the time-dependent fragility analysis methods to incorporate degradations was provided before a detailed description of the five fragility analyses. The goal of this discussion is to provide an overview of test-based, closed-form solution, and simulation based fragility analysis methods that can be used to develop the seismic fragilities of structures and passive components (SPCs). This discussion also laid out approaches to the theoretical time-dependent fragility analysis. The discussed methods and approaches can be used for fragility analysis of other SPCs in addition to the CST in this study, and in particular are intended to become a framework for the Year 4 task in which KAERI staff will perform fragility analyses of other SPCs.

### 6.1 The Year 3 Cases

In the base case fragility analysis of the CST, the CDFM method was implemented in the Mathcad software to obtain the high confidence low probability of failure (HCLPF) fragility capacity. Important aspects of the implementation were summarized to assist the readers to understand the methodology, which is included as Appendix A of this report. The utilization of Mathcad saved considerable time that would be used in developing spreadsheet or in-house code, because the clear presentation of equations avoided much unnecessary debugging time. The HCLPF capacity of the CST was estimated to be 0.426 g, which is governed by the sliding capacity. The estimated HCLPF capacity is conditioned on the RG 1.60 response spectra anchored to 0.426 g. This HCLPF capacity estimate is very close to the value reported by Choun, et al [2008], which is 0.41 g and also sliding capacity governs. This good agreement validates the accuracy of the calculation procedure implemented in Mathcad and provides confidence in the results of the fragility analysis of degraded CST.

A direct assessment of the epistemic and aleatory uncertainties was not performed because of the subjective nature of the uncertainty estimates. Instead, the aleatory uncertainty  $\beta_R$  and the epistemic uncertainty  $\beta_U$  for the median capacity were identified as 0.20 and 0.27, respectively, as reported in Appendix A of NUREG/CR-5270. These uncertainty values are almost identical to those reported by Choun, et al [2008], where the only difference is that the aleatory uncertainty was 0.21. The composite uncertainty  $\beta_C$  can be calculated as 0.34. Based on the HCLPF capacity and the uncertainties, the median fragility capacity can be estimated to be 0.923 g.

The influence of the auxiliary building in between the two CSTs on the HCLPF capacity was also assessed in the study. A simplified check was performed by calculating the rotation angle at the tank base and the maximum horizontal displacement at the roof level. The maximum horizontal displacement at the roof level was estimated to be 0.008" (0.2 mm), which is only about 0.3% of the 3" gap between the CST and the roof of the auxiliary building. Based on this result, it is judged that influence of the auxiliary building on the SME capacity of the CST is minimal. This check has also been performed during the fragility analyses considering various degradation scenarios and no major impact on the HCLPF capacity of the degraded CST was determined.

A series of time-dependent fragility analyses of the CST were performed by incorporating selected aging-related material degradation models into the fragility analysis. For the degradation scenarios involving the degraded stainless tank shell or degraded anchor bolts, degradation models from the Year 2 report were selected for demonstration purposes. For the degradation scenario of cracked anchorage concrete, a hybrid degradation model was developed based on available anchorage test results for cracked concrete and KAERI's recent regression model/data that utilized measurements from Korean NPPs. It is noted that the recorded degradation data were very valuable because such data are not commonly available, as also identified during the Year 2 research. The fourth degradation scenario combines all three degradation scenarios with a perfect correlation among them.

For fragility analysis of the CST with degraded tank shell, the mechanochemical model was selected from the Year 2 Annual report and the parameters were chosen to best match the CST environment. This model resulted in a constant crack growth rate of 0.0075 in/year. Using this material degradation model, the time-dependent fragility analysis of the CST was performed up to 60 years, after which the fragility calculation was not mathematically achievable. At the end of 60 years, the HCLPF capacity drops from 0.426 g to 0.091g, based on the assumed mechanochemical degradation model. The governing failure mode was the sliding mode until 45 years, and then switches to the overturning moment mode. The tank shell degradation (wall thinning) has the most significant impact on the fluid pressure capacity and the least impact on sliding capacity. The fragility capacity (either HCLPF capacity or the median capacity) is clearly dominated by the sliding mode until slightly after 45 years, and then by the overturning mode. Although the fluid pressure mode does not dominate the fragility capacity up to 60 years, it would be dominant shortly after that if the calculation was continued.

For fragility analysis of the CST with degraded anchor bolts, the power model was selected from the Year 2 Annual report. Since the Ulchin NPP, where the subject CST is installed, is located on the coast, a marine environment was assumed in the fragility analysis of the CST for the worst case scenario. Using this power model, the time-dependent fragility analysis of the CST was performed up to 80 years. In a practical sense, the HCLPF fragility is virtually unchanged for a period of 80 years. Sliding capacity dominates the HCLPF capacity for the same period. Even with a degradation level of half of the bolt diameter (approximate 950 years using the power model), the HCLPF capacity was found to be still as high as 0.34 g, compared to 0.426 g for the base case. This high level of HCLPF capacity is believed to be attributed to (1) the large number of bolts (78 in total) and (2) the power model did not lead to a very fast degradation rate even when the worst environment for the model was chosen.

For fragility analysis of the CST with cracked anchorage concrete, a linear rate crack width growth model as provided by KAERI was used. Based on this model, the HCLPF fragility was found to be virtually unchanged for a period of 80 years, with an HCLPF capacity of 0.423 g at the end of 80 years. Sliding capacity dominates the fragility capacity for the entire period of 80

years. In a sensitivity analysis, a different linear rate crack width growth model was also developed based on recorded data in Korean NPPs, which are the same data the KAERI linear model was based on. A very interesting trace of the HCLPF capacity, where the failure mode associated with the fragility capacity changes over time, was determined based on this model: (1) during 0-20 years, with a maximum crack width of 0.156 mm (about half of the crack width specified in the anchor bolt test reported in NUREG/CR-5434), the fragility capacities were unchanged because of the large number of bolts that have no or moderate reduction in their bolt hold-down capacity; (2) between 20 to about 48 years, the fragility capacities were dominated by the sliding mode; (3) before 55 years, the fragility capacities were dominated by the overturning moment mode and the reduction in the bolt hold-down capacity affects the overturning moment capacity; and (4) after 55 years, the fragility capacities continue to be dominated by the overturning moment capacity, the bolts in tension appeared to have been pulled out, and the CST effectively becomes an unanchored tank. The overturning moment capacity starts to be affected dramatically by the bolt hold-down capacity after 20 years until the bolts reach a zero capacity around 55 years. The bolt hold-down capacity does not have as great an impact on the sliding capacity as on the overturning moment capacity, and it does not have any impact on the fluid pressure capacity as expected.

This sensitivity analysis showed that the crack growth model had a great impact on the fragility capacities of the CST. However, the crack growth model in the sensitivity analysis may not be accurate after about 40 years because the crack width estimate after 40 years is extrapolated beyond the test data reported in NUREG/CR-5434. Provided this crack growth model is reasonable, a crack width of 0.429 mm at the end of 55 years corresponds to a pull-out failure of the anchor bolts and a 61% reduction in seismic HCLPF capacity for this CST with a very dense array of anchor bolts (78). This observation shows the importance of concrete cracking in the CST seismic fragility, and certainly leads to a recommendation of regular inspection of the concrete foundation for cracking. It is cautioned that the above observation is based on a greatly simplified conversion from the test results of the tensile strength of anchor bolts of very small size to the large size anchor bolts. It is also emphasized that many uncertain factors were not considered, for example, how the crack depth in conjunction with the crack width affect the bolt hold-down capacity. As discussed in the Year 2 Annual Report, the surface crack may not always be a good indicator of the crack depth.

For fragility analysis of the CST with perfectly correlated degradation cases, the concrete cracking model that was used in the sensitivity analysis was used. Before the end of 45 years, the fragility capacity is dominated by the slow deterioration of the sliding capacity. Between 45 years and 55 years, the dominating failure mode switches to the overturning moment mode and the resultant deterioration rate in the fragility becomes higher. Between 55 and 60, the fragility capacity is still dominated by the overturning moment capacity but levels to a small value, and the CST is believed to have effectively become an unanchored tank. At the end of 65 years, the overturning moment capacity and the fluid pressure capacity are very close, with the latter dominating the fragility capacity. This is the only occasion among all degradation scenarios that the fluid pressure capacity dominates the fragility calculation.

The HCLPF capacities were compared among all 4 degradation cases. It is interesting to note that before 45 years, the HCLPF fragility for the combined degradation case is the same as that for the degradation of the tank shell, indicating that the degradation of anchor bolts and the anchorage concrete cracking have no effect on the fragility. After 45 years, it appears all three degradation scenarios contribute to the HCLPF fragility in the combined degradation case.

## 6.2 The Year 4 Cases

An additional seismic fragility analysis of the undegraded CST was carried out to take into account the operational water level. The elevation of operational water level in the CST is normally maintained by opening/closing the makeup valve. A representative water head was identified as 30'-3" based on the normal water range. The calculation procedure for the base case in the Year 3 research was revised to reflect this change of water level. The representative water level is 19.2% lower than the design water level.

As a result of this revision, the fundamental frequencies of the horizontal impulsive mode and the vertical mode increased about 21.5% and 24%, respectively, while the fundamental frequency of the horizontal convective (sloshing) mode decreased slightly. The lower water level results in lower seismic responses and consequently higher HCLPF capacity. The HCLPF capacity corresponding to the representative operational water level was estimated to be 0.549 g, which is 28.9% higher than the original 0.426 g determined using the design water level. The sliding mode of the CST still governed. The influence of the auxiliary building to the two CSTs was found to be negligible. The median seismic fragility capacity was determined to be 1.2 g, by assuming the overall aleatory and epistemic uncertainties to be 0.2 and 0.27, respectively. The relative change of the median seismic fragility capacity is about 30%, compared to using the design water level.

A case with all three degradation scenarios perfectly correlated was analyzed using the representative operational water level. The Mathcad calculation sheet was derived based on the CDFM procedure described in Appendix F. The purpose of this analysis was to obtain a better mean curve for the simulation-based assessment of the non-perfectly correlated case (to be summarized later). The resultant HCLPF-time relation appeared to have a similar trend to that using the design water level, except for higher HCLPF capacities. Specifically, before the end of 45 years, the fragility capacity is dominated by the slow deterioration of the sliding capacity. At about 50 years, the dominating failure mode switches to the overturning moment mode and the HCLPF capacity deteriorates at a much higher rate. Between 55 and 65, the fragility capacity is still dominated by the overturning moment capacity and levels to a very small value because the CST effectively becomes an unanchored tank.

Non-perfect correlations between the three basic degradation scenarios, namely in the tank shell, in the anchor bolts, and in the foundation concrete, are introduced by three time-invariant random rate factors. The rate factors have unit mean and a specified covariance matrix  $\Sigma$  so that the perfectly correlated case is close to the true mean case. This approach was chosen for its simplicity in achieving the goal of demonstration.

A total of 11 samples were used for the characterization of the deterioration behavior of the HCLPF capacity as the degradations proceed over time. Each sample in the simulation corresponds to a separate Mathcad calculation sheet. To facilitate the repetitive and involved calculation, a set of optimum Latin Hypercube samples (LHS) were identified through the "lhs" package for the R statistical environment [2010]. The generated optimum LHS were uniformly and independently distributed and were transformed to the correlated rate factor samples. The three rate factor random variables were assumed to have lognormal marginal distributions with unit mean and standard deviations 0.2, 0.25, and 0.3, respectively. The correlation coefficients between  $(a,b)$ ,  $(a,c)$ , and  $(b,c)$  were specified as 0.4, 0.4, and 0.7, recognizing that degradations in the anchor bolts and the reinforced concrete foundation have stronger correlation than those involving the stainless steel tank shell.

Based on the simulation results, there are apparently two HCLPF levels of importance. The first is slightly higher than 0.3 g, where the controlling mode changes from the sliding mode to the overturning mode. The second is slightly higher than 0.1 g, where the CST effectively becomes unanchored. The time for the CST to reach these two HCLPF levels varies significantly among the samples but generally lies in the range of about 30 to 40 years.

Two approaches were implemented for determining the mean curve: (1) averaging HCLPF capacities at every 5 years and (2) averaging years to reach a HCLPF level. The average HCLPF capacity can represent well the mean curve up to 30 years but not after 30 years, partly because the number of samples is relatively small. Averaging the years to reach a HCLPF level led to a better mean curve, which is closer to the perfectly correlated case.

The standard deviation in years to reach a HCLPF value generally increases as time proceeds. It is worthwhile to note that this increasing standard deviation occurs while the uncertainties and the correlations in the rate factors are constant. The coefficient of variation (COV) generally increases but not as significantly as that of the standard deviation. The standard deviation in HCLPF also generally increases. More importantly, since the mean HCLPF becomes smaller at a later time, the COV in HCLPF capacity increases at a greater rate. For example, the COV is only about 0.05 at 20 years, and increases to 0.31 at 35 years. In contrast, the COV in years to reach a HCLPF level stays in a range of 0.2 to 0.26.

The overall uncertainties in the seismic fragility of the CST should properly take into account the additional time-dependent uncertainty as observed above. For example, at 20 years, the additional uncertainty  $\beta_A$  associated with a HCLPF capacity does not significantly change the composite uncertainty in the fragility. However, at 35 years, the composite uncertainty in the fragility increases from 0.34 to 0.46.

### **6.3 Additional Remarks**

It should be noted that the impact of degradation on the uncertainties was not directly treated in this study because reliable uncertainty data about the degradation models were not available. However, it should be pointed out that there is no technical difficulty to incorporate updated uncertainties into the time-dependent fragility analysis.

The analyses in this report were based on assumed degradation types and rates and are presented to demonstrate the process of characterizing the deterioration of fragility capacity as a function of age-dependent degradations. These analyses do not take into account the inspection/maintenance programs that are normally established in nuclear power plants. However, the results of these analyses can be utilized for the planning of inspection/maintenance.

It is recognized in this study that the most critical factor for a high quality time-dependent fragility analysis is the identification of accurate and reliable material degradation models. Recorded degradation data in NPPs are not available in a consistent and coherent fashion for use in development of degradation models, but extremely important for performing fragility analysis. Long term measurement/monitoring of the performance of safety significant SPCs remains a high priority to improve future research activities and assist in making operational decisions. As more recorded degradation data in NPPs are obtained in the future, the existing material degradation models and fragility analyses can be updated to improve their accuracy and thereby ensure the continued safe operation of NPPs.



## 7 REFERENCES

AISC (1989). *Manual of Steel Construction - Allowable Stress Design*, 9<sup>th</sup> Edition, American Institute of Steel Construction, Chicago, IL.

Albrecht, P. and Naeemi, A.H. (1984). *Performance of Weathering Steel in Bridges*, Report 272, Nat. Cooperative Highway Res. Program.

ASCE 4-98 (2000). *Seismic Analysis Of Safety-Related Nuclear Structures And Commentary*, American Society of Civil Engineers, Reston, VA.

Bandyopadhyay, K., A. Cornell, C. Costantino, R.P. Kennedy, C. Miller, and A. Veletsos (1995). *Seismic Design and Evaluation Guidelines for the Department of Energy High-Level Waste Storage Tanks and appurtenances*, BNL 52361, Brookhaven National Laboratory, Upton, NY.

Braverman, J.I., G. DeGrassi, G. Martinez-Guridi, R.J. Morante, and C.H. Hofmayer (2005). *Risk-Informed Assessment of Degraded Buried Piping Systems in Nuclear Power Plants*, NUREG/CR-6876, U.S. Nuclear Regulatory Commission, Washington, D.C.

Choun, Y.S., I.K. Choi, and J.M. Seo (2008). "Improvement of the seismic safety of existing nuclear power plants by an increase of the component seismic capacity: a case study," *Nuclear Engineering and Design*, **238**, 1410-1420.

Ellingwood, B.R. (1994). *Validation of Seismic Probabilistic Risk Assessments of Nuclear Power Plants*, NUREG/GR-0008, U.S. Nuclear Regulatory Commission, Washington, D.C.

Ellingwood, B.R. and J. Song (1996). *Impact of Structural Aging on Seismic Risk Assessment of Reinforced Concrete Structures in Nuclear Power Plants*, NUREG/CR-6425, U.S. Nuclear Regulatory Commission, Washington, D.C.

Kaplan, S., V.M. Bier, and D.C. Bley (1989). "A note on families of fragility curves – is the composite curve equivalent to the mean curve?" Transactions, *10<sup>th</sup> International Conference on Structural Mechanics in Reactor Technology*, Vol. **P**, 163-168.

Kennedy, R.P. and M.K. Ravindra (1984). "Seismic fragilities for nuclear power plant risk studies," *Nuclear Engineering and Design*, **79**, 47-68.

Kennedy, R.P., C.A. Cornell, R.D. Campbell, S. Kaplan and H.F. Perla (1984). "Probabilistic seismic safety study of an existing nuclear power plant," *Nuclear Engineering and Design*, **59**, 315-338.

Kennedy, R.P., R.C. Murray, M.K. Ravindra, J.W. Reed, and J.D. Stevenson (1989). *Assessment of seismic margin calculation methods and Supplement 1*, NUREG/CR-5270, U.S. Nuclear Regulatory Commission, Washington, D.C.

Klingner, R.E., J.M. Hallowell, D. Lotze, H.G. Park, M. Rodriguez, and Y.G. Zhang (1998). *Anchor Bolt Behavior and Strength During Earthquakes*, NUREG/CR-5434, U.S. Nuclear Regulatory Commission, Washington, D.C.

Lee, N.H., I.H. Moon, and I.S. Ju (2001). "Failure mechanism for large-sized grouted anchor bolt under tensile load," *16th International Conference on Structural Mechanics in Reactor Technology*, SMiRT-16, Washington, D.C.

Mathcad 14.0 User's Manual (2007).

Mori, Y. (2005). "Reliability-based service life prediction and durability in structural safety assessment." Chapter 7, *Structural Safety and Its Quality Assurance*, Editors: B.R. Ellingwood and J. Kanda, ASCE.

NASA SP-8007 (1968). "Buckling of thin-walled circular cylinders," *NASA Space Vehicle Design Criteria*, National Aeronautics and Space Administration, Washington, D.C.

Naus, D.J., C.B. Oland, and E.G. Arndt (1991). "Ageing management of safety-related concrete structures to provide improved bases for continuing the service of nuclear power plants," *Materials and Structures*, **24**, 308-316.

Naus, D.J., C.B. Oland, and B.R. Ellingwood (1996). *Report on Aging of Nuclear Power Plant Reinforced Concrete Structures*, NUREG/CR-6424, U.S. Nuclear Regulatory Commission, Washington, D.C.

Newmark, N.M. and W.J. Hall (1978). *Development of Criteria for Seismic Review of Selected Nuclear Power Plants*, NUREG/CR-0098, U.S. Nuclear Regulatory Commission, Washington, D.C.

Nie, J., J. Xu, and C. Costantino (2007). *P-CARES: Probabilistic Computer Analysis for Rapid Evaluation of Structures*, NUREG/CR-6922, U.S. Nuclear Regulatory Commission, Washington, D.C.

Nie, J., J.I. Braverman, C.H. Hofmayer, M.K. Kim, and I.K. Choi (2009). *Identification and Assessment of Age-Related Degradation of Structures and Passive Components in Nuclear Power Plants*, Annual Report for Year 2 Task. BNL Report-82249-2009, Brookhaven National Laboratory; KAERI/TR-3757/2009, Korea Atomic Energy Research Institute.

Nie, J., J.I. Braverman, C.H. Hofmayer, Y.S. Choun, M.K. Kim, and I.K. Choi (2008). *Identification and Assessment of Recent Aging-Related Degradation Occurrences in U.S. Nuclear Power Plants*, Annual Report for Year 1 Task. BNL Report-81741-2008, Brookhaven National Laboratory; KAERI/RR-2931/2008, Korea Atomic Energy Research Institute.

Oland, C.B., D.J. Naus, and S. Jerath (1993). "A data base for aging of structural materials," *12th International Conference on Structural Mechanics in Reactor Technology*, SMiRT-12, Stuttgart, Germany.

R Version 2.12.0: A Language and Environment for Statistical Computing, 2010.

Reed, J.W., R.P. Kennedy, D.R. Buttemer, I.M. Idriss, D.P. Moore, T.Barr, K.D. Wooten, and J.E. Simith (1991). "A methodology for assessment of nuclear power plant seismic margin," EPRI NP-6041-SL, Revision 1, *Department of Energy Workshop on Walkthrough Field Guide and SQUG/EPRI Seismic Evaluation Material*, Vol 7.

Regulatory Guide 1.60 (1973). *Design Response Spectra for Seismic Design of Nuclear Power Plants*, Revision 1, U.S. Nuclear Regulatory Commission, Washington, D.C.

Saito, K. and J. Kuniya (2001). "Mechanochemical model to predict stress corrosion crack growth of stainless steel in high temperature water." *Corrosion Science*, **43**, 1751-1766.

SRM/SECY 93-087 (1993). *Staff Requirement Memorandum, Subject: SECY-93-087 - Policy, Technical, and Licensing Issues Pertaining to Evolutionary and Advanced Light-Water Reactor (ALWR) Designs*, U.S. Nuclear Regulatory Commission, Washington, D.C.

Stocki, R. (2005). "A method to improve design reliability using optimal Latin hyper-cube sampling," *Computer Assisted Mechanics and Engineering Sciences*, **12**(4), 393-412.

Tada, H., P.C. Paris, and G.R. Irwin (2000). *The Stress Analysis of Cracks Handbook*, 3<sup>rd</sup> edition, American Society of Mechanical Engineers.

Veletos, A.S. (1984). "Seismic response and design of liquid storage tanks," Chapter 7, *Guidelines for the Seismic Design of Oil and Gas Pipeline Systems*, American Society of Civil Engineers, Reston, VA.



**Appendix A FRAGILITY ANALYSIS OF UNDEGRADED CONDENSATE STORAGE  
TANK**



# KAERI Year 3 Task Fragility Analysis of Condensate Storage Tank

## - baseline analysis without considering degradation

Using Conservative Deterministic Failure Margin (CDFM) method to estimate the High Confidence Low Probability of Failure (HCLPF) seismic capacity, which is then used to generate fragility curves by combining randomness and uncertainty parameters.

The CDFM method described in this and the later appendices utilizes to a large extent the approach presented in NUREG/CR-5270 [Kennedy, et al., 1989] and is supplemented by additional sources as referenced herein.

Design information of the CST and related input data were based on the drawing KEPC Ulchin NPP Unit 3 & 4, Drawing No. M262-DG-A03-01, Rev. 6 and KAERI Email Communication to BNL, 09/29/2009, Document No. 9-251-C118-002, which were provided by KAERI for use in this study.

## H.1 Introduction

KAERI indicated that the seismic DBE in Korea follows the NRC Reg. Guide 1.60 design spectrum shape but with a PGA level scaled down to 0.2 g. Assuming an initial HCLPF capacity as 1.67 times of 0.2 g:

$$SME_e := 1.67 \times 0.2g = 0.334 \cdot g$$

The Mathcad sheets in this appendix solve the various equations iteratively by manually setting  $SME_e$  to different values and the following  $SME_e$  value of 0.426 g represents the converged solution.

$$SME_e := 0.426g$$



Horizontal PGA ( $SME_e$ ):  $A_H := SME_e = 0.426 \cdot g$

Definitions of some useful units:

$$kips \equiv 1000lb_f$$

$$ksi \equiv 1000psi$$

$$GPa \equiv 10^9 Pa$$

$$MPa \equiv 10^6 Pa$$

$$tonf \equiv 2000 lbf$$

$$tonnef = 1 \times 10^3 \cdot kgf$$



## H.2 Response Evaluation



The weight  $W$  and the center of gravity  $X$  (measured as the height above tank base) of various components are calculated as follows:

**Head:** using a conservative uniform thickness of 5/8" to compensate for other attachments. The head configuration is simplified as a spherical cap plus a short cylinder. The spherical cap with a radius  $a = (25' + 5/16")$  and a height  $h = (8.7') \cdot 13mm/16mm = 7.07'$  (estimated from drawing). The short cylinder has a radius of  $(25' + 5/16")$  and a height of 1.63'. The short cylinder is to be combined with the tank shell in this calculation. The total height of the head above the top of fluid level is 8.7'.

Spherical segment of head (following CRD Standard Mathematical Tables, 20 ed., 1972, page 17):

$$a := 25 \cdot ft + \frac{5}{16} \cdot in = 25.026 \cdot ft$$

$$h := 7.07 \cdot ft = 7.07 \cdot ft$$

$$p := \sqrt{a^2 + h^2} = 26.006 \cdot ft$$

$R$  is defined here as the radius of the sphere for the head (to be redefined later as the radius of the tank):

$$R := \frac{p^2}{2 \cdot h} = 47.828 \cdot ft$$

$$t_H := \frac{5}{8} \cdot in = 0.625 \cdot in$$

$$\gamma_{steel} := 0.285 \frac{lbf}{in^3} = 492.48 \cdot \frac{lbf}{ft^3}$$

$$W_H := \pi \cdot p^2 \cdot t_H \cdot \gamma_{steel} = 54.497 \cdot kips$$

$$W_H = 242.413 \cdot kN$$

$$H_S := (37 \cdot ft + 6 \cdot in) + 1.63 \cdot ft = 39.13 \cdot ft$$

$$X_H := \frac{h}{2} + H_S = 42.665 \cdot ft$$

$$X_H = 13.004 \cdot m$$

**Shell** - include the approximated short cylinder (with a height of 0.82ft) from the head.

$$t_S := \frac{5}{8} \cdot in = 0.625 \cdot in$$

$$W_S := (2\pi \cdot a \cdot t_S) H_S \cdot \gamma_{steel} = 157.823 \cdot kips$$

$$W_S = 702.03 \cdot kN$$

$$X_S := H_S \div 2 = 19.565 \cdot ft$$

$$X_S = 5.963 \cdot m$$

**Bottom** - assume a thickness of 7 mm as no English unit is available.

$$t_B := 7 \cdot mm = 0.276 \cdot in$$

$$W_B := t_B \cdot \pi \cdot a^2 \cdot \gamma_{steel} = 22.254 \cdot kips$$

$$W_B = 98.99 \cdot kN$$

$$X_B := t_B \div 2 = 0.011 \cdot ft$$

$$X_B = 3.5 \times 10^{-3} \cdot m$$

**Water** - as KAERI explained, T.L. indicates the top of fluid level.

$$H_W := 37 \cdot ft + 6 \cdot in = 37.5 \cdot ft$$

$$\gamma_W := 62.4 \frac{lbf}{ft^3} = 999.552 \cdot \frac{kgf}{m^3}$$

$$W_W := \pi \cdot a^2 \cdot H_W \cdot \gamma_W = 4604.156 \cdot kips$$

$$W_W = 2.048 \times 10^4 \cdot kN$$

$$X_W := H_W \div 2 = 18.75 \cdot ft$$

$$X_W = 5.715 \cdot m$$

Hydrostatic fluid pressure function,  $P_{ST}$ , as used in Table H-1 (y is pointing downward from TL, with a value of 0ft at TL):

$$P_{ST}(y) := y \cdot \gamma_W$$

$$P_{ST}(0ft) = 0 \cdot psi$$

$$P_{ST}(H_W) = 16.25 \cdot psi$$

In summary, the total weight and the center of gravity are:

$$W_{total} := W_H + W_S + W_B + W_W = 4.839 \times 10^3 \cdot kips$$

$$W_{total} = 2.195 \times 10^6 \cdot kgf$$

$$W_{total} = 2.195 \times 10^3 \cdot tonnef$$

$$X_{total} := \frac{W_H \cdot X_H + W_S \cdot X_S + W_B \cdot X_B + W_W \cdot X_W}{W_{total}} = 18.96 \cdot ft$$

$$X_{total} = 5.779 \cdot m$$

$$X_{tank} := \frac{W_H \cdot X_H + W_S \cdot X_S + W_B \cdot X_B}{W_H + W_S + W_B} = 23.077 \cdot ft$$

### **H.2.1 Horizontal Impulsive Mode Responses:**

$$\rho_L := \gamma_W \div g = 999.552 \frac{kg}{m^3}$$

$$\rho_S := \gamma_{steel} \div g = 7.889 \times 10^3 \frac{kg}{m^3}$$

$$\frac{\rho_L}{\rho_S} = 0.127$$

$$E_S := 29000 \cdot ksi$$

$$\nu_S := 0.3$$

Redefining R back to the radius of the tank:

$$R := a = 25.026 \cdot ft$$

Also defining H as  $H_W$  for compatibility with the equations in the method:

$$H := H_W = 37.5 \cdot ft$$

$$H_W \div R = 1.498 \quad \text{Formulations for } H/R \geq 1.5 \text{ are utilized in the following section.}$$

$$H_S \div R = 1.564$$

$$H_W \div H_S = 0.958$$

$$t_S \div R = 0.0021$$

The evaluation of horizontal impulsive modal frequency in the original CDFM method by Dr. Kennedy used Table 7.4 of Veletsos 1984, "Guidelines for the Seismic Design of Oil and Gas Pipeline Systems." Using the same table, it is determined that  $C_{WI}=0.0916$  for  $t_S/R=0.001$  and  $H_W/R=1.498$ . Using equation 4.18 in BNL 52631(Rev. 10/95):

$$C_{WI} := 0.0916$$

$$C_{LI} := C_{WI} \times \sqrt{\frac{127t_S \cdot \rho_S}{R \cdot \rho_L}} = 0.132$$

The horizontal impulsive mode natural frequency is estimated to be:

$$f_I := \frac{C_{LI}}{2\pi H_W} \cdot \sqrt{\frac{E_S}{\rho_S}} = 9.274 \cdot \text{Hz}$$

As indicated by KAERI, a modified design response spectrum shape as described in Regulatory Guide 1.60 was used in the design and therefore will be used in this calculation to define the SME spectrum shape. The 5% damped acceleration spectrum for a frequency range covering  $f_1=9.274$  Hz from Regulatory Guide 1.60 is used in the following to find the spectral acceleration:

$$Hor\_Freq := (0.25 \ 2.5 \ 9. \ 33.)^T \cdot \text{Hz}$$

$$Hor\_SA\_50 := (0.4 \ 3.13 \ 2.61 \ 1)^T \cdot A_H$$

$$S_{AI} := \text{linterp}(Hor\_Freq, Hor\_SA\_50, f_I) = 1.104 \cdot g$$

$$Hor\_amp\_I := S_{AI} \div A_H = 2.592$$

$$H_W \div R = 1.498 \quad \text{approximately as 1.50, otherwise ASCE 4-98 has the equation for } H/R < 1.5.$$

For the CST with an approximate  $H/R \geq 1.50$ , the effective impulsive weight of the contained water (or other fluid)  $W_I$  and its effective height above the tank base  $X_I$  can be calculated as follows. It is assumed in this calculation that the tank shell is rigid for the effective impulsive weight calculation per ASCE 4-98.

$$W_I := \left(1 - 0.436 \frac{R}{H_W}\right) W_W = 3.264 \times 10^3 \cdot kips \quad W_I = 1.452 \times 10^4 \cdot kN$$

$$X_I := \left(0.5 - 0.188 \frac{R}{H_W}\right) \cdot H_W = 14.045 \cdot ft \quad X_I = 4.281 \cdot m$$

The impulsive mode base shear  $V_I$  and moment  $M_I$  at the base of the tank shell:

$$V_I := \frac{S_{AI}}{g} \cdot (W_H + W_S + W_I) = 3.838 \times 10^3 \cdot kips$$

$$V_I = 1.707 \times 10^4 \cdot kN$$

$$M_I := \frac{S_{AI}}{g} \cdot (W_H \cdot X_H + W_S \cdot X_S + W_I \cdot X_I) = 5.66 \times 10^4 \cdot kips \cdot ft$$

$$M_I = 7.673 \times 10^4 \cdot kN \cdot m$$

For a depth from the top of the fluid greater than 0.15H (5.625 ft), the impulsive hydrodynamic pressure is estimated as:

$$P_I := \frac{W_I \cdot X_I \cdot S_{AI}}{1.36R \cdot H^2 \cdot g} = 7.344 \cdot psi \quad P_I = 50.638 \cdot kPa$$

For depths between 0 ft (fluid surface) to 0.15 H, the impulsive pressure varies linearly with height from 0 psi to the value computed above at 0.15H.

### **H.2.2 Horizontal Convective (Sloshing) Mode Responses:**

The fundamental convective mode frequency:

$$f_C := \sqrt{\frac{1.5ft \div sec^2}{R} \tanh\left(1.835 \frac{H}{R}\right)} = 0.244 \cdot Hz$$

This convective mode is very lightly damped and the damping ratio 0.5 percent is used as suggested by the original CDFM method. Using the fundamental convective frequency 0.244 Hz and 0.5% damping on the modified Regulatory Guide 1.60 spectrum, the convective spectral acceleration  $S_{AC}$  for the given  $SME_e$  can be calculated as follows:

$$Hor\_Freq := (0.1 \ 0.25 \ 2.5 \ 9.)^T \cdot Hz$$

$$Hor\_SA\_05 := (0.12 \ 0.707 \ 5.95 \ 4.96)^T \cdot A_H$$

$$S_{AC} := \text{interp}(Hor\_Freq, Hor\_SA\_05, f_C) = 0.291 \cdot g$$

$$Hor\_amp\_C := S_{AC} \div A_H = 0.683$$

It should be noted that  $f_C$  is slightly smaller than the corner frequency at point D in Regulatory Guide 1.60 horizontal spectrum, and the spectral acceleration values at point D and at frequency 0.1 Hz are determined by reading the horizontal spectral plot in Regulatory Guide 1.60.

The effective convective mode fluid weight and its effective application height:

$$W_C := W_W \cdot \left( 0.46 \frac{R}{H} \tanh \left( 1.835 \frac{H}{R} \right) \right) = 1.402 \times 10^3 \cdot kips \quad W_I = 3.264 \times 10^3 \cdot kips$$

$$W_C = 6.236 \times 10^3 \cdot kN$$

$$X_C := H \cdot \left[ 1.0 - \frac{\cosh \left( 1.835 \frac{H}{R} \right) - 1.0}{1.835 \left( \frac{H}{R} \right) \sinh \left( 1.835 \frac{H}{R} \right)} \right] = 25.501 \cdot ft \quad X_I = 14.045 \cdot ft$$

$$X_C = 7.773 \cdot m$$

$$V_C := \frac{S_{AC}}{g} \cdot W_C = 407.789 \cdot kips \quad V_I = 3.838 \times 10^3 \cdot kips$$

$$V_C = 1.814 \times 10^3 \cdot kN$$

$$M_C := \frac{S_{AC}}{g} \cdot W_C \cdot X_C = 1.04 \times 10^4 \cdot kips \cdot ft \quad M_I = 5.66 \times 10^4 \cdot kips \cdot ft$$

$$M_C = 1.41 \times 10^4 \cdot kN \cdot m$$

The hydrodynamic convective pressure as a function of depth,  $y$  ( $y=0$  at fluid surface and its positive direction is pointing downward), is given by:

$$P_C(y) := \frac{0.267W_W S_{AC}}{R \cdot H \cdot g} \cdot \frac{\cosh\left[1.835\left(\frac{H-y}{R}\right)\right]}{\cosh\left(1.835\frac{H}{R}\right)}$$

$$P_C(0 \cdot ft) = 2.646 \cdot psi$$

$$0.337psi = 2.324 \cdot kPa$$

$$P_C(H - X_C) = 1.119 \cdot psi$$

$$P_C(H - X_I) = 0.532 \cdot psi$$

$$P_C(H) = 0.337 \cdot psi$$

Note:  $P_C(y)$  is smaller at greater depth. The hydrodynamic convective pressures are generally negligible compared to the hydrodynamic impulsive pressure  $P_I$ , or the hydrostatic pressure  $P_{ST}$ , except at very shallow depths. The fundamental mode fluid slosh height  $h_s$  can be estimated to be,

$$h_s := 0.837R \cdot \frac{S_{AC}}{g} = 6.093 \cdot ft \qquad h_s = 1.857 m$$

Note that this sloshing height is more than half of the height of head.

### H.2.3 Vertical Fluid Mode Response:

The method to compute the natural frequency for the vertical fluid-tank system mode, which was used in the original CDFM method, is not applicable to this CST configuration. The example tank in the CDFM method has a  $t/R$  ratio of about 0.001, and the available data in the literature is only applicable to this  $t/R$  ratio. Note that the CST has a  $t/R$  ratio of 0.0021. As an alternative, also mentioned in the CDFM method, equation C3.5-13 in ASCE 4-98 is used instead in the following:

$$\text{Water bulk modulus: } K := 2.2 \times 10^9 Pa = 319.083 \cdot ksi$$

$$f_v := \frac{1}{4H} \left[ \rho L \cdot \left( \frac{2 \cdot R}{t_S \cdot E_S} + \frac{1}{K} \right) \right]^{-0.5} = 9.538 \cdot Hz$$

The CDFM method recommends 5% of critical damping be used when estimating the vertical spectral acceleration. Using the Reg Guide 1.60 vertical acceleration spectra:

$$Ver\_Freq := (0.25 \ 3.5 \ 9.0 \ 33.)^T \cdot Hz \qquad A_H = 0.426 \cdot g$$

$$Ver\_SA\_50 := (0.3 \ 2.98 \ 2.61 \ 1)^T \cdot A_H$$

$$S_{AV} := \text{lininterp}(Ver\_Freq, Ver\_SA\_50, f_v) = 1.096 \cdot g$$

The hydrodynamic vertical fluid response mode pressure:

$$P_V(y) := 0.8 \rho_L \cdot H \cdot S_{AV} \cdot \cos\left(\frac{\pi}{2} \cdot \frac{H-y}{H}\right) \quad P_V(0ft) = 0 \cdot psi$$

$$P_V(H) = 14.254 \cdot psi$$

### H.2.4 Combined Responses:

Define a square root of sum of squares (SRSS) function for convenience ( $v$  must be a column vector):

$$SRSS(v) := \sqrt{v \cdot v}$$

The combined horizontal seismic responses for the base shear  $V_{SH}$ , base moment  $M_{SH}$ , and horizontal seismic hydrodynamic pressures  $P_{SH}$  can be obtained by the SRSS of the horizontal impulsive and convective responses.

$$V_{SH} := SRSS\left[\left(V_I \ V_C\right)^T\right] = 3.86 \times 10^3 \cdot kips \quad V_I = 3.838 \times 10^3 \cdot kips$$

$$M_{SH} := SRSS\left[\left(M_I \ M_C\right)^T\right] = 5.754 \times 10^4 \cdot kips \cdot ft \quad M_I = 5.66 \times 10^4 \cdot kips \cdot ft$$

$$P_{SH}(y) := SRSS\left[\left(P_I \ P_C(y)\right)^T\right] \quad P_{SH}(H) = 7.352 \cdot psi$$

Note that for this CST, the combined horizontal seismic responses are essentially equal to the impulsive mode responses and the influence of the convective mode is negligible.

**(1):** For the purpose of the membrane hoop stress capacity check, the maximum seismic hydrodynamic pressures  $P_{SM}$  can be obtained by SRSS of the horizontal seismic pressures  $P_{SH}$  and the vertical fluid response hydrodynamic pressure  $P_V$ :

$$P_{SM}(y) := SRSS\left[\left(P_{SH}(y) \ P_V(y)\right)^T\right] \quad P_{SM}(H) = 16.039 \cdot psi$$

**(2):** For the purpose of estimating the buckling capacity of the tank shell, it is

necessary to estimate the expected maximum and minimum of the fluid pressures acting against the tank shell near its base at the location of the maximum axial compression during the time of maximum base moment. The expected maximum and minimum compression zone pressure  $P_{C+}$  and  $P_{C-}$ , at the time of maximum base moment can be obtained as,

$$P_{C+} := P_{ST}(H) + P_{SH}(H) + 0.4P_V(H) = 29.304 \cdot psi$$

$$P_{C-} := P_{ST}(H) + P_{SH}(H) - 0.4P_V(H) = 17.901 \cdot psi$$

Where the factor of 0.4 on  $P_V$  is to account for the probable vertical mode hydrodynamic vertical pressure at the time of maximum base moment.

**(3):** Similarly, for the purpose of estimating the expected minimum fluid hold-down forces in the zone of maximum tank wall axial tension, it is required to estimate the minimum tension zone fluid pressure  $P_{T-}$  at the time of maximum moment:

$$P_{T-} := P_{ST}(H) - P_{SH}(H) - 0.4P_V(H) = 3.196 \cdot psi$$

**(4):** For the sliding capacity evaluation, the expected minimum average fluid pressure  $P_a$  on the base plate, at the time of the maximum base shear, can be estimated to be:

$$P_a := P_{ST}(H) - 0.4P_V(H) = 10.548 \cdot psi$$

**(5):** The expected minimum total effective weight  $W_{Te}$  of the tank shell acting on the base, at the time of maximum moment and base shear, can be estimated by (assuming the vertical stiffness of the tank shell and head system results in a frequency greater than 33 Hz):

$$W_{Te} := (W_H + W_S) \cdot \left[ 1 - 0.4 \left( \frac{A_H}{g} \right) \right] = 176.14 \cdot kips$$




---

### H.3 Capacity Assessment



The seismic overturning moment capacity of the CST at its base,  $M_{SC}$ , depends on the axial compressive buckling capacity of the tank shell  $C_m$ , the tensile hold-down capacity of the anchor bolts including their anchorage and attachment to the tank  $T_{BC}$ , and the hold-down capacity of the fluid pressure acting on the tank base plate  $T_e$ .

Although unlikely for larger radius tanks, the tank SME capacity is sometimes

governed by the sliding shear capacity at the tank base,  $V_{SC}$ . Even though it does not appear that any butt welded steel tank has ever failed due to seismic induced membrane hoop stresses due to combined hydrostatic and hydrodynamic fluid pressures, the SME capacity of this failure mode,  $P_{CA}$ , should also be checked.

Additional assessment of the seismic capacity may include the possibility and consequence of the fluid sloshing against the tank roof, foundation failure for soil sites, and possibility of failure of piping or their attachment to the tank.

### **H.3.1 Compressive Buckling Capacity of the Tank Shell:**

The most likely buckling for tanks is the "elephant-foot" buckling near the base of the tank shell. The "elephant-foot" buckling is a combined effect of hoop tension, axial (vertical) compression, and restriction of radial deformation of the tank shell by the base plate. "Elephant-foot" buckling does not necessarily lead to failure of a tank (e.g., leakage). However, there is no simple capability evaluation method that can predict tank performance after the development of "elephant-foot" buckling. Therefore, for a CDFM SME capacity of tanks, the onset of "elephant-foot" buckling will be judged to represent the limit to the compressive buckling capacity of the tank shell. The onset of "elephant-foot" buckling can be estimated using elastic-plastic collapse theory as presented in the following:

The sidewall thickness near the shell base:  $t_s := t_S = 0.625 \cdot in$

The tank internal pressure near its base:  $P := P_{C+} = 2.02 \times 10^5 Pa$

Elastic modulus of the tank:  $E_S = 2.9 \times 10^4 \cdot ksi$

The CST shell is made of SA 204-type 304 stainless steel. This material does not have a flat yield plateau and as strain increases its stress can grow to a minimum ultimate stress capacity of 75 ksi. In the CDFM method, an effective yield stress  $\sigma_{ye}$  is set to  $2.4S_M$  or 45 ksi, in line with the ASME seismic design limit for primary local membrane plus primary bending [ASME 1983, "ASME Boiler & Pressure Vessel Code"]. The potential uncertainty range for  $\sigma_{ye}$  is reported to be between 30 ksi and 60 ksi, according to the original CDFM method description.

$$\sigma_{ye} := 45ksi$$

$$\frac{R}{t_s} = 480.5$$

$$S_I := \frac{R}{t_s} \div 400 = 1.201$$

The "elephant-foot" buckling axial stress of the tank shell can be accurately predicted to be:

$$\sigma_p := \frac{0.6E_S}{R \div t_s} \left[ 1 - \left( \frac{P \cdot R}{\sigma_{ye} \cdot t_s} \right)^2 \right] \cdot \left( 1 - \frac{1}{1.12 + S_I^{1.5}} \right) \cdot \left( \frac{S_I + \frac{\sigma_{ye}}{36 \text{ksi}}}{S_I + 1} \right) = 21.447 \cdot \text{ksi}$$

The compressive buckling capacity for HCLPF capacity computation utilizes a recommended 0.9 reduction factor of the buckling stress:

$$C_m := 0.9 \sigma_p \cdot t_s = 12.064 \cdot \frac{\text{kips}}{\text{in}}$$

Buckling capacity of the supported cylindrical shells under combined axial bending and internal pressure should also be checked although it is unlikely to govern for overall seismic response of fluid containing tanks. The axial bending induced buckling stress,  $\sigma_{CB}$ , for such a load case can be conservatively estimated (essentially lower bound) as follows.

A parameter  $\Delta\gamma$  to be used in the following procedure as an increase factor for internal pressure can be obtained from Figure 6 of "Buckling of Thin-walled Circular Cylinders," [NASA SP-8007].  $\Delta\gamma$  depends on the minimum compression zone pressure at the base of the tank shell,  $P_C$ , corresponding to the time of maximum moment.

Considering the potential range on  $\sigma_{ye}$  of 30 to 60 ksi, the resultant range on  $\sigma_p$  is 16.572 ksi to 26.702 ksi. Consequently,  $C_m$  has a range of 9.322 kips/in to 15.02 kips/in.

$$\frac{P_C \cdot \left( \frac{R}{t_s} \right)^2}{E_S} = 0.143$$

From Figure 6 of NASA SP-8007:  $\Delta\gamma := 0.12$

$$\phi := \frac{1}{16} \cdot \sqrt{\frac{R}{t_s}} = 1.37$$

$$\gamma := 1 - 0.73(1 - e^{-\phi}) = 0.455$$

$$\sigma_{CB} := (0.6\gamma + \Delta\gamma) \frac{E_S}{R \div t_s} = 23.737 \cdot ksi$$

$$0.9\sigma_p = 19.303 \cdot ksi$$

$\sigma_{CB}$  exceeds  $0.9s_p$ , so it does not govern.

### H.3.2 Bolt Hold-down Capacity:

The bolt hold-down capacity should be determined as the smallest of the bolt tensile capacity, anchorage of bolt into concrete foundation, capacity of the top plate of bolt chairs to transfer bolt loads to the vertical chair gussets, attachment of the top plate and vertical chair gussets to the tank shell, and the capacity of tank shell to withstand concentrated loads imposed on it by the bolt chairs.

**Anchor bolt capacity:** the anchor bolt has a diameter of 2 1/2" and is made of A36 steel. The tensile capacity can be determined as:

$$d_{bolt} := 2.5in$$

$$A_{bolt} := \frac{\pi \cdot d_{bolt}^2}{4} = 4.909 \cdot in^2$$

Based on the AISC Code [9th edition, 1989] for threaded A36 bolts:

$$T_{BC} := 1.7A_{bolt} \cdot 19.1ksi = 159.387 \cdot kips \quad T_{BC} = 79.693 \cdot tonf$$

Note that  $T_{BC}$  is the capacity of one bolt and the capacity of the interacting multi-bolts will be considered later.

**Anchor bolt chair capacity check:** according to the drawing, the anchor bolt chairs form a circumferentially continuous construction. Based on the continuous chair construction and the sizing of the plates and weld, it is judged that the anchor bolt chair and its attachment to the tank shell are adequate to transfer the bolt capacity load for the CST. The tank shell is also considered to be adequate in withstanding the concentrated loads imposed on it by bolt chairs, especially because the "elephant-foot" buckling capacity is also checked.

$$t_{chair} := \left(1 + \frac{3}{8}\right)in = 1.375 \cdot in$$

Weld width is 15 mm (5/8") according to the drawing.

**Capacity of bolt anchorage into concrete foundation:** the anchorage is constructed using non-shrinking grout. The tensile failure of bolt anchorage mainly consists of bolt failure, plug pull-out, and concrete cone failure, the last two of which typically are a combination of tensile failure of concrete in the upper portion of the anchorage that results in a partial depth cone-shaped spall and bond failure at the grout-concrete interface in the lower portion of the anchorage.

$$\text{Bolt spacing: } \Delta d := \pi \cdot \left[ 50ft + \left( 9 + \frac{1}{16} \right) in \right] \div 78 = 2.044 \cdot ft$$

Lee, et al [2001] described an experimental and analytical work on the pull-out strength of large-sized anchor bolt, in a SMiRT 16 paper entitled "failure mechanism for large-sized grouted anchor bolt under tensile load." The test specimens were selected based on the real construction of a CST in the Yonggwang Nuclear Power Plant of Korea. The anchor bolt is 2-1/2 inches in diameter, and has an embedment length of 2 ft 2-3/8 inches. The anchor bolt material is ASTM A36. Non-shrinking grout was used in the post-installed anchorage construction. These construction variables are basically very similar to those of the subject CST for fragility analysis, except that the subject CST anchors have a slightly shorter embedment length of 2 ft 1 inch. The concrete strength of the subject CST foundation is not available, and is assumed to be the same as in this SMiRT 16 paper, which has a compressive strength of 4500 psi. The circumferential spacing is about 2 ft for both tanks. The test included 5 anchor bolt specimens.

As reported by Lee, et al [2001], the average 7 day and 28 day compressive strength of the concrete were 5419 psi and 7180 psi, respectively. The actual average compressive strength of non-shrinking grout at 7 days and 21 days were 7550 psi and 11100 psi, respectively. The non-shrinking grout has obviously larger compressive strength than the concrete, as expected for normal construction of anchorage. The reported bond strength of the non-shrinking grout (Masterflow 870) was 40 kgf/cm<sup>2</sup> (569 psi). The Young's modulus of A36 is 2.9\*10<sup>7</sup> psi and the Poisson's ratio is 0.3.

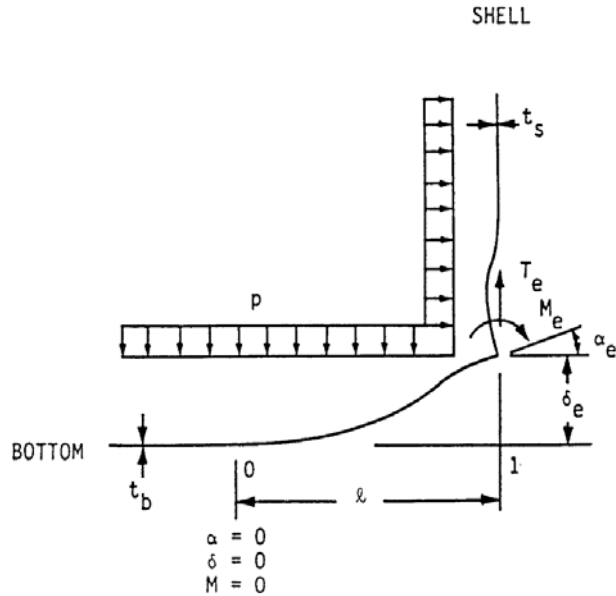
The test first confirmed a minimum required load of 50 tons (100 kips). Three of the five grouted anchors were tested further until failure. Two specimens was judged to have failed by tensile failure of grout at the lower portion of the grout block, bonding failure between grout and the concrete, and tensile failure of concrete. The other specimen showed abrasion of anchor bolt thread. All specimens achieved at least 100 tons (200kips), after which the load-deformation curve became significantly flatter and the ultimate failure load scatters between 100 tons and 120 tons.

Based on the test, the anchorage capacity should be 200 kips, which is about 26% higher than the estimate based on tensile strength of the anchor bolt. It should be noted that in the test, one specimen had abrasion in its thread, suggesting the anchor bolt capacity should be also close to 200 kips. However, since the

embedment in the test was about 1-3/8 inch longer than the subject CST case, the spacing of anchor bolts in the test is twice as long as in the subject CST case, and the lab test condition usually have a higher quality control, the estimate of 159.387 kips will be assumed as the anchorage capacity.

$$T_{BC} = 159.387 \cdot kips$$

### H.3.3 Fluid Hold-down Forces:



**Schematic Illustration of Tank Bottom Behavior Near Tensile Region of Tank Shell [NUREG/CR-5270]**

The hold-down force  $T_e$  increases with increasing fluid pressure  $P$ , which consequently assumes the minimum tension zone fluid press  $P_T$ . A number of other related parameters are also defined below.

$$P := P_T = 3.196 \cdot psi$$

$$\nu := 0.3$$

$$I_b := \frac{t_B^3}{12(1 - \nu^2)} = 1.917 \times 10^{-3} \cdot in^3$$

$$t_S = 0.625 \cdot in$$

$$t_B = 7 \cdot mm$$

$$K := \frac{E_S \cdot t_S^3}{12(1 - \nu^2)} = 7.325 \times 10^4 J$$

$$\kappa := \left[ \frac{R}{t_S} \cdot \sqrt{3(1 - \nu^2)} \right]^{0.5} = 28.177$$

$$MFP := \frac{R \cdot t_S}{\sqrt{12(1 - \nu^2)}} \left( 1 - \frac{R}{H \cdot \kappa} \right) = 0.036 m^2 \quad \text{MFP is a shortcut to } M_F / P$$

$$K_S := \frac{2 \cdot K \cdot \kappa}{R} = 5.412 \times 10^5 N$$

The uplift height  $\delta_e$ , the hold down tension  $T_e$ , moment  $M_e$ , rotation  $a_e$ , and maximum positive moment  $M_+$  can then be defined as functions of uplift length  $l$ :

$$F(l) := 1 + \frac{K_S \cdot l}{2E_S \cdot I_b}$$

$$\delta_e(l) := \left[ \frac{l^4}{24} - \frac{1}{F(l)} \left( \frac{K_S \cdot l^5}{72E_S \cdot I_b} + MFP \cdot \frac{l^2}{6} \right) \right] \cdot \left( \frac{P}{E_S \cdot I_b} \right)$$

$$T_e(l) := P \cdot \left[ \frac{l}{2} + \frac{1}{F(l)} \cdot \left( \frac{K_S \cdot l^2}{12E_S \cdot I_b} + \frac{MFP}{l} \right) \right]$$

Note: this equation as in the original CDFM method is singular at  $L = 0$  ft. The  $MFP/L$  term only has a minor effect on  $T_e$  when  $L$  is very small. The linear approximation in the original CDFM method can effectively avoid this singularity.

$$M_e(l) := P \cdot \left( \frac{1}{F(l)} \right) \cdot \left( \frac{K_S \cdot l^3}{12E_S \cdot I_b} + MFP \right)$$

$$M_+(l) := P \cdot \left( \frac{l^2}{8} - \frac{M_e(l)}{2P} + \frac{M_e(l)^2}{2P^2 \cdot l^2} \right)$$

The singularity in this equation can be similarly avoided by the linear approximation.

$$\alpha_e(l) := \frac{P \cdot l^3}{12E_S \cdot I_b} - \frac{M_e(l) \cdot l}{2E_S \cdot I_b}$$

Given

$$l := 0 \text{ in}$$

$$\frac{l^2}{24} - \frac{1}{F(l)} \left( \frac{K_S \cdot l^3}{72E_S \cdot I_b} + MFP \cdot \frac{1}{6} \right) = 0$$

$$l_{min} := \text{Find}(l) = 7.65 \cdot \text{in}$$

Given

$$l_{max} := 10 \text{ in}$$

$$\delta_e(l_{max}) = 0.165 \text{ in}$$

$$l_{max} := \text{Find}(l_{max}) = 21.207 \cdot \text{in}$$

$$l := l_{min}, l_{min} + 0.1 \text{ in} .. l_{max}$$

Linear Approximation:

$$i := 0 .. \frac{(l_{max} - l_{min})}{0.1 \text{ in}}$$

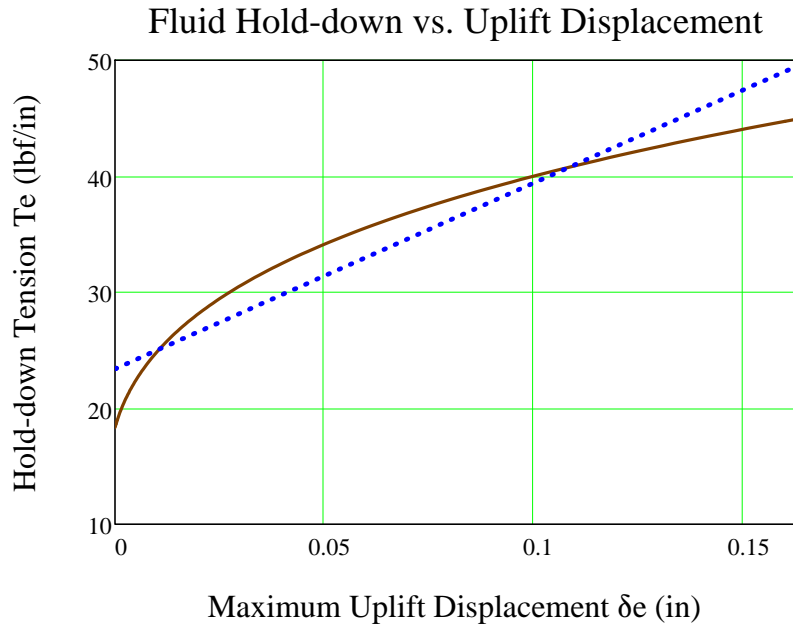
$$l_{vec_i} := l_{min} + i \cdot 0.1 \cdot \text{in}$$

$$\begin{pmatrix} T_{e0} \\ T_{e1} \end{pmatrix} := \text{line} \left[ \begin{array}{c} \overrightarrow{\delta_e(l_{vec})} \\ \text{in} \end{array}, \begin{array}{c} \overrightarrow{T_e(l_{vec}) \cdot \frac{\text{in}}{\text{lbf}}} \\ \left( T_e(l_{vec}) \cdot \frac{\text{in}}{\text{lbf}} \right) \end{array} \right] = \begin{pmatrix} 23.391 \\ 160.234 \end{pmatrix}$$

$$T_{e0} := \text{if}(P_{T-} > 0 \text{ psi}, T_{e0}, 0) \cdot \frac{\text{lbf}}{\text{in}} = 23.391 \cdot \frac{\text{lbf}}{\text{in}}$$

$$T_{e1} := \text{if}(P_{T-} > 0 \text{ psi}, T_{e1}, 0) \cdot \frac{\text{lbf}}{\text{in}^2} = 160.234 \cdot \frac{\text{lbf}}{\text{in}^2}$$

$$T_{e\_lin}(\delta_e) := T_{e0} + T_{e1} \cdot \delta_e$$



It should be noted that these equations are derived based on small displacement theory, and are applicable to the following conditions:

1.  $L / R \leq 0.15$ . The solution does not consider the stiffening effect of hoop behavior on the base plate and consequently conservatively overpredicts the displacement  $\delta_e$ , as the ratio of  $L/R$  becomes larger.
2.  $\delta_e / t_b \leq 0.6$ . As the solution is based on small displacement assumption, which ignores the beneficial influence of the membrane tension in the base plate to reduce  $\delta_e$  for a given  $T_e$  as in large displacement theory. For unanchored tanks, Manos (in "earthquake tank-wall stability of unanchored tanks," *Journal of Structural Engineering*, Vol 112, No. 8, ASCE, 1986) and Haroun and Badawi (in "nonlinear axisymmetric uplift of circular plates," *Dynamics of Structures*, ASCE, 1987) showed that large displacement membrane theory greatly increases the fluid hold-down force  $T_e$  and consequently the uplift  $\delta_e$ . Nevertheless, for anchored tanks like the subject CST, the uplift is not expected to be very large.
3.  $M_e/M_{pb} \leq 0.9$ ;  $M_e/M_{ps} \leq 0.9$ ; and  $M_+/M_{pb} \leq 0.9$ , where  $M_{pb}$  and  $M_{ps}$  are the plastic moment capacity of the base plate and shell sidewalls, respectively. These equations are derived from elastic solution, and these conditions prevent the potential unconservatism.

$$0.6t_B = 0.165 \cdot \text{in}$$

The second requirement leads to maximum  $\delta_e$  of 0.165 in, beyond which the small displacement theory becomes increasingly conservative. The original CDFM solved the problem by making a linear approximation of the  $\delta_e$ - $T_e$  curve in a range of  $\delta_e = 0$  to  $0.6t_B$ , and then use the linear equation to extrapolate beyond the  $0.6t_B$  to partially account for membrane tension effects. This approach will also be used in this study.

$$T_e := T_{e\_lin}$$

**Assessment of the upper limit on the fluid hold-down force:** based on a yield stress  $\sigma_y$  of 30 ksi, and an ultimate stress of 75 ksi, the fully plastic moment capacity  $M_{pb}$  of the 7 mm base plate is estimated to be 0.949 kips-inch/inch when the outer fiber reaches 75 ksi. It is also assumed that the effective hoop compressive yield stress  $\sigma_{ye}$  is equal to 45 ksi. The upper limit of the horizontal component of the membrane tension  $F_H$  can be found to be:

$$\sigma_{ye} = 45 \cdot \text{ksi}$$

$$M_{pb} := \frac{t_B^3}{12} \div \left( \frac{t_B}{2} \right) \cdot 75 \text{ksi} = 0.949 \cdot \frac{\text{kips} \cdot \text{in}}{\text{in}}$$

$$F_H := \frac{\sigma_{ye} \cdot t_S}{2\kappa} + \frac{M_{pb} \cdot \kappa}{R} = 0.588 \cdot \frac{\text{kips}}{\text{in}}$$

$$(4M_{pb}P_T)^{0.5} = 110.169 \cdot \frac{\text{lb}f}{\text{in}}$$

$$\frac{F_H}{2M_{pb}} = 0.31 \cdot \frac{1}{\text{in}}$$

Thus, the upper limit of the fluid hold-down force is estimated to be:

$$T_m(\delta_e) := 168.841 \frac{\text{lb}f}{\text{in}} \left( 1 + \frac{0.31 \cdot \delta_e}{\text{in}} \right)^{0.5}$$

The maximum  $\delta_e$  can be found by equating  $T_e$  and  $T_m$ :

*Given*

$$\delta_{ee} := 0.15in$$

$$T_e(\delta_{ee}) = T_m(\delta_{ee})$$

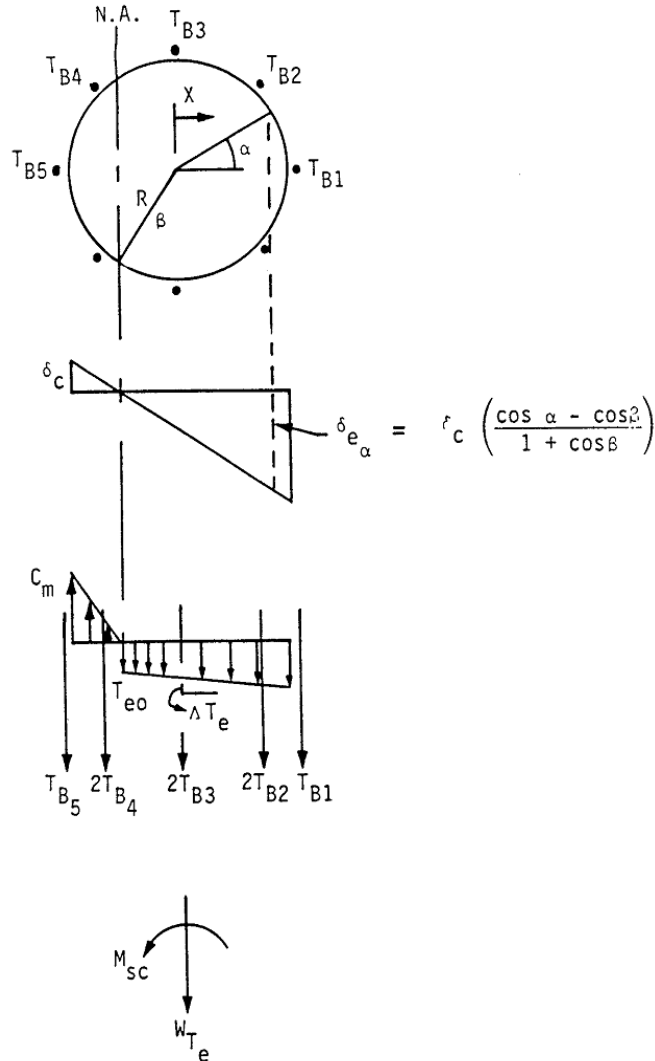
$$\delta_{ee} := Find(\delta_{ee}) = 1.07 \cdot in$$

Therefore, the linearized equation for  $T_e$  should not be extrapolated beyond  $\delta_e = 1.07$  inch.

Note that linearization is necessary later when developing overturning moment capacity.



### H.3.4 Overturning Moment Capacity:



#### Vertical Loading on Tank Shell at Base [NUREG/CR-5270]

The overturning moment capacity  $M_{SC}$  can be estimated using the compressive buckling capacity of the tank shell ( $C_B$ ), the anchor bolt hold-down capacity ( $T_{BC}$ ), and the relationship between fluid hold-down force and uplift displacement. The estimation approach in the CDFM method requires several conservative but reasonable assumptions as noted below:

1. The bottom of the tank shell is assumed to rotate rigidly about

the neutral axis (plane sections remain plane).

2. The cross-section of the tank at the top of the top plate of the bolt chairs ( $h_c$  above the base) is assumed to remain horizontal so that all vertical tank distortions needed to result in base uplift and mobilization of the anchor bolts must be accommodated over the height  $h_c$ .
3. The compressive stress varies linearly from zero at the neutral axis ( $\alpha=\beta$  as in the figure above) to its maximum value  $C_m$  at  $\alpha=180^\circ$ , as given by  $C_m = E_s t_s \delta_c / h_c \leq C_B$  (by converting eq. H-39), where  $\delta_c$  is the maximum compressive shortening.

Summary of parameters:

$$C_m = 12.064 \cdot \frac{\text{kips}}{\text{in}} \quad T_{BC} = 159.387 \cdot \text{kips}$$

$$T_{e0} = 0.023 \cdot \frac{\text{kips}}{\text{in}} \quad T_{e1} = 0.16 \cdot \frac{\text{kips}}{\text{in}^2}$$

$$W_{Te} = 176.14 \cdot \text{kips} \quad A_B := A_{bolt} \quad A_B = 4.909 \cdot \text{in}^2$$

$$E_B := 29 \times 10^3 \text{ ksi}$$

$$R = 25.026 \cdot \text{ft}$$

$$t_s = 0.625 \cdot \text{in} \quad E_s := E_S = 29 \times 10^3 \cdot \text{ksi}$$

$$h_c := 207 \text{ mm} = 8.15 \cdot \text{in}$$

$$h_a := 2 \text{ ft} + 1 \text{ in} = 25 \cdot \text{in}$$

Using the approach outlined in NUREG/CR-5270 instead of the EPRI NP-6041-SL appendix H in the following:

$$\delta_c := \frac{C_m \cdot h_c}{E_s \cdot t_s} = 5.424 \times 10^{-3} \cdot \text{in}$$

$$K_B := \frac{\delta_c \cdot A_B \cdot E_B}{h_a + h_c} = 23.294 \cdot \text{kips}$$

$$\Delta T_e := T_{e1} \cdot \delta_c = 8.692 \times 10^{-4} \cdot \frac{\text{kips}}{\text{in}}$$

$$\delta_{ea}(a,b) := \delta_c \cdot \left( \frac{\cos(a) - \cos(b)}{1 + \cos(b)} \right)$$

Because the bolt pretension  $T_{BP}$  is unreliable after a number of years in service, it is conservatively assumed to be 0.

$$T_{BP} := 0 \text{ kips}$$

The neutral axis angle  $\beta$  can be determined iteratively using the following procedure.

Bolt locations:  $i := 0..77$

$$\alpha_i := \frac{2\pi}{78}i$$

$$Tfunc(\alpha, \beta) := \begin{cases} c \leftarrow T_{BP} + K_B \cdot \frac{\cos(\alpha) - \cos(\beta)}{1 + \cos(\beta)} \\ c \leftarrow T_{BC} \text{ if } c > T_{BC} \\ c \leftarrow 0 \text{ if } c < 0 \end{cases}$$

$$C_1(\beta) := \frac{1 + \cos(\beta)}{\sin(\beta) + (\pi - \beta)\cos(\beta)}$$

$$C_2(\beta) := \frac{\sin(\beta)\cos(\beta) + \pi - \beta}{1 + \cos(\beta)}$$

$$C_3(\beta) := \frac{\sin(\beta) - \beta \cdot \cos(\beta)}{\sin(\beta) + (\pi - \beta)\cos(\beta)}$$

$$C_4(\beta) := \frac{\beta - \sin(\beta)\cos(\beta)}{1 + \cos(\beta)}$$

$$T_B(\alpha, \beta) := \overrightarrow{Tfunc(\alpha, \beta)}$$

$$Cf'_m(\alpha, \beta) := \left( \frac{W_{Te} + \sum T_B(\alpha, \beta)}{2R} + T_{e0} \cdot \beta \right) \cdot C_1(\beta) + \Delta T_e \cdot C_3(\beta)$$

Equating  $Cf'_m$  and  $C_m$  to determine  $\beta$ :

$$func(\alpha, \beta) := Cf'_m(\alpha, \beta) - C_m$$

$$\beta := \text{root}(\text{func}(\alpha, \beta), \beta, 0, 3.1)$$

$$\beta = 2.29114 \quad \beta \cdot \frac{180}{\pi} = 131.273$$

$$C'_m := C_f'_m(\alpha, \beta) = 12.064 \cdot \frac{\text{kips}}{\text{in}} \quad C_m = 12.064 \cdot \frac{\text{kips}}{\text{in}}$$

Use  $C'_m$  and  $\beta$  to find the overturning moment capacity  $M_{SC}$ :

$$M_{SC} := C'_m \cdot C_2(\beta) \cdot R^2 + \sum \overrightarrow{(T_B(\alpha, \beta) \cdot R \cdot \cos(\alpha))} + T_{e0} \cdot R^2 \cdot 2 \cdot \sin(\beta) + \Delta T_e \cdot C_4(\beta) \cdot R^2$$

$$M_{SC} = 154055.156 \cdot \text{kips} \cdot \text{ft}$$

$$\sum T_B(\alpha, \beta) = 3.846 \times 10^3 \cdot \text{kips}$$

The largest bolt elongation (at  $\alpha=0$ ) should be checked to ensure that the anchorage has the capability:

$$\delta_{e0} := \delta_{ea}(\alpha_0, \beta) = 0.026 \cdot \text{in}$$

$$\text{Elongation ratio: } \frac{\delta_{e0}}{h_a + h_c} = 0.08\%$$

The maximum elongation ratio is much smaller than 1%, which is recommended in the original CDFM method for the A307 bolt. One percent is also considered to be an appropriate percentage value for the A36 anchor bolt used in the subject CST construction.

The maximum tank shell uplift distortion  $\delta_{e0} = 0.026$  in, which is much less than the limit of 0.165 in for the small displacement theory to be applicable in developing the fluid hold-down capacity.

Because there are 78 anchor bolts (the example tank in the original CDFM method had only 8), the case where  $\alpha=0$  lies midway between bolts need not be checked.

The uncertainty in HCLPF buckling capacity of the tank shell due to the uncertain  $\sigma_{ye}$  can lead to an  $M_{SC}$  as low as 119133.414 kips-ft or as high as 192156.702 kips-ft. It should be noted that unlike in the original CDFM method,  $M_{SC}$  is sensitive to the estimate of  $C_m$ .

Inelastic energy absorption reduction factor  $k$  can be applied to linearly computed

seismic response to obtain the actual overturning moment capacity. The combined bolt yielding and tank shell buckling failure mode for overturning moment is not brittle so that  $k$  can be less than unity. However, as stated in the original CDFM method, it is difficult to make an appropriate estimate of  $k$  for this failure mode. Therefore, it is conservatively assumed to be unity.

$$k := 1.0$$



$$SME_M := \frac{M_{SC}}{k \cdot M_{SH}} \cdot SME_e \qquad SME_M = 1.14 \cdot g$$

Since  $SME_M$  is substantially different from  $SME_e$ , the above procedure should be iterated to obtain the appropriate SME estimate. Since there are more capacities that need to be assessed, the iteration is conducted considering all capacities.

### **H.3.5 Sliding Capacity:**



The base plate of the CST has a slight cone (with a slope of 1 to 96) so that the fluid will always drain away from the center of the tank. This cone is generally created by variable thickness of the oiled sand cushion between the tank bottom plate and its foundation. Therefore, the coefficient of friction between the tank base and its foundation is reasonably assumed to have a conservative value of 0.7 in the original CDFM method. For steel over concrete, the coefficient of friction is more reasonably set to 0.55, as suggested in BNL 52361 [Bandyopadhyay, et al., 1995]. For this study, the lower coefficient of friction of 0.55 is used.

$$COF := 0.55$$

The sliding shear capacity can then be calculated as,

$$V_{SC} := COF \cdot \left( W_{Te} + P_a \cdot \pi \cdot R^2 + \sum T_B(\alpha, \beta) \right) = 3.856 \times 10^3 \cdot kips$$

The shear capacity of the bolts should not be considered because (a) there is a large space between the concrete foundation and the anchor bolt chair, and (b) there is a 1/4" diametric clearance in the hole in the anchor bolt chair.



The sliding capacity with a unit inelastic absorption factor as suggested by the original CDFM method:

$$SME_V := \frac{V_{SC}}{k \cdot V_{SH}} \cdot SME_e \qquad SME_V = 0.426 \cdot g$$

By varying  $SME_e$ , the HCLPF shear capacity is found to be 0.426g.

Unlike the example tank in the original CDFM method, the capacity of the CST appears to be governed by the sliding capacity. The sliding capacity considers only the friction between the bottom plate and the foundation.

### H.3.6 Fluid Pressure Capacity:

The inelastic energy absorption seismic response reduction factor  $k_u$  is suggested to be 0.8 for HCLPF capacity evaluation:

$$k_u := 0.8$$

For the CDFM hoop membrane stress capacity, it is recommended that the ASME seismic design limit of  $2 S_M$  for primary stress should be used, which is 37.5 ksi for SA240-type 304 stainless steel:

$$\sigma_a := 37.5 \text{ ksi}$$

The pressure capacity,  $P_{CA}$ , at the bottom of the tank shell (the CST has a uniform shell thickness), can be estimated to be:

$$P_{CA}(t) := \frac{\sigma_a \cdot t}{R}$$

$$P_{CA}(t_S) = 78.044 \cdot \text{psi}$$

The maximum seismic induced hydrodynamic pressures  $P_{SM}$  and the hydrostatic pressure  $P_{ST}$  at the bottom of the tank shell are:

$$P_{SM}(H) = 16.039 \cdot \text{psi}$$

$$P_{ST}(H) = 16.25 \cdot \text{psi}$$

The HCLPF fluid pressure capacity  $SME_p$  can be determined as:

$$SME_p := \frac{P_{CA}(t_S) - P_{ST}(H)}{k_u \cdot P_{SM}(H)} \cdot SME_e = 2.052 \cdot g$$

The HCLPF fluid pressure capacity does not govern. This agrees with seismic experience that the fluid pressure capacity seldom appears to govern the seismic

capacity for normal flat bottomed steel tanks with butt-welded side plates.

Summary of SME capacities:

$$SME_M = 1.14 \cdot g$$

$$SME_V = 0.426 \cdot g$$

$$SME_p = 2.052 \cdot g$$

$$SME_{cr} := \min(SME_M, SME_V, SME_p) = 0.426 \cdot g$$

$$SME_e = 0.426 \cdot g$$

It should be noted that the controlling SME capacity of 0.426 g based on the CDFM method is similar to 0.41 g as reported by Choun, et al [2008]. Both capacities are associated with the sliding failure mode.

### **H.3.7 Consideration of Other Capacities:**

(1) Slosh height for roof damage: note that even with a  $SME_e = 0.334$  g (the initial guess), the slosh height is about 4.8 ft. With the HCLPF shear capacity of  $SME_e = 0.426$  g, the sloshing height can be about 6.1 ft, which is lower than the total height of the head (8.7', as approximated in the beginning part of this calculation).

$$h_s = 6.093 \cdot ft$$

$$SME_e = 0.426 \cdot g$$

The increase of sloshing height is not significant as  $SME_e$  increases from 0.334 g to 0.555 g. In addition, as pointed out in the original CDFM method, even if roof damage might be expected, such damage usually does not impair the ability of the tank to contain fluid.

(2) The CST is assumed to sit on rock/very stiff soil; therefore, soil-tank foundation interaction is not considered.

(3) Piping failure or failure of nozzles may lead to loss of fluid in the tank, and more importantly, may impair the normal function of the condensation system. As reported in the original CDFM method, a significant fraction of the cases of seismic induced loss of tank contents have been due to piping/nozzle failures because of poor detailing. The CDFM method also stated that a SME evaluation of piping/nozzle failure is necessary only when poor seismic detailing is found in the involved piping attached to the tank. This analysis assumes that the subject CST is appropriately detailed, i.e. the piping and nozzle directly attached to the tank are properly designed and constructed so that sufficient piping flexibility can

be achieved to accommodate large relative seismic anchor movements.

(4) The influence of the building in between the two CSTs on the SME is assessed in the following. The gap between the auxiliary building and the CSTs at the roof level is filled with elastomeric sealant.

The maximum tank shell uplift distortion is found to be 0.026 in, which corresponds to a neutral axis angle  $\beta$  of 2.29161 rad. Since the horizontal plane at the anchor bolt chair is assumed to remain plane and all distortion is assumed to occur below this level, the rotation angle around the neutral axis can be estimated to be:

$$\delta_{e0} = 0.026 \cdot \text{in}$$

$$\text{Rotation} := \frac{\delta_{e0}}{R \cdot (1 - \cos(\beta))} = 5.307 \times 10^{-5}$$

$$\beta = 2.291 \quad \cos(\beta) = -0.66$$

The maximum horizontal displacement at the roof of the auxiliary building, which is at an elevation of 114' 9" (Parapet elevation, compared to the tank floor elevation of 101' 9"), can be estimated to be:

$$\text{Rotation} \cdot 13\text{ft} = 8.279 \times 10^{-3} \cdot \text{in}$$

This horizontal displacement is much less than the width of the seismic separation joint at the roof elevation, which is 3 in. Therefore, the influence of the auxiliary building to the two CSTs is considered minimal.

## The Fragility of CST

$$SME_{HCLPF} := SME_e = 0.426 \cdot g$$

It should be emphasized that the HCLPF SME capacity assumes the Regulatory Guide 1.60 spectra anchored to the HCLPF SME PGA.

To determine the seismic fragility of the CST, one needs to convert the HCLPF SME PGA to median SME PGA. This conversion requires the estimate of both aleatory and epistemic uncertainties ( $\beta_R$  and  $\beta_U$ ). The Fragility Method, also presented along with the original CDFM method, estimates the aleatory and epistemic uncertainties to be 0.2 and 0.27, respectively. These uncertainties are nearly identical to those reported by Choun, et al [2008]. The SME median  $SME_m$  can then be estimated as well.

$$\beta_R := 0.2$$

$$\beta_U := 0.27$$

$$\beta_C := \sqrt{\beta_R^2 + \beta_U^2} = 0.336$$

$$SME_m := SME_{HCLPF} \cdot \exp[1.645(\beta_R + \beta_U)] = 0.923 \cdot g$$

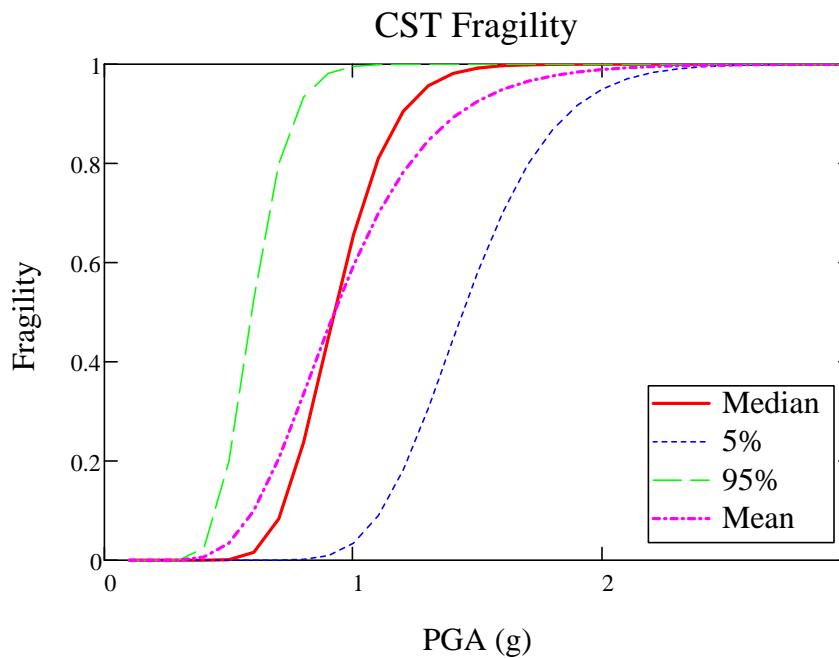
The fragility for the CST can now be calculated using the equations given below.

$$F(Q, a) := cnorm\left(\frac{\ln\left(\frac{a \cdot g}{SME_m}\right) + \beta_U \cdot qnorm(Q, 0, 1)}{\beta_R}\right)$$

$$F_{mean}(a) := cnorm\left(\frac{\ln\left(\frac{a \cdot g}{SME_m}\right)}{\beta_C}\right)$$

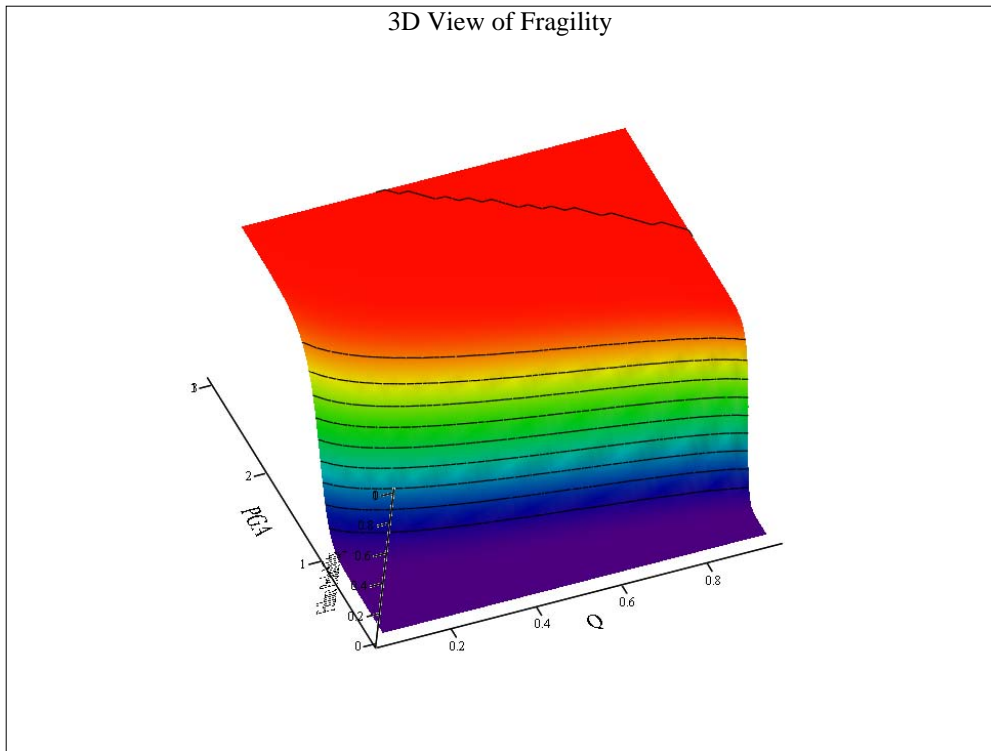
$$sa := 0.1, 0.2 \dots 3$$

The fragility curves for the median, 5% and 95% confidence levels, and the mean are shown in the figure below.



$Q := 0.05, 0.1 \dots 0.95$

A 3D surface plot of the fragility of the CST in terms of PGA and confidence level Q is shown below. The ordinate value is the probability of failure.



**Appendix B FRAGILITY ANALYSIS OF THE CST WITH DEGRADED STAINLESS  
TANK SHELL**



# KAERI Year 3 Task Fragility Analysis of Condensate Storage Tank

## - Degradation Case (A) Stainless Steel Shell Degradation

This calculation is based on the base case CDFM fragility analysis of the subject CST tank.

The thickness of the tank is reduced for strength calculation, but not for the weight and frequency calculation. The assumption is that the degradation occurs locally at the base.

For each thickness representing a degradation stage,  $SME_e$  must be determined manually because Mathcad does not support nested solve blocks (using the *given* keyword). Therefore, the calculated  $SME_e$  will be saved in a vector.

SCC crack rate was determined using the mechanochemical model for stress corrosion cracking (SCC) [Nie, et al, 2009, Saito and Kuniya, 2001]. See Section 4.1.1 of this report for more details.

$$year \equiv 3600s \cdot 24 \cdot 365$$

$$scc\_rate := 7.494 \cdot 10^{-3} \frac{in}{year}$$

$$years := 60 \text{ year}$$

$$tshell\_degraded := \frac{5}{8}in - scc\_rate \cdot years = 0.175 \cdot in$$

## H.1 Introduction

KAERI indicated that the seismic DBE in Korea follows the NRC Reg. Guide 1.60 design spectrum shape but with a PGA level scaled down to 0.2 g. An initial HCLPF capacity was assumed to be 1.67 times of 0.2 g. However, since the Mathcad sheets in this appendix solve the various equations iteratively by manually setting  $SME_e$  to different values, the following  $SME_e$  value of 0.091 g represents the converged solution for the degradation level of the stainless steel tank shell at 60 years.

$$SME_e := 0.091g$$



## H.2 Response Evaluation

Section H.2 of this appendix is the same as Section H.2 of Appendix A.

---

### H.3 Capacity Assessment

---

The seismic overturning moment capacity of the CST at its base,  $M_{SC}$ , depends on the axial compressive buckling capacity of the tank shell  $C_m$ , the tensile hold-down capacity of the anchor bolts including their anchorage and attachment to the tank  $T_{BC}$ , and the hold-down capacity of the fluid pressure acting on the tank base plate  $T_e$ .

Although unlikely for larger radius tanks, the tank SME capacity is sometimes governed by the sliding shear capacity at the tank base,  $V_{SC}$ . Even though it does not appear that any butt welded steel tank has ever failed due to seismic induced membrane hoop stresses due to combined hydrostatic and hydrodynamic fluid pressures, the SME capacity of this failure mode,  $P_{CA}$ , should also be checked.

Additional assessment of the seismic capacity may include the possibility and consequence of the fluid sloshing against the tank roof, foundation failure for soil sites, and possibility of failure of piping or their attachment to the tank.

#### **H.3.1 Compressive Buckling Capacity of the Tank Shell:**

The most likely buckling for tanks is the "elephant-foot" buckling near the base of the tank shell. The "elephant-foot" buckling is a combined effect of hoop tension, axial (vertical) compression, and restriction of radial deformation of the tank shell by the base plate. "Elephant-foot" buckling does not necessarily lead to failure of a tank (e.g., leakage). However, there is no simple capability evaluation method that can predict tank performance after the development of "elephant-foot" buckling. Therefore, for a CDFM SME capacity of tanks, the onset of "elephant-foot" buckling will be judged to represent the limit to the compressive buckling capacity of the tank shell. The onset of "elephant-foot" buckling can be estimated using elastic-plastic collapse theory as presented in the following:

The sidewall thickness near the shell base:  $t_s := t_{shell\_degraded} = 0.175 \cdot in$

The tank internal pressure near its base:  $P := P_{C+} = 1.313 \times 10^5 Pa$

Elastic modulus of the tank:  $E_S = 2.9 \times 10^4 \cdot ksi$

The CST shell is made of SA 204-type 304 stainless steel. This material does not have a flat yield plateau and as strain increases its stress can grow to a minimum ultimate stress capacity of 75 ksi. In the CDFM method, an effective yield stress  $\sigma_{ye}$  is set to  $2.4S_M$  or 45 ksi, in line with the ASME seismic design limit for primary local membrane plus primary bending [ASME 1983, "ASME Boiler & Pressure Vessel

Code"]. The potential uncertainty range for  $\sigma_{ye}$  is reported to be between 30 ksi and 60 ksi, according to the original CDFM method description.

$$\sigma_{ye} := 45 \text{ ksi}$$

$$\frac{R}{t_s} = 1.713 \times 10^3$$

$$S_I := \frac{R}{t_s} \div 400 = 4.281$$

The "elephant-foot" buckling axial stress of the tank shell can be accurately predicted to be:

$$\sigma_p := \frac{0.6E_S}{R \div t_s} \cdot \left[ 1 - \left( \frac{P \cdot R}{\sigma_{ye} \cdot t_s} \right)^2 \right] \cdot \left( 1 - \frac{1}{1.12 + S_I^{1.5}} \right) \cdot \left( \frac{S_I + \frac{\sigma_{ye}}{36 \text{ ksi}}}{S_I + 1} \right) = 4.548 \cdot \text{ksi}$$

The compressive buckling capacity for HCLPF capacity computation utilizes a recommended 0.9 reduction factor of the buckling stress:

$$C_m := 0.9 \sigma_p \cdot t_s = 0.718 \cdot \frac{\text{kips}}{\text{in}}$$

Buckling capacity of the supported cylindrical shells under combined axial bending and internal pressure should also be checked although it is unlikely to govern for overall seismic response of fluid containing tanks. The axial bending induced buckling stress,  $\sigma_{CB}$ , for such a load case can be conservatively estimated (essentially lower bound) as follows.

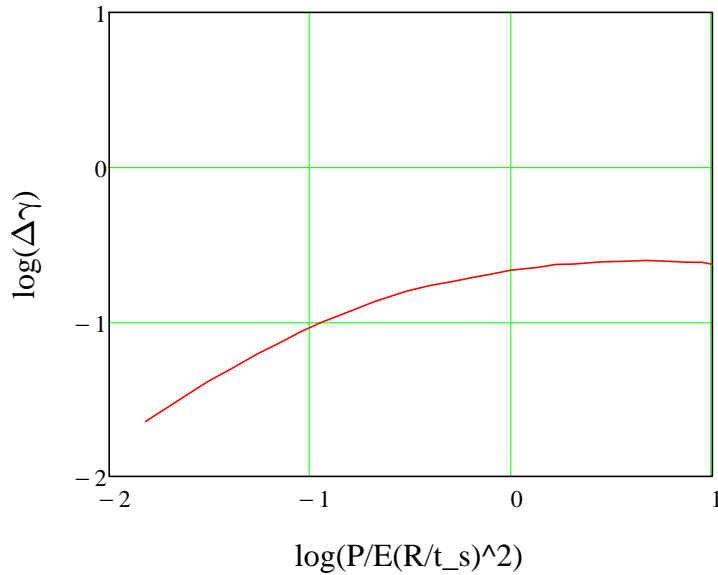
A parameter  $\Delta\gamma$  to be used in the following procedure as an increase factor for internal pressure can be obtained from Figure 6 of "Buckling of Thin-walled Circular Cylinders," [NASA SP-8007].  $\Delta\gamma$  depends on the minimum compression zone pressure at the base of the tank shell,  $P_C$ , corresponding to the time of maximum moment.

Considering the potential range on  $\sigma_{ye}$  of 30 to 60 ksi, the resultant range on  $\sigma_p$  is 16.572 ksi to 26.702 ksi. Consequently,  $C_m$  has a range of 9.322 kips/in to 15.02 kips/in.

Since  $\Delta\gamma$  is to be evaluated based on Figure 6 of NASA SP-8007, this figure is digitized and defined by the following two vectors, in log scale:

$$\begin{array}{r}
 \text{fig6x} := \left( \begin{array}{l}
 -1.8197 \\
 -1.5124 \\
 -1.395 \\
 -1.264 \\
 -1.1422 \\
 -1.0519 \\
 -0.94817 \\
 -0.81296 \\
 -0.67999 \\
 -0.52011 \\
 -0.40087 \\
 -0.28846 \\
 -0.18951 \\
 -0.09283 \\
 -0.00063874 \\
 0.12966 \\
 0.22407 \\
 0.3071 \\
 0.45083 \\
 0.57204 \\
 0.67305 \\
 0.78519 \\
 0.86144 \\
 0.94893 \\
 1.0004
 \end{array} \right)
 \end{array}
 \quad
 \begin{array}{r}
 \text{fig6y} := \left( \begin{array}{l}
 -1.6448 \\
 -1.3884 \\
 -1.3056 \\
 -1.2088 \\
 -1.1297 \\
 -1.0676 \\
 -1.0058 \\
 -0.93763 \\
 -0.86938 \\
 -0.8017 \\
 -0.76514 \\
 -0.7391 \\
 -0.71278 \\
 -0.68996 \\
 -0.66704 \\
 -0.64849 \\
 -0.62918 \\
 -0.62739 \\
 -0.61269 \\
 -0.60816 \\
 -0.60321 \\
 -0.60915 \\
 -0.61434 \\
 -0.6162 \\
 -0.62796
 \end{array} \right)
 \end{array}$$

Figure 6 of NASA SP-8007: Increase in Axial-Compressive Buckling-Stress Coefficient of Cylinders due to Internal Pressure



$$10^{\text{linterp}(\text{fig6x}, \text{fig6y}, \log(0.166))} = 0.12004$$

$$\text{ipx} := \frac{P_C}{E_S} \left( \frac{R}{t_s} \right)^2 = 1.679$$

$$\frac{P_C}{E_S} \left( \frac{R}{t_s} \right)^2 = 0.132$$

$$\Delta\gamma := 10^{\text{linterp}(\text{fig6x}, \text{fig6y}, \log(\text{ipx}))} = 0.235$$

$$\phi := \frac{1}{16} \cdot \sqrt{\frac{R}{t_s}} = 2.586$$

$$\gamma := 1 - 0.73(1 - e^{-\phi}) = 0.325$$

Note: there is not experimental data for  $R/t > 1500$ .

$$\frac{R}{t_s} = 1.713 \times 10^3$$

$$\sigma_{CB} := (0.6\gamma + \Delta\gamma) \frac{E_S}{R \div t_s} = 7.279 \cdot \text{ksi}$$

$$0.9\sigma_p = 4.094 \cdot \text{ksi}$$

$\sigma_{CB}$  exceeds  $0.9\sigma_p$ , so it does not govern.

### H.3.2 Bolt Hold-down Capacity:

The bolt hold-down capacity should be determined as the smallest of the bolt tensile capacity, anchorage of bolt into concrete foundation, capacity of the top plate of bolt chairs to transfer bolt loads to the vertical chair gussets, attachment of the top plate and vertical chair gussets to the tank shell, and the capacity of tank shell to withstand concentrated loads imposed on it by the bolt chairs.

**Anchor bolt capacity:** the anchor bolt has a diameter of 2 1/2" and is made of A36 steel. The tensile capacity can be determined as:

$$d_{bolt} := 2.5in$$
$$A_{bolt} := \frac{\pi \cdot d_{bolt}^2}{4} = 4.909 \cdot in^2$$

Based on the AISC Code [9th edition, 1989] for threaded A36 bolts:

$$T_{BC} := 1.7A_{bolt} \cdot 19.1ksi = 159.387 \cdot kips \quad T_{BC} = 79.693 \cdot tonf$$

Note that  $T_{BC}$  is the capacity of one bolt and the capacity of the interacting multi-bolts will be considered later.

**Anchor bolt chair capacity check:** according to the drawing, the anchor bolt chairs form a circumferentially continuous construction. Based on the continuous chair construction and the sizing of the plates and weld, it is judged that the anchor bolt chair and its attachment to the tank shell is adequate to transfer the bolt capacity load for the CST tank. The tank shell is also considered to be adequate in withstanding the concentrated loads imposed on it by bolt chairs, especially because the "elephant-foot" buckling capacity is also checked.

$$t_{chair} := \left(1 + \frac{3}{8}\right)in = 1.375 \cdot in$$

Weld width is 15 mm (5/8") according to the drawing.

**Capacity of bolt anchorage into concrete foundation:** the anchorage is constructed using non-shrinking grout. The tensile failure of bolt anchorage mainly consists of bolt failure, plug pull-out, and concrete cone failure, the last two of which typically are a combination of tensile failure of concrete in the upper portion of the anchorage that results in a partial depth cone-shaped spall and bond failure at the grout-concrete interface in the lower portion of the anchorage.

$$\text{Bolt spacing:} \quad \Delta d := \pi \cdot \left[50ft + \left(9 + \frac{1}{16}\right)in\right] \div 78 = 2.044 \cdot ft$$

Lee, et al [2001] described an experimental and analytical work on the pull-out strength of large-sized anchor bolt, in a SMiRT 16 paper entitled "failure mechanism for large-sized grouted anchor bolt under tensile load." The test

specimens were selected based on the real construction of a CST in the Yonggwang Nuclear Power Plant of Korea. The anchor bolt is 2-1/2 inches in diameter, and has an embedment length of 2 ft 2-3/8 inches. The anchor bolt material is ASTM A36. Non-shrinking grout was used in the post-installed anchorage construction. These construction variables are basically very similar to those of the subject CST for fragility analysis, except that the subject CST anchors have a slightly shorter embedment length of 2 ft 1 inch. The concrete strength of the subject CST foundation is not available, and is assumed to be the same as in this SMiRT 16 paper, which has a compressive strength of 4500 psi. The circumferential spacing is about 2 ft for both tanks. The test included 5 anchor bolt specimens.

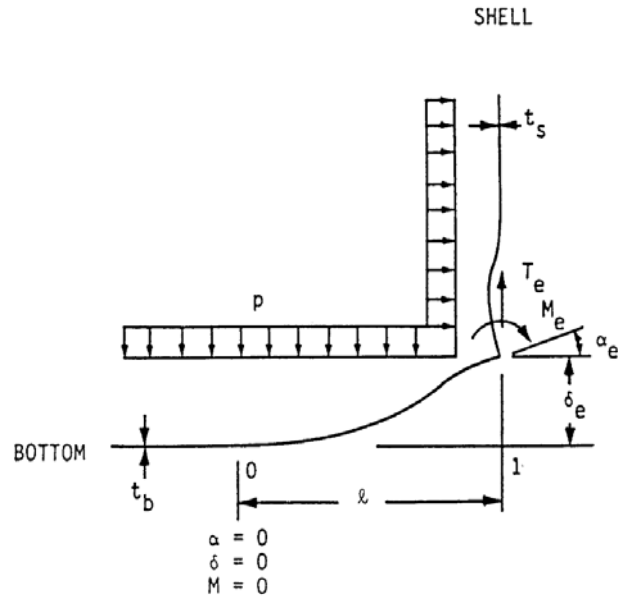
As reported by Lee, et al [2001], the average 7 day and 28 day compressive strength of the concrete were 5419 psi and 7180 psi, respectively. The actual average compressive strength of non-shrinking grout at 7 days and 21 days were 7550 psi and 11100 psi, respectively. The non-shrinking grout has obviously larger compressive strength than the concrete, as expected for normal construction of anchorage. The reported bond strength of the non-shrinking grout (Masterflow 870) was 40 kgf/cm<sup>2</sup> (569 psi). The Young's modulus of A36 is 2.9\*10<sup>7</sup> psi and the Poisson's ratio is 0.3.

The test first confirmed a minimum required load of 50 tons (100 kips). Three of the five grouted anchors were tested further until failure. Two specimens was judged to have failed by tensile failure of grout at the lower portion of the grout block, bonding failure between grout and the concrete, and tensile failure of concrete. The other specimen showed abrasion of anchor bolt thread. All specimens achieved at least 100 tons (200kips), after which the load-deformation curve became significantly flatter and the ultimate failure load scatters between 100 tons and 120 tons.

Based on the test, the anchorage capacity should be 200 kips, which is about 26% higher than the estimate based on tensile strength of the anchor bolt. It should be noted that in the test, one specimen had abrasion in its thread, suggesting the anchor bolt capacity should be also close to 200 kips. However, since the embedment in the test was about 1-3/8 inch longer than the subject CST case, the spacing of anchor bolts in the test is twice as long as in the subject CST case, and the lab test condition usually have a higher quality control, the estimate of 159.387 kips will be assumed as the anchorage capacity.

$$T_{BC} = 159.387 \cdot kips$$

### H.3.3 Fluid Hold-down Forces:



**Schematic Illustration of Tank Bottom Behavior Near Tensile Region of Tank Shell [NUREG/CR-5270]**

The hold-down force  $T_e$  increases with increasing fluid pressure  $P$ , which consequently assumes the minimum tension zone fluid press  $P_{T-}$ . A number of other related parameters are also defined below.

$$P := P_{T-} = 13.461 \cdot psi$$

$$\nu := 0.3$$

$$I_b := \frac{t_B^3}{12(1 - \nu^2)} = 1.917 \times 10^{-3} \cdot in^3$$

$$t_S = 0.625 \cdot in$$

$$t_S = 0.175 \cdot in$$

$$K := \frac{E_S \cdot t_S^3}{12(1 - \nu^2)} = 1.618 \times 10^3 J$$

$$t_B = 7 \cdot mm$$

$$\kappa := \left[ \frac{R}{t_S} \cdot \sqrt{3(1 - \nu^2)} \right]^{-0.5} = 53.194$$

$$MFP := \frac{R \cdot t_S}{\sqrt{12(1 - \nu^2)}} \left( 1 - \frac{R}{H \cdot \kappa} \right) = 0.01 m^2$$

MFP is a shortcut to  $M_F / P$

$$K_S := \frac{2 \cdot K \cdot \kappa}{R} = 2.257 \times 10^4 N$$

The uplift height  $\delta_e$ , the hold down tension  $T_e$ , moment  $M_e$ , rotation  $\alpha_e$ , and maximum positive moment  $M_+$  can then be defined as functions of uplift length  $l$ :

$$F(l) := 1 + \frac{K_S \cdot l}{2E_S \cdot I_b}$$

$$\delta_e(l) := \left[ \frac{l^4}{24} - \frac{1}{F(l)} \left( \frac{K_S \cdot l^5}{72E_S \cdot I_b} + MFP \cdot \frac{l^2}{6} \right) \right] \cdot \left( \frac{P}{E_S \cdot I_b} \right)$$

$$T_e(l) := P \cdot \left[ \frac{l}{2} + \frac{1}{F(l)} \cdot \left( \frac{K_S \cdot l^2}{12E_S \cdot I_b} + \frac{MFP}{l} \right) \right]$$

Note: this equation as in the original CDFM method is singular at  $L=0$  ft. The  $MFP/L$  term only has a minor effect on  $T_e$  when  $L$  is very small. The linear approximation in the original CDFM method can effectively avoid this singularity.

$$M_e(l) := P \cdot \left( \frac{1}{F(l)} \right) \cdot \left( \frac{K_S \cdot l^3}{12E_S \cdot I_b} + MFP \right)$$

$$M_+(l) := P \cdot \left( \frac{l^2}{8} - \frac{M_e(l)}{2P} + \frac{M_e(l)^2}{2P^2 \cdot l^2} \right)$$

The singularity in this equation can be similarly avoided by the linear approximation.

$$\alpha_e(l) := \frac{P \cdot l^3}{12E_S \cdot I_b} - \frac{M_e(l) \cdot l}{2E_S \cdot I_b}$$

Given

$l := 0$  in

$$\frac{l^2}{24} - \frac{1}{F(l)} \left( \frac{K_S \cdot l^3}{72E_S \cdot I_b} + MFP \cdot \frac{1}{6} \right) = 0$$

$$l_{min} := Find(l) = 7.516 \cdot in$$

Given

$$l_{max} := 10in$$

$$\delta_e(l_{max}) = 0.165in$$

$$l_{max} := Find(l_{max}) = 13.278 \cdot in$$

$$l := l_{min}, l_{min} + 0.1in .. l_{max}$$

Linear Approximation:

$$i := 0 .. \frac{(l_{max} - l_{min})}{0.1in}$$

$$l_{vec_i} := l_{min} + i \cdot 0.1 \cdot in$$

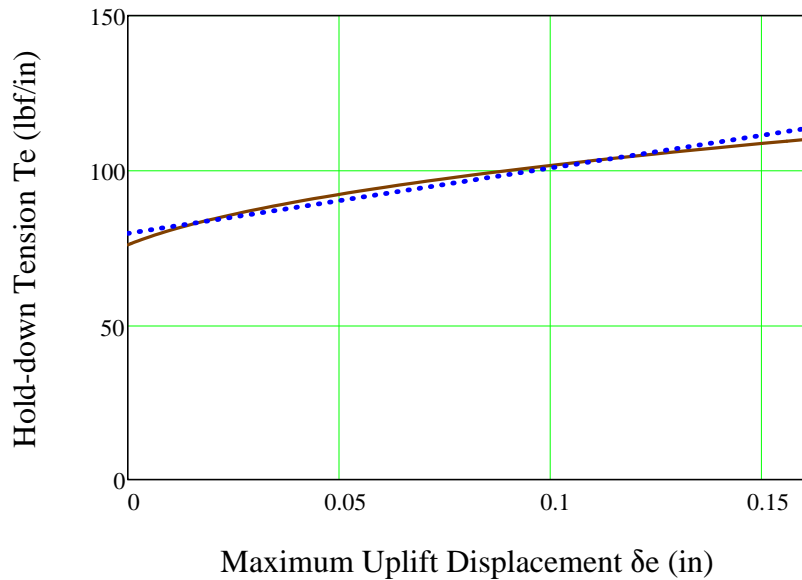
$$\begin{pmatrix} T_{e0} \\ T_{e1} \end{pmatrix} := line \left[ \frac{\delta_e(l_{vec})}{in}, \left( T_e(l_{vec}) \cdot \frac{in}{lbf} \right) \right] = \begin{pmatrix} 79.594 \\ 211.542 \end{pmatrix}$$

$$T_{e0} := if(P_{T-} > 0psi, T_{e0}, 0) \frac{lbf}{in} = 79.594 \cdot \frac{lbf}{in}$$

$$T_{e1} := if(P_{T-} > 0psi, T_{e1}, 0) \cdot \frac{lbf}{in^2} = 211.542 \cdot \frac{lbf}{in^2}$$

$$T_{e\_lin}(\delta_e) := T_{e0} + T_{e1} \cdot \delta_e$$

## Fluid Hold-down vs Uplift Displacement



It should be noted that these equations are derived based on small displacement theory, and are applicable to the following conditions:

1.  $L/R \leq 0.15$ . The solution does not consider the stiffening effect of hoop behavior on the base plate and consequently conservatively overpredicts the displacement  $\delta_e$ , as the ratio of  $L/R$  becomes larger.
  
2.  $\delta_e/t_b \leq 0.6$ . As the solution is based on small displacement assumption, which ignores the beneficial influence of the membrane tension in the base plate to reduce  $\delta_e$  for a given  $T_e$  as in large displacement theory. For unanchored tanks, Manos (in "earthquake tank-wall stability of unanchored tanks," *Journal of Structural Engineering*, Vol 112, No. 8, ASCE, 1986) and Haroun and Badawi (in "nonlinear axisymmetric uplift of circular plates," *Dynamics of Structures*, ASCE, 1987) showed that large displacement membrane theory greatly increases the fluid hold-down force  $T_e$  and consequently the uplift  $\delta_e$ . Nevertheless, for anchored tanks like the subject CST, the uplift is not expected to be very large.
  
3.  $M_e/M_{pb} \leq 0.9$ ;  $M_e/M_{ps} \leq 0.9$ ; and  $M_+/M_{pb} \leq 0.9$ , where  $M_{pb}$  and  $M_{ps}$  are the plastic moment capacity of the base plate and shell sidewalls, respectively. These equations are derived from elastic solution, and these conditions prevent the potential unconservatism.

$$0.6t_B = 0.165 \cdot in$$

The second requirement leads to maximum  $\delta_e$  of 0.165 in, beyond which the small displacement theory becomes increasingly conservative. The original CDFM solved the problem by making a linear approximation of the  $\delta_e$ - $T_e$  curve in a range of  $\delta_e=0$  to  $0.6t_B$ , and then use the linear equation to extrapolate beyond the  $0.6t_B$  to partially account for membrane tension effects. This approach will also be used in this study.

$$T_e := T_{e\_lin}$$

**Assessment of the upper limit on the fluid hold-down force:** based on a yield stress  $\sigma_y$  of 30 ksi, and an ultimate stress of 75 ksi, the fully plastic moment capacity  $M_{pb}$  of the 7 mm base plate is estimated to be 0.949 kips-inch/inch when the outer fiber reaches 75 ksi. It is also assumed that the effective hoop compressive yield stress  $\sigma_{ye}$  is equal to 45 ksi. The upper limit of the horizontal component of the membrane tension  $F_H$  can be found to be:

$$\sigma_{ye} = 45 \cdot \text{ksi}$$

$$M_{pb} := \frac{t_B^3}{12} \div \left( \frac{t_B}{2} \right) \cdot 75 \text{ksi} = 0.949 \cdot \frac{\text{kips} \cdot \text{in}}{\text{in}} \quad t_B = 7 \cdot \text{mm}$$

$$F_H := \frac{\sigma_{ye} \cdot t_s}{2\kappa} + \frac{M_{pb} \cdot \kappa}{R} = 0.242 \cdot \frac{\text{kips}}{\text{in}}$$

$$(4M_{pb}P_{T-})^{0.5} = 226.098 \cdot \frac{\text{lb} \cdot \text{f}}{\text{in}}$$

$$\frac{F_H}{2M_{pb}} = 0.128 \cdot \frac{1}{\text{in}}$$

Thus, the upper limit of the fluid hold-down force is estimated to be:

$$T_m(\delta_e) := 168.841 \frac{\text{lb} \cdot \text{f}}{\text{in}} \left( 1 + \frac{0.31 \cdot \delta_e}{\text{in}} \right)^{0.5}$$

The maximum  $\delta_e$  can be found by equating  $T_e$  and  $T_m$ :

Given

$$\delta_{ee} := 0.15 \text{in}$$

$$T_e(\delta_{ee}) = T_m(\delta_{ee})$$

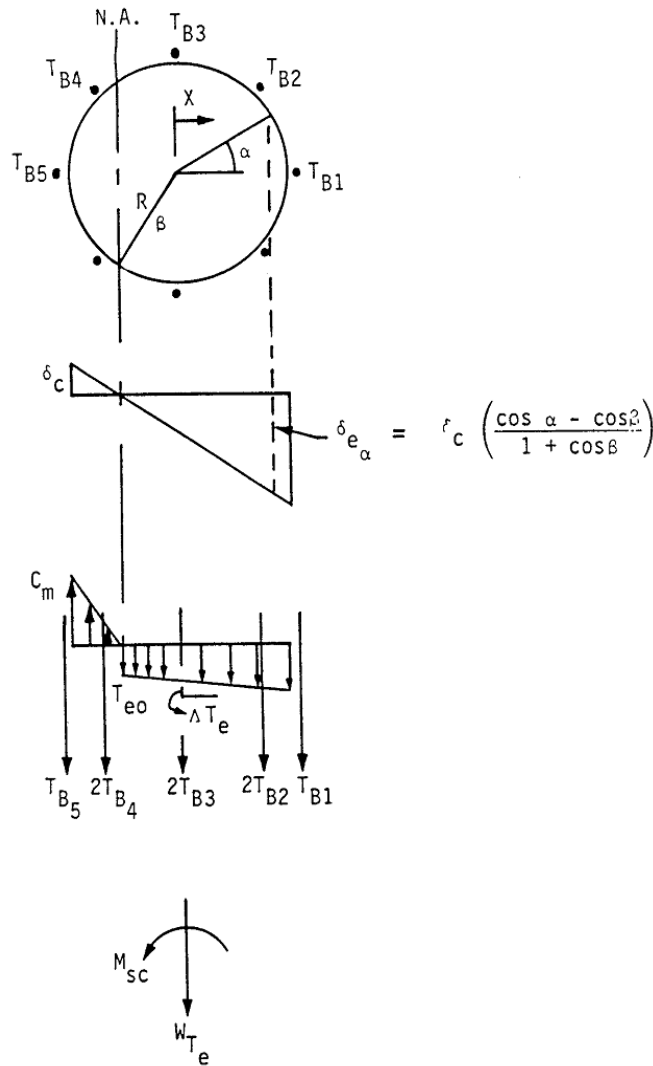
$$\delta_{ee} := \text{Find}(\delta_{ee}) = 0.479 \cdot \text{in}$$

Therefore, the linearized equation for  $T_e$  should not be extrapolated beyond  $\delta_{ee}$ .

Note that linearization is necessary later when developing overturning moment capacity.



### H.3.4 Overturning Moment Capacity:



### Vertical Loading on Tank Shell at Base [NUREG/CR-5270]

The overturning moment capacity  $M_{SC}$  can be estimated using the compressive buckling capacity of the tank shell ( $C_B$ ), the anchor bolt hold-down capacity ( $T_{BC}$ ), and the relationship between fluid hold-down force and uplift displacement. The estimation approach in the CDFM method requires several

conservative but reasonable assumptions as noted below:

1. The bottom of the tank shell is assumed to rotate rigidly about the neutral axis (plane sections remain plane).
2. The cross-section of the tank at the top of the top plate of the bolt chairs ( $h_c$  above the base) is assumed to remain horizontal so that all vertical tank distortions needed to result in base uplift and mobilization of the anchor bolts must be accommodated over the height  $h_c$ .
3. The compressive stress varies linearly from zero at the neutral axis ( $\alpha=\beta$  as in the figure above) to its maximum value  $C_m$  at  $\alpha=180^\circ$ , as given by  $C_m = E_s t_s \delta_c / h_c \leq C_B$  (by converting eq. H-39), where  $\delta_c$  is the maximum compressive shortening.

Summary of parameters:

$$C_m = 0.718 \cdot \frac{\text{kips}}{\text{in}} \quad T_{BC} = 159.387 \cdot \text{kips}$$

$$T_{e0} = 0.08 \cdot \frac{\text{kips}}{\text{in}} \quad T_{eI} = 0.212 \cdot \frac{\text{kips}}{\text{in}^2}$$

$$W_{Te} = 204.591 \cdot \text{kips} \quad A_B := A_{bolt} \quad A_B = 4.909 \cdot \text{in}^2$$

$$E_B := 29 \times 10^3 \text{ ksi}$$

$$R = 25.026 \cdot \text{ft}$$

$$t_s = 0.175 \cdot \text{in} \quad E_s := E_S = 29 \times 10^3 \cdot \text{ksi}$$

$$h_c := 207 \text{ mm} = 8.15 \cdot \text{in}$$

$$h_a := 2 \text{ ft} + 1 \text{ in} = 25 \cdot \text{in}$$

Using the approach outlined in NUREG/CR-5270 instead of the EPRI NP-6041-SL appendix H in the following:

$$\delta_c := \frac{C_m \cdot h_c}{E_s \cdot t_s} = 1.15 \times 10^{-3} \cdot \text{in}$$

$$K_B := \frac{\delta_c \cdot A_B \cdot E_B}{h_a + h_c} = 4.94 \cdot \text{kips}$$

$$\Delta T_e := T_{eI} \cdot \delta_c = 2.434 \times 10^{-4} \cdot \frac{\text{kips}}{\text{in}}$$

$$\delta_{ea}(a,b) := \delta_c \cdot \left( \frac{\cos(a) - \cos(b)}{1 + \cos(b)} \right)$$

Because the bolt pretension  $T_{BP}$  is unreliable after a number of years in service, it is conservatively assumed to be 0.

$$T_{BP} := 0 \text{ kips}$$

The neutral axis angle  $\beta$  can be determined iteratively using the following procedure.

Bolt locations:  $i := 0..77$

$$\alpha_i := \frac{2\pi}{78}i$$

$$Tfunc(\alpha, \beta) := \begin{cases} c \leftarrow T_{BP} + K_B \cdot \frac{\cos(\alpha) - \cos(\beta)}{1 + \cos(\beta)} \\ c \leftarrow T_{BC} \text{ if } c > T_{BC} \\ c \leftarrow 0 \text{ if } c < 0 \end{cases}$$

$$C_1(\beta) := \frac{1 + \cos(\beta)}{\sin(\beta) + (\pi - \beta)\cos(\beta)}$$

$$C_2(\beta) := \frac{\sin(\beta)\cos(\beta) + \pi - \beta}{1 + \cos(\beta)}$$

$$C_3(\beta) := \frac{\sin(\beta) - \beta \cdot \cos(\beta)}{\sin(\beta) + (\pi - \beta)\cos(\beta)}$$

$$C_4(\beta) := \frac{\beta - \sin(\beta)\cos(\beta)}{1 + \cos(\beta)}$$

$$T_B(\alpha, \beta) := \overrightarrow{Tfunc(\alpha, \beta)}$$

$$Cf'_m(\alpha, \beta) := \left( \frac{W_{Te} + \sum T_B(\alpha, \beta)}{2R} + T_{e0} \cdot \beta \right) \cdot C_1(\beta) + \Delta T_e \cdot C_3(\beta)$$

Equating  $Cf'_m$  and  $C_m$  to determine  $\beta$ :

$$func(\alpha, \beta) := Cf'_m(\alpha, \beta) - C_m$$

$$\beta := \text{root}(func(\alpha, \beta), \beta, 0, 3.14159)$$

$$\beta = 1.61646 \quad \beta \cdot \frac{180}{\pi} = 92.617$$

$$C'_m := C_f'_m(\alpha, \beta) = 0.718 \cdot \frac{\text{kips}}{\text{in}} \quad C_m = 0.718 \cdot \frac{\text{kips}}{\text{in}}$$

Use  $C'_m$  and  $\beta$  to find the overturning moment capacity  $M_{SC}$ :

$$M_{SC} := C'_m \cdot C_2(\beta) \cdot R^2 + \sum \overrightarrow{(T_B(\alpha, \beta) \cdot R \cdot \cos(\alpha))} + T_{e0} \cdot R^2 \cdot 2 \cdot \sin(\beta) + \Delta T_e \cdot C_4(\beta) \cdot R^2$$

$$M_{SC} = 12235.299 \cdot \text{kips} \cdot \text{ft}$$

$$\sum T_B(\alpha, \beta) = 137.826 \cdot \text{kips}$$

The largest bolt elongation (at  $\alpha=0$ ) should be checked to ensure that the anchorage has the capability:

$$\delta_{e0} := \delta_{ea}(\alpha_0, \beta) = 1.26 \times 10^{-3} \cdot \text{in}$$

$$\text{Elongation ratio: } \frac{\delta_{e0}}{h_a + h_c} = 3.802 \times 10^{-3} \cdot \%$$

The maximum elongation ratio is much smaller than 1%, which is recommended in the original CDFM method for the A307 bolt. One percent is also considered to be an appropriate percentage value for the A36 anchor bolt used in the subject CST construction.

The maximum tank shell uplift distortion  $\delta_{e0} = 0.026$  in, which is much less than the limit of 0.165 in for the small displacement theory to be applicable in developing the fluid hold-down capacity.

Because there are 78 anchor bolts (the example tank in the original CDFM method had only 8), the case where  $\alpha=0$  lies midway between bolts need not be checked.

The uncertainty in HCLPF buckling capacity of the tank shell due to the uncertain  $\sigma_{ye}$  can lead to an  $M_{SC}$  as low as 119133.414 kips-ft or as high as 192156.702 kips-ft. It should be noted that unlike in the original CDFM method,  $M_{SC}$  is sensitive to the estimate of  $C_m$ .

Inelastic energy absorption reduction factor  $k$  can be applied to linearly computed seismic response to obtain the actual overturning moment capacity. The combined bolt yielding and tank shell buckling failure mode for overturning moment is not brittle so that  $k$  can be less than unity. However, as stated in the original CDFM method, it is difficult to make an appropriate estimate of  $k$  for this failure mode. Therefore, it is conservatively assumed to be unity.

$$k := 1.0$$

$$SME_M := \frac{M_{SC}}{k \cdot M_{SH}} \cdot SME_e \qquad SME_M = 0.091 \cdot g$$

Since  $SME_M$  is substantially different from  $SME_e$ , the above procedure should be iterated to obtain the appropriate SME estimate. The resultant  $SME_e$  is found to be 0.97g.



### H.3.5 Sliding Capacity:



The base plate of the CST has a slight cone (with a slope of 1 to 96) so that the fluid will always drain away from the center of the tank. This cone is generally created by variable thickness of the oiled sand cushion between the tank bottom plate and its foundation. Therefore, the coefficient of friction between the tank base and its foundation is reasonably assumed to have a conservative value of 0.55:

$$COF := 0.55$$

The sliding shear capacity can then be calculated as,

$$V_{SC} := COF \cdot \left( W_{Te} + P_a \cdot \pi \cdot R^2 + \sum T_B(\alpha, \beta) \right) = 2.531 \times 10^3 \cdot kips$$

The shear capacity of the bolts should not be considered because (a) there is a large space between the concrete foundation and the anchor bolt chair, and (b) there is a 1/4" diametric clearance in the hole in the anchor bolt chair.

The sliding capacity with a unit inelastic absorption factor as suggested by the original CDFM method:

$$SME_V := \frac{V_{SC}}{k \cdot V_{SH}} \cdot SME_e \qquad SME_V = 0.279 \cdot g$$

Unlike the example tank in the original CDFM method, the capacity of the CST appears to be governed by the sliding capacity. The sliding capacity considers only the friction between the bottom plate and the foundation.



### H.3.6 Fluid Pressure Capacity:

---



The inelastic energy absorption seismic response reduction factor  $k_u$  is suggested to be 0.8 for HCLPF capacity evaluation:

$$k_u := 0.8$$

For the CDFM hoop membrane stress capacity, it is recommended that the ASME seismic design limit of  $2 S_M$  for primary stress should be used, which is 37.5 ksi for SA240-type 304 stainless steel:

$$\sigma_a := 37.5 \text{ ksi}$$

The pressure capacity,  $P_{CA}$ , at the bottom of the tank shell (the CST has a uniform shell thickness), can be estimated to be:

$$P_{CA}(t) := \frac{\sigma_a \cdot t}{R}$$

$$P_{CA}(t_s) = 21.897 \cdot \text{psi}$$

The maximum seismic induced hydrodynamic pressures  $P_{SM}$  and the hydrostatic pressure  $P_{ST}$  at the bottom of the tank shell are:

$$P_{SM}(H) = 2.362 \times 10^4 \text{ Pa}$$

$$P_{ST}(H) = 1.12 \times 10^5 \text{ Pa}$$

The HCLPF fluid pressure capacity  $SME_p$  can be determined as:

$$SME_p := \frac{P_{CA}(t_s) - P_{ST}(H)}{k_u \cdot P_{SM}(H)} \cdot SME_e = 0.187 \cdot g$$

By varying  $SME_e$ , the HCLPF fluid pressure capacity can be found to be 2.191 g, which does not govern. This agrees with seismic experience that the fluid pressure capacity seldom appears to govern the seismic capacity for normal flat bottomed steel tanks with butt-welded side plates.



Summary of SME capacities:

$$SME_M = 0.091 \cdot g$$

$$SME_V = 0.279 \cdot g$$

$$SME_p = 0.187 \cdot g$$

$$SME_{cr} := \min(SME_M, SME_V, SME_p) = 0.091 \cdot g$$

$$SME_e = 0.091 \cdot g$$

$$if[SME_{cr} = SME_M, "Moment", (if(SME_{cr} = SME_V, "Shear", "Fluid Pressure"))] = "Moment"$$

$$t_s = 0.175 \cdot in$$

Summary of results:

Years:	0	5	10	15	20	25	30	35	40
ts (in):	0.625	0.591	0.557	0.523	0.489	0.455	0.421	0.387	0.353
SME:	0.426	0.409	0.393	0.376	0.360	0.343	0.326	0.310	0.294
SMEM:	1.14	1.047	0.953	0.858	0.762	0.667	0.571	0.476	0.383
SMEV:	0.426	0.409	0.393	0.376	0.360	0.343	0.326	0.310	0.294
SMEP:	2.052	1.896	1.741	1.586	1.430	1.275	1.120	0.964	0.809
Mode:	Shear	Shear	Shear	Shear	Shear	Shear	Shear	Shear	Shear
Years:	45	50	55	60	65	70	75	80	
ts (in):	0.319	0.285	0.251	0.217	0.184	0.150			
SME:	0.278	0.218	0.152	0.091	NA				
SMEM:	0.290	0.218	0.152	0.091	NA				
SMEV:	0.278	0.276	0.277	0.28	NA				
SMEP:	0.654	0.498	0.343	0.187	NA				
Mode:	Shear	Moment	Moment	Moment	NA				

**H.3.7 Consideration of Other Capacities:**

(1) Slosh height for roof damage: note that even with a  $SME_e = 0.334 \text{ g}$  (the initial guess), the slosh height is about 4.8 ft. With the HCLPF shear capacity of  $SME_e = 0.555 \text{ g}$ , the sloshing height can be about 7.9 ft, which is close to the total height of the head (8.7', as approximated in the beginning part of this calculation).

$$h_s = 1.302 \cdot ft$$

$$SME_e = 0.091 \cdot g$$

The increase of sloshing height is not significant as  $SME_e$  increases from 0.334 g to 0.555 g. In addition, as pointed out in the original CDFM method, even if roof damage might be expected, such damage usually does not impair the ability of the tank to contain fluid.

(2) The CST is assumed to sit on rock/very stiff soil; therefore, soil-tank foundation interaction is not considered.

(3) Piping failure or failure of nozzles may lead to loss of fluid in the tank, and more importantly, may impair the normal function of the condensation system. As reported in the original CDFM method, a significant fraction of the cases of seismic induced loss of tank contents have been due to piping/nozzle failures because of poor detailing. The CDFM method also stated that a SME evaluation of piping/nozzle failure is only necessary when poor seismic detailing is found in the involved piping attached to the tank. This analysis assumes that the subject CST is appropriately detailed, i.e. the piping and nozzle directly attached to the tank are properly designed and constructed so that sufficient piping flexibility can be achieved to accommodate large relative seismic anchor movements.

(4) The influence of the building in between the two CSTs on the SME are assessed in the following. The gap between the auxiliary building and the CSTs at the roof level is filled with elastomeric sealant.

The maximum tank shell uplift distortion is found to be 0.026 in, which corresponds to a neutral axis angle  $\beta$  of 2.29161 rad. Since the horizontal plane at the anchor bolt chair is assumed to remain plane and all distortion is assumed to occur below this level, the rotation angle around the neutral axis can be estimated to be:

$$Rotation := \frac{\delta_{e0}}{R \cdot (1 - \cos(\beta))} = 4.014 \times 10^{-6}$$

$$\beta = 1.616 \quad \cos(\beta) = -0.046$$

The maximum horizontal displacement at the roof of the auxiliary building, which is at an elevation of 114' 9" (Parapet elevation, compared to the tank floor elevation of 101' 9"), can be estimated to be:

$$Rotation \cdot 13ft = 0.000626 \cdot in$$

This horizontal displacement is much less than the width of the seismic separation joint at the roof elevation, which is 3 in. Therefore, the influence of the auxiliary building to the two CSTs is considered minimal.

## The Fragility of CST Based on Degraded Conditions

Summary of results:

Years:	0	5	10	15	20	25	30	35	40
ts (in):	0.625	0.591	0.557	0.523	0.489	0.455	0.421	0.387	0.353
SME:	0.426	0.409	0.393	0.376	0.360	0.343	0.326	0.310	0.294
SMEM:	1.14	1.047	0.953	0.858	0.762	0.667	0.571	0.476	0.383
SMEV:	0.426	0.409	0.393	0.376	0.360	0.343	0.326	0.310	0.294
SMEP:	2.052	1.896	1.741	1.586	1.430	1.275	1.120	0.964	0.809
Mode:	Shear								
Years:	45	50	55	60	65	70	75	80	
ts (in):	0.319	0.285	0.251	0.217	0.184	0.150			



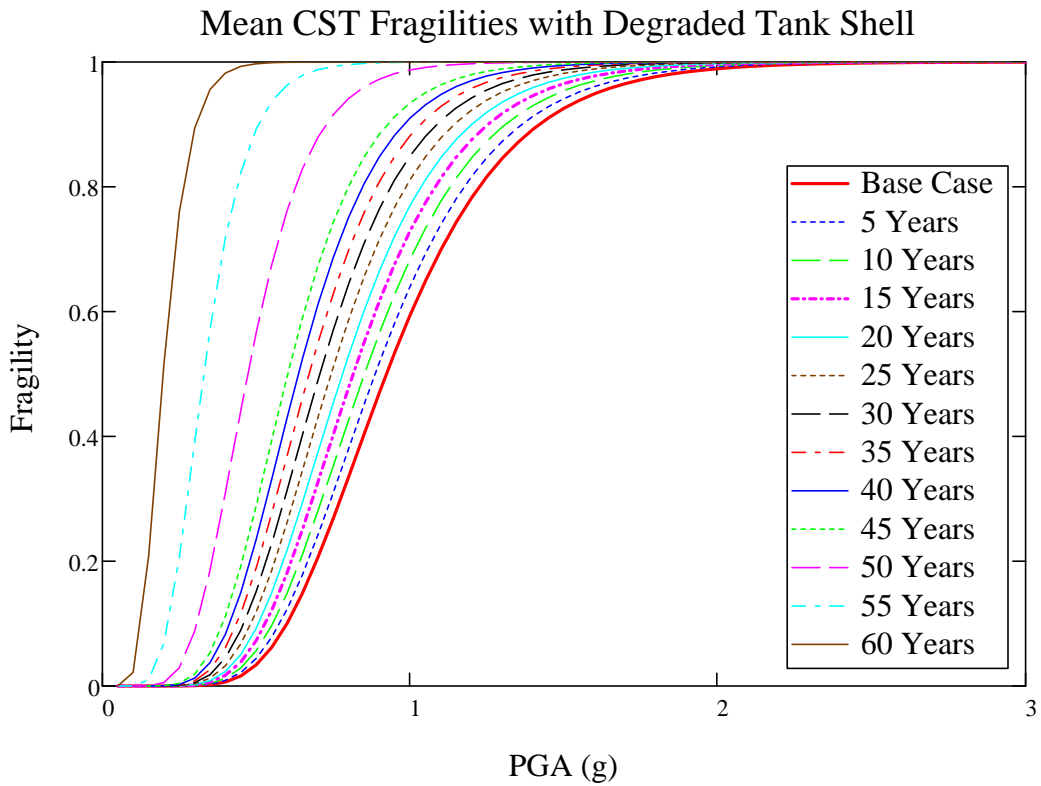
$$SME_{Vm_i} := SME_{V_i} \cdot Hm$$

$$SME_{Pm_i} := SME_{P_i} \cdot Hm$$

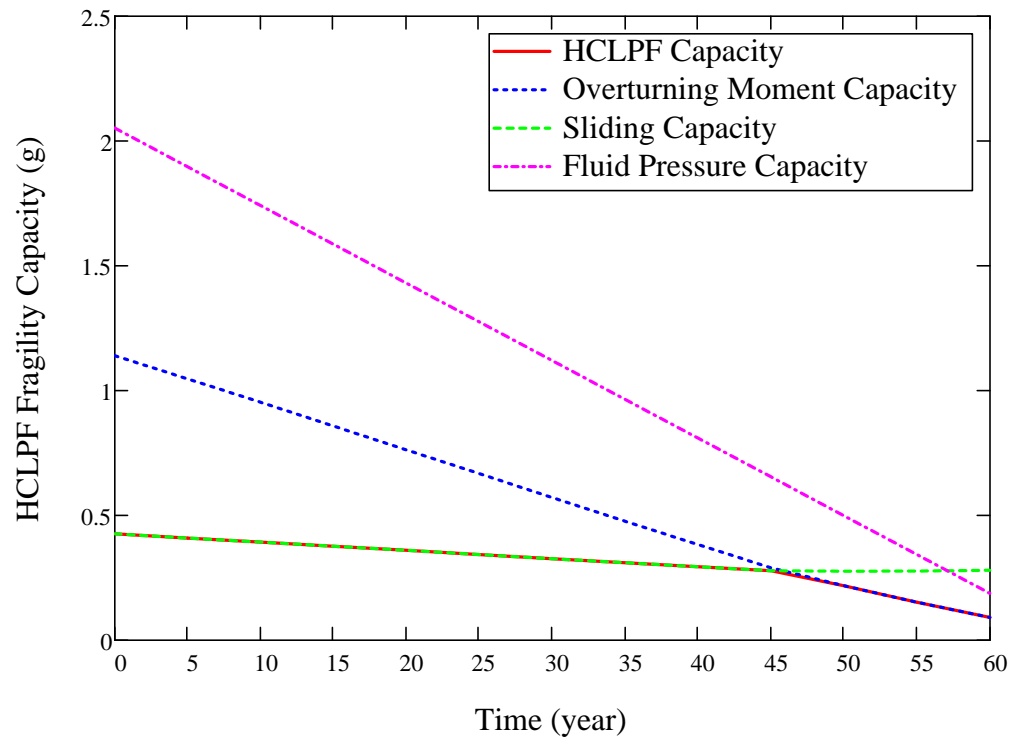
$$F(Q, a) := cnorm \left( \frac{\ln \left( \frac{a \cdot g}{SME_m} \right) + \beta_U \cdot qnorm(Q, 0, 1)}{\beta_R} \right)$$

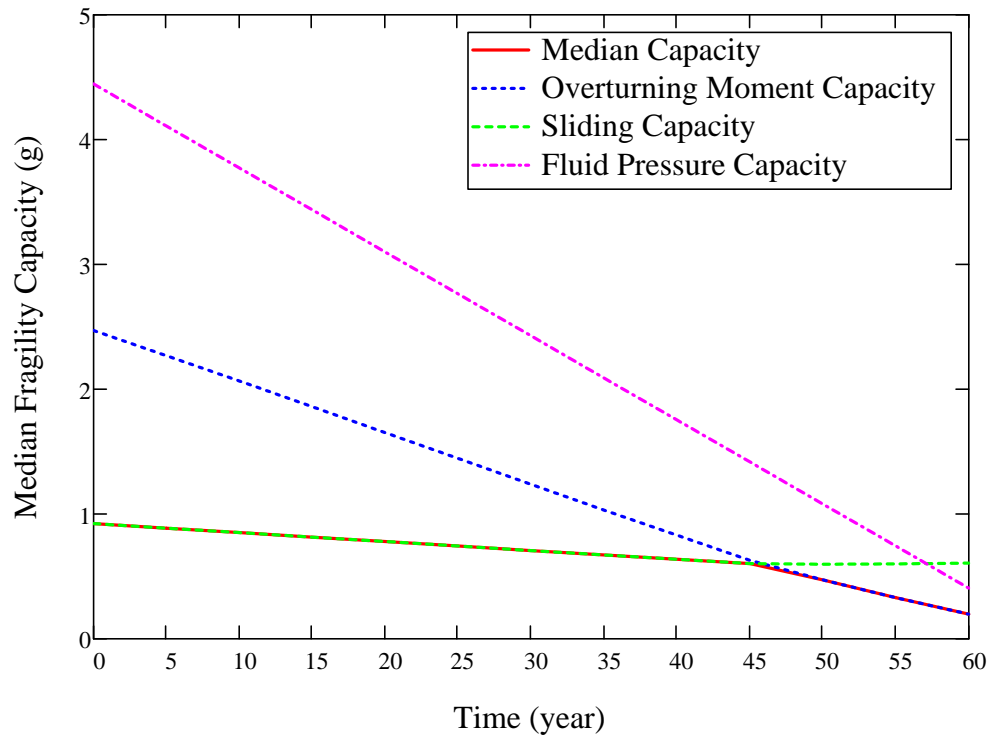
$$F_{mean}(a) := cnorm \left( \frac{\ln \left( \frac{a \cdot g}{SME_m} \right)}{\beta_C} \right)$$

sa := 0.05, 0.1 .. 3



year<sub>i</sub> := i · 5





118 0.152 0.091)<sup>T</sup>·g

152 0.091)<sup>T</sup>·g

277 0.28)<sup>T</sup>·g

343 0.187)<sup>T</sup>·g

THESE DATA ARE THE CONTINUATION OF PAGE B-21.



**Appendix C FRAGILITY ANALYSIS OF THE CST WITH DEGRADED ANCHOR BOLTS**



# KAERI Year 3 Task

## Fragility Analysis of Condensate Storage Tank

### - Degradation Case (B) A36 Anchor Bolt



The power model for steel corrosion was chosen for modeling the degradation of the anchor bolts, from the Year 2 annual report [Nie, et al, 2009]. Parameters  $C$  and  $\alpha$  are identified based on "Performance of weathering steel in bridges," by Albrecht and Naeemi [1984].

For severity consideration, it is conservatively assumed that the Ulchin NPP units 3 & 4 are exposed to a marine condition.

$$C := 70.6$$

$$\alpha := 0.79$$

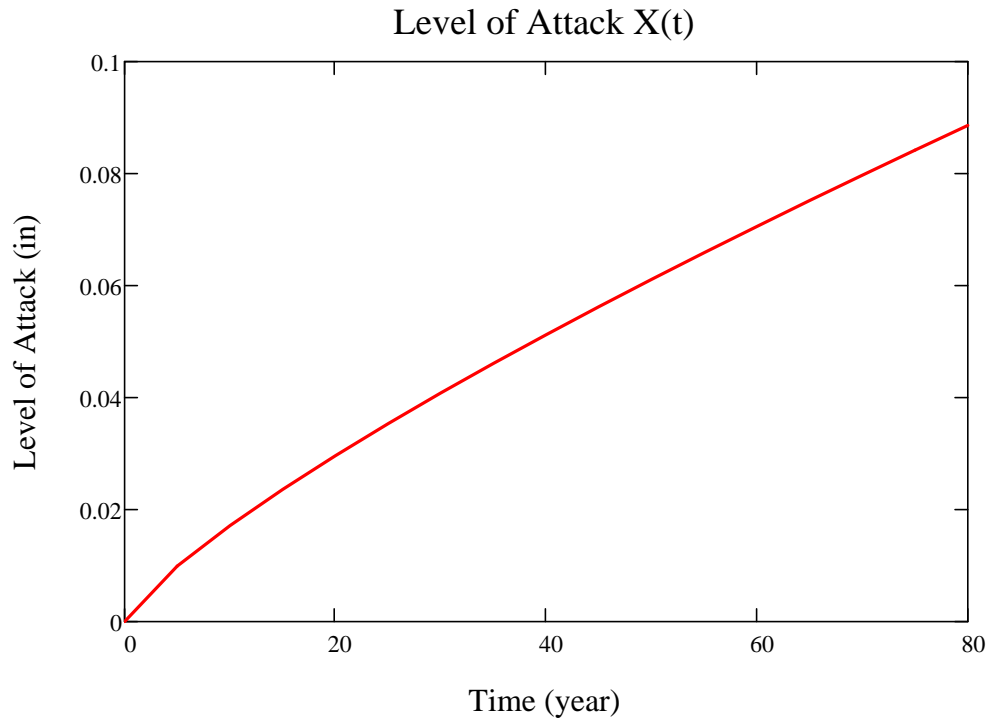
$$X(t) := C \cdot t^\alpha \cdot \mu m$$

$$y := 0,5 \dots 80$$

$$X(y) =$$

0
$9.912 \cdot 10^{-3}$
0.017
0.024
0.03
0.035
0.041
0.046
0.051
...

*·in*



$year := 950$

$Dbolt\_degraded := 2.5in - 2 \cdot X(year) = 1.24858 \cdot in$

## H.1 Introduction

KAERI indicated that the seismic DBE in Korea follows the NRC Reg. Guide 1.60 design spectrum shape but with a PGA level scaled down to 0.2 g. Assuming an initial HCLPF capacity as 1.67 times of 0.2 g:

$$SME_e := 0.34g$$



## H.2 Response Evaluation

Same as Appendix A, Section H.2.



## H.3 Capacity Assessment



The seismic overturning moment capacity of the CST at its base,  $M_{SC}$ , depends

on the axial compressive buckling capacity of the tank shell  $C_m$ , the tensile hold-down capacity of the anchor bolts including their anchorage and attachment to the tank  $T_{BC}$ , and the hold-down capacity of the fluid pressure acting on the tank base plate  $T_e$ .

Although unlikely for larger radius tanks, the tank SME capacity is sometimes governed by the sliding shear capacity at the tank base,  $V_{SC}$ . Even though it does not appear that any butt welded steel tank has ever failed due to seismic induced membrane hoop stresses due to combined hydrostatic and hydrodynamic fluid pressures, the SME capacity of this failure mode,  $P_{CA}$ , should also be checked.

Additional assessment of the seismic capacity may include the possibility and consequence of the fluid sloshing against the tank roof, foundation failure for soil sites, and possibility of failure of piping or their attachment to the tank.

### **H.3.1 Compressive Buckling Capacity of the Tank Shell:**

The most likely buckling for tanks is the "elephant-foot" buckling near the base of the tank shell. The "elephant-foot" buckling is a combined effect of hoop tension, axial (vertical) compression, and restriction of radial deformation of the tank shell by the base plate. "Elephant-foot" buckling does not necessarily lead to failure of a tank (e.g., leakage). However, there is no simple capacity evaluation method that can predict tank performance after the development of "elephant-foot" buckling. Therefore, for a CDFM SME capacity of tanks, the onset of "elephant-foot" buckling will be judged to represent the limit to the compressive buckling capacity of the tank shell. The onset of "elephant-foot" buckling can be estimated using elastic-plastic collapse theory as presented in the following:

The sidewall thickness near the shell base:  $t_s := t_G = 0.625 \cdot in$

The tank internal pressure near its base:  $P := P_{C+} = 1.839 \times 10^5 Pa$

Elastic modulus of the tank:  $E_G = 2.9 \times 10^4 \cdot ksi$

The CST shell is made of SA 204-type 304 stainless steel. This material does not have a flat yield plateau and as strain increases its stress can grow to a minimum ultimate stress capacity of 75 ksi. In the CDFM method, an effective yield stress  $\sigma_{ye}$  is set to  $2.4S_M$  or 45 ksi, in line with the ASME seismic design limit for primary local membrane plus primary bending [ASME 1983, "ASME Boiler & Pressure Vessel Code"]. The potential uncertainty range for  $\sigma_{ye}$  is reported to be between 30 ksi and 60 ksi, according to the original CDFM method description.

$$\sigma_{ye} := 45ksi$$

$$\frac{R}{t_s} = 480.5$$

$$S_I := \frac{R}{t_s} \div 400 = 1.201$$

The "elephant-foot" buckling axial stress of the tank shell can be accurately predicted to be:

$$\sigma_p := \frac{0.6E_S}{R \div t_s} \left[ 1 - \left( \frac{P \cdot R}{\sigma_{ye} \cdot t_s} \right)^2 \right] \cdot \left( 1 - \frac{1}{1.12 + S_I^{1.5}} \right) \cdot \left( \frac{S_I + \frac{\sigma_{ye}}{36 \text{ksi}}}{S_I + 1} \right) = 21.847 \cdot \text{ksi}$$

The compressive buckling capacity for HCLPF capacity computation utilizes a recommended 0.9 reduction factor of the buckling stress:

$$C_m := 0.9 \sigma_p \cdot t_s = 12.289 \cdot \frac{\text{kips}}{\text{in}}$$

Buckling capacity of the supported cylindrical shells under combined axial bending and internal pressure should also be checked although it is unlikely to govern for overall seismic response of fluid containing tanks. The axial bending induced buckling stress,  $\sigma_{CB}$ , for such a load case can be conservatively estimated (essentially lower bound) as follows.

A parameter  $\Delta\gamma$  to be used in the following procedure as an increase factor for internal pressure can be obtained from Figure 6 of "Buckling of Thin-walled Circular Cylinders," [NASA SP-8007].  $\Delta\gamma$  depends on the minimum compression zone pressure at the base of the tank shell,  $P_C$ , corresponding to the time of maximum moment.

Considering the potential range on  $\sigma_{ye}$  of 30 to 60 ksi, the resultant range on  $\sigma_p$  is 16.572 ksi to 26.702 ksi. Consequently,  $C_m$  has a range of 9.322 kips/in to 15.02 kips/in.

$$\frac{P_C \cdot \left( \frac{R}{t_s} \right)^2}{E_S} = 0.14$$

From Figure 6 of NASA SP-8007:  $\Delta\gamma := 0.12$

$$\phi := \frac{1}{16} \cdot \sqrt{\frac{R}{t_s}} = 1.37$$

$$\gamma := 1 - 0.73(1 - e^{-\phi}) = 0.455$$

$$\sigma_{CB} := (0.6\gamma + \Delta\gamma) \frac{E_S}{R \div t_s} = 23.737 \cdot ksi$$

$$0.9\sigma_p = 19.663 \cdot ksi$$

$\sigma_{CB}$  exceeds  $0.9s_p$ , so it does not govern.

### H.3.2 Bolt Hold-down Capacity:

The bolt hold-down capacity should be determined as the smallest of the bolt tensile capacity, anchorage of bolt into concrete foundation, capacity of the top plate of bolt chairs to transfer bolt loads to the vertical chair gussets, attachment of the top plate and vertical chair gussets to the tank shell, and the capacity of tank shell to withstand concentrated loads imposed on it by bolt chairs.

**Anchor bolt capacity:** the anchor bolt has a diameter of 2 1/2" and is made of A36 steel. The tensile capacity can be determined as:

$$d_{bolt} := Dbolt\_degraded = 1.249 \cdot in$$

$$A_{bolt} := \frac{\pi \cdot d_{bolt}^2}{4} = 1.224 \cdot in^2$$

Based on the AISC Code [9th edition, 1989] for threaded A36 bolts:

$$T_{BC} := 1.7A_{bolt} \cdot 19.1ksi = 39.756 \cdot kips \quad T_{BC} = 19.878 \cdot tonf$$

Note that  $T_{BC}$  is the capacity of one bolt and the capacity of the interacting multi-bolts will be considered later.

**Anchor bolt chair capacity check:** according to the drawing, the anchor bolt chairs form a circumferentially continuous construction. Based on the continuous chair construction and the sizing of the plates and weld, it is judged that the anchor bolt chair and its attachment to the tank shell is adequate to transfer the bolt capacity load for the CST. The tank shell is also considered to be adequate in withstanding the concentrated loads imposed on it by bolt chairs, especially because the "elephant-foot" buckling capacity is also checked.

$$t_{chair} := \left(1 + \frac{3}{8}\right) in = 1.375 \cdot in$$

Weld width is 15 mm (5/8") according to the drawing.

**Capacity of bolt anchorage into concrete foundation:** the anchorage is constructed using non-shrinking grout. The tensile failure of bolt anchorage mainly consists of bolt failure, plug pull-out, and concrete cone failure, the last two of

which typically are a combination of tensile failure of concrete in the upper portion of the anchorage that results in a partial depth cone-shaped spall and bond failure at the grout-concrete interface in the lower portion of the anchorage.

$$\text{Bolt spacing: } \Delta d := \pi \cdot \left[ 50\text{ft} + \left( 9 + \frac{1}{16} \right) \text{in} \right] \div 78 = 2.044 \cdot \text{ft}$$

Lee, et al [2001] described an experimental and analytical work on the pull-out strength of large-sized anchor bolt, in a SMiRT 16 paper entitled "failure mechanism for large-sized grouted anchor bolt under tensile load." The test specimens were selected based on the real construction of CST in the Yonggwang Nuclear Power Plant of Korea. The anchor bolt is 2-1/2 inches in diameter, and has an embedment length of 2 ft 2-3/8 inches. The anchor bolt material is ASTM A36. Non-shrinking grout was used in the post-installed anchorage construction. These construction variables are basically very similar to those of the subject CST for fragility analysis, except that the subject CST anchors have a slightly shorter embedment length of 2 ft 1 inch. The concrete strength of the subject CST foundation is not available, and is assumed to be the same as in this SMiRT 16 paper, which has a compressive strength of 4500 psi. The circumferential spacing is about 2 ft for both tanks. The test included 5 anchor bolt specimens.

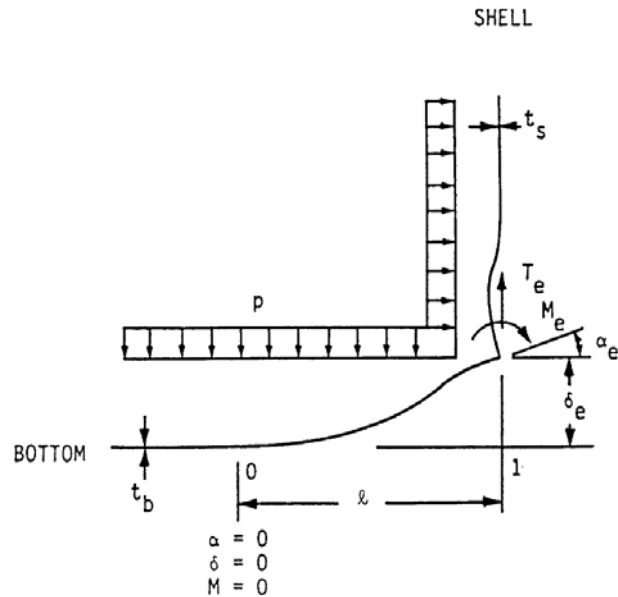
As reported by Lee, et al [2001], the average 7 day and 28 day compressive strength of the concrete were 5419 psi and 7180 psi, respectively. The actual average compressive strength of non-shrinking grout at 7 days and 21 days were 7550 psi and 11100 psi, respectively. The non-shrinking grout has obviously larger compressive strength than the concrete, as expected for normal construction of anchorage. The reported bond strength of the non-shrinking grout (Masterflow 870) was 40 kgf/cm<sup>2</sup> (569 psi). The Young's modulus of A36 is 2.9\*10<sup>7</sup> psi and the Poisson's ratio is 0.3.

The test first confirmed a minimum required load of 50 tons (100 kips). Three of the five grouted anchors were tested further until failure. Two specimens was judged to have failed by tensile failure of grout at the lower portion of the grout block, bonding failure between grout and the concrete, and tensile failure of concrete. The other specimen showed abrasion of anchor bolt thread. All specimens achieved at least 100 tons (200kips), after which the load-deformation curve became significantly flatter and the ultimate failure load scatters between 100 tons and 120 tons.

Based on the test, the anchorage capacity should be 200 kips, which is about 26% higher than the estimate based on tensile strength of the anchor bolt. It should be noted that in the test, one specimen had abrasion in its thread, suggesting the anchor bolt capacity should be also close to 200 kips. However, since the embedment in the test was about 1-3/8 inch longer than the subject CST case, the spacing of anchor bolts in the test is twice as long as in the subject CST case, and the lab test condition usually have a higher quality control, the estimate of 159.387 kips will be assumed as the anchorage capacity.

$$T_{BC} = 39.756 \cdot \text{kips}$$

### H.3.3 Fluid Hold-down Forces:



**Schematic Illustration of Tank Bottom Behavior Near Tensile Region of Tank Shell [NUREG/CR-5270]**

The hold-down force  $T_e$  increases with increasing fluid pressure  $P$ , which consequently assumes the minimum tension zone fluid press  $P_T$ . A number of other related parameters are also defined below.

$$P := P_T = 5.831 \cdot psi$$

$$\nu := 0.3$$

$$I_b := \frac{t_B^3}{12(1 - \nu^2)} = 1.917 \times 10^{-3} \cdot in^3$$

$$t_S = 0.625 \cdot in$$

$$t_B = 7 \cdot mm$$

$$K := \frac{E_S \cdot t_S^3}{12(1 - \nu^2)} = 7.325 \times 10^4 J$$

$$\kappa := \left[ \frac{R}{t_S} \cdot \sqrt{3(1 - \nu^2)} \right]^{0.5} = 28.177$$

$$MFP := \frac{R \cdot t_S}{\sqrt{12(1 - \nu^2)}} \left( 1 - \frac{R}{H \cdot \kappa} \right) = 0.036 m^2$$

MFP is a shortcut to  $M_F / P$

$$K_S := \frac{2 \cdot K \cdot \kappa}{R} = 5.412 \times 10^5 N$$

The uplift height  $\delta_e$ , the hold down tension  $T_e$ , moment  $M_e$ , rotation  $\alpha_e$ , and maximum positive moment  $M_+$  can then be defined as functions of uplift length  $l$ :

$$F(l) := 1 + \frac{K_S \cdot l}{2E_S \cdot I_b}$$

$$\delta_e(l) := \left[ \frac{l^4}{24} - \frac{1}{F(l)} \left( \frac{K_S \cdot l^5}{72E_S \cdot I_b} + MFP \cdot \frac{l^2}{6} \right) \right] \cdot \left( \frac{P}{E_S \cdot I_b} \right)$$

$$T_e(l) := P \cdot \left[ \frac{l}{2} + \frac{1}{F(l)} \cdot \left( \frac{K_S \cdot l^2}{12E_S \cdot I_b} + \frac{MFP}{l} \right) \right]$$

Note: this equation as in the original CDFM method is singular at  $L = 0$  ft. The  $MFP/L$  term only has a minor effect on  $L/R \leq 0.15$ . The solution does not consider the stiffening effect of hoop behavior on the base plate and consequently conservatively overpredicts the displacement  $\delta_e$ , as the ratio of  $L/R$  becomes larger.  $T_e$  when  $L$  is very small. The linear approximation in the original CDFM method can effectively avoid this singularity.

$$M_e(l) := P \cdot \left( \frac{1}{F(l)} \right) \cdot \left( \frac{K_S \cdot l^3}{12E_S \cdot I_b} + MFP \right)$$

$$M_+(l) := P \cdot \left( \frac{l^2}{8} - \frac{M_e(l)}{2P} + \frac{M_e(l)^2}{2P^2 \cdot l^2} \right)$$

The singularity in this equation can be similarly avoided by the linear approximation.

$$\alpha_e(l) := \frac{P \cdot l^3}{12E_S \cdot I_b} - \frac{M_e(l) \cdot l}{2E_S \cdot I_b}$$

Given

$$l := 0 \text{ in}$$

$$\frac{l^2}{24} - \frac{1}{F(l)} \left( \frac{K_S \cdot l^3}{72E_S \cdot I_b} + MFP \cdot \frac{1}{6} \right) = 0$$

$$lmin := Find(l) = 7.65 \cdot in$$

Given

$$lmax := 10in$$

$$\delta_e(lmax) = 0.165in$$

$$lmax := Find(lmax) = 18.34 \cdot in$$

$$l := lmin, lmin + 0.1in .. lmax$$

Linear Approximation:

$$i := 0 .. \frac{(lmax - lmin)}{0.1in}$$

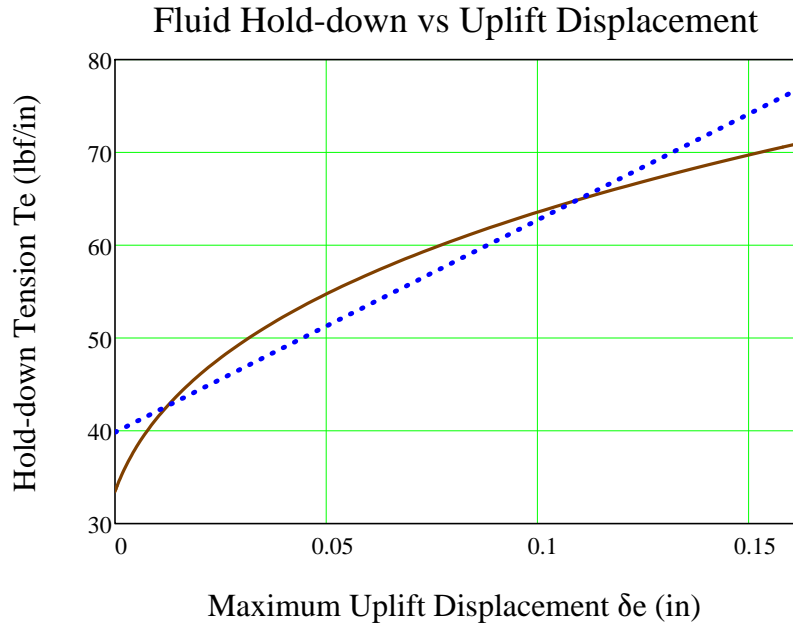
$$l\_vec_i := lmin + i \cdot 0.1 \cdot in$$

$$\begin{pmatrix} T_{e0} \\ T_{e1} \end{pmatrix} := line \left[ \frac{\delta_e(l\_vec)}{in}, \left( T_e(l\_vec) \cdot \frac{in}{lbf} \right) \right] = \begin{pmatrix} 39.846 \\ 228.734 \end{pmatrix}$$

$$T_{e0} := if(P_{T-} > 0psi, T_{e0}, 0) \frac{lbf}{in} = 39.846 \cdot \frac{lbf}{in}$$

$$T_{e1} := if(P_{T-} > 0psi, T_{e1}, 0) \cdot \frac{lbf}{in^2} = 228.734 \cdot \frac{lbf}{in^2}$$

$$T_{e\_lin}(\delta_e) := T_{e0} + T_{e1} \cdot \delta_e$$



It should be noted that these equations are derived based on small displacement theory, and are applicable to the following conditions:

1.  $L / R \leq 0.15$ . The solution does not consider the stiffening effect of hoop behavior on the base plate and consequently conservatively overpredicts the displacement  $\delta_e$ , as the ratio of  $L/R$  becomes larger.
2.  $\delta_e / t_b \leq 0.6$ . As the solution is based on small displacement assumption, which ignores the beneficial influence of the membrane tension in the base plate to reduce  $\delta_e$  for a given  $T_e$  as in large displacement theory. For unanchored tanks, Manos (in "earthquake tank-wall stability of unanchored tanks," *Journal of Structural Engineering*, Vol 112, No. 8, ASCE, 1986) and Haroun and Badawi (in "nonlinear axisymmetric uplift of circular plates," *Dynamics of Structures*, ASCE, 1987) showed that large displacement membrane theory greatly increases the fluid hold-down force  $T_e$  and consequently the uplift  $\delta_e$ . Nevertheless, for anchored tanks like the subject CST, the uplift is not expected to be very large.
3.  $M_e/M_{pb} \leq 0.9$ ;  $M_e/M_{ps} \leq 0.9$ ; and  $M_+/M_{pb} \leq 0.9$ , where  $M_{pb}$  and  $M_{ps}$  are the plastic moment capacity of the base plate and shell sidewalls, respectively. These equations are derived from elastic solution, and these conditions prevent the potential unconservatism.

$$0.6t_B = 0.165 \cdot in$$

The second requirement leads to maximum  $\delta_e$  of 0.165 in, beyond which the small displacement theory becomes increasingly conservative. The original CDFM solved the problem by making a linear approximation of the  $\delta_e$ - $T_e$  curve in a range of  $\delta_e=0$  to  $0.6t_B$ , and then use the linear equation to extrapolate beyond the  $0.6t_B$  to partially account for membrane tension effects. This approach will also be used in this study.

$$T_e := T_{e\_lin}$$

**Assessment of the upper limit on the fluid hold-down force:** based on a yield stress  $\sigma_y$  of 30 ksi, and an ultimate stress of 75 ksi, the fully plastic moment capacity  $M_{pb}$  of the 7 mm base plate is estimated to be 0.949 kips-inch/inch when the outer fiber reaches 75 ksi. It is also assumed that the effective hoop compressive yield stress  $\sigma_{ye}$  is equal to 45 ksi. The upper limit of the horizontal component of the membrane tension  $F_H$  can be found to be:

$$\sigma_{ye} = 45 \cdot \text{ksi}$$

$$M_{pb} := \frac{t_B^3}{12} \div \left( \frac{t_B}{2} \right) \cdot 75 \text{ksi} = 0.949 \cdot \frac{\text{kips} \cdot \text{in}}{\text{in}}$$

$$F_H := \frac{\sigma_{ye} \cdot t_S}{2\kappa} + \frac{M_{pb} \cdot \kappa}{R} = 0.588 \cdot \frac{\text{kips}}{\text{in}}$$

$$(4M_{pb}P_T)^{0.5} = 148.811 \cdot \frac{\text{lb}f}{\text{in}}$$

$$\frac{F_H}{2M_{pb}} = 0.31 \cdot \frac{1}{\text{in}}$$

Thus, the upper limit of the fluid hold-down force is estimated to be:

$$T_m(\delta_e) := 168.841 \frac{\text{lb}f}{\text{in}} \left( 1 + \frac{0.31 \cdot \delta_e}{\text{in}} \right)^{0.5}$$

The maximum  $\delta_e$  can be found by equating  $T_e$  and  $T_m$ :

Given

$$\delta_{ee} := 0.15 \text{in}$$

$$T_e(\delta_{ee}) = T_m(\delta_{ee})$$

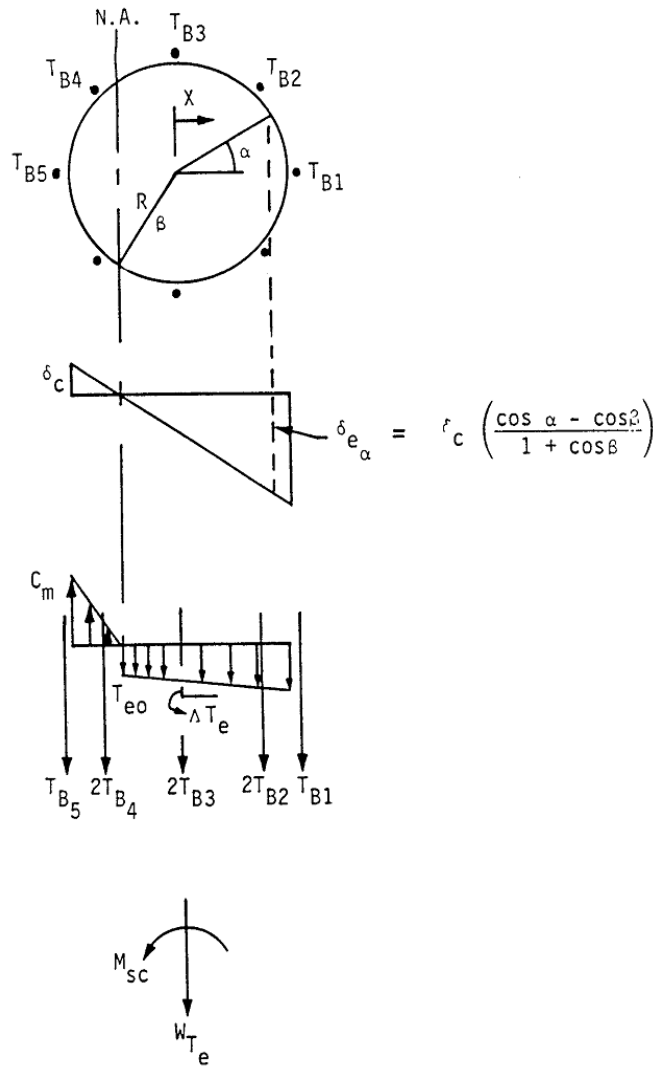
$$\delta_{ee} := \text{Find}(\delta_{ee}) = 0.633 \cdot \text{in}$$

Therefore, the linearized equation for  $T_e$  should not be extrapolated beyond  $\delta_e = 1.805$  inch.

Note that linearization is necessary later when developing overturning moment capacity.



### H.3.4 Overturning Moment Capacity:



### Vertical Loading on Tank Shell at Base [NUREG/CR-5270]

The overturning moment capacity  $M_{SC}$  can be estimated using the compressive

buckling capacity of the tank shell ( $C_B$ ), the anchor bolt hold-down capacity ( $T_{BC}$ ), and the relationship between fluid hold-down force and uplift displacement. The estimation approach in the CDFM method requires several conservative but reasonable assumptions as noted below:

1. The bottom of the tank shell is assumed to rotate rigidly about the neutral axis (plane sections remain plane).
2. The cross-section of the tank at the top of the top plate of the bolt chairs ( $h_c$  above the base) is assumed to remain horizontal so that all vertical tank distortions needed to result in base uplift and mobilization of the anchor bolts must be accommodated over the height  $h_c$ .
3. The compressive stress varies linearly from zero at the neutral axis ( $\alpha=\beta$  as in the figure above) to its maximum value  $C_m$  at  $\alpha=180^\circ$ , as given by  $C_m = E_s t_s \delta_c / h_c \leq C_B$  (by converting eq. H-39), where  $\delta_c$  is the maximum compressive shortening.

Summary of parameters:

$$C_m = 12.289 \cdot \frac{\text{kips}}{\text{in}} \quad T_{BC} = 39.756 \cdot \text{kips}$$

$$T_{e0} = 0.04 \cdot \frac{\text{kips}}{\text{in}} \quad T_{e1} = 0.229 \cdot \frac{\text{kips}}{\text{in}^2}$$

$$W_{Te} = 183.444 \cdot \text{kips} \quad A_B := A_{bolt} \quad A_B = 1.224 \cdot \text{in}^2$$

$$E_B := 29 \times 10^3 \text{ksi}$$

$$R = 25.026 \cdot \text{ft}$$

$$t_s = 0.625 \cdot \text{in} \quad E_s := E_S = 29 \times 10^3 \cdot \text{ksi}$$

$$h_c := 207 \text{mm} = 8.15 \cdot \text{in}$$

$$h_a := 2 \text{ft} + 1 \text{in} = 25 \cdot \text{in}$$

Using the approach outlined in NUREG/CR-5270 instead of the EPRI NP-6041-SL appendix H in the following:

$$\delta_c := \frac{C_m \cdot h_c}{E_s \cdot t_s} = 5.526 \times 10^{-3} \cdot \text{in}$$

$$K_B := \frac{\delta_c \cdot A_B \cdot E_B}{h_a + h_c} = 5.919 \cdot \text{kips}$$

$$\Delta T_e := T_{eI} \cdot \delta_c = 1.264 \times 10^{-3} \cdot \frac{\text{kips}}{\text{in}}$$

$$\delta_{ea}(a,b) := \delta_c \cdot \left( \frac{\cos(a) - \cos(b)}{1 + \cos(b)} \right)$$

Because the bolt pretension  $T_{BP}$  is unreliable after a number of years in service, it is conservatively assumed to be 0.

$$T_{BP} := 0 \text{ kips}$$

The neutral axis angle  $\beta$  can be determined iteratively using the following procedure.

Bolt locations:  $i := 0..77$

$$\alpha_i := \frac{2\pi}{78} i$$

$$T_{func}(\alpha, \beta) := \begin{cases} c \leftarrow T_{BP} + K_B \cdot \frac{\cos(\alpha) - \cos(\beta)}{1 + \cos(\beta)} \\ c \leftarrow T_{BC} \text{ if } c > T_{BC} \\ c \leftarrow 0 \text{ if } c < 0 \end{cases}$$

$$C_1(\beta) := \frac{1 + \cos(\beta)}{\sin(\beta) + (\pi - \beta)\cos(\beta)}$$

$$C_2(\beta) := \frac{\sin(\beta)\cos(\beta) + \pi - \beta}{1 + \cos(\beta)}$$

$$C_3(\beta) := \frac{\sin(\beta) - \beta \cdot \cos(\beta)}{\sin(\beta) + (\pi - \beta)\cos(\beta)}$$

$$C_4(\beta) := \frac{\beta - \sin(\beta)\cos(\beta)}{1 + \cos(\beta)}$$

$$T_B(\alpha, \beta) := \overrightarrow{T_{func}(\alpha, \beta)}$$

$$Cf'_m(\alpha, \beta) := \left( \frac{W_{Te} + \sum T_B(\alpha, \beta)}{2R} + T_{e0} \cdot \beta \right) \cdot C_1(\beta) + \Delta T_e \cdot C_3(\beta)$$

Equating  $Cf'_m$  and  $C_m$  to determine  $\beta$ :

$$func(\alpha, \beta) := Cf'_m(\alpha, \beta) - C_m$$

$$\beta := \text{root}(func(\alpha, \beta), \beta, 0, 3.1)$$

$$\beta = 2.65998 \quad \beta \cdot \frac{180}{\pi} = 152.406$$

$$C'_m := C'_m(\alpha, \beta) = 12.289 \cdot \frac{\text{kips}}{\text{in}} \quad C_m = 12.289 \cdot \frac{\text{kips}}{\text{in}}$$

Use  $C'_m$  and  $\beta$  to find the overturning moment capacity  $M_{SC}$ :

$$M_{SC} := C'_m \cdot C_2(\beta) \cdot R^2 + \sum \left( \overrightarrow{T_B(\alpha, \beta) \cdot R \cdot \cos(\alpha)} \right) + T_{e0} \cdot R^2 \cdot 2 \cdot \sin(\beta) + \Delta T_e \cdot C_4(\beta) \cdot R^2$$

$$M_{SC} = 78565.847 \cdot \text{kips} \cdot \text{ft}$$

$$\sum T_B(\alpha, \beta) = 2.095 \times 10^3 \cdot \text{kips}$$

The largest bolt elongation (at  $\alpha=0$ ) should be checked to ensure that the anchorage has the capability:

$$\delta_{e0} := \delta_{ea}(\alpha_0, \beta) = 0.092 \cdot \text{in}$$

$$\text{Elongation ratio: } \frac{\delta_{e0}}{h_a + h_c} = 0.276 \cdot \%$$

The maximum elongation ratio is much smaller than 1%, which is recommended in the original CDFM method for the A307 bolt. One percent is also considered to be an appropriate percentage value for the A36 anchor bolt used in the subject CST construction.

The maximum tank shell uplift distortion  $\delta_{e0} = 0.026$  in, which is much less than the limit of 0.165 in for the small displacement theory to be applicable in developing the fluid hold-down capacity.

Because there are 78 anchor bolts (the example tank in the original CDFM method had only 8), the case where  $\alpha=0$  lies midway between bolts need not be checked.

The uncertainty in HCLPF buckling capacity of the tank shell due to the uncertain  $\sigma_{ye}$  can lead to an  $M_{SC}$  as low as 119133.414 kips-ft or as high as 192156.702 kips-ft. It should be noted that unlike in the original CDFM method,  $M_{SC}$  is sensitive to the estimate of  $C_m$ .

Inelastic energy absorption reduction factor  $k$  can be applied to linearly computed seismic response to obtain the actual overturning moment capacity. The combined bolt yielding and tank shell buckling failure mode for overturning moment is not brittle so that  $k$  can be less than unity. However, as stated in the original CDFM method, it

is difficult to make an appropriate estimate of  $k$  for this failure mode. Therefore, it is conservatively assumed to be unity.

$$k := 1.0$$

$$SME_M := \frac{M_{SC}}{k \cdot M_{SH}} \cdot SME_e \qquad SME_M = 0.582 \cdot g$$

Since  $SME_M$  is substantially different from  $SME_e$ , the above procedure should be iterated to obtain the appropriate SME estimate. The resultant  $SME_e$  is found to be 0.97g.



### **H.3.5 Sliding Capacity:**



The base plate of the CST has a slight cone ( with a slope of 1 to 96) so that the fluid will always drain away from the center of the tank. This cone is generally created by variable thickness of the oiled sand cushion between the tank bottom plate and its foundation. Therefore, the coefficient of friction between the tank base and its foundation is reasonably assumed to have a conservative value of 0.55:

$$COF := 0.55$$

The sliding shear capacity can then be calculated as,

$$V_{SC} := COF \cdot \left( W_{Te} + P_a \cdot \pi \cdot R^2 + \sum T_B(\alpha, \beta) \right) = 3.076 \times 10^3 \cdot kips$$

The shear capacity of the bolts should not be considered because (a) there is a large space between the concrete foundation and the anchor bolt chair, and (b) there is a 1/4" diametric clearance in the hole in the anchor bolt chair.

The sliding capacity with a unit inelastic absorption factor as suggested by the original CDFM method:

$$SME_V := \frac{V_{SC}}{k \cdot V_{SH}} \cdot SME_e \qquad SME_V = 0.339 \cdot g$$

By varying  $SME_e$ , the HCLPF shear capacity is found to be 0.555g.

Unlike the example tank in the original CDFM method, the capacity of the CST appears to be governed by the sliding capacity. The sliding capacity considers only the friction between the bottom plate and the foundation.



### H.3.6 Fluid Pressure Capacity:

---



The inelastic energy absorption seismic response reduction factor  $k_u$  is suggested to be 0.8 for HCLPF capacity evaluation:

$$k_u := 0.8$$

For the CDFM hoop membrane stress capacity, it is recommended that the ASME seismic design limit of  $2 S_M$  for primary stress should be used, which is 37.5 ksi for SA240-type 304 stainless steel:

$$\sigma_a := 37.5 \text{ ksi}$$

The pressure capacity,  $P_{CA}$ , at the bottom of the tank shell (the CST has a uniform shell thickness), can be estimated to be:

$$P_{CA}(t) := \frac{\sigma_a \cdot t}{R}$$
$$P_{CA}(t_S) = 78.044 \cdot \text{psi}$$

The maximum seismic induced hydrodynamic pressures  $P_{SM}$  and the hydrostatic pressure  $P_{ST}$  at the bottom of the tank shell are:

$$P_{SM}(H) = 8.826 \times 10^4 \text{ Pa}$$

$$P_{ST}(H) = 1.12 \times 10^5 \text{ Pa}$$

The HCLPF fluid pressure capacity  $SME_p$  can be determined as:

$$SME_p := \frac{P_{CA}(t_S) - P_{ST}(H)}{k_u \cdot P_{SM}(H)} \cdot SME_e = 2.052 \cdot g$$

By varying  $SME_e$ , the HCLPF fluid pressure capacity can be found to be 2.191 g, which does not govern. This agrees with seismic experience that the fluid pressure capacity seldom appears to govern the seismic capacity for normal flat bottomed steel tanks with butt-welded side plates.



---

Summary of SME capacities:

$$SME_M = 0.582 \cdot g$$

$$SME_V = 0.339 \cdot g$$

$$SME_p = 2.052 \cdot g$$

$$SME_{cr} := \min(SME_M, SME_V, SME_p) = 0.339 \cdot g$$

$$SME_e = 0.34 \cdot g$$

$$if[SME_{cr} = SME_M, "Moment", (if(SME_{cr} = SME_V, "Shear", "Fluid Pressure"))] = "Shear"$$

$$d_{bolt} = 1.249 \cdot in$$

Summary of results:

Years:	0	5	10	15	20	25	30	35	40
db (in):	2.5	2.48	2.466	2.453	2.441	2.429	2.418	2.408	2.398
SME:	0.426	0.425	0.424	0.423	0.423	0.422	0.422	0.422	0.421
SMEM:	1.140	1.136	1.132	1.129	1.126	1.123	1.120	1.117	1.115
SMEV:	0.426	0.425	0.424	0.423	0.423	0.422	0.422	0.422	0.421
SMEP:	2.052	2.052	2.052	2.052	2.052	2.052	2.052	2.052	2.052
Mode:	Shear								
Years:	45	50	55	60	65	70	75	80	
db (in):								2.323	
SME:		0.42		0.42		0.419		0.418	
SMEM:		1.11		1.105		1.100		1.095	
SMEV:		0.42		0.42		0.419		0.418	
SMEP:		2.052		2.052		2.052		2.052	
Mode:	Shear								

Even with a degradation level of half of bolt diameter, the SME is still as high as 0.34 g and shear failure mode still dominates. The overturning moment capacity is about 0.582 g at this level of degradation (approximate 950 years using the current power model) and the fluid pressure capacity remains unchanged as expected. This high level of SME capacity and reliability is believed to be attributed to the large number of bolts.

### H.3.7 Consideration of Other Capacities:

(1) Slosh height for roof damage: note that even with a  $SME_e = 0.334 \text{ g}$  (the initial guess), the slosh height is about 4.8 ft. With the HCLPF shear capacity of  $SME_e = 0.555 \text{ g}$ , the sloshing height can be about 7.9 ft, which is close to the total height of the head (8.7', as approximated in the beginning part of this calculation).

$$h_s = 4.863 \cdot ft$$

$$SME_e = 0.34 \cdot g$$

The increase of sloshing height is not significant as  $SME_e$  increases from 0.334 g to 0.555 g. In addition, as pointed out in the original CDFM method, even if roof damage might be expected, such damage usually does not impair the ability of the tank to contain fluid.

(2) The CST is assumed to sit on rock/very stiff soil; therefore, soil-tank foundation interaction is not considered.

(3) Piping failure or failure of nozzles may lead to loss of fluid in the tank, and more importantly, may impair the normal function of the condensation system. As reported in the original CDFM method, a significant fraction of the cases of seismic induced loss of tank contents have been due to piping/nozzle failures because of poor detailing. The CDFM method also stated that a SME evaluation of piping/nozzle failure is only necessary when poor seismic detailing is found in the involved piping attached to the tank. This analysis assumes that the subject CST is appropriately detailed, i.e. the piping and nozzle directly attached to the tank are properly designed and constructed so that sufficient piping flexibility can be achieved to accommodate large relative seismic anchor movements.

(4) The influence of the building in between the two CSTs on the SME are assessed in the following. The gap between the auxiliary building and the CSTs at the roof level is filled with elastomeric sealant.

The maximum tank shell uplift distortion is found to be 0.026 in, which corresponds to a neutral axis angle  $\beta$  of 2.29161 rad. Since the horizontal plane at the anchor bolt chair is assumed to remain plane and all distortion is assumed to occur below this level, the rotation angle around the neutral axis can be estimated to be:

$$Rotation := \frac{\delta_{e0}}{R \cdot (1 - \cos(\beta))} = 1.618 \times 10^{-4}$$

$$\beta = 2.66 \quad \cos(\beta) = -0.886$$

The maximum horizontal displacement at the roof of the auxiliary building, which is at an elevation of 114' 9" (Parapet elevation, compared to the tank floor elevation of 101' 9"), can be estimated to be:

$$Rotation \cdot 13ft = 0.025 \cdot in$$

This horizontal displacement is much less than the width of the seismic separation joint at the roof elevation, which is 3 in. Therefore, the influence of the auxiliary building to the two CSTs is considered minimal.

## The Fragility of CST

### Summary of results:

Years:	0	5	10	15	20	25	30	35	40
db (in):	2.5	2.48	2.466	2.453	2.441	2.429	2.418	2.408	2.398
SME:	0.426	0.425	0.424	0.423	0.423	0.422	0.422	0.422	0.421
SMEM:	1.140	1.136	1.132	1.129	1.126	1.123	1.120	1.117	1.115
SMEV:	0.426	0.425	0.424	0.423	0.423	0.422	0.422	0.422	0.421
SMEP:	2.052	2.052	2.052	2.052	2.052	2.052	2.052	2.052	2.052
Mode:	Shear								

Years:	45	50	55	60	65	70	75	80
db (in):								2.323
SME:		0.42		0.42		0.419		0.418
SMEM:		1.11		1.105		1.100		1.095
SMEV:		0.42		0.42		0.419		0.418
SMEP:		2.052		2.052		2.052		2.052
Mode:	Shear							

$$SME_{HCLPF} := (0.426 \ 0.425 \ 0.424 \ 0.423 \ 0.423 \ 0.423 \ 0.422 \ 0.422 \ 0.422 \ 0.421 \ 0.42 \ 0.42 \ 0.42)$$

$$SME_M := (1.140 \ 1.136 \ 1.132 \ 1.129 \ 1.126 \ 1.123 \ 1.120 \ 1.117 \ 1.115 \ 1.11 \ 1.105 \ 1.100)$$

$$SME_V := (0.426 \ 0.425 \ 0.424 \ 0.423 \ 0.423 \ 0.422 \ 0.422 \ 0.422 \ 0.421 \ 0.42 \ 0.42 \ 0.419)$$

$$SME_P := (2.052 \ 2.052 \ 2.052 \ 2.052 \ 2.052 \ 2.052 \ 2.052 \ 2.052 \ 2.052 \ 2.052 \ 2.052 \ 2.052)$$

It should be emphasized that the HCLPF SME capacity assumes the Regulatory Guide 1.60 spectra anchored to the HCLPF SME PGA.

To determine the seismic fragility of the CST, one needs to convert the HCLPF SME PGA to median SME PGA. This conversion requires the estimate of both aleatory and epistemic uncertainties ( $\beta_R$  and  $\beta_U$ ). The Fragility Method, also presented along with the original CDFM method, estimates the aleatory and epistemic uncertainties to be 0.2 and 0.27, respectively. These uncertainties are nearly identical to those reported by Choun, et al [2008]. The SME median  $SME_m$  can then be estimated as well.

$$i := 0, 1 \dots 12$$

$$\beta_R := 0.2$$

$$\beta_U := 0.27$$

$$\beta_C := \sqrt{\beta_R^2 + \beta_U^2} = 0.336$$

$$Hm := \exp[1.645(\beta_R + \beta_U)] = 2.167$$

$$SME_{m_i} := SME_{HCLPF_i} \cdot Hm$$

$$SME_{Mm_i} := SME_{M_i} \cdot Hm$$

$$SME_{Vm_i} := SME_{V_i} \cdot Hm$$

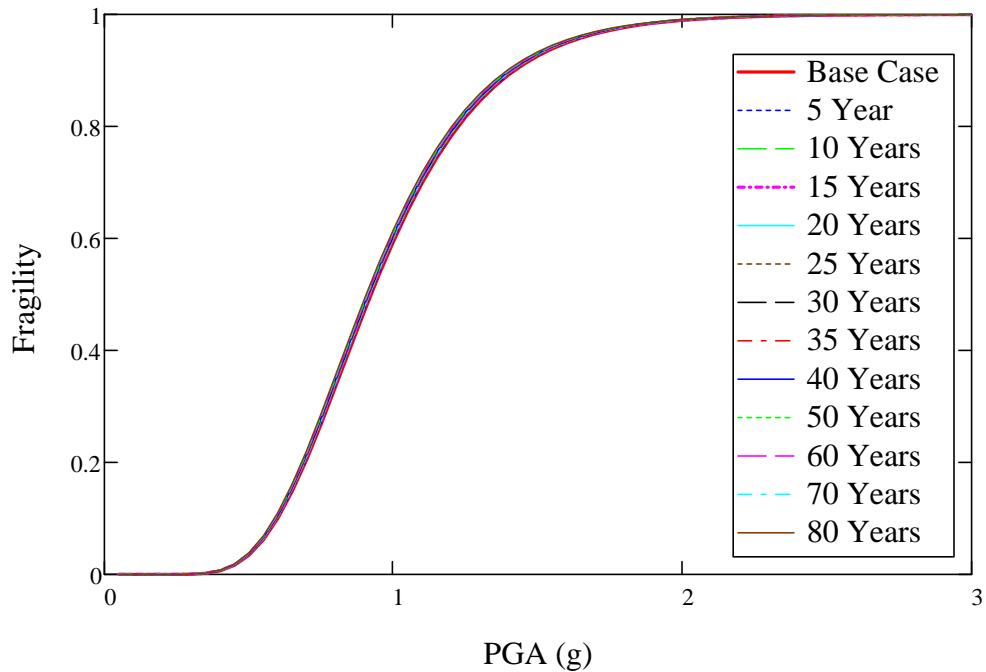
$$SME_{Pm_i} := SME_{P_i} \cdot Hm$$

$$F(Q, a) := cnorm \left( \frac{\ln \left( \frac{a \cdot g}{SME_m} \right) + \beta_U \cdot qnorm(Q, 0, 1)}{\beta_R} \right)$$

$$F_{mean}(a) := cnorm \left( \frac{\ln \left( \frac{a \cdot g}{SME_m} \right)}{\beta_C} \right)$$

sa := 0.05, 0.1 .. 3

Mean CST Fragilities with Degradation of Anchor Bolts



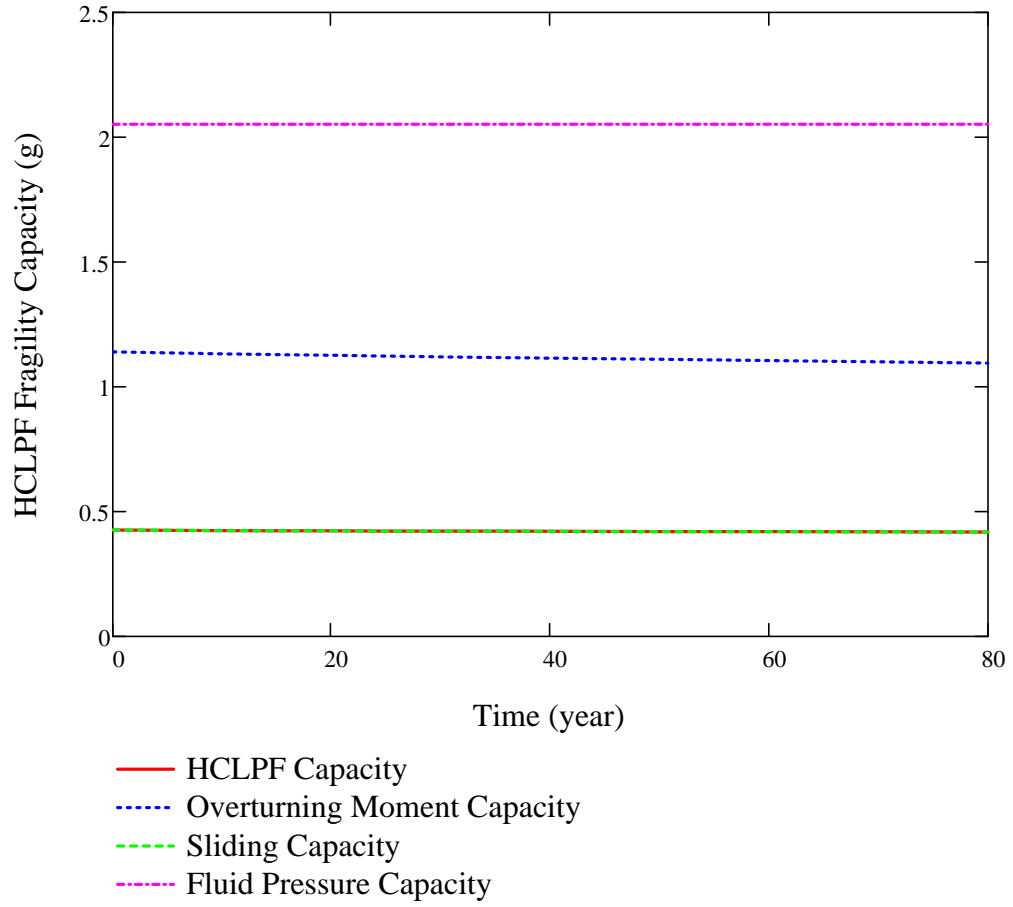
year<sub>i</sub> := i · 5

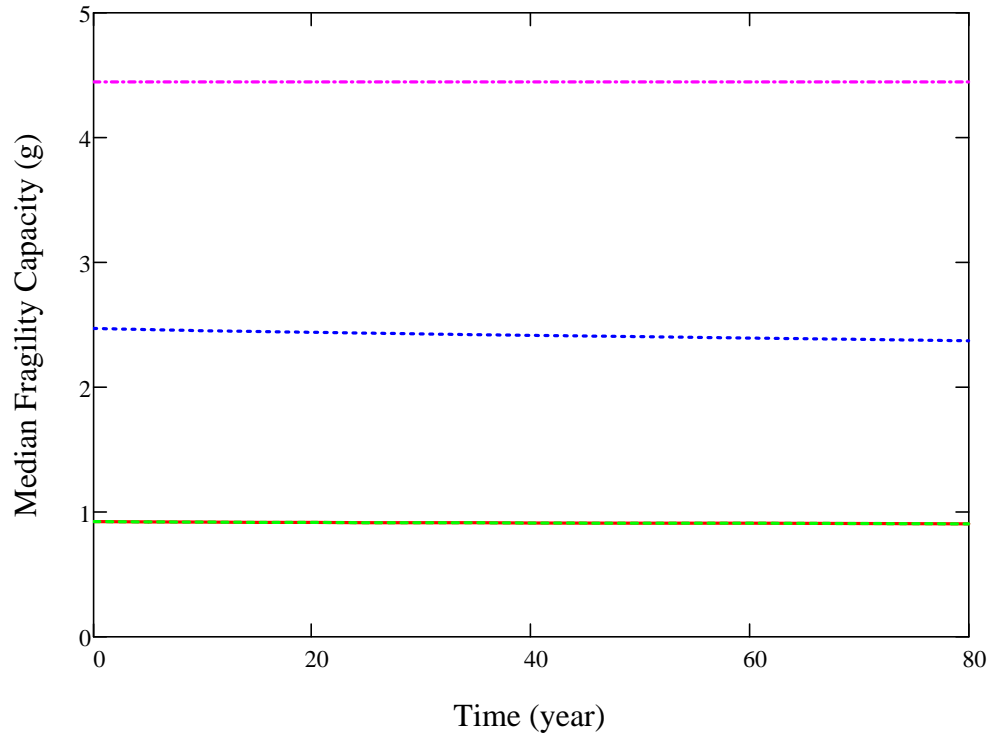
year<sub>9</sub> := 50

year<sub>11</sub> := 70

$year_{10} := 60$

$year_{12} := 80$





0.419 0.418)<sup>T</sup>.g

1 1.095)<sup>T</sup>.g

0.418)<sup>T</sup>.g

2 2.052)<sup>T</sup>.g

THESE DATA ARE THE CONTINUATION OF PAGE C-20.

**Appendix D FRAGILITY ANALYSIS OF THE CST WITH FOUNDATION CONCRETE  
CRACKING – APPLICATION OF MODEL C-1**



# KAERI Year 3 Task

## Fragility Analysis of Condensate Storage Tank

### - Degradation Case (C-1) Anchorage (concrete) Degradation

---



This case utilizes the concrete degradation data recorded in Korea NPPs and test data of dynamic anchorage strength with simulated cracks in concrete as reported in NUREG/CR-5434.

The anchorage strength is the smaller of the bolt strength (base case) and the anchorage strength attributed to concrete with various levels of degradation.

The grouted anchors used NURE/CR-5434 have a diameter of 3/4" and (effective) embedment of 4". Both dimensions are much smaller than the anchorage in the CST construction. Therefore, the data in NUREG/CR-5434 will be used as scaling factors.

Crack width regression curve provided by KAERI data is used to predict the crack width.



$$year := 80$$

$$crack := (0.001194818398 \cdot year + 0.1079928957) \cdot mm = 0.204 \cdot mm$$

## H.1 Introduction

KAERI indicated that the seismic DBE in Korea follows the NRC Reg. Guide 1.60 design spectrum shape but with a PGA level scaled down to 0.2 g. An initial HCLPF capacity was assumed to be 1.67 times of 0.2 g. However, since the Mathcad sheets in this appendix solve the various equations iteratively by manually setting  $SME_e$  to different values, the following  $SME_e$  value of 0.423 g represents the converged solution for the degradation level of the anchorage (concrete) at 80 years.

$$SME_e := 0.423g$$



## H.2 Response Evaluation

Same as Appendix A, Section H.2.



## H.3 Capacity Assessment



The seismic overturning moment capacity of the CST at its base,  $M_{SC}$ , depends on the axial compressive buckling capacity of the tank shell  $C_m$ , the tensile hold-down capacity of the anchor bolts including their anchorage and attachment to the tank  $T_{BC}$ , and the hold-down capacity of the fluid pressure acting on the tank base plate  $T_e$ .

Although unlikely for larger radius tanks, the tank SME capacity is sometimes governed by the sliding shear capacity at the tank base,  $V_{SC}$ . Even though it does not appear that any butt welded steel tank has ever failed due to seismic induced membrane hoop stresses due to combined hydrostatic and hydrodynamic fluid pressures, the SME capacity of this failure mode,  $P_{CA}$ , should also be checked.

Additional assessment of the seismic capacity may include the possibility and consequence of the fluid sloshing against the tank roof, foundation failure for soil sites, and possibility of failure of piping or their attachment to the tank.

### H.3.1 Compressive Buckling Capacity of the Tank Shell:

The most likely buckling for tanks is the "elephant-foot" buckling near the base of the tank shell. The "elephant-foot" buckling is a combined effect of hoop tension, axial (vertical) compression, and restriction of radial deformation of the tank shell by the base plate. "Elephant-foot" buckling does not necessarily lead to failure of a tank (e.g., leakage). However, there is no simple capability evaluation method that can predict tank performance after the development of "elephant-foot" buckling. Therefore, for a CDFM SME capacity of tanks, the onset of "elephant-foot" buckling will be judged to represent the limit to the compressive buckling capacity of the tank shell. The onset of "elephant-foot" buckling can be estimated using elastic-plastic collapse theory as presented in the following:

The sidewall thickness near the shell base:  $t_s := t_S = 0.625 \cdot in$

The tank internal pressure near its base:  $P := P_{C+} = 2.014 \times 10^5 Pa$

Elastic modulus of the tank:  $E_S = 2.9 \times 10^4 \cdot ksi$

The CST shell is made of SA 204-type 304 stainless steel. This material does not have a flat yield plateau and as strain increases its stress can grow to a minimum ultimate stress capacity of 75 ksi. In the CDFM method, an effective yield stress  $\sigma_{ye}$  is set to  $2.4S_M$  or 45 ksi, in line with the ASME seismic design limit for primary local membrane plus primary bending [ASME 1983, "ASME Boiler & Pressure Vessel Code"]. The potential uncertainty range for  $\sigma_{ye}$  is reported to be between 30 ksi and 60 ksi, according to the original CDFM method description.

$$\sigma_{ye} := 45 \text{ksi}$$

$$\frac{R}{t_s} = 480.5$$

$$S_I := \frac{R}{t_s} \div 400 = 1.201$$

The "elephant-foot" buckling axial stress of the tank shell can be accurately predicted to be:

$$\sigma_p := \frac{0.6E_S}{R \div t_s} \left[ 1 - \left( \frac{P \cdot R}{\sigma_{ye} \cdot t_s} \right)^2 \right] \cdot \left( 1 - \frac{1}{1.12 + S_I^{1.5}} \right) \cdot \left( \frac{S_I + \frac{\sigma_{ye}}{36 \text{ksi}}}{S_I + 1} \right) = 21.462 \cdot \text{ksi}$$

The compressive buckling capacity for HCLPF capacity computation utilizes a recommended 0.9 reduction factor of the buckling stress:

$$C_m := 0.9 \sigma_p \cdot t_s = 12.072 \cdot \frac{\text{kips}}{\text{in}}$$

Buckling capacity of the supported cylindrical shells under combined axial bending and internal pressure should also be checked although it is unlikely to govern for overall seismic response of fluid containing tanks. The axial bending induced buckling stress,  $\sigma_{CB}$ , for such a load case can be conservatively estimated (essentially lower bound) as follows.

A parameter  $\Delta\gamma$  to be used in the following procedure as an increase factor for internal pressure can be obtained from Figure 6 of "Buckling of Thin-walled Circular Cylinders," [NASA SP-8007].  $\Delta\gamma$  depends on the minimum compression zone pressure at the base of the tank shell,  $P_{C-}$ , corresponding to the time of maximum moment.

Considering the potential range on  $\sigma_{ye}$  of 30 to 60 ksi, the resultant range on  $\sigma_p$  is 16.572 ksi to 26.702 ksi. Consequently,  $C_m$  has a range of 9.322 kips/in to 15.02 kips/in.

$$\frac{P_{C-}}{E_S} \left( \frac{R}{t_s} \right)^2 = 0.142$$

From Figure 6 of NASA SP-8007:  $\Delta\gamma := 0.12$

$$\phi := \frac{1}{16} \cdot \sqrt{\frac{R}{t_s}} = 1.37$$

$$\gamma := 1 - 0.73(1 - e^{-\phi}) = 0.455$$

$$\sigma_{CB} := (0.6\gamma + \Delta\gamma) \frac{E_S}{R \div t_s} = 23.737 \cdot ksi$$

$$0.9\sigma_p = 19.316 \cdot ksi$$

$\sigma_{CB}$  exceeds  $0.9\sigma_p$ , so it does not govern.

### H.3.2 Bolt Hold-down Capacity:

The bolt hold-down capacity should be determined as the smallest of the bolt tensile capacity, anchorage of bolt into concrete foundation, capacity of the top plate of bolt chairs to transfer bolt loads to the vertical chair gussets, attachment of the top plate and vertical chair gussets to the tank shell, and the capacity of tank shell to withstand concentrated loads imposed on it by bolt chairs.

**Anchor bolt capacity:** the anchor bolt has a diameter of 2 1/2" and is made of A36 steel. The tensile capacity can be determined as:

$$d_{bolt} := 2.5in$$

$$A_{bolt} := \frac{\pi \cdot d_{bolt}^2}{4} = 4.909 \cdot in^2$$

Based on the AISC Code [9th edition, 1989] for threaded A36 bolts:

$$T_{BC} := 1.7A_{bolt} \cdot 19.1ksi = 159.387 \cdot kips \quad T_{BC} = 79.693 \cdot tonf$$

Note that  $T_{BC}$  is the capacity of one bolt and the capacity of the interacting multi-bolts will be considered later.

**Anchor bolt chair capacity check:** according to the drawing, the anchor bolt chairs form a circumferentially continuous construction. Based on the continuous chair construction and the sizing of the plates and weld, it is judged that the anchor bolt chair and its attachment to the tank shell is adequate to transfer the bolt capacity load for the CST. The tank shell is also considered to be adequate in withstanding the concentrated loads imposed on it by bolt chairs, especially because the "elephant-foot" buckling capacity is also checked.

$$t_{chair} := \left(1 + \frac{3}{8}\right)in = 1.375 \cdot in$$

Weld width is 15 mm (5/8") according to the drawing.

**Capacity of bolt anchorage into concrete foundation:** the anchorage is constructed using non-shrinking grout. The tensile failure of bolt anchorage mainly

consists of bolt failure, plug pull-out, and concrete cone failure, the last two of which typically are a combination of tensile failure of concrete in the upper portion of the anchorage that results in a partial depth cone-shaped spall and bond failure at the grout-concrete interface in the lower portion of the anchorage.

$$\text{Bolt spacing: } \Delta d := \pi \cdot \left[ 50\text{ft} + \left( 9 + \frac{1}{16} \right) \text{in} \right] \div 78 = 2.044 \cdot \text{ft}$$

Lee, et al [2001] described an experimental and analytical work on the pull-out strength of large-sized anchor bolt, in a SMiRT 16 paper entitled "failure mechanism for large-sized grouted anchor bolt under tensile load." The test specimens were selected based on the real construction of CST in the Yonggwang Nuclear Power Plant of Korea. The anchor bolt is 2-1/2 inches in diameter, and has an embedment length of 2 ft 2-3/8 inches. The anchor bolt material is ASTM A36. Non-shrinking grout was used in the post-installed anchorage construction. These construction variables are basically very similar to those of the subject CST for fragility analysis, except that the subject CST anchors have a slightly shorter embedment length of 2 ft 1 inch. The concrete strength of the subject CST foundation is not available, and is assumed to be the same as in this SMiRT 16 paper, which has a compressive strength of 4500 psi. The circumferential spacing is about 2 ft for both tanks. The test included 5 anchor bolt specimens.

As reported by Lee, et al [2001], the average 7 day and 28 day compressive strength of the concrete were 5419 psi and 7180 psi, respectively. The actual average compressive strength of non-shrinking grout at 7 days and 21 days were 7550 psi and 11100 psi, respectively. The non-shrinking grout has obviously larger compressive strength than the concrete, as expected for normal construction of anchorage. The reported bond strength of the non-shrinking grout (Masterflow 870) was 40 kgf/cm<sup>2</sup> (569 psi). The Young's modulus of A36 is 2.9\*10<sup>7</sup> psi and the Poisson's ratio is 0.3.

The test first confirmed a minimum required load of 50 tons (100 kips). Three of the five grouted anchors were tested further until failure. Two specimens was judged to have failed by tensile failure of grout at the lower portion of the grout block, bonding failure between grout and the concrete, and tensile failure of concrete. The other specimen showed abrasion of anchor bolt thread. All specimens achieved at least 100 tons (200kips), after which the load-deformation curve became significantly flatter and the ultimate failure load scatters between 100 tons and 120 tons.

Based on the test, the anchorage capacity should be 200 kips, which is about 26% higher than the estimate based on tensile strength of the anchor bolt. It should be noted that in the test, one specimen had abrasion in its thread, suggesting the anchor bolt capacity should be also close to 200 kips. However, since the embedment in the test was about 1-3/8 inch longer than the subject CST case, the spacing of anchor bolts in the test is twice as long as in the subject CST case, and the lab test condition usually have a higher quality control, the estimate of 159.387 kips will be assumed as the anchorage capacity.

The effective embedment for the anchorage in the subject CST is estimated to be 23", which is determined by subtracting 1" from the total embedment of 2' 1" to

account for the nuts.

$$h_{eff} := 23in$$

The compressive strength of the concrete is assumed to be 4500 psi, according to the above mentioned paper. It should be pointed out that the measured strength in the test is higher.

$$f_c := 4500psi$$

Base case of the anchor bolt strength based on concrete based on NUREG/CR-5434 (Figure 5.20):

$$k := 57$$

$$T_{AC} := k \cdot \left( \frac{h_{eff}}{in} \right)^{1.5} \cdot \sqrt{\frac{f_c}{psi}} \cdot lbf = 421.767 \cdot kips$$

Note that this  $T_{AC}$  capacity calculated based on NUREG/CR-5434 is greater than 200 kips as determined in the test as reported in a SMiRT paper by Lee, et al. [2001]. The anchor bolts in the tests reported in NUREG/CR-5434 have a diameter of 3/4" and an embedment of 4", which are much smaller than those used in the CST construction. Therefore, the test data in NUREG/CR-5434 will be used as factors to scale the test data as reported in the paper by Lee, et al. [2001].

$$f_{TAC} := \frac{200kips}{421.767kips} = 0.474$$

Strengths for a crack width of 0mm and 0.3 mm can be assumed to be, based on Figure 5.20 of NUREG/CR-5434:

$$T_{AC\_00} := 200kips$$

$$T_{AC\_03} := 200kips \cdot \frac{15.5}{57} = 54.386 \cdot kips$$

$T_{AC}$  as a function of crack width can be established as:

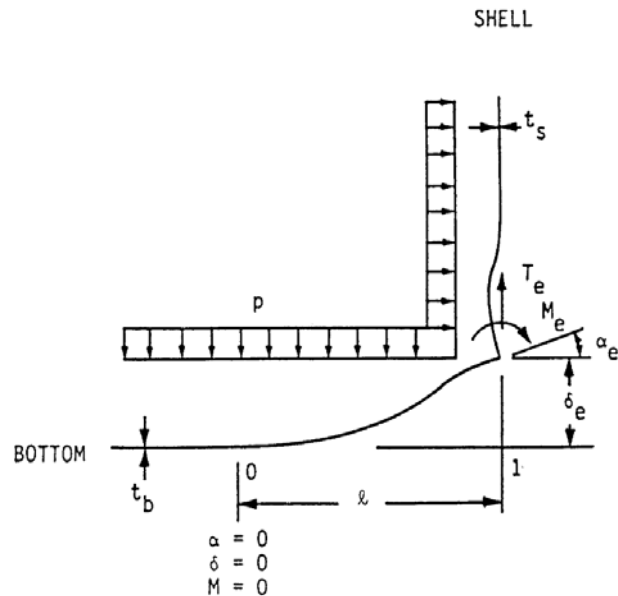
$$T_{AC}(c) := \max \left[ T_{AC\_00} + \frac{c}{0.3mm} \cdot (T_{AC\_03} - T_{AC\_00}), 0kips \right]$$

$$T_{AC}(crack) = 101.187 \cdot kips$$

$$T_{BC} = 159.387 \cdot kips$$

$$T_{BC} := \min(T_{BC}, T_{AC}(crack)) = 101.187 \cdot kips$$

### H.3.3 Fluid Hold-down Forces:



**Schematic Illustration of Tank Bottom Behavior Near Tensile Region of Tank Shell [NUREG/CR-5270]**

The hold-down force  $T_e$  increases with increasing fluid pressure  $P$ , which consequently assumes the minimum tension zone fluid press  $P_{T-}$ . A number of other related parameters are also defined below.

$$P := P_{T-} = 3.288 \cdot \text{psi}$$

$$\nu := 0.3$$

$$I_b := \frac{t_B^3}{12(1 - \nu^2)} = 1.917 \times 10^{-3} \cdot \text{in}^3$$

$$t_S = 0.625 \cdot \text{in}$$

$$t_B = 7 \cdot \text{mm}$$

$$K := \frac{E_S \cdot t_S^3}{12(1 - \nu^2)} = 7.325 \times 10^4 J$$

$$\kappa := \left[ \frac{R}{t_S} \cdot \sqrt{3(1 - \nu^2)} \right]^{0.5} = 28.177$$

$$MFP := \frac{R \cdot t_S}{\sqrt{12(1 - \nu^2)}} \left( 1 - \frac{R}{H \cdot \kappa} \right) = 0.036 m^2$$

MFP is a shortcut to  $M_F / P$

$$K_S := \frac{2 \cdot K \cdot \kappa}{R} = 5.412 \times 10^5 N$$

The uplift height  $\delta_e$ , the hold down tension  $T_e$ , moment  $M_e$ , rotation  $\alpha_e$ , and maximum positive moment  $M_+$  can then be defined as functions of uplift length  $l$ :

$$F(l) := 1 + \frac{K_S \cdot l}{2E_S \cdot I_b}$$

$$\delta_e(l) := \left[ \frac{l^4}{24} - \frac{1}{F(l)} \left( \frac{K_S \cdot l^5}{72E_S \cdot I_b} + MFP \cdot \frac{l^2}{6} \right) \right] \cdot \left( \frac{P}{E_S \cdot I_b} \right)$$

$$T_e(l) := P \cdot \left[ \frac{l}{2} + \frac{1}{F(l)} \cdot \left( \frac{K_S \cdot l^2}{12E_S \cdot I_b} + \frac{MFP}{l} \right) \right]$$

Note: this equation as in the original CDFM method is singular at  $L=0$  ft. The  $MFP/L$  term only has a minor effect on  $T_e$  when  $L$  is very small. The linear approximation in the original CDFM method can effectively avoid this singularity.

$$M_e(l) := P \cdot \left( \frac{1}{F(l)} \right) \cdot \left( \frac{K_S \cdot l^3}{12E_S \cdot I_b} + MFP \right)$$

$$M_+(l) := P \cdot \left( \frac{l^2}{8} - \frac{M_e(l)}{2P} + \frac{M_e(l)^2}{2P^2 \cdot l^2} \right)$$

The singularity in this equation can be similarly avoided by the linear approximation.

$$\alpha_e(l) := \frac{P \cdot l^3}{12E_S \cdot I_b} - \frac{M_e(l) \cdot l}{2E_S \cdot I_b}$$

Given

$$l := 0 \text{ in}$$

$$\frac{l^2}{24} - \frac{1}{F(l)} \left( \frac{K_S \cdot l^3}{72E_S \cdot I_b} + MFP \cdot \frac{1}{6} \right) = 0$$

$$lmin := Find(l) = 7.65 \cdot in$$

Given

$$lmax := 10in$$

$$\delta_e(lmax) = 0.165in$$

$$lmax := Find(lmax) = 21.061 \cdot in$$

$$l := lmin, lmin + 0.1in .. lmax$$

Linear Approximation:

$$i := 0 .. \frac{(lmax - lmin)}{0.1in}$$

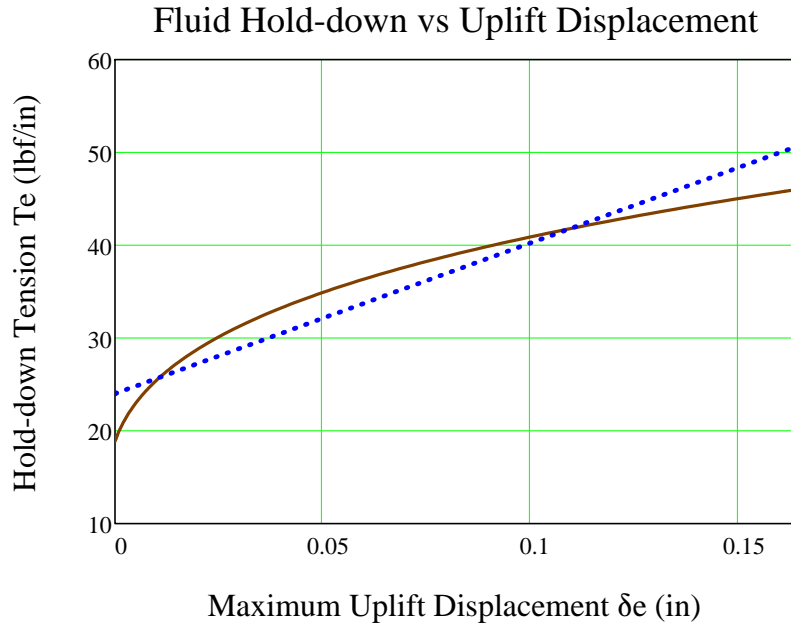
$$l\_vec_i := lmin + i \cdot 0.1 \cdot in$$

$$\begin{pmatrix} T_{e0} \\ T_{e1} \end{pmatrix} := line \left[ \frac{\delta_e(l\_vec)}{in}, \left( T_e(l\_vec) \cdot \frac{in}{lbf} \right) \right] = \begin{pmatrix} 24.007 \\ 162.111 \end{pmatrix}$$

$$T_{e0} := if(P_{T_} > 0psi, T_{e0}, 0) \frac{lbf}{in} = 24.007 \cdot \frac{lbf}{in}$$

$$T_{e1} := if(P_{T_} > 0psi, T_{e1}, 0) \cdot \frac{lbf}{in^2} = 162.111 \cdot \frac{lbf}{in^2}$$

$$T_{e\_lin}(\delta_e) := T_{e0} + T_{e1} \cdot \delta_e$$



It should be noted that these equations are derived based on small displacement theory, and are applicable to the following conditions:

1.  $L / R \leq 0.15$ . The solution does not consider the stiffening effect of hoop behavior on the base plate and consequently conservatively overpredicts the displacement  $\delta_e$ , as the ratio of  $L/R$  becomes larger.
2.  $\delta_e / t_b \leq 0.6$ . As the solution is based on small displacement assumption, which ignores the beneficial influence of the membrane tension in the base plate to reduce  $\delta_e$  for a given  $T_e$  as in large displacement theory. For unanchored tanks, Manos (in "earthquake tank-wall stability of unanchored tanks," *Journal of Structural Engineering*, Vol 112, No. 8, ASCE, 1986) and Haroun and Badawi (in "nonlinear axisymmetric uplift of circular plates," *Dynamics of Structures*, ASCE, 1987) showed that large displacement membrane theory greatly increases the fluid hold-down force  $T_e$  and consequently the uplift  $\delta_e$ . Nevertheless, for anchored tanks like the subject CST, the uplift is not expected to be very large.
3.  $M_e/M_{pb} \leq 0.9$ ;  $M_e/M_{ps} \leq 0.9$ ; and  $M_+/M_{pb} \leq 0.9$ , where  $M_{pb}$  and  $M_{ps}$  are the plastic moment capacity of the base plate and shell sidewalls, respectively. These equations are derived from elastic solution, and these conditions prevent the potential unconservatism.

$$0.6t_B = 0.165 \cdot in$$

The second requirement leads to maximum  $\delta_e$  of 0.165 in, beyond which the small displacement theory becomes increasingly conservative. The original CDFM solved the problem by making a linear approximation of the  $\delta_e$ - $T_e$  curve in a range of  $\delta_e=0$  to  $0.6t_B$ , and then use the linear equation to extrapolate beyond the  $0.6t_B$  to partially account for membrane tension effects. This approach will also be used in this study.

$$T_e := T_{e\_lin}$$

**Assessment of the upper limit on the fluid hold-down force:** based on a yield stress  $\sigma_y$  of 30 ksi, and an ultimate stress of 75 ksi, the fully plastic moment capacity  $M_{pb}$  of the 7 mm base plate is estimated to be 0.949 kips-inch/inch when the outer fiber reaches 75 ksi. It is also assumed that the effective hoop compressive yield stress  $\sigma_{ye}$  is equal to 45 ksi. The upper limit of the horizontal component of the membrane tension  $F_H$  can be found to be:

$$\sigma_{ye} = 45 \cdot \text{ksi}$$

$$M_{pb} := \frac{t_B^3}{12} \div \left( \frac{t_B}{2} \right) \cdot 75 \text{ksi} = 0.949 \cdot \frac{\text{kips} \cdot \text{in}}{\text{in}}$$

$$F_H := \frac{\sigma_{ye} \cdot t_S}{2\kappa} + \frac{M_{pb} \cdot \kappa}{R} = 0.588 \cdot \frac{\text{kips}}{\text{in}}$$

$$(4M_{pb}P_T)^{0.5} = 111.742 \cdot \frac{\text{lb}f}{\text{in}}$$

$$\frac{F_H}{2M_{pb}} = 0.31 \cdot \frac{1}{\text{in}}$$

Thus, the upper limit of the fluid hold-down force is estimated to be:

$$T_m(\delta_e) := 168.841 \frac{\text{lb}f}{\text{in}} \left( 1 + \frac{0.31 \cdot \delta_e}{\text{in}} \right)^{0.5}$$

The maximum  $\delta_e$  can be found by equating  $T_e$  and  $T_m$ :

Given

$$\delta_{ee} := 0.15 \text{in}$$

$$T_e(\delta_{ee}) = T_m(\delta_{ee})$$

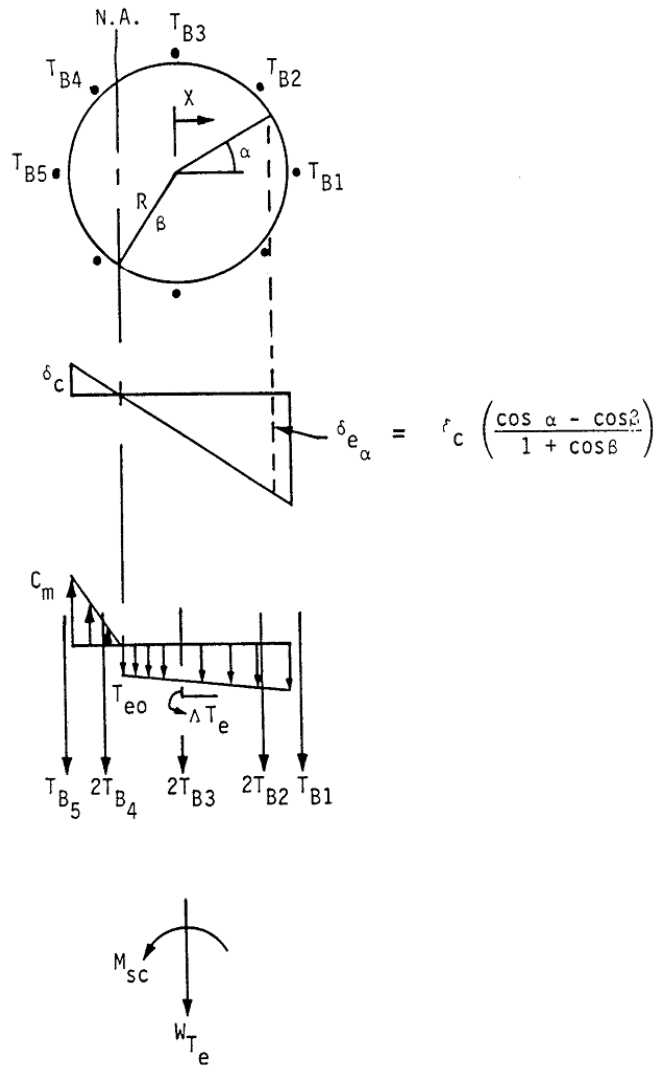
$$\delta_{ee} := \text{Find}(\delta_{ee}) = 1.051 \cdot \text{in}$$

Therefore, the linearized equation for  $T_e$  should not be extrapolated beyond  $\delta_e = 1.805$  inch.

Note that linearization is necessary later when developing overturning moment capacity.



### H.3.4 Overturning Moment Capacity:



**Vertical Loading on Tank Shell at Base [NUREG/CR-5270]**

The overturning moment capacity  $M_{SC}$  can be estimated using the compressive buckling capacity of the tank shell ( $C_B$ ), the anchor bolt hold-down capacity ( $T_{BC}$ ), and the relationship between fluid hold-down force and uplift

displacement. The estimation approach in the CDFM method requires several conservative but reasonable assumptions as noted below:

1. The bottom of the tank shell is assumed to rotate rigidly about the neutral axis (plane sections remain plane).
2. The cross-section of the tank at the top of the top plate of the bolt chairs ( $h_c$  above the base) is assumed to remain horizontal so that all vertical tank distortions needed to result in base uplift and mobilization of the anchor bolts must be accommodated over the height  $h_c$ .
3. The compressive stress varies linearly from zero at the neutral axis ( $\alpha=\beta$  as in the figure above) to its maximum value  $C_m$  at  $\alpha=180^\circ$ , as given by  $C_m = E_s t_s \delta_c / h_c \leq C_B$  (by converting eq. H-39), where  $\delta_c$  is the maximum compressive shortening.

Summary of parameters:

$$C_m = 12.072 \cdot \frac{\text{kips}}{\text{in}} \quad T_{BC} = 101.187 \cdot \text{kips}$$

$$T_{e0} = 0.024 \cdot \frac{\text{kips}}{\text{in}} \quad T_{e1} = 0.162 \cdot \frac{\text{kips}}{\text{in}^2}$$

$$W_{Te} = 176.395 \cdot \text{kips} \quad A_B := A_{\text{bolt}} \quad A_B = 4.909 \cdot \text{in}^2$$

$$E_B := 29 \times 10^3 \text{ksi}$$

$$R = 25.026 \cdot \text{ft}$$

$$t_s = 0.625 \cdot \text{in} \quad E_s := E_S = 29 \times 10^3 \cdot \text{ksi}$$

$$h_c := 207 \text{mm} = 8.15 \cdot \text{in}$$

$$h_a := 2 \text{ft} + 1 \text{in} = 25 \cdot \text{in}$$

Using the approach outlined in NUREG/CR-5270 instead of the EPRI NP-6041-SL appendix H in the following:

$$\delta_c := \frac{C_m \cdot h_c}{E_s \cdot t_s} = 5.428 \times 10^{-3} \cdot \text{in}$$

$$K_B := \frac{\delta_c \cdot A_B \cdot E_B}{h_a + h_c} = 23.31 \cdot \text{kips}$$

$$\Delta T_e := T_{e1} \cdot \delta_c = 8.8 \times 10^{-4} \cdot \frac{\text{kips}}{\text{in}}$$

$$\delta_{ea}(a,b) := \delta_c \cdot \left( \frac{\cos(a) - \cos(b)}{1 + \cos(b)} \right)$$

Because the bolt pretension  $T_{BP}$  is unreliable after a number of years in service, it is conservatively assumed to be 0.

$$T_{BP} := 0 \text{ kips}$$

The neutral axis angle  $\beta$  can be determined iteratively using the following procedure.

Bolt locations:  $i := 0..77$

$$\alpha_i := \frac{2\pi}{78}i$$

$$Tfunc(\alpha, \beta) := \begin{cases} c \leftarrow T_{BP} + K_B \cdot \frac{\cos(\alpha) - \cos(\beta)}{1 + \cos(\beta)} \\ c \leftarrow T_{BC} \text{ if } c > T_{BC} \\ c \leftarrow 0 \text{ if } c < 0 \end{cases}$$

$$C_1(\beta) := \frac{1 + \cos(\beta)}{\sin(\beta) + (\pi - \beta)\cos(\beta)}$$

$$C_2(\beta) := \frac{\sin(\beta)\cos(\beta) + \pi - \beta}{1 + \cos(\beta)}$$

$$C_3(\beta) := \frac{\sin(\beta) - \beta \cdot \cos(\beta)}{\sin(\beta) + (\pi - \beta)\cos(\beta)}$$

$$C_4(\beta) := \frac{\beta - \sin(\beta)\cos(\beta)}{1 + \cos(\beta)}$$

$$T_B(\alpha, \beta) := \overrightarrow{Tfunc(\alpha, \beta)}$$

$$Cf'_m(\alpha, \beta) := \left( \frac{W_{Te} + \sum T_B(\alpha, \beta)}{2R} + T_{e0} \cdot \beta \right) \cdot C_1(\beta) + \Delta T_e \cdot C_3(\beta)$$

Equating  $Cf'_m$  and  $C_m$  to determine  $\beta$ :

$$func(\alpha, \beta) := Cf'_m(\alpha, \beta) - C_m$$

$$\beta := \text{root}(func(\alpha, \beta), \beta, 0, 3.1)$$

$$\beta = 2.302 \qquad \beta \cdot \frac{180}{\pi} = 131.895$$

$$C'_m := C_f'_m(\alpha, \beta) = 12.072 \cdot \frac{\text{kips}}{\text{in}} \qquad C_m = 12.072 \cdot \frac{\text{kips}}{\text{in}}$$

Use  $C'_m$  and  $\beta$  to find the overturning moment capacity  $M_{SC}$ :

$$M_{SC} := C'_m \cdot C_2(\beta) \cdot R^2 + \sum \overrightarrow{(T_B(\alpha, \beta) \cdot R \cdot \cos(\alpha))} + T_{e0} \cdot R^2 \cdot 2 \cdot \sin(\beta) + \Delta T_e \cdot C_4(\beta) \cdot R^2$$

$$M_{SC} = 150617.311 \cdot \text{kips} \cdot \text{ft}$$

$$\sum T_B(\alpha, \beta) = 3.796 \times 10^3 \cdot \text{kips}$$

The largest bolt elongation (at  $\alpha=0$ ) should be checked to ensure that the anchorage has the capability:

$$\delta_{e0} := \delta_{ea}(\alpha_0, \beta) = 0.027 \cdot \text{in}$$

$$\text{Elongation ratio: } \frac{\delta_{e0}}{h_a + h_c} = 0.082 \cdot \%$$

The maximum elongation ratio is much smaller than 1%, which is recommended in the original CDFM method for the A307 bolt. One percent is also considered to be an appropriate percentage value for the A36 anchor bolt used in the subject CST construction.

The maximum tank shell uplift distortion  $\delta_{e0} = 0.026$  in, which is much less than the limit of 0.165 in for the small displacement theory to be applicable in developing the fluid hold-down capacity.

Because there are 78 anchor bolts (the example tank in the original CDFM method had only 8), the case where  $\alpha=0$  lies midway between bolts need not be checked.

The uncertainty in HCLPF buckling capacity of the tank shell due to the uncertain  $\sigma_{ye}$  can lead to an  $M_{SC}$  as low as 119133.414 kips-ft or as high as 192156.702 kips-ft. It should be noted that unlike in the original CDFM method,  $M_{SC}$  is sensitive to the estimate of  $C_m$ .

Inelastic energy absorption reduction factor  $k$  can be applied to linearly computed seismic response to obtain the actual overturning moment capacity. The combined bolt yielding and tank shell buckling failure mode for overturning moment is not brittle so that  $k$  can be less than unity. However, as stated in the original CDFM method, it is difficult to make an appropriate estimate of  $k$  for this failure mode. Therefore, it is

conservatively assumed to be unity.

$$k := 1.0$$

$$SME_M := \frac{M_{SC}}{k \cdot M_{SH}} \cdot SME_e \qquad SME_M = 1.115 \cdot g$$

Since  $SME_M$  is substantially different from  $SME_e$ , the above procedure should be iterated to obtain the appropriate SME estimate. The resultant  $SME_e$  is found to be 0.97g.



### H.3.5 Sliding Capacity:



The base plate of the CST has a slight cone ( with a slope of 1 to 96) so that the fluid will always drain away from the center of the tank. This cone is generally created by variable thickness of the oiled sand cushion between the tank bottom plate and its foundation. Therefore, the coefficient of friction between the tank base and its foundation is reasonably assumed to have a conservative value of 0.55:

$$COF := 0.55$$

The sliding shear capacity can then be calculated as,

$$V_{SC} := COF \cdot \left( W_{Te} + P_a \cdot \pi \cdot R^2 + \sum T_B(\alpha, \beta) \right) = 3.835 \times 10^3 \cdot kips$$

The shear capacity of the bolts should not be considered because (a) there is a large space between the concrete foundation and the anchor bolt chair, and (b) there is a 1/4" diametric clearance in the hole in the anchor bolt chair.

The sliding capacity with a unit inelastic absorption factor as suggested by the original CDFM method:

$$SME_V := \frac{V_{SC}}{k \cdot V_{SH}} \cdot SME_e \qquad SME_V = 0.423 \cdot g$$

By varying  $SME_e$ , the HCLPF shear capacity is found to be 0.555g.

Unlike the example tank in the original CDFM method, the capacity of the CST appears to be governed by the sliding capacity. The sliding capacity considers only the friction between the bottom plate and the foundation.



### H.3.6 Fluid Pressure Capacity:

---



The inelastic energy absorption seismic response reduction factor  $k_u$  is suggested to be 0.8 for HCLPF capacity evaluation:

$$k_u := 0.8$$

For the CDFM hoop membrane stress capacity, it is recommended that the ASME seismic design limit of  $2 S_M$  for primary stress should be used, which is 37.5 ksi for SA240-type 304 stainless steel:

$$\sigma_a := 37.5 \text{ ksi}$$

The pressure capacity,  $P_{CA}$ , at the bottom of the tank shell (the CST has a uniform shell thickness), can be estimated to be:

$$P_{CA}(t) := \frac{\sigma_a \cdot t}{R}$$
$$P_{CA}(t_S) = 78.044 \cdot \text{psi}$$

The maximum seismic induced hydrodynamic pressures  $P_{SM}$  and the hydrostatic pressure  $P_{ST}$  at the bottom of the tank shell are:

$$P_{SM}(H) = 1.098 \times 10^5 \text{ Pa}$$

$$P_{ST}(H) = 1.12 \times 10^5 \text{ Pa}$$

The HCLPF fluid pressure capacity  $SME_p$  can be determined as:

$$SME_p := \frac{P_{CA}(t_S) - P_{ST}(H)}{k_u \cdot P_{SM}(H)} \cdot SME_e = 2.052 \cdot g$$

By varying  $SME_e$ , the HCLPF fluid pressure capacity can be found to be 2.191 g, which does not govern. This agrees with seismic experience that the fluid pressure capacity seldom appears to govern the seismic capacity for normal flat bottomed steel tanks with butt-welded side plates.



---

Summary of SME capacities:

$$SME_M = 1.115 \cdot g$$

$$SME_V = 0.423 \cdot g$$

$$SME_p = 2.052 \cdot g$$

$$SME_{cr} := \min(SME_M, SME_V, SME_p) = 0.423 \cdot g$$

$$SME_e = 0.423 \cdot g$$

$$if[SME_{cr} = SME_M, "Moment", (if(SME_{cr} = SME_V, "Shear", "Fluid Pressure"))] = "Shear"$$

$$crack = 0.204 \cdot mm$$

Summary of results:

Years:	0	5	10	15	20	25	30	35	40
cr (mm):	0.108	0.114	0.120	0.126	0.132	0.138	0.144	0.150	0.156
SME:	0.426	0.426	0.426	0.426	0.426	0.426	0.426	0.426	0.426
SMEM:	1.140	1.140	1.140	1.140	1.140	1.140	1.140	1.140	1.140
SMEV:	0.426	0.426	0.426	0.426	0.426	0.426	0.426	0.426	0.426
SMEP:	2.052	2.052	2.052	2.052	2.052	2.052	2.052	2.052	2.052
Mode:	Shear								
Years:	45	50	55	60	65	70	75	80	
cr (mm):	0.162	0.168	0.174	0.180	0.186	0.192	0.198	0.204	
SME:	0.426	0.426	0.426	0.426	0.425	0.425	0.424	0.423	
SMEM:	1.140	1.140	1.140	1.140	1.137	1.131	1.124	1.115	
SMEV:	0.426	0.426	0.426	0.426	0.425	0.425	0.424	0.423	
SMEP:	2.052	2.052	2.052	2.052	2.052	2.052	2.052	2.052	
Mode:	Shear								

### H.3.7 Consideration of Other Capacities:

(1) Slosh height for roof damage: note that even with a  $SME_e = 0.334 \text{ g}$  (the initial guess), the slosh height is about 4.8 ft. With the HCLPF shear capacity of  $SME_e = 0.555 \text{ g}$ , the sloshing height can be about 7.9 ft, which is close to the total height of the head (8.7', as approximated in the beginning part of this calculation).

$$h_s = 6.05 \cdot ft$$

$$SME_e = 0.423 \cdot g$$

The increase of sloshing height is not significant as  $SME_e$  increases from 0.334 g to 0.555 g. In addition, as pointed out in the original CDFM method, even if roof damage might be expected, such damage usually does not impair the ability of the tank to contain fluid.

(2) The CST is assumed to sit on rock/very stiff soil; therefore, soil-tank foundation interaction is not considered.

(3) Piping failure or failure of nozzles may lead to loss of fluid in the tank, and more importantly, may impair the normal function of the condensation system. As reported in the original CDFM method, a significant fraction of the cases of seismic induced loss of tank contents have been due to piping/nozzle failures because of poor detailing. The CDFM method also stated that a SME evaluation

of piping/nozzle failure is only necessary when poor seismic detailing is found in the involved piping attached to the tank. This analysis assumes that the subject CST is appropriately detailed, i.e. the piping and nozzle directly attached to the tank are properly designed and constructed so that sufficient piping flexibility can be achieved to accommodate large relative seismic anchor movements.

(4) The influence of the building in between the two CSTs on the SME are assessed in the following. The gap between the auxiliary building and the CSTs at the roof level is filled with elastomeric sealant.

The maximum tank shell uplift distortion is found to be 0.026 in, which corresponds to a neutral axis angle  $\beta$  of 2.29161 rad. Since the horizontal plane at the anchor bolt chair is assumed to remain plane and all distortion is assumed to occur below this level, the rotation angle around the neutral axis can be estimated to be:

$$Rotation := \frac{\delta_{e0}}{R \cdot (1 - \cos(\beta))} = 5.44 \times 10^{-5}$$

$$\beta = 2.302 \quad \cos(\beta) = -0.668$$

The maximum horizontal displacement at the roof of the auxiliary building, which is at an elevation of 114' 9" (Parapet elevation, compared to the tank floor elevation of 101' 9"), can be estimated to be:

$$Rotation \cdot 13ft = 8.487 \times 10^{-3} \cdot in$$

This horizontal displacement is much less than the width of the seismic separation joint at the roof elevation, which is 3 in. Therefore, the influence of the auxiliary building to the two CSTs is considered minimal.

## The Fragility of CST

### Summary of results:

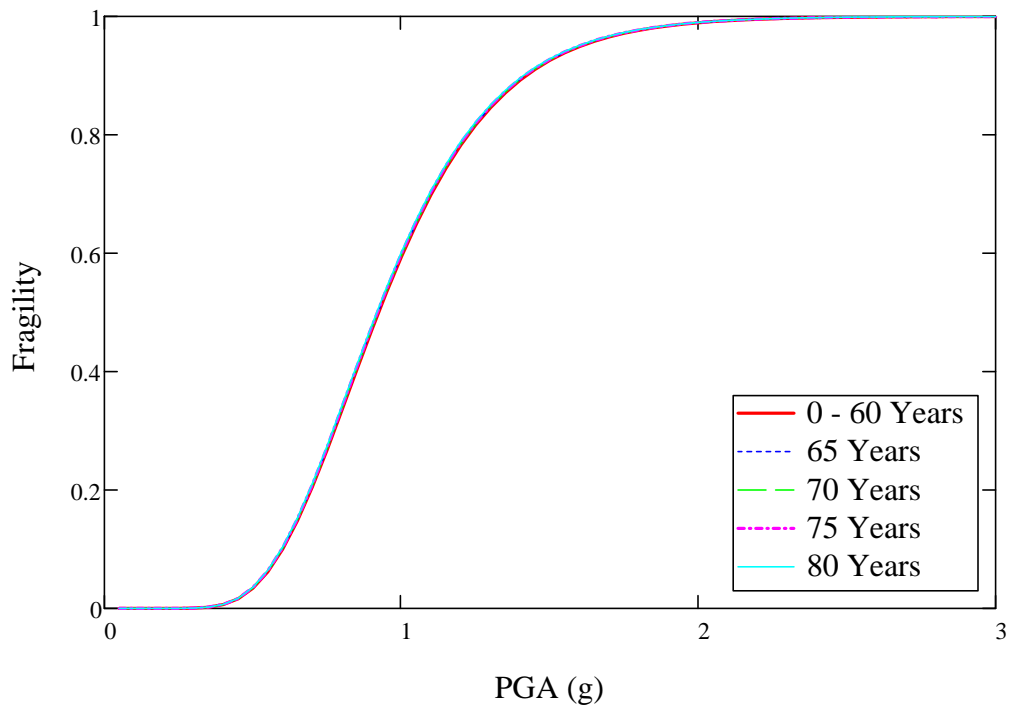
Years:	0	5	10	15	20	25	30	35	40
cr (mm):	0.108	0.114	0.120	0.126	0.132	0.138	0.144	0.150	0.156
SME:	0.426	0.426	0.426	0.426	0.426	0.426	0.426	0.426	0.426
SMEM:	1.140	1.140	1.140	1.140	1.140	1.140	1.140	1.140	1.140
SMEV:	0.426	0.426	0.426	0.426	0.426	0.426	0.426	0.426	0.426
SMEP:	2.052	2.052	2.052	2.052	2.052	2.052	2.052	2.052	2.052
Mode:	Shear								
Years:	45	50	55	60	65	70	75	80	
cr (mm):	0.162	0.168	0.174	0.180	0.186	0.192	0.198	0.204	
SME:	0.426	0.426	0.426	0.426	0.425	0.425	0.424	0.423	
SMEM:	1.140	1.140	1.140	1.140	1.137	1.131	1.124	1.115	
SMEV:	0.426	0.426	0.426	0.426	0.425	0.425	0.424	0.423	
SMEP:	2.052	2.052	2.052	2.052	2.052	2.052	2.052	2.052	
Mode:	Shear								



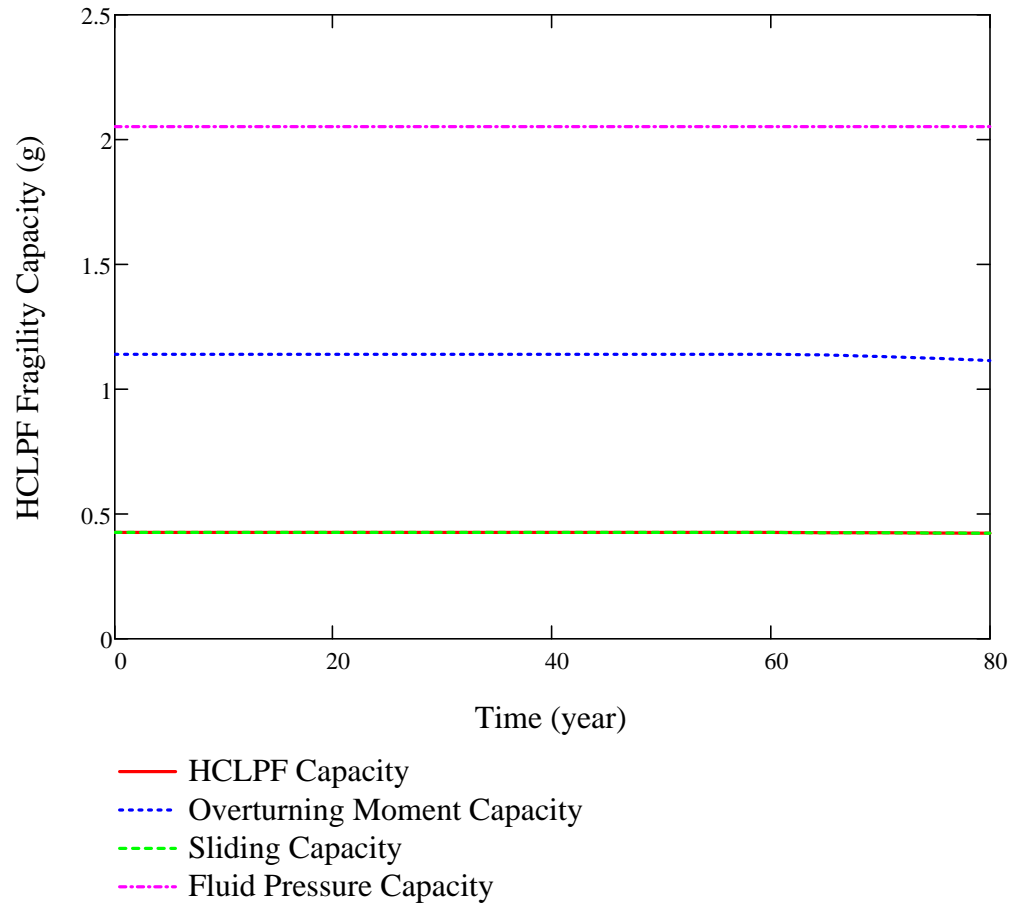
$$F(Q,a) := cnorm\left(\frac{\ln\left(\frac{a \cdot g}{SME_m}\right) + \beta_U \cdot qnorm(Q,0,1)}{\beta_R}\right)$$

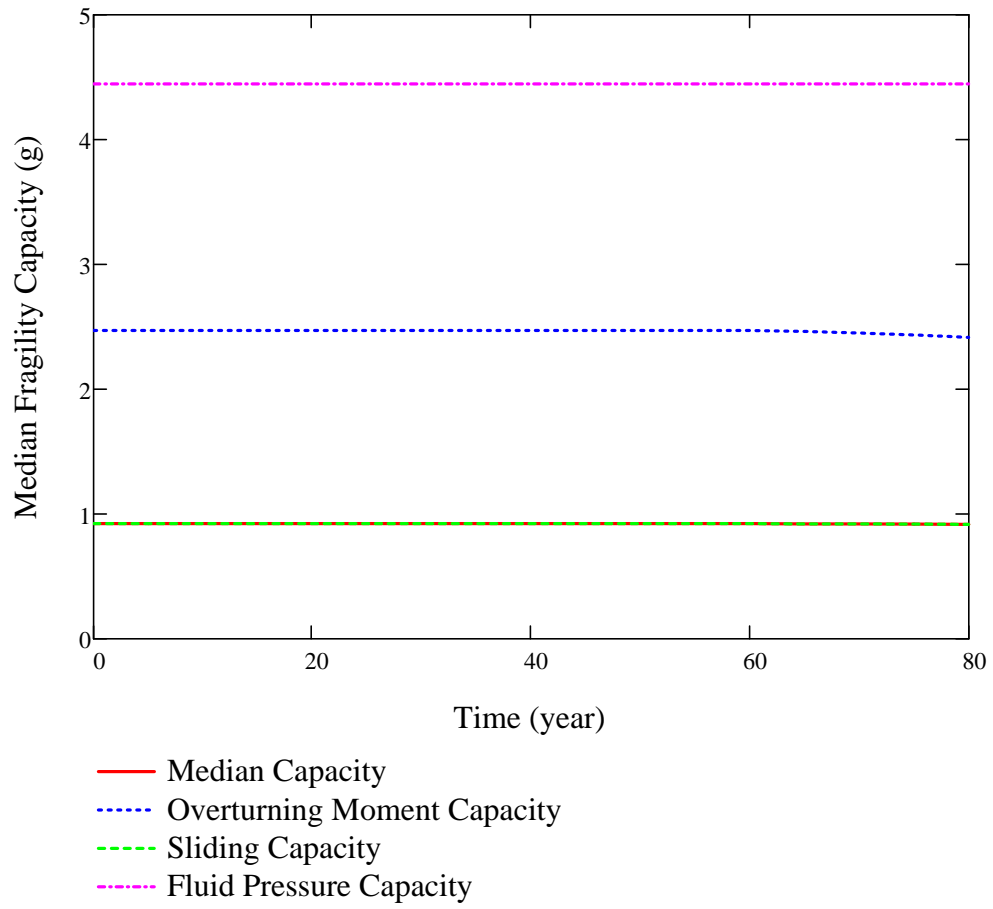
$$F_{mean}(a) := cnorm\left(\frac{\ln\left(\frac{a \cdot g}{SME_m}\right)}{\beta_C}\right)$$

$sa := 0.05, 0.1 \dots 3$



$year_i := i \cdot 5$





16 0.426 0.426 0.425 0.425 0.424 0.423)<sup>T</sup>.g

140 1.140 1.137 1.131 1.124 1.115)<sup>T</sup>.g

126 0.426 0.425 0.425 0.424 0.423)<sup>T</sup>.g

52 2.052 2.052 2.052 2.052 2.052)<sup>T</sup>.g

THESE DATA ARE THE CONTINUATION OF PAGE D-20.

**Appendix E FRAGILITY ANALYSIS OF THE CST WITH FOUNDATION CONCRETE  
CRACKING – APPLICATION OF MODEL C-2**



# KAERI Year 3 Task

## Fragility Analysis of Condensate Storage Tank

### - Degradation Case (C-2) Anchorage (concrete) Degradation



This case utilizes the concrete degradation data recorded in Korea NPPs and test data of dynamic anchorage strength with simulated cracks in concrete as reported in NUREG/CR-5434.

The anchorage strength is the smaller of the bolt strength (base case) and the anchorage strength attributed to concrete with various levels of degradation.

The grouted anchors used NURE/CR-5434 have a diameter of 3/4" and (effective) embedment of 4". Both dimensions are much smaller than the anchorage in the CST construction. Therefore, the data in NUREG/CR-5434 will be used as scaling factors.

Crack width regression curve developed by BNL based on KAERI data is used to predict the crack width.



$$year := 80$$

$$crack := 0.0078 \cdot year \cdot mm = 0.624 \cdot mm$$

## H.1 Introduction

KAERI indicated that the seismic DBE in Korea follows the NRC Reg. Guide 1.60 design spectrum shape but with a PGA level scaled down to 0.2 g. An initial HCLPF capacity was assumed to be 1.67 times of 0.2 g. However, since the Mathcad sheets in this appendix solve the various equations iteratively by manually setting  $SME_e$  to different values, the following  $SME_e$  value of 0.165 g represents the converged solution for the degradation level of the anchorage (concrete) at 80 years.

$$SME_e := 0.165g$$



## H.2 Response Evaluation

Same as Appendix A, Section H.2.

---

## ▣ H.3 Capacity Assessment

---

- ▣ The seismic overturning moment capacity of the CST at its base,  $M_{SC}$ , depends on the axial compressive buckling capacity of the tank shell  $C_m$ , the tensile hold-down capacity of the anchor bolts including their anchorage and attachment to the tank  $T_{BC}$ , and the hold-down capacity of the fluid pressure acting on the tank base plate  $T_e$ .

Although unlikely for larger radius tanks, the tank SME capacity is sometimes governed by the sliding shear capacity at the tank base,  $V_{SC}$ . Even though it does not appear that any butt welded steel tank has ever failed due to seismic induced membrane hoop stresses due to combined hydrostatic and hydrodynamic fluid pressures, the SME capacity of this failure mode,  $P_{CA}$ , should also be checked.

Additional assessment of the seismic capacity may include the possibility and consequence of the fluid sloshing against the tank roof, foundation failure for soil sites, and possibility of failure of piping or their attachment to the tank.

### **H.3.1 Compressive Buckling Capacity of the Tank Shell:**

The most likely buckling for tanks is the "elephant-foot" buckling near the base of the tank shell. The "elephant-foot" buckling is a combined effect of hoop tension, axial (vertical) compression, and restriction of radial deformation of the tank shell by the base plate. "Elephant-foot" buckling does not necessarily lead to failure of a tank (e.g., leakage). However, there is no simple capability evaluation method that can predict tank performance after the development of "elephant-foot" buckling. Therefore, for a CDFM SME capacity of tanks, the onset of "elephant-foot" buckling will be judged to represent the limit to the compressive buckling capacity of the tank shell. The onset of "elephant-foot" buckling can be estimated using elastic-plastic collapse theory as presented in the following:

The sidewall thickness near the shell base:  $t_s := t_S = 0.625 \cdot in$

The tank internal pressure near its base:  $P := P_{C+} = 1.469 \times 10^5 Pa$

Elastic modulus of the tank:  $E_S = 2.9 \times 10^4 \cdot ksi$

The CST shell was made of SA 204-type 304 stainless steel. This material does not have a flat yield plateau and as strain increases its stress can grow to a minimum ultimate stress capacity of 75 ksi. In the CDFM method, an effective yield stress  $\sigma_{ye}$  is set to  $2.4S_M$  or 45 ksi, in line with the ASME seismic design limit for primary local membrane plus primary bending [ASME 1983, "ASME Boiler & Pressure Vessel Code"]. The potential uncertainty range for  $\sigma_{ye}$  is reported to be between 30 ksi and 60 ksi, according to the original CDFM method description.

$$\sigma_{ye} := 45ksi$$

$$\frac{R}{t_s} = 480.5$$

$$S_I := \frac{R}{t_s} \div 400 = 1.201$$

The "elephant-foot" buckling axial stress of the tank shell can be accurately predicted to be:

$$\sigma_p := \frac{0.6E_S}{R \div t_s} \left[ 1 - \left( \frac{P \cdot R}{\sigma_{ye} \cdot t_s} \right)^2 \right] \cdot \left( 1 - \frac{1}{1.12 + S_I^{1.5}} \right) \cdot \left( \frac{S_I + \frac{\sigma_{ye}}{36ksi}}{S_I + 1} \right) = 22.545 \cdot ksi$$

The compressive buckling capacity for HCLPF capacity computation utilizes a recommended 0.9 reduction factor of the buckling stress:

$$C_m := 0.9\sigma_p \cdot t_s = 12.681 \cdot \frac{kips}{in}$$

Buckling capacity of the supported cylindrical shells under combined axial bending and internal pressure should also be checked although it is unlikely to govern for overall seismic response of fluid containing tanks. The axial bending induced buckling stress,  $\sigma_{CB}$ , for such a load case can be conservatively estimated (essentially lower bound) as follows.

A parameter  $\Delta\gamma$  to be used in the following procedure as an increase factor for internal pressure can be obtained from Figure 6 of "Buckling of Thin-walled Circular Cylinders", [NASA SP-8007].  $\Delta\gamma$  depends on the minimum compression zone pressure at the base of the tank shell,  $P_{C-}$ , corresponding to the time of maximum moment.

Considering the potential range on  $\sigma_{ye}$  of 30 to 60 ksi, the resultant range on  $\sigma_p$  is 16.572 ksi to 26.702 ksi. Consequently,  $C_m$  has a range of 9.322 kips/in to 15.02 kips/in.

$$\frac{P_{C-}}{E_S} \left( \frac{R}{t_s} \right)^2 = 0.134$$

From Figure 6 of NASA SP-8007:  $\Delta\gamma := 0.12$

$$\phi := \frac{1}{16} \cdot \sqrt{\frac{R}{t_s}} = 1.37$$

$$\gamma := 1 - 0.73(1 - e^{-\phi}) = 0.455$$

$$\sigma_{CB} := (0.6\gamma + \Delta\gamma) \frac{E_S}{R \div t_s} = 23.737 \cdot ksi$$

$$0.9\sigma_p = 20.29 \cdot ksi$$

$\sigma_{CB}$  exceeds  $0.9\sigma_p$ , so it does not govern.

### H.3.2 Bolt Hold-down Capacity:

The bolt hold-down capacity should be determined as the smallest of the bolt tensile capacity, anchorage of bolt into concrete foundation, capacity of the top plate of bolt chairs to transfer bolt loads to the vertical chair gussets, attachment of the top plate and vertical chair gussets to the tank shell, and the capacity of tank shell to withstand concentrated loads imposed on it by bolt chairs.

**Anchor bolt capacity:** the anchor bolt has a diameter of 2 1/2" and is made of A36 steel. The tensile capacity can be determined as:

$$d_{bolt} := 2.5in$$

$$A_{bolt} := \frac{\pi \cdot d_{bolt}^2}{4} = 4.909 \cdot in^2$$

Based on the AISC Code [9th edition, 1989] for threaded A36 bolts:

$$T_{BC} := 1.7A_{bolt} \cdot 19.1ksi = 159.387 \cdot kips \quad T_{BC} = 79.693 \cdot tonf$$

Note that  $T_{BC}$  is the capacity of one bolt and the capacity of the interacting multi-bolts will be considered later.

**Anchor bolt chair capacity check:** according to the drawing, the anchor bolt chairs form a circumferentially continuous construction. Based on the continuous chair construction and the sizing of the plates and weld, it is judged that the anchor bolt chair and its attachment to the tank shell is adequate to transfer the bolt capacity load for the CST tank. The tank shell is also considered to be adequate in withstanding the concentrated loads imposed on it by bolt chairs, especially because the "elephant-foot" buckling capacity is also checked.

$$t_{chair} := \left(1 + \frac{3}{8}\right)in = 1.375 \cdot in$$

Weld width is 15 mm (5/8") according to the drawing.

**Capacity of bolt anchorage into concrete foundation:** the anchorage is constructed using non-shrinking grout. The tensile failure of bolt anchorage mainly

consists of bolt failure, plug pull-out, and concrete cone failure, the last two of which typically are a combination of tensile failure of concrete in the upper portion of the anchorage that results in a partial depth cone-shaped spall and bond failure at the grout-concrete interface in the lower portion of the anchorage.

$$\text{Bolt spacing: } \Delta d := \pi \cdot \left[ 50\text{ft} + \left( 9 + \frac{1}{16} \right) \text{in} \right] \div 78 = 2.044 \cdot \text{ft}$$

Lee, et al [2001] described an experimental and analytical work on the pull-out strength of large-sized anchor bolt, in a SMiRT 16 paper entitled "failure mechanism for large-sized grouted anchor bolt under tensile load." The test specimens were selected based on the real construction of CST in the Yonggwang Nuclear Power Plant of Korea. The anchor bolt is 2-1/2 inches in diameter, and has an embedment length of 2 ft 2-3/8 inches. The anchor bolt material is ASTM A36. Non-shrinking grout was used in the post-installed anchorage construction. These construction variables are basically very similar to those of the subject CST for fragility analysis, except that the subject CST anchors have a slightly shorter embedment length of 2 ft 1 inch. The concrete strength of the subject CST foundation is not available, and is assumed to be the same as in this SMiRT 16 paper, which has a compressive strength of 4500 psi. The circumferential spacing is about 2 ft for both tanks. The test included 5 anchor bolt specimens.

As reported by Lee, et al [2001], the average 7 day and 28 day compressive strength of the concrete were 5419 psi and 7180 psi, respectively. The actual average compressive strength of non-shrinking grout at 7 days and 21 days were 7550 psi and 11100 psi, respectively. The non-shrinking grout has obviously larger compressive strength than the concrete, as expected for normal construction of anchorage. The reported bond strength of the non-shrinking grout (Masterflow 870) was 40 kgf/cm<sup>2</sup> (569 psi). The Young's modulus of A36 is 2.9\*10<sup>7</sup> psi and the Poisson's ratio is 0.3.

The test first confirmed a minimum required load of 50 tons (100 kips). Three of the five grouted anchors were tested further until failure. Two specimens was judged to have failed by tensile failure of grout at the lower portion of the grout block, bonding failure between grout and the concrete, and tensile failure of concrete. The other specimen showed abrasion of anchor bolt thread. All specimens achieved at least 100 tons (200kips), after which the load-deformation curve became significantly flatter and the ultimate failure load scatters between 100 tons and 120 tons.

Based on the test, the anchorage capacity should be 200 kips, which is about 26% higher than the estimate based on tensile strength of the anchor bolt. It should be noted that in the test, one specimen had abrasion in its thread, suggesting the anchor bolt capacity should be also close to 200 kips. However, since the embedment in the test was about 1-3/8 inch longer than the subject CST case, the spacing of anchor bolts in the test is twice as long as in the subject CST case, and the lab test condition usually have a higher quality control, the estimate of 159.387 kips will be assumed as the anchorage capacity.

The effective embedment for the anchorage in the subject CST is estimated to be 23", which is determined by subtracting 1" from the total embedment of 2' 1" to

account for the nuts.

$$h_{eff} := 23in$$

The compressive strength of the concrete is assumed to be 4500 psi, according to the above mentioned paper. It should be pointed out that the measured strength in the test is higher.

$$f_c := 4500psi$$

Base case of the anchor bolt strength based on concrete based on NUREG/CR-5434 (Figure 5.20):

$$k := 57$$

$$T_{AC} := k \cdot \left( \frac{h_{eff}}{in} \right)^{1.5} \cdot \sqrt{\frac{f_c}{psi}} \cdot lbf = 421.767 \cdot kips$$

Note that this  $T_{AC}$  capacity calculated based on NUREG/CR-5434 is greater than 200 kips as determined in the test as reported in a SMiRT paper by Lee, et al. [2001]. The anchor bolts in the tests reported in NUREG/CR-5434 have a diameter of 3/4" and an embedment of 4", which are much smaller than those used in the CST construction. Therefore, the test data in NUREG/CR-5434 will be used as factors to scale the test data as reported in the paper by Lee, et al. [2001].

$$f_{TAC} := \frac{200kips}{421.767kips} = 0.474$$

Strengths for a crack width of 0mm and 0.3 mm can be assumed to be, based on Figure 5.20 of NUREG/CR-5434:

$$T_{AC\_00} := 200kips$$

$$T_{AC\_03} := 200kips \cdot \frac{15.5}{57} = 54.386 \cdot kips$$

$T_{AC}$  as a function of crack width can be established as:

$$T_{AC}(c) := \max \left[ T_{AC\_00} + \frac{c}{0.3mm} \cdot (T_{AC\_03} - T_{AC\_00}), 0kips \right]$$

$$T_{AC}(crack) = 0 \cdot kips$$

$$T_{BC} = 159.387 \cdot kips$$

$$T_{BC} := \min(T_{BC}, T_{AC}(crack)) = 0 \cdot kips$$



$$K_S := \frac{2 \cdot K \cdot \kappa}{R} = 5.412 \times 10^5 N$$

The uplift height  $\delta_e$ , the hold down tension  $T_e$ , moment  $M_e$ , rotation  $\alpha_e$ , and maximum positive moment  $M_+$  can then be defined as functions of uplift length  $l$ :

$$F(l) := 1 + \frac{K_S \cdot l}{2E_S \cdot I_b}$$

$$\delta_e(l) := \left[ \frac{l^4}{24} - \frac{1}{F(l)} \left( \frac{K_S \cdot l^5}{72E_S \cdot I_b} + MFP \cdot \frac{l^2}{6} \right) \right] \cdot \left( \frac{P}{E_S \cdot I_b} \right)$$

$$T_e(l) := P \cdot \left[ \frac{l}{2} + \frac{1}{F(l)} \cdot \left( \frac{K_S \cdot l^2}{12E_S \cdot I_b} + \frac{MFP}{l} \right) \right]$$

Note: this equation as in the original CDFM method is singular at  $L=0$  ft. The  $MFP/L$  term only has a minor effect on  $T_e$  when  $L$  is very small. The linear approximation in the original CDFM method can effectively avoid this singularity.

$$M_e(l) := P \cdot \left( \frac{1}{F(l)} \right) \cdot \left( \frac{K_S \cdot l^3}{12E_S \cdot I_b} + MFP \right)$$

$$M_+(l) := P \cdot \left( \frac{l^2}{8} - \frac{M_e(l)}{2P} + \frac{M_e(l)^2}{2P^2 \cdot l^2} \right)$$

The singularity in this equation can be similarly avoided by the linear approximation.

$$\alpha_e(l) := \frac{P \cdot l^3}{12E_S \cdot I_b} - \frac{M_e(l) \cdot l}{2E_S \cdot I_b}$$

Given

$$l := 0 \text{ in}$$

$$\frac{l^2}{24} - \frac{1}{F(l)} \left( \frac{K_S \cdot l^3}{72E_S \cdot I_b} + MFP \cdot \frac{1}{6} \right) = 0$$

$$lmin := Find(l) = 7.65 \cdot in$$

Given

$$lmax := 10in$$

$$\delta_e(lmax) = 0.165in$$

$$lmax := Find(lmax) = 15.735 \cdot in$$

$$l := lmin, lmin + 0.1in .. lmax$$

Linear Approximation:

$$i := 0 .. \frac{(lmax - lmin)}{0.1in}$$

$$l\_vec_i := lmin + i \cdot 0.1 \cdot in$$

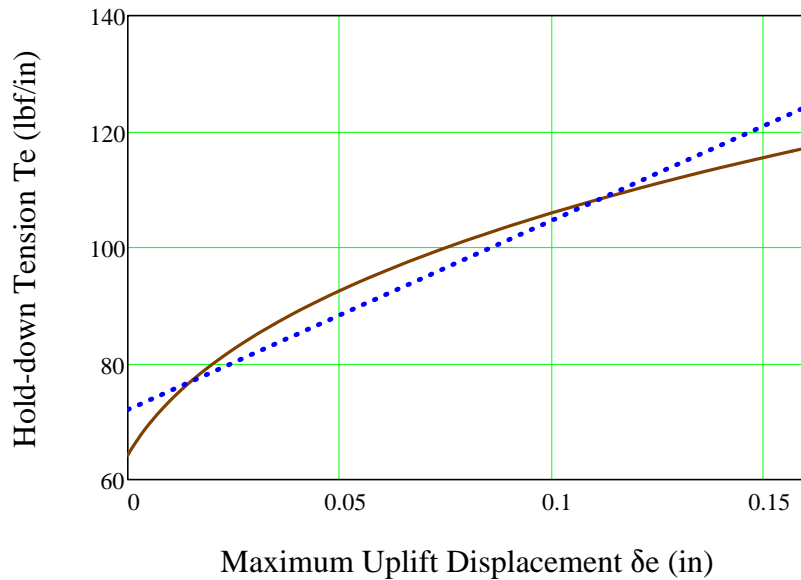
$$\begin{pmatrix} T_{e0} \\ T_{e1} \end{pmatrix} := line \left[ \frac{\delta_e(l\_vec)}{in}, \left( T_e(l\_vec) \cdot \frac{in}{lbf} \right) \right] = \begin{pmatrix} 72.042 \\ 326.372 \end{pmatrix}$$

$$T_{e0} := if(P_{T-} > 0psi, T_{e0}, 0) \frac{lbf}{in} = 72.042 \cdot \frac{lbf}{in}$$

$$T_{e1} := if(P_{T-} > 0psi, T_{e1}, 0) \cdot \frac{lbf}{in^2} = 326.372 \cdot \frac{lbf}{in^2}$$

$$T_{e\_lin}(\delta_e) := T_{e0} + T_{e1} \cdot \delta_e$$

## Fluid Hold-down vs Uplift Displacement



It should be noted that these equations are derived based on small displacement theory, and are applicable to the following conditions:

1.  $L / R \leq 0.15$ . The solution does not consider the stiffening effect of hoop behavior on the base plate and consequently conservatively overpredicts the displacement  $\delta_e$ , as the ratio of  $L/R$  becomes larger.
2.  $\delta_e / t_b \leq 0.6$ . As the solution is based on small displacement assumption, which ignores the beneficial influence of the membrane tension in the base plate to reduce  $\delta_e$  for a given  $T_e$  as in large displacement theory. For unanchored tanks, Manos (in "earthquake tank-wall stability of unanchored tanks," *Journal of Structural Engineering*, Vol 112, No. 8, ASCE, 1986) and Haroun and Badawi (in "nonlinear axisymmetric uplift of circular plates," *Dynamics of Structures*, ASCE, 1987) showed that large displacement membrane theory greatly increases the fluid hold-down force  $T_e$  and consequently the uplift  $\delta_e$ . Nevertheless, for anchored tanks like the subject CST, the uplift is not expected to be very large.
3.  $M_e/M_{pb} \leq 0.9$ ;  $M_e/M_{ps} \leq 0.9$ ; and  $M_+/M_{pb} \leq 0.9$ , where  $M_{pb}$  and  $M_{ps}$  are the plastic moment capacity of the base plate and shell sidewalls, respectively. These equations are derived from elastic solution, and these conditions prevent the potential unconservatism.

$$0.6t_B = 0.165 \cdot in$$

The second requirement leads to maximum  $\delta_e$  of 0.165 in, beyond which the small displacement theory becomes increasingly conservative. The original CDFM solved the problem by making a linear approximation of the  $\delta_e$ - $T_e$  curve in a range of  $\delta_e=0$  to  $0.6t_B$ , and then use the linear equation to extrapolate beyond the  $0.6t_B$  to partially account for membrane tension effects. This approach will also be used in this study.

$$T_e := T_{e\_lin}$$

**Assessment of the upper limit on the fluid hold-down force:** based on a yield stress  $\sigma_y$  of 30 ksi, and an ultimate stress of 75 ksi, the fully plastic moment capacity  $M_{pb}$  of the 7 mm base plate is estimated to be 0.949 kips-inch/inch when the outer fiber reaches 75 ksi. It is also assumed that the effective hoop compressive yield stress  $\sigma_{ye}$  is equal to 45 ksi. The upper limit of the horizontal component of the membrane tension  $F_H$  can be found to be:

$$\sigma_{ye} = 45 \cdot \text{ksi}$$

$$M_{pb} := \frac{t_B^3}{12} \div \left( \frac{t_B}{2} \right) \cdot 75 \text{ksi} = 0.949 \cdot \frac{\text{kips} \cdot \text{in}}{\text{in}}$$

$$F_H := \frac{\sigma_{ye} \cdot t_S}{2\kappa} + \frac{M_{pb} \cdot \kappa}{R} = 0.588 \cdot \frac{\text{kips}}{\text{in}}$$

$$(4M_{pb}P_T)^{0.5} = 206.177 \cdot \frac{\text{lb} \cdot \text{f}}{\text{in}}$$

$$\frac{F_H}{2M_{pb}} = 0.31 \cdot \frac{1}{\text{in}}$$

Thus, the upper limit of the fluid hold-down force is estimated to be:

$$T_m(\delta_e) := 168.841 \frac{\text{lb} \cdot \text{f}}{\text{in}} \left( 1 + \frac{0.31 \cdot \delta_e}{\text{in}} \right)^{0.5}$$

The maximum  $\delta_e$  can be found by equating  $T_e$  and  $T_m$ :

Given

$$\delta_{ee} := 0.15 \text{in}$$

$$T_e(\delta_{ee}) = T_m(\delta_{ee})$$

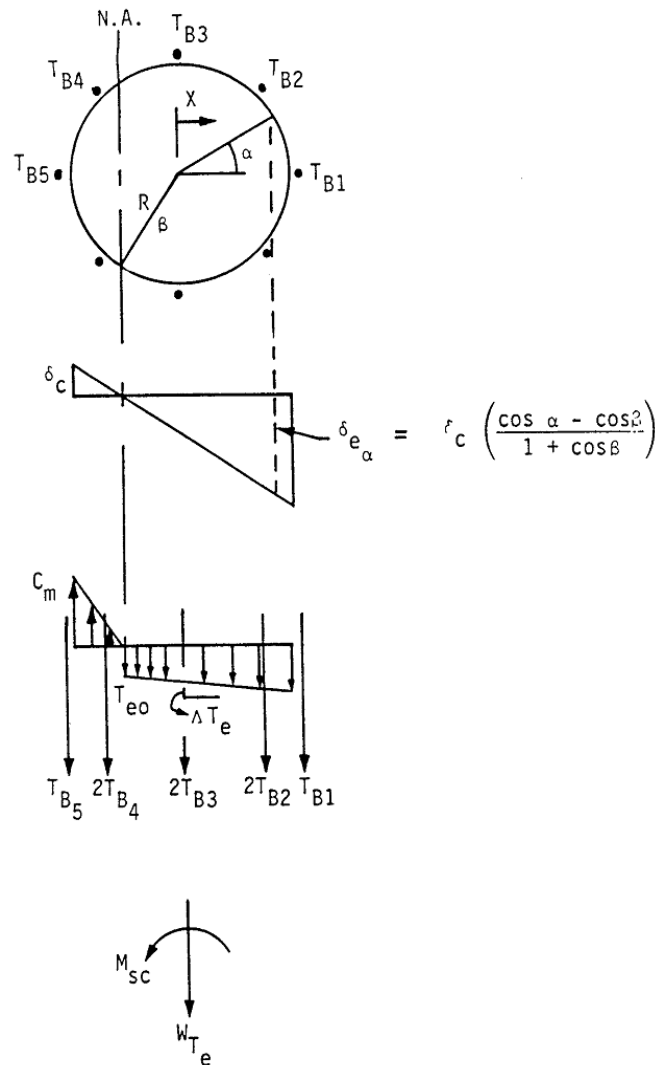
$$\delta_{ee} := \text{Find}(\delta_{ee}) = 0.322 \cdot \text{in}$$

Therefore, the linearized equation for  $T_e$  should not be extrapolated beyond  $\delta_e = 1.805$  inch.

Note that linearization is necessary later when developing overturning moment capacity.



### H.3.4 Overturning Moment Capacity:



### Vertical Loading on Tank Shell at Base [NUREG/CR-5270]

The overturning moment capacity  $M_{SC}$  can be estimated using the compressive buckling capacity of the tank shell ( $C_B$ ), the anchor bolt hold-down capacity

( $T_{BC}$ ), and the relationship between fluid hold-down force and uplift displacement. The estimation approach in the CDFM method requires several conservative but reasonable assumptions as noted below:

1. The bottom of the tank shell is assumed to rotate rigidly about the neutral axis (plane sections remain plane).
2. The cross-section of the tank at the top of the top plate of the bolt chairs ( $h_c$  above the base) is assumed to remain horizontal so that all vertical tank distortions needed to result in base uplift and mobilization of the anchor bolts must be accommodated over the height  $h_c$ .
3. The compressive stress varies linearly from zero at the neutral axis ( $\alpha=\beta$  as in the figure above) to its maximum value  $C_m$  at  $\alpha=180^\circ$ , as given by  $C_m = E_s t_s \delta_c / h_c \leq C_B$  (by converting eq. H-39), where  $\delta_c$  is the maximum compressive shortening.

Summary of parameters:

$$C_m = 12.681 \cdot \frac{\text{kips}}{\text{in}}$$

$$T_{BC} = 0 \cdot \text{kips}$$

$$T_{e0} = 0.072 \cdot \frac{\text{kips}}{\text{in}}$$

$$T_{e1} = 0.326 \cdot \frac{\text{kips}}{\text{in}^2}$$

$$W_{Te} = 198.306 \cdot \text{kips}$$

$$A_B := A_{bolt}$$

$$A_B = 4.909 \cdot \text{in}^2$$

$$E_B := 29 \times 10^3 \text{ksi}$$

$$R = 25.026 \cdot \text{ft}$$

$$t_s = 0.625 \cdot \text{in}$$

$$E_S := E_S = 29 \times 10^3 \cdot \text{ksi}$$

$$h_c := 207 \text{mm} = 8.15 \cdot \text{in}$$

$$h_a := 2 \text{ft} + 1 \text{in} = 25 \cdot \text{in}$$

Using the approach outlined in NUREG/CR-5270 instead of the EPRI NP-6041-SL appendix H in the following:

$$\delta_c := \frac{C_m \cdot h_c}{E_s \cdot t_s} = 5.702 \times 10^{-3} \cdot \text{in}$$

$$K_B := \frac{\delta_c \cdot A_B \cdot E_B}{h_a + h_c} = 24.486 \cdot \text{kips}$$

$$\Delta T_e := T_{eI} \cdot \delta_c = 1.861 \times 10^{-3} \cdot \frac{\text{kips}}{\text{in}}$$

$$\delta_{ea}(a, b) := \delta_c \cdot \left( \frac{\cos(a) - \cos(b)}{1 + \cos(b)} \right)$$

Because the bolt pretension  $T_{BP}$  is unreliable after a number of years in service, it is conservatively assumed to be 0.

$$T_{BP} := 0 \text{ kips}$$

The neutral axis angle  $\beta$  can be determined iteratively using the following procedure.

Bolt locations:  $i := 0..77$

$$\alpha_i := \frac{2\pi}{78} i$$

$$Tfunc(\alpha, \beta) := \begin{cases} c \leftarrow T_{BP} + K_B \cdot \frac{\cos(\alpha) - \cos(\beta)}{1 + \cos(\beta)} \\ c \leftarrow T_{BC} \text{ if } c > T_{BC} \\ c \leftarrow 0 \text{ if } c < 0 \end{cases}$$

$$C_1(\beta) := \frac{1 + \cos(\beta)}{\sin(\beta) + (\pi - \beta)\cos(\beta)}$$

$$C_2(\beta) := \frac{\sin(\beta)\cos(\beta) + \pi - \beta}{1 + \cos(\beta)}$$

$$C_3(\beta) := \frac{\sin(\beta) - \beta \cdot \cos(\beta)}{\sin(\beta) + (\pi - \beta)\cos(\beta)}$$

$$C_4(\beta) := \frac{\beta - \sin(\beta)\cos(\beta)}{1 + \cos(\beta)}$$

$$T_B(\alpha, \beta) := \xrightarrow{\hspace{1.5cm}} Tfunc(\alpha, \beta)$$

$$Cf'_m(\alpha, \beta) := \left( \frac{W_{Te} + \sum T_B(\alpha, \beta)}{2R} + T_{e0} \cdot \beta \right) \cdot C_1(\beta) + \Delta T_e \cdot C_3(\beta)$$

Equating  $Cf'_m$  and  $C_m$  to determine  $\beta$ :

$$func(\alpha, \beta) := Cf'_m(\alpha, \beta) - C_m$$

$$\beta := \text{root}(func(\alpha, \beta), \beta, 0, 3.1)$$

$$\beta = 3.00419 \quad \beta \cdot \frac{180}{\pi} = 172.128$$

$$C'_m := C_f'_m(\alpha, \beta) = 12.681 \cdot \frac{kips}{in} \quad C_m = 12.681 \cdot \frac{kips}{in}$$

Use  $C'_m$  and  $\beta$  to find the overturning moment capacity  $M_{SC}$ :

$$M_{SC} := C'_m \cdot C_2(\beta) \cdot R^2 + \sum \left( \overrightarrow{T_B(\alpha, \beta) \cdot R \cdot \cos(\alpha)} \right) + T_{e0} \cdot R^2 \cdot 2 \cdot \sin(\beta) + \Delta T_e \cdot C_4(\beta) \cdot R^2$$

$$M_{SC} = 22230.13 \cdot kips \cdot ft$$

$$\sum T_B(\alpha, \beta) = 0 \cdot kips$$

The largest bolt elongation (at  $\alpha=0$ ) should be checked to ensure that the anchorage has the capability:

$$\delta_{e0} := \delta_{ea}(\alpha_0, \beta) = 1.204 \cdot in$$

$$\text{Elongation ratio: } \frac{\delta_{e0}}{h_a + h_c} = 3.633\%$$

Elongation assessment is valid here at the end of 80 years because the bolts at tension will be pulled out. The following text is kept for other years.

The maximum elongation ratio is larger than 1%, which is recommended in the original CDFM method for the A307 bolt. One percent is also considered to be an appropriate percentage value for the A36 anchor bolt used in the subject CST construction.

The maximum tank shell uplift distortion  $\delta_{e0} = 0.026$  in, which is much less than the limit of 0.165 in for the small displacement theory to be applicable in developing the fluid hold-down capacity.

Because there are 78 anchor bolts (the example tank in the original CDFM method had only 8), the case where  $\alpha=0$  lies midway between bolts need not be checked.

The uncertainty in HCLPF buckling capacity of the tank shell due to the uncertain  $\sigma_{ye}$  can lead to an  $M_{SC}$  as low as 119133.414 kips-ft or as high as 192156.702 kips-ft. It should be noted that unlike in the original CDFM method,  $M_{SC}$  is sensitive to the estimate of  $C_m$ .

Inelastic energy absorption reduction factor  $k$  can be applied to linearly computed seismic response to obtain the actual overturning moment capacity. The combined bolt yielding and tank shell buckling failure mode for overturning moment is not brittle

so that k can be less than unity. However, as stated in the original CDFM method, it is difficult to make an appropriate estimate of k for this failure mode. Therefore, it is conservatively assumed to be unity.

$$k := 1.0$$

$$SME_M := \frac{M_{SC}}{k \cdot M_{SH}} \cdot SME_e \qquad SME_M = 0.165 \cdot g$$

Since  $SME_M$  is substantially different from  $SME_e$ , the above procedure should be iterated to obtain the appropriate SME estimate. The resultant  $SME_e$  is found to be 0.97g.



### H.3.5 Sliding Capacity:



The base plate of the CST has a slight cone ( with a slope of 1 to 96) so that the fluid will always drain away from the center of the tank. This cone is generally created by variable thickness of the oiled sand cushion between the tank bottom plate and its foundation. Therefore, the coefficient of friction between the tank base and its foundation is reasonably assumed to have a conservative value of 0.55:

$$COF := 0.55$$

The sliding shear capacity can then be calculated as,

$$V_{SC} := COF \cdot \left( W_{Te} + P_a \cdot \pi \cdot R^2 + \sum T_B(\alpha, \beta) \right) = 2.297 \times 10^3 \cdot kips$$

The shear capacity of the bolts should not be considered because (a) there is a large space between the concrete foundation and the anchor bolt chair, and (b) there is a 1/4" diametric clearance in the hole in the anchor bolt chair.

The sliding capacity with a unit inelastic absorption factor as suggested by the original CDFM method:

$$SME_V := \frac{V_{SC}}{k \cdot V_{SH}} \cdot SME_e \qquad SME_V = 0.254 \cdot g$$

By varying  $SME_e$ , the HCLPF shear capacity is found to be 0.426g.

Unlike the example tank in the original CDFM method, the capacity of the CST appears to be governed by the sliding capacity. The sliding capacity considers only the friction between the bottom plate and the foundation.



### H.3.6 Fluid Pressure Capacity:

---



The inelastic energy absorption seismic response reduction factor  $k_u$  is suggested to be 0.8 for HCLPF capacity evaluation:

$$k_u := 0.8$$

For the CDFM hoop membrane stress capacity, it is recommended that the ASME seismic design limit of  $2 S_M$  for primary stress should be used, which is 37.5 ksi for SA240-type 304 stainless steel:

$$\sigma_a := 37.5 \text{ ksi}$$

The pressure capacity,  $P_{CA}$ , at the bottom of the tank shell (the CST has a uniform shell thickness), can be estimated to be:

$$P_{CA}(t) := \frac{\sigma_a \cdot t}{R}$$
$$P_{CA}(t_S) = 78.044 \cdot \text{psi}$$

The maximum seismic induced hydrodynamic pressures  $P_{SM}$  and the hydrostatic pressure  $P_{ST}$  at the bottom of the tank shell are:

$$P_{SM}(H) = 4.283 \times 10^4 \text{ Pa}$$
$$P_{ST}(H) = 1.12 \times 10^5 \text{ Pa}$$

The HCLPF fluid pressure capacity  $SME_p$  can be determined as:

$$SME_p := \frac{P_{CA}(t_S) - P_{ST}(H)}{k_u \cdot P_{SM}(H)} \cdot SME_e = 2.052 \cdot g$$

By varying  $SME_e$ , the HCLPF fluid pressure capacity can be found to be 2.191 g, which does not govern. This agrees with seismic experience that the fluid pressure capacity seldom appears to govern the seismic capacity for normal flat bottomed steel tanks with butt-welded side plates.



---

Summary of SME capacities:

$$SME_M = 0.165 \cdot g$$

$$SME_V = 0.254 \cdot g$$

$$SME_p = 2.052 \cdot g$$

$$SME_{cr} := \min(SME_M, SME_V, SME_p) = 0.165 \cdot g$$

$$SME_e = 0.165 \cdot g$$

$$if[SME_{cr} = SME_M, "Moment", (if(SME_{cr} = SME_V, "Shear", "Fluid Pressure"))] = "Moment"$$

$$year = 80$$

$$crack = 0.624 \cdot mm$$

Summary of results:

Years:	0	5	10	15	20	25	30	35	40
cr (mm):	0.	0.039	0.078	0.117	0.156	0.194	0.234	0.273	0.312
SME:	0.426	0.426	0.426	0.426	0.426	0.424	0.416	0.399	0.371
SMEM:	1.140	1.140	1.140	1.140	1.140	1.127	1.045	0.900	0.704
SMEV:	0.426	0.426	0.426	0.426	0.426	0.424	0.416	0.399	0.371
SMEP:	2.052	2.052	2.052	2.052	2.052	2.052	2.052	2.052	2.052
Mode:	Shear	Shear	Shear	Shear	Shear	Shear	Shear	Shear	Shear
Years:	45	50	55	60	65	70	75	80	
cr (mm):	0.351	0.390	0.429	0.468	0.507	0.546	0.585	0.624	
SME:	0.330	0.240	0.165	0.165	0.165	0.165	0.165	0.165	
SMEM:	0.472	0.240	0.165	0.165	0.165	0.165	0.165	0.165	
SMEV:	0.330	0.282	0.254	0.254	0.254	0.254	0.254	0.254	
SMEP:	2.052	2.052	2.052	2.052	2.052	2.052	2.052	2.052	
Mode:	Shear	Moment							

### H.3.7 Consideration of Other Capacities:

(1) Slosh height for roof damage: note that even with a  $SME_e = 0.334 \text{ g}$  (the initial guess), the slosh height is about 4.8 ft. With the HCLPF shear capacity of  $SME_e = 0.555 \text{ g}$ , the sloshing height can be about 7.9 ft, which is close to the total height of the head (8.7', as approximated in the beginning part of this calculation).

$$h_s = 2.36 \cdot ft$$

$$SME_e = 0.165 \cdot g$$

The increase of sloshing height is not significant as  $SME_e$  increases from 0.334 g to 0.555 g. In addition, as pointed out in the original CDFM method, even if roof damage might be expected, such damage usually does not impair the ability of the tank to contain fluid.

(2) The CST is assumed to sit on rock/very stiff soil; therefore, soil-tank foundation interaction is not considered.

(3) Piping failure or failure of nozzles may lead to loss of fluid in the tank, and more importantly, may impair the normal function of the condensation system. As reported in the original CDFM method, a significant fraction of the cases of seismic induced loss of tank contents have been due to piping/nozzle failures because of poor detailing. The CDFM method also stated that a SME evaluation of piping/nozzle failure is only necessary when poor seismic detailing is found in

the involved piping attached to the tank. This analysis assumes that the subject CST is appropriately detailed, i.e. the piping and nozzle directly attached to the tank are properly designed and constructed so that sufficient piping flexibility can be achieved to accommodate large relative seismic anchor movements.

(4) The influence of the building in between the two CSTs on the SME are assessed in the following. The gap between the auxiliary building and the CSTs at the roof level is filled with elastomeric sealant.

The maximum tank shell uplift distortion is found to be 0.026 in, which corresponds to a neutral axis angle  $\beta$  of 2.29161 rad. Since the horizontal plane at the anchor bolt chair is assumed to remain plane and all distortion is assumed to occur below this level, the rotation angle around the neutral axis can be estimated to be:

$$Rotation := \frac{\delta_{e0}}{R \cdot (1 - \cos(\beta))} = 2.015 \times 10^{-3}$$

$$\beta = 3.004 \quad \cos(\beta) = -0.991$$

The maximum horizontal displacement at the roof of the auxiliary building, which is at an elevation of 114' 9" (Parapet elevation, compared to the tank floor elevation of 101' 9"), can be estimated to be:

$$Rotation \cdot 13ft = 0.314 \cdot in$$

This horizontal displacement is much less than the width of the seismic separation joint at the roof elevation, which is 3 in. Therefore, the influence of the auxiliary building to the two CSTs is considered minimal.

## The Fragility of CST

Summary of results:

Years:	0	5	10	15	20	25	30	35	40
cr (mm):	0.	0.039	0.078	0.117	0.156	0.194	0.234	0.273	0.312
SME:	0.426	0.426	0.426	0.426	0.426	0.424	0.416	0.399	0.371
SMEM:	1.140	1.140	1.140	1.140	1.140	1.127	1.045	0.900	0.704
SMEV:	0.426	0.426	0.426	0.426	0.426	0.424	0.416	0.399	0.371
SMEP:	2.052	2.052	2.052	2.052	2.052	2.052	2.052	2.052	2.052
Mode:	Shear	Shear	Shear	Shear	Shear	Shear	Shear	Shear	Shear
Years:	45	50	55	60	65	70	75	80	
cr (mm):	0.351	0.390	0.429	0.468	0.507	0.546	0.585	0.624	
SME:	0.330	0.240	0.165	0.165	0.165	0.165	0.165	0.165	
SMEM:	0.472	0.240	0.165	0.165	0.165	0.165	0.165	0.165	
SMEV:	0.330	0.282	0.254	0.254	0.254	0.254	0.254	0.254	
SMEP:	2.052	2.052	2.052	2.052	2.052	2.052	2.052	2.052	
Mode:	Shear	Moment							

$$SME_{HCLPF} := (0.426 \ 0.426 \ 0.426 \ 0.426 \ 0.426 \ 0.424 \ 0.416 \ 0.399 \ 0.371 \ 0.330 \ 0.240)$$

$$SME_M := (1.140 \ 1.140 \ 1.140 \ 1.140 \ 1.140 \ 1.127 \ 1.045 \ 0.900 \ 0.704 \ 0.472 \ 0.240 \ 0.16)$$

$$SME_V := (0.426 \ 0.426 \ 0.426 \ 0.426 \ 0.426 \ 0.424 \ 0.416 \ 0.399 \ 0.371 \ 0.330 \ 0.282 \ 0.25)$$

$$SME_P := (2.052 \ 2.052 \ 2.052 \ 2.052 \ 2.052 \ 2.052 \ 2.052 \ 2.052 \ 2.052 \ 2.052 \ 2.052 \ 2.052)$$

It should be emphasized that the HCLPF SME capacity assumes the Regulatory Guide 1.60 spectra anchored to the HCLPF SME PGA.

To determine the seismic fragility of the CST tank, one needs to convert the HCLPF SME PGA to median SME PGA. This conversion requires the estimate of both aleatory and epistemic uncertainties ( $\beta_R$  and  $\beta_U$ ). The Fragility Method, also presented along with the original CDFM method, estimates the aleatory and epistemic uncertainties to be 0.2 and 0.27, respectively. These uncertainties are nearly identical to those reported by Choun, et al [2008]. The SME median  $SME_m$  can then be estimated as well.

$$i := 0, 1 \dots 16$$

$$\beta_R := 0.2$$

$$\beta_U := 0.27$$

$$\beta_C := \sqrt{\beta_R^2 + \beta_U^2} = 0.336$$

$$Hm := \exp[1.645(\beta_R + \beta_U)] = 2.167$$

$$SME_{m_i} := SME_{HCLPF_i} \cdot Hm$$

$$SME_{Mm_i} := SME_{M_i} \cdot Hm$$

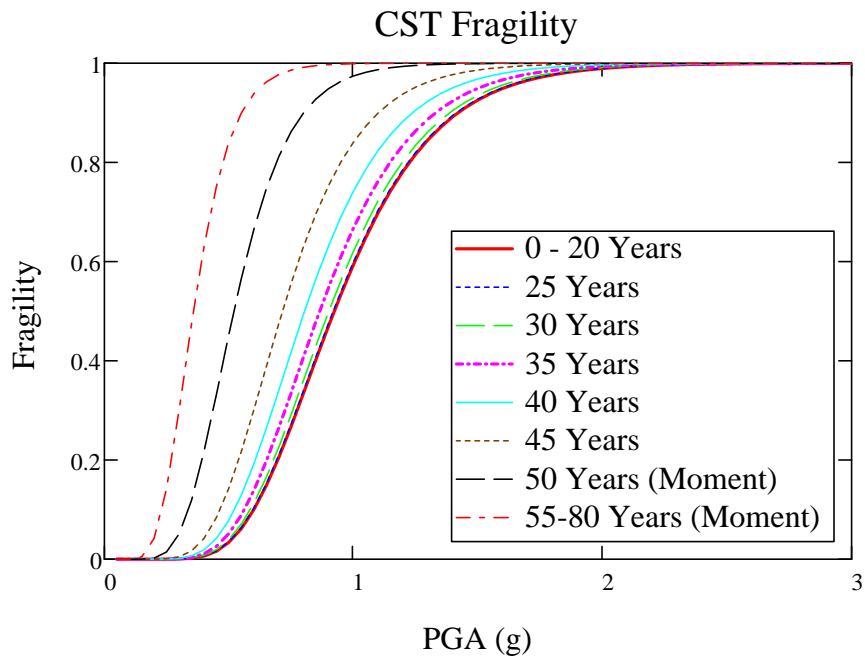
$$SME_{Vm_i} := SME_{V_i} \cdot Hm$$

$$SME_{Pm_i} := SME_{P_i} \cdot Hm$$

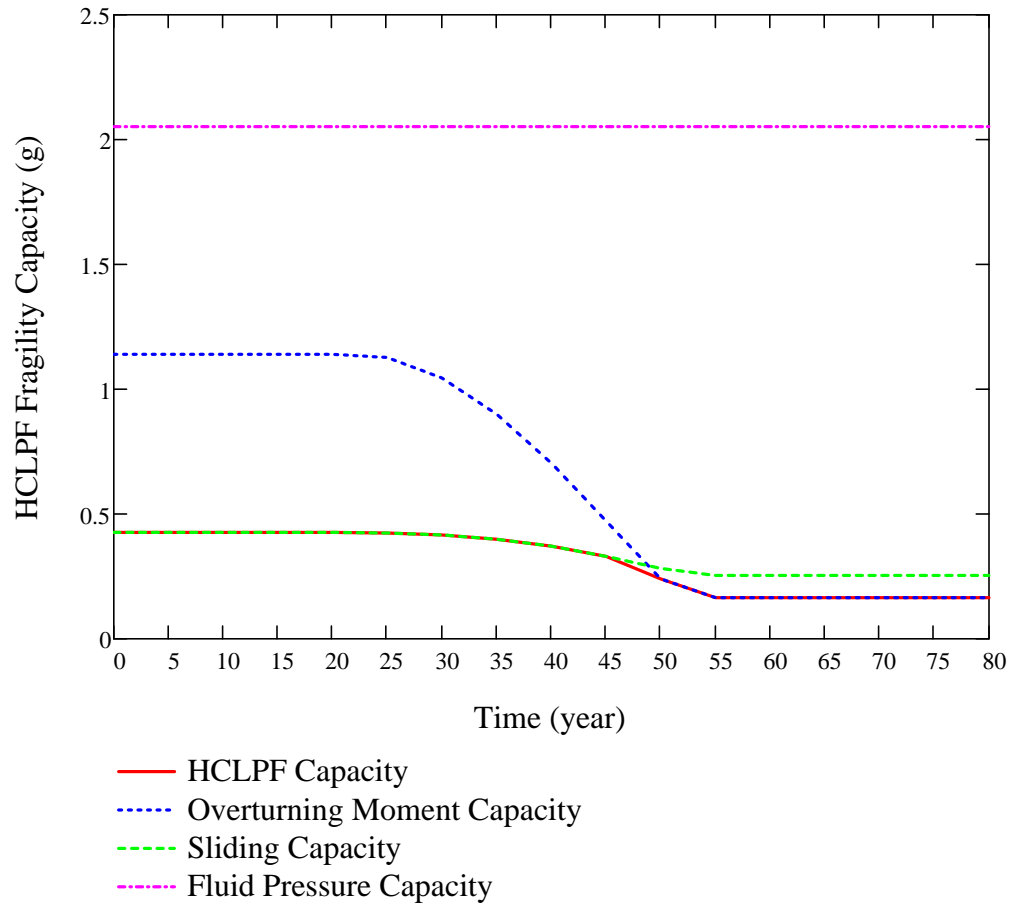
$$F(Q,a) := cnorm \left( \frac{\ln \left( \frac{a \cdot g}{SME_m} \right) + \beta_U \cdot qnorm(Q,0,1)}{\beta_R} \right)$$

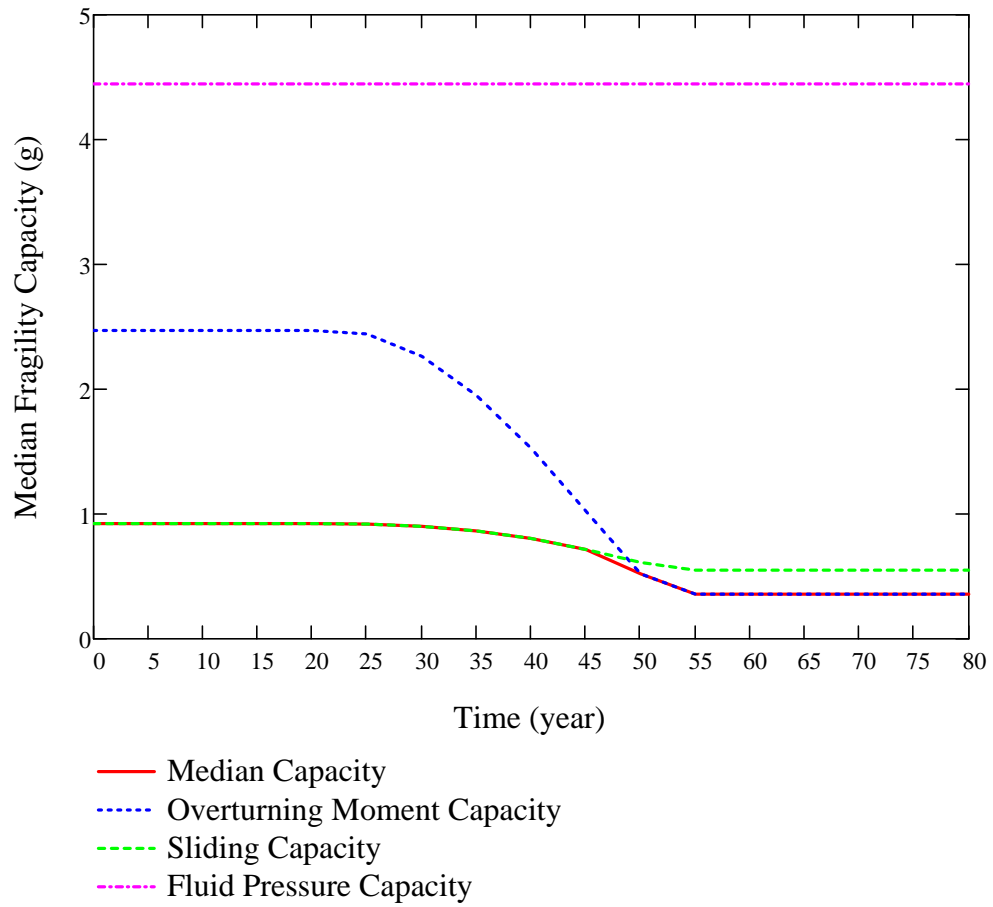
$$F_{mean}(a) := cnorm \left( \frac{\ln \left( \frac{a \cdot g}{SME_m} \right)}{\beta_C} \right)$$

$sa := 0.05, 0.1 \dots 3$



$year_i := i \cdot 5$





1 0.165 0.165 0.165 0.165 0.165 0.165)<sup>T</sup>·g

55 0.165 0.165 0.165 0.165 0.165)<sup>T</sup>·g

4 0.254 0.254 0.254 0.254 0.254)<sup>T</sup>·g

2 2.052 2.052 2.052 2.052 2.052)<sup>T</sup>·g

THESE DATA ARE THE CONTINUATION OF PAGE E-20.

**Appendix F FRAGILITY ANALYSIS OF THE CST WITH MULTIPLE  
DEGRADATIONS**



# KAERI Year 3 Task

## Fragility Analysis of Condensate Storage Tank

### - Combining Degradation Cases A, B, and C

This calculation combines degradation cases (A) stainless steel tank shell, (B) anchor bolts, and (C-2) anchorage concrete cracking. In this evaluation, all three degradations are assumed to occur simultaneously and to be perfectly correlated.

$$year := 65$$

$$SME_e := 0.032g$$



Degradation Case A: Stainless Steel Tank Shell

$$scc\_rate := 7.494 \times 10^{-3} \text{ in}$$

$$tshell\_degraded := \frac{5}{8} \text{ in} - scc\_rate \cdot year = 0.138 \cdot \text{in}$$

Degradation Case B: Anchor Bolts

$$C := 70.6$$

$$\alpha := 0.79$$

$$X(t) := C \cdot t^\alpha \cdot \mu m$$

$$Dbolt\_degraded := 2.5 \text{ in} - 2 \cdot X(\text{year}) = 2.34962 \cdot \text{in}$$

Degradation Case C: Anchorage concrete cracking - BNL model

$$crack := 0.0078 \cdot year \cdot mm = 0.02 \cdot \text{in}$$



## H.1 Introduction

KAERI indicated that the seismic DBE in Korea follows the NRC Reg. Guide 1.60 design spectrum shape but with a PGA level scaled down to 0.2 g. An initial HCLPF capacity was assumed to be 1.67 times of 0.2 g. However, since the Mathcad

sheets in this appendix solve the various equations iteratively by manually setting  $SME_e$  to different values, the above  $SME_e$  value of 0.032 g represents the converged solution for the degradation level of the combined degradations at 65 years.



---

## H.2 Response Evaluation

Same as Appendix A, Section H.2.



---

## H.3 Capacity Assessment



The seismic overturning moment capacity of the CST at its base,  $M_{SC}$ , depends on the axial compressive buckling capacity of the tank shell  $C_m$ , the tensile hold-down capacity of the anchor bolts including their anchorage and attachment to the tank  $T_{BC}$ , and the hold-down capacity of the fluid pressure acting on the tank base plate  $T_e$ .

Although unlikely for larger radius tanks, the tank SME capacity is sometimes governed by the sliding shear capacity at the tank base,  $V_{SC}$ . Even though it does not appear that any butt welded steel tank has ever failed due to seismic induced membrane hoop stresses due to combined hydrostatic and hydrodynamic fluid pressures, the SME capacity of this failure mode,  $P_{CA}$ , should also be checked.

Additional assessment of the seismic capacity may include the possibility and consequence of the fluid sloshing against the tank roof, foundation failure for soil sites, and possibility of failure of piping or their attachment to the tank.

### ***H.3.1 Compressive Buckling Capacity of the Tank Shell:***

The most likely buckling for tanks is the "elephant-foot" buckling near the base of the tank shell. The "elephant-foot" buckling is a combined effect of hoop tension, axial (vertical) compression, and restriction of radial deformation of the tank shell by the base plate. "Elephant-foot" buckling does not necessarily lead to failure of a tank (e.g., leakage). However, there is no simple capability evaluation method that can predict tank performance after the development of "elephant-foot" buckling. Therefore, for a CDFM SME capacity of tanks, the onset of "elephant-foot" buckling will be judged to represent the limit to the compressive buckling capacity of the tank shell. The onset of "elephant-foot" buckling can be estimated using elastic-plastic collapse theory as presented in the following:

The sidewall thickness near the shell base:  $t_s := t_{shell\_degraded} = 0.138 \cdot in$

The tank internal pressure near its base:

$$P := P_{C+} = 1.188 \times 10^5 Pa$$

Elastic modulus of the tank:

$$E_S = 2.9 \times 10^4 \cdot ksi$$

The CST shell was made of SA 204-type 304 stainless steel. This material does not have a flat yield plateau and as strain increases its stress can grow to a minimum ultimate stress capacity of 75 ksi. In the CDFM method, an effective yield stress  $\sigma_{ye}$  is set to  $2.4S_M$  or 45 ksi, in line with the ASME seismic design limit for primary local membrane plus primary bending [ASME 1983, "ASME Boiler & Pressure Vessel Code"]. The potential uncertainty range for  $\sigma_{ye}$  is reported to be between 30 ksi and 60 ksi, according to the original CDFM method description.

$$\sigma_{ye} := 45ksi$$

$$\frac{R}{t_s} = 2.178 \times 10^3$$

$$S_I := \frac{R}{t_s} \div 400 = 5.445$$

The "elephant-foot" buckling axial stress of the tank shell can be accurately predicted to be:

$$\sigma_p := \frac{0.6E_S}{R \div t_s} \cdot \left[ 1 - \left( \frac{P \cdot R}{\sigma_{ye} \cdot t_s} \right)^2 \right] \cdot \left( 1 - \frac{1}{1.12 + S_I^{1.5}} \right) \cdot \left( \frac{S_I + \frac{\sigma_{ye}}{36ksi}}{S_I + 1} \right) = 2.345 \cdot ksi$$

The compressive buckling capacity for HCLPF capacity computation utilizes a recommended 0.9 reduction factor of the buckling stress:

$$C_m := 0.9\sigma_p \cdot t_s = 0.291 \cdot \frac{kips}{in}$$

Buckling capacity of the supported cylindrical shells under combined axial bending and internal pressure should also be checked although it is unlikely to govern for overall seismic response of fluid containing tanks. The axial bending induced buckling stress,  $\sigma_{CB}$ , for such a load case can be conservatively estimated (essentially lower bound) as follows.

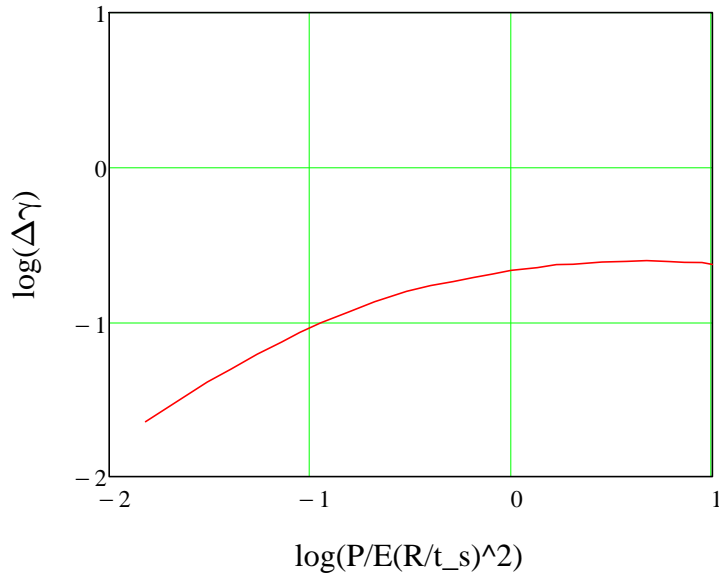
A parameter  $\Delta\gamma$  to be used in the following procedure as an increase factor for internal pressure can be obtained from Figure 6 of "Buckling of Thin-walled Circular Cylinders," [NASA SP-8007].  $\Delta\gamma$  depends on the minimum compression zone pressure at the base of the tank shell,  $P_{C-}$ , corresponding to the time of maximum moment.

Considering the potential range on  $\sigma_{ye}$  of 30 to 60 ksi, the resultant range on  $\sigma_p$  is 16.572 ksi to 26.702 ksi. Consequently,  $C_m$  has a range of 9.322 kips/in to 15.02 kips/in.

Since  $\Delta\gamma$  is to be evaluated based on Figure 6 of NASA SP-8007, this figure is digitized and defined by the following two vectors, in log scale:

$$\begin{array}{l}
 \text{fig6x} := \left( \begin{array}{l}
 -1.8197 \\
 -1.5124 \\
 -1.395 \\
 -1.264 \\
 -1.1422 \\
 -1.0519 \\
 -0.94817 \\
 -0.81296 \\
 -0.67999 \\
 -0.52011 \\
 -0.40087 \\
 -0.28846 \\
 -0.18951 \\
 -0.09283 \\
 -0.00063874 \\
 0.12966 \\
 0.22407 \\
 0.3071 \\
 0.45083 \\
 0.57204 \\
 0.67305 \\
 0.78519 \\
 0.86144 \\
 0.94893 \\
 1.0004
 \end{array} \right)
 \end{array}
 \qquad
 \begin{array}{l}
 \text{fig6y} := \left( \begin{array}{l}
 -1.6448 \\
 -1.3884 \\
 -1.3056 \\
 -1.2088 \\
 -1.1297 \\
 -1.0676 \\
 -1.0058 \\
 -0.93763 \\
 -0.86938 \\
 -0.8017 \\
 -0.76514 \\
 -0.7391 \\
 -0.71278 \\
 -0.68996 \\
 -0.66704 \\
 -0.64849 \\
 -0.62918 \\
 -0.62739 \\
 -0.61269 \\
 -0.60816 \\
 -0.60321 \\
 -0.60915 \\
 -0.61434 \\
 -0.6162 \\
 -0.62796
 \end{array} \right)
 \end{array}$$

Figure 6 of NASA SP-8007: Increase in Axial-Compressive Buckling-Stress Coefficient of Cylinders due to Internal Pressure



$$10^{\text{linterp}(\text{fig6x}, \text{fig6y}, \log(0.166))} = 0.12004$$

$$\text{ipx} := \frac{P_C}{E_S} \left( \frac{R}{t_s} \right)^2 = 2.678$$

$$\frac{P_C}{E_S} \left( \frac{R}{t_s} \right)^2 = 0.13$$

$$\Delta\gamma := 10^{\text{linterp}(\text{fig6x}, \text{fig6y}, \log(\text{ipx}))} = 0.243$$

$$\phi := \frac{1}{16} \cdot \sqrt{\frac{R}{t_s}} = 2.917$$

$$\gamma := 1 - 0.73(1 - e^{-\phi}) = 0.309$$

Note: there is not experimental data for  $R/t > 1500$ .

$$\frac{R}{t_s} = 2.178 \times 10^3$$

$$\sigma_{CB} := (0.6\gamma + \Delta\gamma) \frac{E_S}{R \div t_s} = 5.704 \cdot \text{ksi}$$

$$0.9\sigma_p = 2.11 \cdot \text{ksi}$$

$\sigma_{CB}$  exceeds  $0.9s_p$ , so it does not govern.

### H.3.2 Bolt Hold-down Capacity:

The bolt hold-down capacity should be determined as the smallest of the bolt tensile capacity, anchorage of bolt into concrete foundation, capacity of the top plate of bolt chairs to transfer bolt loads to the vertical chair gussets, attachment of the top plate and vertical chair gussets to the tank shell, and the capacity of tank shell to withstand concentrated loads imposed on it by bolt chairs.

**Anchor bolt capacity:** the anchor bolt has a diameter of 2 1/2" and is made of A36 steel. The tensile capacity can be determined as:

$$d_{bolt} := D_{bolt\_degraded} = 2.35 \cdot in$$

$$A_{bolt} := \frac{\pi \cdot d_{bolt}^2}{4} = 4.336 \cdot in^2$$

Based on the AISC Code [9th edition, 1989] for threaded A36 bolts:

$$T_{BC} := 1.7A_{bolt} \cdot 19.1ksi = 140.788 \cdot kips \quad T_{BC} = 70.394 \cdot tonf$$

Note that  $T_{BC}$  is the capacity of one bolt and the capacity of the interacting multi-bolts will be considered later.

**Anchor bolt chair capacity check:** according to the drawing, the anchor bolt chairs form a circumferentially continuous construction. Based on the continuous chair construction and the sizing of the plates and weld, it is judged that the anchor bolt chair and its attachment to the tank shell is adequate to transfer the bolt capacity load for the CST tank. The tank shell is also considered to be adequate in withstanding the concentrated loads imposed on it by bolt chairs, especially because the "elephant-foot" buckling capacity is also checked.

$$t_{chair} := \left(1 + \frac{3}{8}\right)in = 1.375 \cdot in$$

Weld width is 15 mm (5/8") according to the drawing.

**Capacity of bolt anchorage into concrete foundation:** the anchorage is constructed using non-shrinking grout. The tensile failure of bolt anchorage mainly consists of bolt failure, plug pull-out, and concrete cone failure, the last two of which typically are a combination of tensile failure of concrete in the upper portion of the anchorage that results in a partial depth cone-shaped spall and bond failure at the grout-concrete interface in the lower portion of the anchorage.

Bolt spacing: 
$$\Delta d := \pi \cdot \left[ 50ft + \left( 9 + \frac{1}{16} \right) in \right] \div 78 = 2.044 \cdot ft$$

Lee, et al [2001] described an experimental and analytical work on the pull-out strength of large-sized anchor bolt, in a SMiRT 16 paper entitled "failure mechanism for large-sized grouted anchor bolt under tensile load." The test specimens were selected based on the real construction of CST in the Yonggwang Nuclear Power Plant of Korea. The anchor bolt is 2-1/2 inches in diameter, and has an embedment length of 2 ft 2-3/8 inches. The anchor bolt material is ASTM A36. Non-shrinking grout was used in the post-installed anchorage construction. These construction variables are basically very similar to those of the subject CST for fragility analysis, except that the subject CST anchors have a slightly shorter embedment length of 2 ft 1 inch. The concrete strength of the subject CST foundation is not available, and is assumed to be the same as in this SMiRT 16 paper, which has a compressive strength of 4500 psi. The circumferential spacing is about 2 ft for both tanks. The test included 5 anchor bolt specimens.

As reported by Lee, et al [2001], the average 7 day and 28 day compressive strength of the concrete were 5419 psi and 7180 psi, respectively. The actual average compressive strength of non-shrinking grout at 7 days and 21 days were 7550 psi and 11100 psi, respectively. The non-shrinking grout has obviously larger compressive strength than the concrete, as expected for normal construction of anchorage. The reported bond strength of the non-shrinking grout (Masterflow 870) was 40 kgf/cm<sup>2</sup> (569 psi). The Young's modulus of A36 is 2.9\*10<sup>7</sup> psi and the Poisson's ratio is 0.3.

The test first confirmed a minimum required load of 50 tons (100 kips). Three of the five grouted anchors were tested further until failure. Two specimens was judged to have failed by tensile failure of grout at the lower portion of the grout block, bonding failure between grout and the concrete, and tensile failure of concrete. The other specimen showed abrasion of anchor bolt thread. All specimens achieved at least 100 tons (200kips), after which the load-deformation curve became significantly flatter and the ultimate failure load scatters between 100 tons and 120 tons.

Based on the test, the anchorage capacity should be 200 kips, which is about 26% higher than the estimate based on tensile strength of the anchor bolt. It should be noted that in the test, one specimen had abrasion in its thread, suggesting the anchor bolt capacity should be also close to 200 kips. However, since the embedment in the test was about 1-3/8 inch longer than the subject CST case, the spacing of anchor bolts in the test is twice as long as in the subject CST case, and the lab test condition usually have a higher quality control, the estimate of 159.387 kips will be assumed as the anchorage capacity.

The effective embedment for the anchorage in the subject CST is estimated to be 23", which is determined by subtracting 1" from the total embedment of 2' 1" to account for the nuts.

$$h_{eff} := 23in$$

The compressive strength of the concrete is assumed to be 4500 psi, according to the above mentioned paper. It should be pointed out that the measured strength in the test is higher.

$$f_c := 4500psi$$

Base case of the anchor bolt strength based on concrete based on NUREG/CR-5434 (Figure 5.20):

$$k := 57$$

$$T_{AC} := k \cdot \left( \frac{h_{eff}}{in} \right)^{1.5} \cdot \sqrt{\frac{f_c}{psi}} \cdot lbf = 421.767 \cdot kips$$

Note that this  $T_{AC}$  capacity calculated based on NUREG/CR-5434 is greater than 200 kips as determined in the test as reported in a SMiRT paper by Lee, et al. [2001]. The anchor bolts in the tests reported in NUREG/CR-5434 have a diameter of 3/4" and an embedment of 4", which are much smaller than those used in the CST construction. Therefore, the test data in NUREG/CR-5434 will be used as factors to scale the test data as reported in the paper by Lee, et al. [2001].

$$f_{TAC} := \frac{200kips}{421.767kips} = 0.474$$

Strengths for a crack width of 0mm and 0.3 mm can be assumed to be, based on Figure 5.20 of NUREG/CR-5434:

$$T_{AC\_00} := 200kips$$

$$T_{AC\_03} := 200kips \cdot \frac{15.5}{57} = 54.386 \cdot kips$$

$T_{AC}$  as a function of crack width can be established as:

$$T_{AC}(c) := \max \left[ T_{AC\_00} + \frac{c}{0.3mm} \cdot (T_{AC\_03} - T_{AC\_00}), 0kips \right]$$

$$T_{AC}(crack) = 0 \cdot kips$$

$$T_{BC} = 140.788 \cdot kips$$

$$T_{BC} := \min(T_{BC}, T_{AC}(crack)) = 0 \cdot kips$$



$$MFP := \frac{R \cdot t_s}{\sqrt{12(1 - \nu^2)}} \left( 1 - \frac{R}{H \cdot \kappa} \right) = 7.995 \times 10^{-3} m^2$$

$$K_S := \frac{2 \cdot K \cdot \kappa}{R} = 1.237 \times 10^4 N$$

MFP is a shortcut to  $M_F / P$

The uplift height  $\delta_e$ , the hold down tension  $T_e$ , moment  $M_e$ , rotation  $\alpha_e$ , and maximum positive moment  $M_+$  can then be defined as functions of uplift length  $l$ :

$$F(l) := 1 + \frac{K_S \cdot l}{2E_S \cdot I_b}$$

$$\delta_e(l) := \left[ \frac{l^4}{24} - \frac{1}{F(l)} \left( \frac{K_S \cdot l^5}{72E_S \cdot I_b} + MFP \cdot \frac{l^2}{6} \right) \right] \cdot \left( \frac{P}{E_S \cdot I_b} \right)$$

$$T_e(l) := P \cdot \left[ \frac{l}{2} + \frac{1}{F(l)} \cdot \left( \frac{K_S \cdot l^2}{12E_S \cdot I_b} + \frac{MFP}{l} \right) \right]$$

Note: this equation as in the original CDFM method is singular at  $L = 0$  ft. The  $MFP/L$  term only has a minor effect on  $T_e$  when  $L$  is very small. The linear approximation in the original CDFM method can effectively avoid this singularity.

$$M_e(l) := P \cdot \left( \frac{1}{F(l)} \right) \cdot \left( \frac{K_S \cdot l^3}{12E_S \cdot I_b} + MFP \right)$$

$$M_+(l) := P \cdot \left( \frac{l^2}{8} - \frac{M_e(l)}{2P} + \frac{M_e(l)^2}{2P^2 \cdot l^2} \right)$$

The singularity in this equation can be similarly avoided by the linear approximation.

$$\alpha_e(l) := \frac{P \cdot l^3}{12E_S \cdot I_b} - \frac{M_e(l) \cdot l}{2E_S \cdot I_b}$$

Given

$$l := 0 \text{ in}$$

$$\frac{l^2}{24} - \frac{1}{F(l)} \left( \frac{K_S \cdot l^3}{72E_S \cdot I_b} + MFP \cdot \frac{1}{6} \right) = 0$$

$$l_{min} := Find(l) = 6.848 \cdot in$$

Given

$$l_{max} := 10in$$

$$\delta_e(l_{max}) = 0.165in$$

$$l_{max} := Find(l_{max}) = 12.46 \cdot in$$

$$l := l_{min}, l_{min} + 0.1in .. l_{max}$$

Linear Approximation:

$$i := 0 .. \frac{(l_{max} - l_{min})}{0.1in}$$

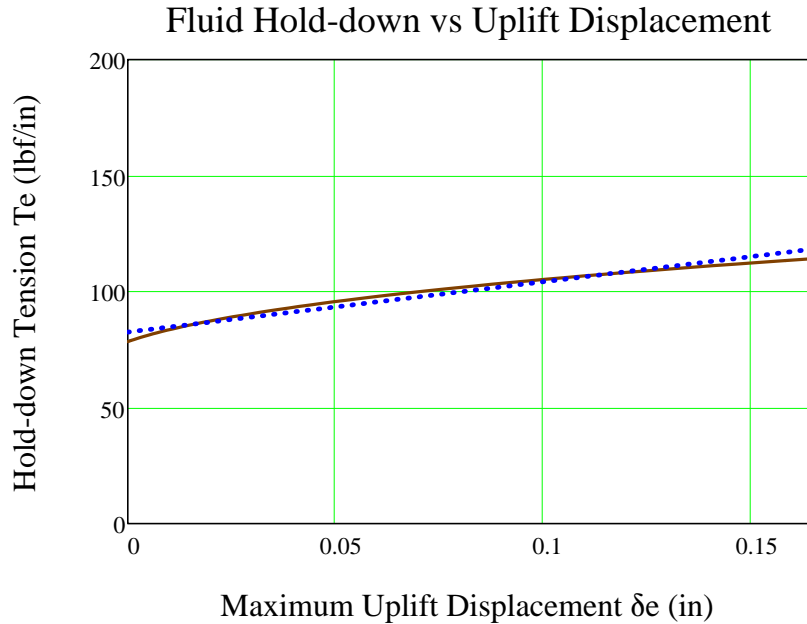
$$l_{vec_i} := l_{min} + i \cdot 0.1 \cdot in$$

$$\begin{pmatrix} T_{e0} \\ T_{e1} \end{pmatrix} := line \left[ \begin{array}{c} \overrightarrow{\delta_e(l_{vec})} \\ in \end{array}, \begin{array}{c} \overrightarrow{T_e(l_{vec}) \cdot \frac{in}{lbf}} \\ \end{array} \right] = \begin{pmatrix} 82.56 \\ 216.98 \end{pmatrix}$$

$$T_{e0} := if(P_{T-} > 0psi, T_{e0}, 0) \frac{lbf}{in} = 82.56 \cdot \frac{lbf}{in}$$

$$T_{e1} := if(P_{T-} > 0psi, T_{e1}, 0) \cdot \frac{lbf}{in^2} = 216.98 \cdot \frac{lbf}{in^2}$$

$$T_{e\_lin}(\delta_e) := T_{e0} + T_{e1} \cdot \delta_e$$



It should be noted that these equations are derived based on small displacement theory, and are applicable to the following conditions:

1.  $L / R \leq 0.15$ . The solution does not consider the stiffening effect of hoop behavior on the base plate and consequently conservatively overpredicts the displacement  $\delta_e$ , as the ratio of  $L/R$  becomes larger.
2.  $\delta_e / t_b \leq 0.6$ . As the solution is based on small displacement assumption, which ignores the beneficial influence of the membrane tension in the base plate to reduce  $\delta_e$  for a given  $T_e$  as in large displacement theory. For unanchored tanks, Manos (in "earthquake tank-wall stability of unanchored tanks," *Journal of Structural Engineering*, Vol 112, No. 8, ASCE, 1986) and Haroun and Badawi (in "nonlinear axisymmetric uplift of circular plates," *Dynamics of Structures*, ASCE, 1987) showed that large displacement membrane theory greatly increases the fluid hold-down force  $T_e$  and consequently the uplift  $\delta_e$ . Nevertheless, for anchored tanks like the subject CST, the uplift is not expected to be very large.
3.  $M_e/M_{pb} \leq 0.9$ ;  $M_e/M_{ps} \leq 0.9$ ; and  $M_+/M_{pb} \leq 0.9$ , where  $M_{pb}$  and  $M_{ps}$  are the plastic moment capacity of the base plate and shell sidewalls, respectively. These equations are derived from elastic solution, and these conditions prevent the potential unconservatism.

$$0.6t_B = 0.165 \cdot in$$

The second requirement leads to maximum  $\delta_e$  of 0.165 in, beyond which the small displacement theory becomes increasingly conservative. The original CDFM solved the problem by making a linear approximation of the  $\delta_e$ - $T_e$  curve in a range of  $\delta_e=0$  to  $0.6t_B$ , and then use the linear equation to extrapolate beyond the  $0.6t_B$  to partially account for membrane tension effects. This approach will also be used in this study.

$$T_e := T_{e\_lin}$$

**Assessment of the upper limit on the fluid hold-down force:** based on a yield stress  $\sigma_y$  of 30 ksi, and an ultimate stress of 75 ksi, the fully plastic moment capacity  $M_{pb}$  of the 7 mm base plate is estimated to be 0.949 kips-inch/inch when the outer fiber reaches 75 ksi. It is also assumed that the effective hoop compressive yield stress  $\sigma_{ye}$  is equal to 45 ksi. The upper limit of the horizontal component of the membrane tension  $F_H$  can be found to be:

$$\sigma_{ye} = 45 \cdot \text{ksi}$$

$$M_{pb} := \frac{t_B^3}{12} \div \left( \frac{t_B}{2} \right) \cdot 75 \text{ksi} = 0.949 \cdot \frac{\text{kips} \cdot \text{in}}{\text{in}} \quad t_B = 7 \cdot \text{mm}$$

$$F_H := \frac{\sigma_{ye} \cdot t_s}{2\kappa} + \frac{M_{pb} \cdot \kappa}{R} = 0.241 \cdot \frac{\text{kips}}{\text{in}}$$

$$(4M_{pb}P_T)^{0.5} = 240.802 \cdot \frac{\text{lb} \cdot \text{f}}{\text{in}}$$

$$\frac{F_H}{2M_{pb}} = 0.127 \cdot \frac{1}{\text{in}}$$

Thus, the upper limit of the fluid hold-down force is estimated to be:

$$T_m(\delta_e) := 168.841 \frac{\text{lb} \cdot \text{f}}{\text{in}} \left( 1 + \frac{0.31 \cdot \delta_e}{\text{in}} \right)^{0.5}$$

The maximum  $\delta_e$  can be found by equating  $T_e$  and  $T_m$ :

Given

$$\delta_{ee} := 0.15 \text{in}$$

$$T_e(\delta_{ee}) = T_m(\delta_{ee})$$

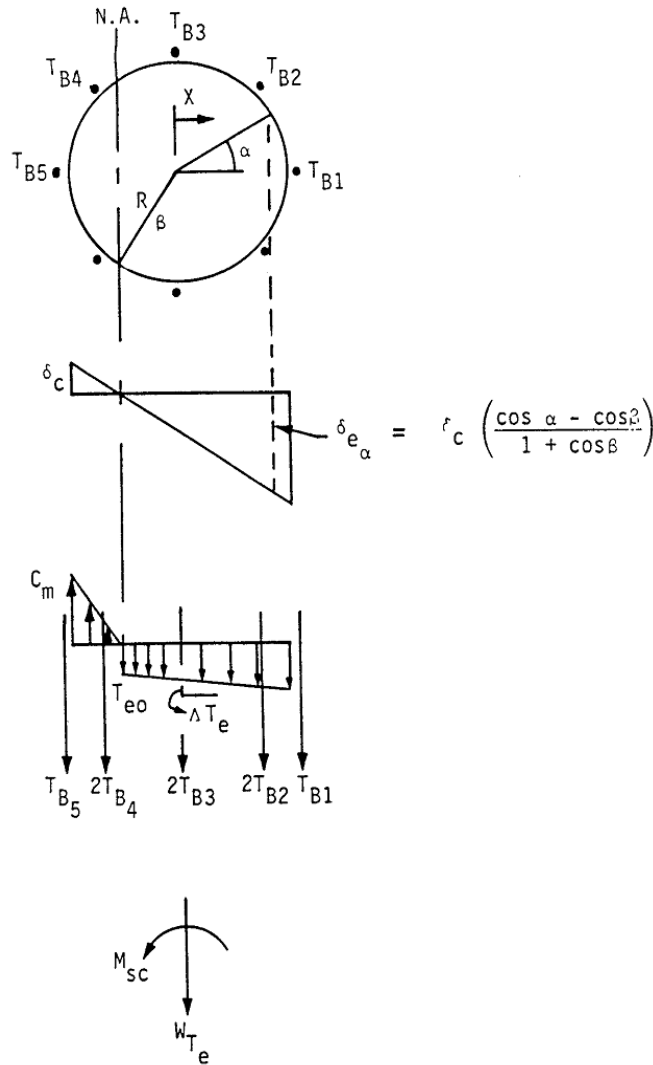
$$\delta_{ee} := \text{Find}(\delta_{ee}) = 0.45 \cdot \text{in}$$

Therefore, the linearized equation for  $T_e$  should not be extrapolated beyond  $\delta_{ee}$ .

Note that linearization is necessary later when developing overturning moment capacity.



### H.3.4 Overturning Moment Capacity:



#### Vertical Loading on Tank Shell at Base [NUREG/CR-5270]

The overturning moment capacity  $M_{SC}$  can be estimated using the compressive buckling capacity of the tank shell ( $C_B$ ), the anchor bolt hold-down capacity ( $T_{BC}$ ), and the relationship between fluid hold-down force and uplift displacement. The estimation approach in the CDFM method requires several

conservative but reasonable assumptions as noted below:

1. The bottom of the tank shell is assumed to rotate rigidly about the neutral axis (plane sections remain plane).
2. The cross-section of the tank at the top of the top plate of the bolt chairs ( $h_c$  above the base) is assumed to remain horizontal so that all vertical tank distortions needed to result in base uplift and mobilization of the anchor bolts must be accommodated over the height  $h_c$ .
3. The compressive stress varies linearly from zero at the neutral axis ( $\alpha=\beta$  as in the figure above) to its maximum value  $C_m$  at  $\alpha=180^\circ$ , as given by  $C_m = E_s t_s \delta_c / h_c \leq C_B$  (by converting eq. H-39), where  $\delta_c$  is the maximum compressive shortening.

Summary of parameters:

$$C_m = 0.291 \cdot \frac{\text{kips}}{\text{in}} \qquad T_{BC} = 0 \cdot \text{kips}$$

$$T_{e0} = 0.083 \cdot \frac{\text{kips}}{\text{in}} \qquad T_{e1} = 0.217 \cdot \frac{\text{kips}}{\text{in}^2}$$

$$W_{Te} = 209.601 \cdot \text{kips} \qquad A_B := A_{bolt} \qquad A_B = 4.336 \cdot \text{in}^2$$

$$E_B := 29 \times 10^3 \text{ ksi}$$

$$R = 25.026 \cdot \text{ft}$$

$$t_s = 0.138 \cdot \text{in} \qquad E_s := E_S = 29 \times 10^3 \cdot \text{ksi}$$

$$h_c := 207 \text{ mm} = 8.15 \cdot \text{in}$$

$$h_a := 2 \text{ ft} + 1 \text{ in} = 25 \cdot \text{in}$$

Using the approach outlined in NUREG/CR-5270 instead of the EPRI NP-6041-SL appendix H in the following:

$$\delta_c := \frac{C_m \cdot h_c}{E_s \cdot t_s} = 5.931 \times 10^{-4} \cdot \text{in}$$

$$K_B := \frac{\delta_c \cdot A_B \cdot E_B}{h_a + h_c} = 2.25 \cdot \text{kips}$$

$$\Delta T_e := T_{eI} \cdot \delta_c = 1.287 \times 10^{-4} \cdot \frac{\text{kips}}{\text{in}}$$

$$\delta_{ea}(a,b) := \delta_c \cdot \left( \frac{\cos(a) - \cos(b)}{1 + \cos(b)} \right)$$

Because the bolt pretension  $T_{BP}$  is unreliable after a number of years in service, it is conservatively assumed to be 0.

$$T_{BP} := 0 \text{ kips}$$

The neutral axis angle  $\beta$  can be determined iteratively using the following procedure.

Bolt locations:  $i := 0..77$

$$\alpha_i := \frac{2\pi}{78} i$$

$$Tfunc(\alpha, \beta) := \begin{cases} c \leftarrow T_{BP} + K_B \cdot \frac{\cos(\alpha) - \cos(\beta)}{1 + \cos(\beta)} \\ c \leftarrow T_{BC} \text{ if } c > T_{BC} \\ c \leftarrow 0 \text{ if } c < 0 \end{cases}$$

$$C_1(\beta) := \frac{1 + \cos(\beta)}{\sin(\beta) + (\pi - \beta)\cos(\beta)}$$

$$C_2(\beta) := \frac{\sin(\beta)\cos(\beta) + \pi - \beta}{1 + \cos(\beta)}$$

$$C_3(\beta) := \frac{\sin(\beta) - \beta \cdot \cos(\beta)}{\sin(\beta) + (\pi - \beta)\cos(\beta)}$$

$$C_4(\beta) := \frac{\beta - \sin(\beta)\cos(\beta)}{1 + \cos(\beta)}$$

$$T_B(\alpha, \beta) := \overrightarrow{Tfunc(\alpha, \beta)}$$

$$Cf'_m(\alpha, \beta) := \left( \frac{W_{Te} + \sum T_B(\alpha, \beta)}{2R} + T_{e0} \cdot \beta \right) \cdot C_1(\beta) + \Delta T_e \cdot C_3(\beta)$$

Equating  $Cf'_m$  and  $C_m$  to determine  $\beta$ :

$$func(\alpha, \beta) := Cf'_m(\alpha, \beta) - C_m$$

$$\beta := \text{root}(func(\alpha, \beta), \beta, 0, 3.14159)$$

$$\beta = 0.7382 \quad \beta \cdot \frac{180}{\pi} = 42.296$$

$$C'_m := C_f'_m(\alpha, \beta) = 0.291 \cdot \frac{kips}{in} \quad C_m = 0.291 \cdot \frac{kips}{in}$$

Use  $C'_m$  and  $\beta$  to find the overturning moment capacity  $M_{SC}$ :

$$M_{SC} := C'_m \cdot C_2(\beta) \cdot R^2 + \sum \left( \overrightarrow{T_B(\alpha, \beta) \cdot R \cdot \cos(\alpha)} \right) + T_{e0} \cdot R^2 \cdot 2 \cdot \sin(\beta) + \Delta T_e \cdot C_4(\beta) \cdot R^2$$

$$M_{SC} = 4482.412 \cdot kips \cdot ft$$

$$\sum T_B(\alpha, \beta) = 0 \cdot kips$$

The largest bolt elongation (at  $\alpha=0$ ) should be checked to ensure that the anchorage has the capability:

$$\delta_{e0} := \delta_{ea}(\alpha_0, \beta) = 8.874 \times 10^{-5} \cdot in$$

$$\text{Elongation ratio: } \frac{\delta_{e0}}{h_a + h_c} = 2.677 \times 10^{-4} \cdot \%$$

The maximum elongation ratio is much smaller than 1%, which is recommended in the original CDFM method for the A307 bolt. One percent is also considered to be an appropriate percentage value for the A36 anchor bolt used in the subject CST construction.

The maximum tank shell uplift distortion  $\delta_{e0} = 0.026$  in, which is much less than the limit of 0.165 in for the small displacement theory to be applicable in developing the fluid hold-down capacity.

Because there are 78 anchor bolts (the example tank in the original CDFM method had only 8), the case where  $\alpha=0$  lies midway between bolts need not be checked.

The uncertainty in HCLPF buckling capacity of the tank shell due to the uncertain  $\sigma_{ye}$  can lead to an  $M_{SC}$  as low as 119133.414 kips-ft or as high as 192156.702 kips-ft. It should be noted that unlike in the original CDFM method,  $M_{SC}$  is sensitive to the estimate of  $C_m$ .

Inelastic energy absorption reduction factor  $k$  can be applied to linearly computed seismic response to obtain the actual overturning moment capacity. The combined bolt yielding and tank shell buckling failure mode for overturning moment is not brittle so that  $k$  can be less than unity. However, as stated in the original CDFM method, it is difficult to make an appropriate estimate of  $k$  for this failure mode. Therefore, it is conservatively assumed to be unity.

$$k := 1.0$$

$$SME_M := \frac{M_{SC}}{k \cdot M_{SH}} \cdot SME_e \qquad SME_M = 0.033 \cdot g$$

Since  $SME_M$  is substantially different from  $SME_e$ , the above procedure should be iterated to obtain the appropriate SME estimate. The resultant  $SME_e$  is found to be 0.97g.



### **H.3.5 Sliding Capacity:**



The base plate of the CST has a slight cone (with a slope of 1 to 96) so that the fluid will always drain away from the center of the tank. This cone is generally created by variable thickness of the oiled sand cushion between the tank bottom plate and its foundation. Therefore, the coefficient of friction between the tank base and its foundation is reasonably assumed to have a conservative value of 0.55:

$$COF := 0.55$$

The sliding shear capacity can then be calculated as,

$$V_{SC} := COF \cdot \left( W_{Te} + P_a \cdot \pi \cdot R^2 + \sum T_B(\alpha, \beta) \right) = 2.581 \times 10^3 \cdot kips$$

The shear capacity of the bolts should not be considered because (a) there is a large space between the concrete foundation and the anchor bolt chair, and (b) there is a 1/4" diametric clearance in the hole in the anchor bolt chair.

The sliding capacity with a unit inelastic absorption factor as suggested by the original CDFM method:

$$SME_V := \frac{V_{SC}}{k \cdot V_{SH}} \cdot SME_e \qquad SME_V = 0.285 \cdot g$$

By varying  $SME_e$ , the HCLPF shear capacity is found to be 0.555g.

Unlike the example tank in the original CDFM method, the capacity of the CST appears to be governed by the sliding capacity. The sliding capacity considers only the friction between the bottom plate and the foundation.



### **H.3.6 Fluid Pressure Capacity:**



The inelastic energy absorption seismic response reduction factor  $k_u$  is suggested

to be 0.8 for HCLPF capacity evaluation:

$$k_u := 0.8$$

For the CDFM hoop membrane stress capacity, it is recommended that the ASME seismic design limit of  $2 S_M$  for primary stress should be used, which is 37.5 ksi for SA240-type 304 stainless steel:

$$\sigma_a := 37.5 \text{ ksi}$$

The pressure capacity,  $P_{CA}$ , at the bottom of the tank shell (the CST has a uniform shell thickness), can be estimated to be:

$$P_{CA}(t) := \frac{\sigma_a \cdot t}{R}$$

$$P_{CA}(t_s) = 17.218 \cdot \text{psi}$$

The maximum seismic induced hydrodynamic pressures  $P_{SM}$  and the hydrostatic pressure  $P_{ST}$  at the bottom of the tank shell are:

$$P_{SM}(H) = 8.307 \times 10^3 \text{ Pa}$$

$$P_{ST}(H) = 1.12 \times 10^5 \text{ Pa}$$

The HCLPF fluid pressure capacity  $SME_p$  can be determined as:

$$SME_p := \frac{P_{CA}(t_s) - P_{ST}(H)}{k_u \cdot P_{SM}(H)} \cdot SME_e = 0.032 \cdot g$$

By varying  $SME_e$ , the HCLPF fluid pressure capacity can be found to be 2.191 g, which does not govern. This agrees with seismic experience that the fluid pressure capacity seldom appears to govern the seismic capacity for normal flat bottomed steel tanks with butt-welded side plates.



Summary of SME capacities:

$$SME_M = 0.033 \cdot g \quad SME_V = 0.285 \cdot g \quad SME_p = 0.032 \cdot g$$

$$SME_{cr} := \min(SME_M, SME_V, SME_p) = 0.032 \cdot g$$

$$SME_e = 0.032 \cdot g$$

$$\text{if} \left[ SME_{cr} = SME_M, \text{"Moment"} , \left( \text{if} \left( SME_{cr} = SME_V, \text{"Shear"} , \text{"Fluid Pressure"} \right) \right) \right] = \text{"Fluid Pressure"}$$

$$\text{year} = 65 \quad t_s = 0.138 \cdot \text{in} \quad d_{bolt} = 2.35 \cdot \text{in} \quad \text{crack} = 0.507 \cdot \text{mm}$$

Summary of results:

Years:	0	5	10	15	20	25	30	35	40
ts (in):	0.625	0.588	0.550	0.513	0.475	0.438	0.400	0.363	0.325
dbolt(in):	2.5	2.48	2.466	2.453	2.441	2.429	2.418	2.408	2.398
cr(mm):	0	0.039	0.078	0.117	0.156	0.195	0.234	0.273	0.312
SME:	0.426	0.408	0.392	0.375	0.358	0.341	0.325	0.309	0.293
SMEM:	1.140	1.042	0.946	0.849	0.752	0.657	0.561	0.467	0.372
SMEV:	0.426	0.408	0.392	0.375	0.358	0.341	0.325	0.309	0.293
SMEP:	2.052	1.896	1.741	1.586	1.430	1.275	1.120	0.964	0.809
Mode:	Shear	Shear	Shear	Shear	Shear	Shear	Shear	Shear	Shear
Years:	45	50	55	60	65	70	75	80	
ts (in):	0.288	0.250	0.213	0.175	0.138				
dbolt(in):	2.388	2.378	2.368	2.359	2.35				
cr(mm):	0.351	0.390	0.429	0.468	0.507				
SME:	0.277	0.182	0.068	0.061	0.032	NA			
SMEM:	0.284	0.182	0.068	0.061	0.033				
SMEV:	0.277	0.279	0.276	0.278	0.285				
SMEP:	0.654	0.498	0.343	0.187	0.032				
Mode:	Shear	Moment	Moment	Moment	Fluid	Pressure			

### H.3.7 Consideration of Other Capacities:



(1) Slosh height for roof damage: note that even with a  $SME_e = 0.334 g$  (the initial guess), the slosh height is about 4.8 ft. With the HCLPF shear capacity of  $SME_e = 0.555 g$ , the sloshing height can be about 7.9 ft, which is close to the total height of the head (8.7', as approximated in the beginning part of this calculation).

$$h_s = 0.458 \cdot ft \qquad SME_e = 0.032 \cdot g$$

The increase of sloshing height is not significant as  $SME_e$  increases from 0.334 g to 0.555 g. In addition, as pointed out in the original CDFM method, even if roof damage might be expected, such damage usually does not impair the ability of the tank to contain fluid.

(2) The CST is assumed to sit on rock/very stiff soil; therefore, soil-tank foundation interaction is not considered.

(3) Piping failure or failure of nozzles may lead to loss of fluid in the tank, and more importantly, may impair the normal function of the condensation system. As reported in the original CDFM method, a significant fraction of the cases of seismic induced loss of tank contents have been due to piping/nozzle failures because of poor detailing. The CDFM method also stated that a SME evaluation of piping/nozzle failure is only necessary when poor seismic detailing is found in the involved piping attached to the tank. This analysis assumes that the subject CST is appropriately detailed, i.e. the piping and nozzle directly attached to the tank are properly designed and constructed so that sufficient piping flexibility can be achieved to accommodate large relative seismic anchor movements.

(4) The influence of the building in between the two CSTs on the SME are

assessed in the following. The gap between the auxiliary building and the CSTs at the roof level is filled with elastomeric sealant.

The maximum tank shell uplift distortion is found to be 0.026 in, which corresponds to a neutral axis angle  $\beta$  of 2.29161 rad. Since the horizontal plane at the anchor bolt chair is assumed to remain plane and all distortion is assumed to occur below this level, the rotation angle around the neutral axis can be estimated to be:

$$Rotation := \frac{\delta_{e0}}{R \cdot (1 - \cos(\beta))} = 1.135 \times 10^{-6}$$

$$\beta = 0.738 \quad \cos(\beta) = 0.74$$

The maximum horizontal displacement at the roof of the auxiliary building, which is at an elevation of 114' 9" (Parapet elevation, compared to the tank floor elevation of 101' 9"), can be estimated to be:

$$Rotation \cdot 13ft = 1.771 \times 10^{-4} \cdot in$$

This horizontal displacement is much less than the width of the seismic separation joint at the roof elevation, which is 3 in. Therefore, the influence of the auxiliary building to the two CSTs is considered minimal.



## The Fragility of CST Based on Degraded Conditions



Summary of results:

Years:	0	5	10	15	20	25	30	35	40
ts (in):	0.625	0.588	0.550	0.513	0.475	0.438	0.400	0.363	0.325
dbolt(in):2.5	2.48	2.466	2.453	2.441	2.429	2.418	2.408	2.398	
cr(mm): 0	0.039	0.078	0.117	0.156	0.195	0.234	0.273	0.312	
SME:	0.426	0.408	0.392	0.375	0.358	0.341	0.325	0.309	0.293
SMEM:	1.140	1.042	0.946	0.849	0.752	0.657	0.561	0.467	0.372
SMEV:	0.426	0.408	0.392	0.375	0.358	0.341	0.325	0.309	0.293
SMEP:	2.052	1.896	1.741	1.586	1.430	1.275	1.120	0.964	0.809
Mode:	Shear	Shear	Shear	Shear	Shear	Shear	Shear	Shear	Shear
Years:	45	50	55	60	65	70	75	80	
ts (in):	0.288	0.250	0.213	0.175	0.138				
dbolt(in):2.388	2.378	2.368	2.359	2.35					
cr(mm): 0.351	0.390	0.429	0.468	0.507					
SME:	0.277	0.182	0.068	0.061	0.032	NA			
SMEM:	0.284	0.182	0.068	0.061	0.033				
SMEV:	0.277	0.279	0.276	0.278	0.285				
SMEP:	0.654	0.498	0.343	0.187	0.032				
Mode:	Shear	Moment	Moment	Moment	Fluid	Pressure			

$$SME_{HCLPF} := (0.426 \ 0.408 \ 0.392 \ 0.375 \ 0.358 \ 0.341 \ 0.325 \ 0.309 \ 0.293 \ 0.277 \ 0.18$$

$$SME_M := (1.140 \ 1.042 \ 0.946 \ 0.849 \ 0.752 \ 0.657 \ 0.561 \ 0.467 \ 0.372 \ 0.284 \ 0.182 \ 0.1$$

$$SME_V := (0.426 \ 0.408 \ 0.392 \ 0.375 \ 0.358 \ 0.341 \ 0.325 \ 0.309 \ 0.293 \ 0.277 \ 0.279 \ 0.2$$

$$SME_P := (2.052 \ 1.896 \ 1.741 \ 1.586 \ 1.430 \ 1.275 \ 1.120 \ 0.964 \ 0.809 \ 0.654 \ 0.498 \ 0.3$$

It should be emphasized that the HCLPF SME capacity assumes the Regulatory Guide 1.60 spectra anchored to the HCLPF SME PGA.

To determine the seismic fragility of the CST tank, one needs to convert the HCLPF SME PGA to median SME PGA. This conversion requires the estimate of both aleatory and epistemic uncertainties ( $\beta_R$  and  $\beta_U$ ). The Fragility Method, also presented along with the original CDFM method, estimates the aleatory and epistemic uncertainties to be 0.2 and 0.27, respectively. These uncertainties are nearly identical to those reported by Choun, et al [2008]. The SME median  $SME_m$  can then be estimated as well.

$$i := 0, 1 \dots 13$$

$$\beta_R := 0.2$$

$$\beta_U := 0.27$$

$$\beta_C := \sqrt{\beta_R^2 + \beta_U^2} = 0.336$$

$$Hm := \exp[1.645(\beta_R + \beta_U)] = 2.167$$

$$SME_{m_i} := SME_{HCLPF_i} \cdot Hm$$

$$SME_{Mm_i} := SME_{M_i} \cdot Hm$$

$$SME_{Vm_i} := SME_{V_i} \cdot Hm$$

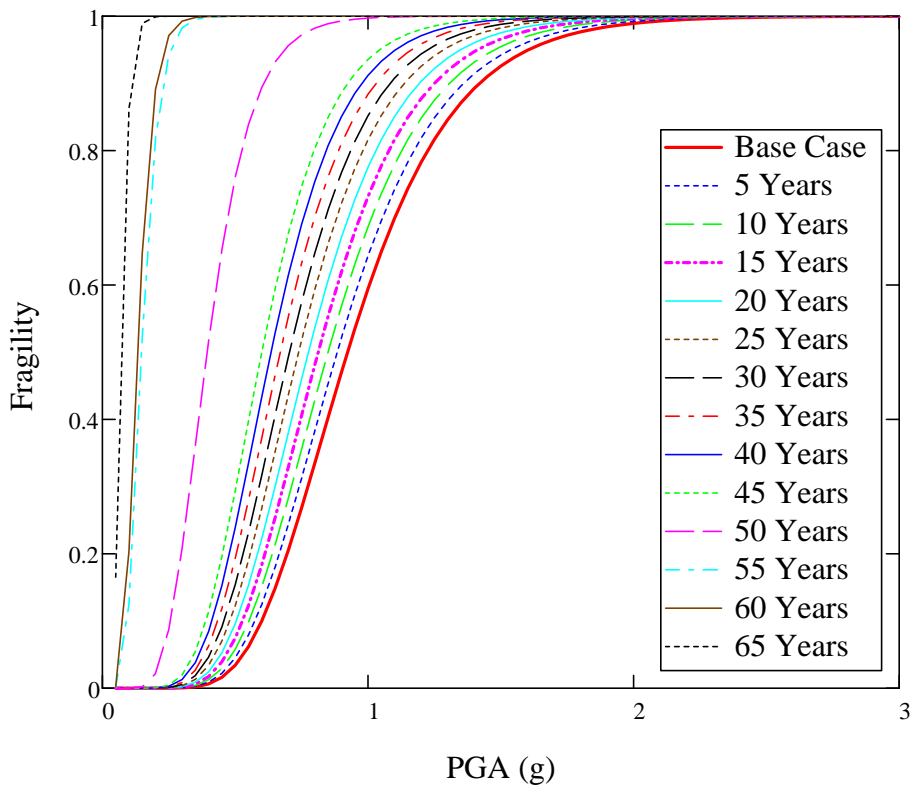
$$SME_{Pm_i} := SME_{P_i} \cdot Hm$$

$$F(Q,a) := cnorm \left( \frac{\ln \left( \frac{a \cdot g}{SME_m} \right) + \beta_U \cdot qnorm(Q,0,1)}{\beta_R} \right)$$

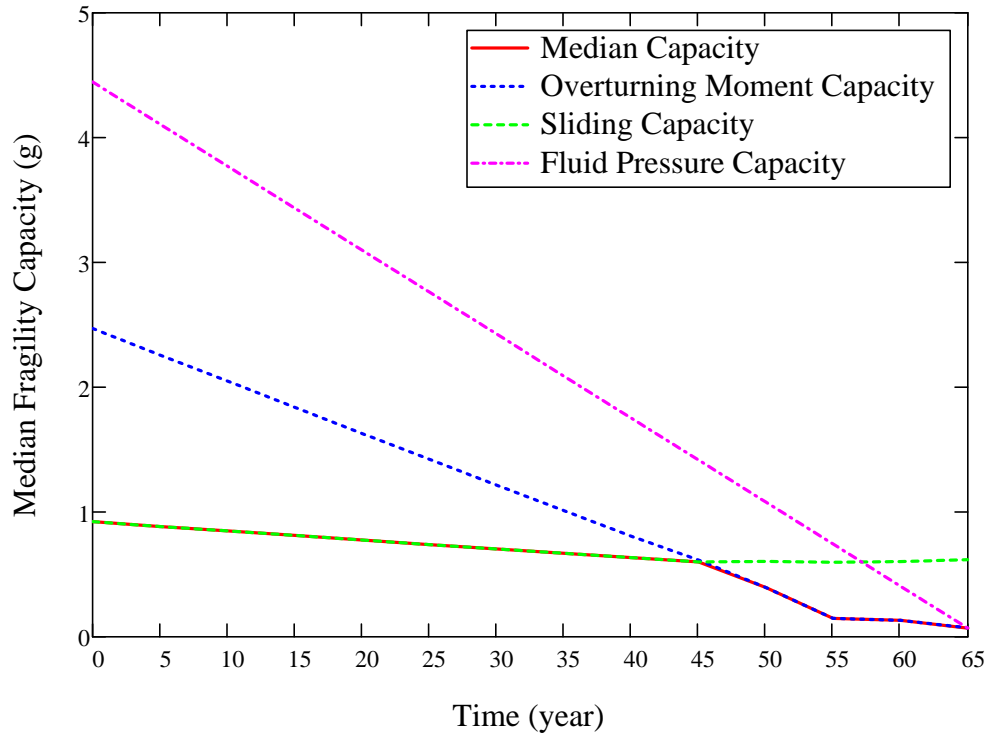
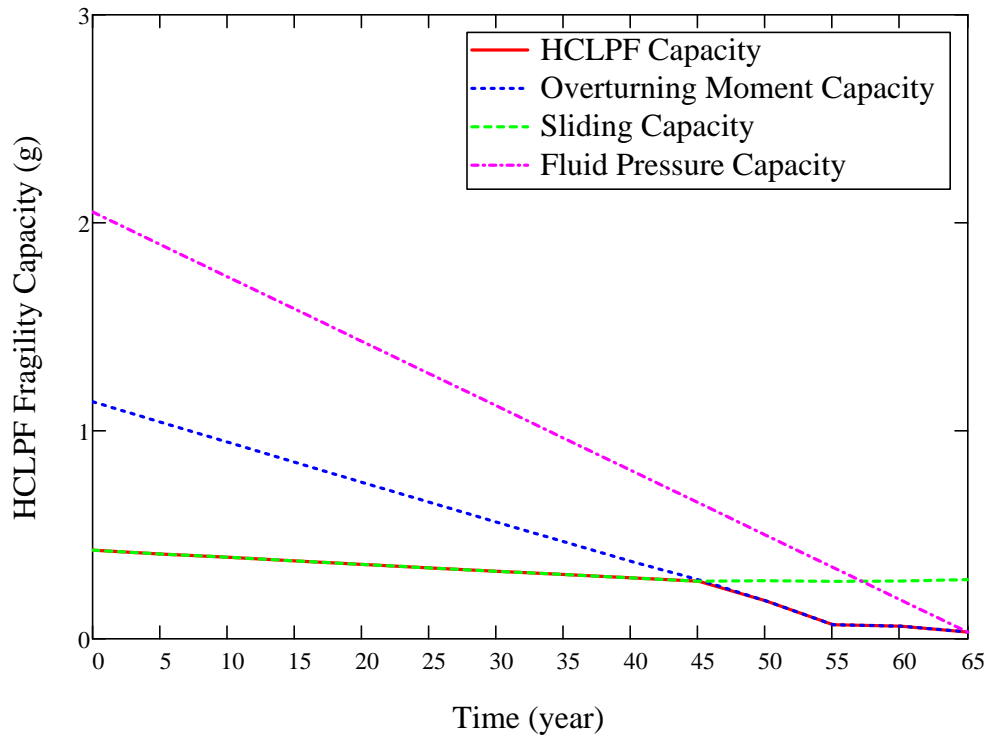
$$F_{mean}(a) := cnorm \left( \frac{\ln \left( \frac{a \cdot g}{SME_m} \right)}{\beta_C} \right)$$

$sa := 0.05, 0.1 \dots 3$

Mean CST Fragilities with Combined Degradations



$year_i := i \cdot 5$



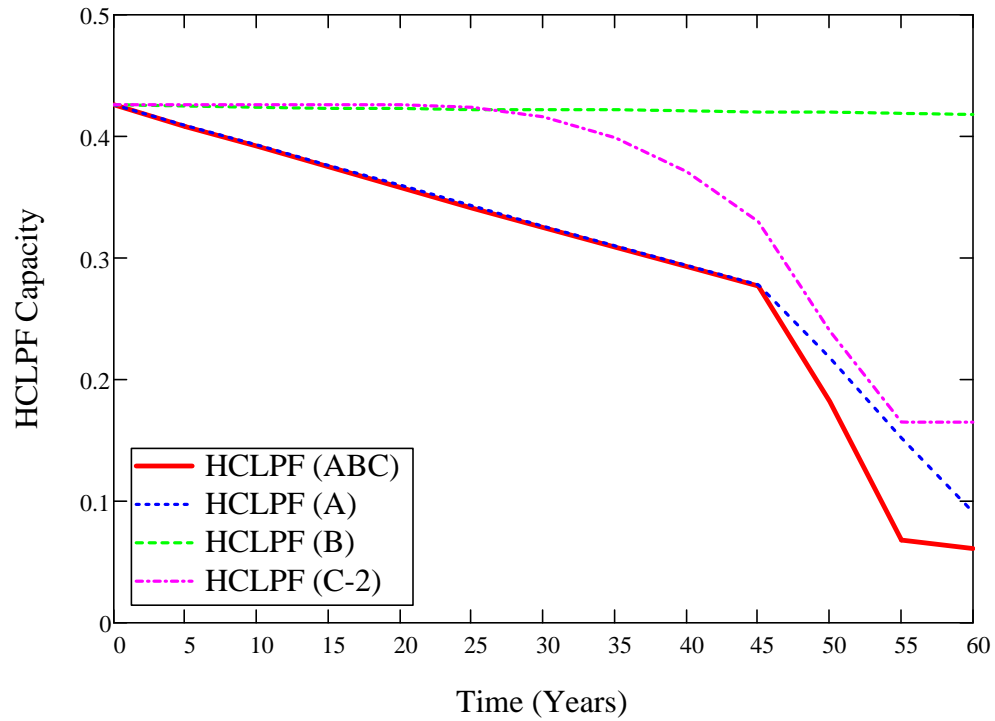
ii := 0,1..12

$year_{ii} := ii \cdot 5$

$HCLPF_A := (0.426 \ 0.409 \ 0.393 \ 0.376 \ 0.360 \ 0.343 \ 0.326 \ 0.310 \ 0.294 \ 0.278 \ 0.218$

$HCLPF_B := (0.426 \ 0.425 \ 0.424 \ 0.423 \ 0.423 \ 0.422 \ 0.422 \ 0.422 \ 0.421 \ 0.42 \ 0.42 \ 0$

$HCLPF_C := (0.426 \ 0.426 \ 0.426 \ 0.426 \ 0.426 \ 0.424 \ 0.416 \ 0.399 \ 0.371 \ 0.330 \ 0.240$



12 0.068 0.061 0.032)<sup>T</sup>.g

068 0.061 0.033)<sup>T</sup>.g

76 0.278 0.285)<sup>T</sup>.g

43 0.187 0.032)<sup>T</sup>.g

THESE DATA ARE THE CONTINUATION OF PAGE F-22.

$0.152 \ 0.091)^T \cdot g$

$.419 \ 0.418)^T \cdot g$

$0.165 \ 0.165 \ 0.165 \ 0.165 \ 0.165 \ 0.165)^T \cdot g$

THESE DATA ARE THE CONTINUATION OF PAGE F-25.

---



**Appendix G FRAGILITY ANALYSIS OF UNDEGRADED CST WITH OPERATIONAL  
WATER LEVEL**



# KAERI Year 4 Task

## Fragility Analysis of Condensate Storage Tank

- baseline analysis without considering degradation
- using water level in normal operation

Based on newly available information during the BNL-KAERI 10/13-15, 2010 meeting, the water level in the CST for normal operation is between 29'-8" and 30'-6". An elevation of 132 ft, which is about the middle of the above range, was picked during the meeting as a representative water level in this calculation.

Using Conservative Deterministic Failure Margin (CDFM) method to estimate the High Confidence Low Probability of Failure (HCLPF) seismic capacity, which is then used to generate fragility curves by combining randomness and uncertainty parameters.

The CDFM method described in this and the later appendices utilizes to a large extent the approach presented in NUREG/CR-5270 [Kennedy, et al., 1989] and is supplemented by additional sources as referenced herein.

Design information of the CST and related input data were based on the drawing KEPC Ulchin NPP Unit 3 & 4, Drawing No. M262-DG-A03-01, Rev. 6 and KAERI Email Communication to BNL, 09/29/2009, Document No. 9-251-C118-002, which were provided by KAERI for use in this study.

### H.1 Introduction

KAERI indicated that the seismic DBE in Korea follows the NRC Reg. Guide 1.60 design spectrum shape but with a PGA level scaled down to 0.2 g. Assuming an initial HCLPF capacity as 1.67 times of 0.2 g:

$$SME_e := 1.67 \times 0.2g = 0.334 \cdot g$$

The Mathcad sheets in this appendix solve the various equations iteratively by manually setting  $SME_e$  to different values and the following  $SME_e$  value of 0.426 g represents the converged solution.

$$SME_e := 0.549g$$



Horizontal PGA ( $SME_e$ ):  $A_H := SME_e = 0.549 \cdot g$

Definitions of some useful units:

$$kips \equiv 1000lb_f$$

$$ksi \equiv 1000psi$$

$$GPa \equiv 10^9 Pa$$

$$MPa \equiv 10^6 Pa$$

$$tonf \equiv 2000lb_f$$

$$tonne_f = 1 \times 10^3 \cdot kg_f$$



## H.2 Response Evaluation



The weight  $W$  and the center of gravity  $X$  (measured as the height above tank base) of various components are calculated as follows:

**Head:** using a conservative uniform thickness of 5/8" to compensate for other attachments. The head configuration is simplified as a spherical cap plus a short cylinder. The spherical cap with a radius  $a = (25' + 5/16")$  and a height  $h = (8.7') \cdot 13mm/16mm = 7.07'$  (estimated from drawing). The short cylinder has a radius of  $(25' + 5/16")$  and a height of 1.63'. The short cylinder is to be combined with the tank shell in this calculation. The total height of the head above the top of fluid level is 8.7'.

Spherical segment of head (following CRD Standard Mathematical Tables, 20 ed., 1972, page 17):

$$a := 25 \cdot ft + \frac{5}{16} \cdot in = 25.026 \cdot ft$$

$$h := 7.07 \cdot ft = 7.07 \cdot ft$$

$$p := \sqrt{a^2 + h^2} = 26.006 \cdot ft$$

$R$  is defined here as the radius of the sphere for the head (to be redefined later as the radius of the tank):

$$R := \frac{p^2}{2 \cdot h} = 47.828 \cdot ft$$

$$t_H := \frac{5}{8} \cdot in = 0.625 \cdot in$$

$$\gamma_{steel} := 0.285 \frac{lb_f}{in^3} = 492.48 \cdot \frac{lb_f}{ft^3}$$

$$W_H := \pi \cdot p^2 \cdot t_H \cdot \gamma_{steel} = 54.497 \cdot kips \quad W_H = 242.413 \cdot kN$$

$$H_S := (37ft + 6in) + 1.63ft = 39.13 \cdot ft$$

$$X_H := \frac{h}{2} + H_S = 42.665 \cdot ft \quad X_H = 13.004 \cdot m$$

$$X_H = 511.98 \cdot in$$

**Shell** - include the approximated short cylinder (with a height of 0.82ft) from the head.

$$t_S := \frac{5}{8}in = 0.625 \cdot in$$

$$W_S := (2\pi \cdot a \cdot t_S)H_S \cdot \gamma_{steel} = 157.823 \cdot kips \quad W_S = 702.03 \cdot kN$$

$$X_S := H_S \div 2 = 19.565 \cdot ft \quad X_S = 5.963 \cdot m$$

**Bottom** - assume a thickness of 7 mm as no English unit is available.

$$t_B := 7 \cdot mm = 0.276 \cdot in$$

$$W_B := t_B \cdot \pi \cdot a^2 \cdot \gamma_{steel} = 22.254 \cdot kips \quad W_B = 98.99 \cdot kN$$

$$X_B := t_B \div 2 = 0.011 \cdot ft \quad X_B = 3.5 \times 10^{-3} \cdot m$$

**Water** - as KAERI explained, T.L. indicates the top of fluid level.

Using the operational water height, per discussion with KAERI on 10/13/2010:

$$H_W := 37ft + 6in = \blacksquare \cdot ft \quad \text{Maximum design water level used for Year 3 task: 37'-6" (11.43 m)}$$

$$H_W := 132ft - (101ft + 9in) = 9.22m \quad H_W = 30.25 \cdot ft$$

$$\gamma_W := 62.4 \frac{lb_f}{ft^3} = 999.552 \cdot \frac{kg_f}{m^3}$$

$$W_W := \pi \cdot a^2 \cdot H_W \cdot \gamma_W = 3714.019 \cdot kips \quad W_W = 1.652 \times 10^4 \cdot kN$$

$$X_W := H_W \div 2 = 15.125 \cdot ft \quad X_W = 4.61 \cdot m$$

Hydrostatic fluid pressure function,  $P_{ST}$ , as used in Table H-1 (y is pointing

downward from TL, with a value of 0ft at TL):

$$P_{ST}(y) := y \cdot \gamma_W \qquad P_{ST}(0ft) = 0 \cdot psi$$

$$P_{ST}(H_W) = 13.108 \cdot psi$$

In summary, the total weight and the center of gravity are:

$$W_{total} := W_H + W_S + W_B + W_W = 3.949 \times 10^3 \cdot kips \qquad \frac{3939}{4839} = 0.814$$

$$W_{total} = 1.791 \times 10^6 \cdot kgf$$

$$W_{total} = 1.791 \times 10^3 \cdot tonnef$$

$$X_{total} := \frac{W_H \cdot X_H + W_S \cdot X_S + W_B \cdot X_B + W_W \cdot X_W}{W_{total}} = 15.597 \cdot ft$$

$$X_{total} = 4.754 \cdot m$$

$$X_{tank} := \frac{W_H \cdot X_H + W_S \cdot X_S + W_B \cdot X_B}{W_H + W_S + W_B} = 23.077 \cdot ft$$

### **H.2.1 Horizontal Impulsive Mode Responses:**

$$\rho_L := \gamma_W \div g = 999.552 \frac{kg}{m^3}$$

$$\rho_S := \gamma_{steel} \div g = 7.889 \times 10^3 \frac{kg}{m^3}$$

$$\frac{\rho_L}{\rho_S} = 0.127$$

$$E_S := 29000ksi$$

$$\nu_S := 0.3$$

Redefining R back to the radius of the tank:

$$R := a = 25.026 \cdot ft$$

Also defining H as H<sub>W</sub> for compatibility with the equations in the method:

$$H := H_W = 30.25 \cdot ft$$

$$H_W \div R = 1.209$$

$$H_S \div R = 1.564$$

$$H_W \div H_S = 0.773$$

$$t_S \div R = 0.0021$$

The evaluation of horizontal impulsive modal frequency in the original CDFM method by Dr. Kennedy used Table 7.4 of Veletsos 1984, "Guidelines for the Seismic Design of Oil and Gas Pipeline Systems." Using the same table, it is determined that  $C_{WI}=0.0904$  for  $t_S/R=0.001$  and  $H_W/R=1.209$ . Using equation 4.18 in BNL 52631(Rev. 10/95):

$$C_{WI} := 0.0904$$

$$C_{LI} := C_{WI} \times \sqrt{\frac{127 t_S \cdot \rho_S}{R \cdot \rho_L}} = 0.131$$

The horizontal impulsive mode natural frequency is estimated to be:

$$f_I := \frac{C_{LI}}{2\pi H_W} \cdot \sqrt{\frac{E_S}{\rho_S}} = 11.346 \cdot Hz$$

As indicated by KAERI, a modified design response spectrum shape as described in Regulatory Guide 1.60 was used in the design and therefore will be used in this calculation to define the SME spectrum shape. The 5% damped acceleration spectrum for a frequency range covering  $f_1=11.346$  Hz from Regulatory Guide 1.60 is used in the following to find the spectral acceleration:

$$Hor\_Freq := (0.25 \ 2.5 \ 9. \ 33.)^T \cdot Hz$$

$$Hor\_SA\_50 := (0.4 \ 3.13 \ 2.61 \ 1)^T \cdot A_H$$

$$S_{AI} := \text{interp}(Hor\_Freq, Hor\_SA\_50, f_I) = 1.346 \cdot g$$

$$Hor\_amp\_I := S_{AI} \div A_H = 2.453$$

$$H_W \div R = 1.209$$

For the CST with an approximate  $H/R < 1.50$ , the effective impulsive weight of the contained water (or other fluid)  $W_I$  and its effective height above the tank base  $X_I$  can be calculated as follows. It is assumed in this calculation that the tank shell is rigid for the effective impulsive weight calculation per ASCE 4-98.

$$W_I := \frac{\tanh\left(\sqrt{3} \cdot \frac{R}{H_W}\right)}{\sqrt{3} \cdot \frac{R}{H_W}} \cdot W_W = 2.313 \times 10^3 \cdot kips \quad W_I = 1.029 \times 10^4 \cdot kN$$

$$X_I := 0.375 \cdot H_W = 11.344 \cdot ft \quad X_I = 3.458 \cdot m$$

The impulsive mode base shear  $V_I$  and moment  $M_I$  at the base of the tank shell:

$$V_I := \frac{S_{AI}}{g} \cdot (W_H + W_S + W_I) = 3.4 \times 10^3 \cdot kips$$

$$V_I = 1.512 \times 10^4 \cdot kN$$

$$M_I := \frac{S_{AI}}{g} \cdot (W_H \cdot X_H + W_S \cdot X_S + W_I \cdot X_I) = 4.261 \times 10^4 \cdot kips \cdot ft$$

$$M_I = 5.777 \times 10^4 \cdot kN \cdot m$$

For a depth from the top of the fluid greater than  $0.15H$  (5.625 ft), the impulsive hydrodynamic pressure is estimated as:

$$P_I := \frac{W_I \cdot X_I \cdot S_{AI}}{1.36R \cdot H^2 \cdot g} = 7.876 \cdot psi \quad P_I = 54.305 \cdot kPa$$

For depths between 0 ft (fluid surface) to  $0.15H$ , the impulsive pressure varies linearly with height from 0 psi to the value computed above at  $0.15H$ .

## **H.2.2 Horizontal Convective (Sloshing) Mode Responses:**

The fundamental convective mode frequency:

$$f_C := \sqrt{\frac{1.5ft \div sec^2}{R} \tanh\left(1.835 \frac{H}{R}\right)} = 0.242 \cdot Hz$$

This convective mode is very lightly damped and the damping ratio 0.5 percent is used as suggested by the original CDFM method. Using the fundamental convective frequency 0.242 Hz and 0.5% damping on the modified Regulatory Guide 1.60 spectrum, the convective spectral acceleration  $S_{AC}$  for the given  $SME_e$  can be calculated as follows:

$$Hor\_Freq := (0.1 \ 0.25 \ 2.5 \ 9.)^T \cdot Hz$$

$$Hor\_SA\_05 := (0.12 \ 0.707 \ 5.95 \ 4.96)^T \cdot A_H$$

$$S_{AC} := \text{linterp}(Hor\_Freq, Hor\_SA\_05, f_C) = 0.371 \cdot g$$

$$Hor\_amp\_C := S_{AC} \div A_H = 0.675$$

It should be noted that  $f_C$  is slightly smaller than the corner frequency at point D in Regulatory Guide 1.60 horizontal spectrum, and the spectral acceleration values at point D and at frequency 0.1 Hz are determined by reading the horizontal spectral plot in Regulatory Guide 1.60.

The effective convective mode fluid weight and its effective application height:

$$W_C := W_W \cdot \left(0.46 \frac{R}{H} \tanh\left(1.835 \frac{H}{R}\right)\right) = 1.38 \times 10^3 \cdot kips \quad W_I = 2.313 \times 10^3 \cdot kips$$

$$W_C = 6.14 \times 10^3 \cdot kN$$

$$X_C := H \cdot \left[1.0 - \frac{\cosh\left(1.835 \frac{H}{R}\right) - 1.0}{1.835 \left(\frac{H}{R}\right) \sinh\left(1.835 \frac{H}{R}\right)}\right] = 19.289 \cdot ft \quad X_I = 11.344 \cdot ft$$

$$X_C = 5.879 \cdot m$$

$$V_C := \frac{S_{AC}}{g} \cdot W_C = 511.86 \cdot kips \quad V_I = 3.4 \times 10^3 \cdot kips$$

$$V_C = 2.277 \times 10^3 \cdot kN$$

$$M_C := \frac{S_{AC}}{g} \cdot W_C \cdot X_C = 9.873 \times 10^3 \cdot kips \cdot ft \quad M_I = 4.261 \times 10^4 \cdot kips \cdot ft$$

$$M_C = 1.339 \times 10^4 \cdot kN \cdot m$$

The hydrodynamic convective pressure as a function of depth,  $y$  ( $y=0$  at fluid surface and its positive direction is pointing downward), is given by:

$$P_C(y) := \frac{0.267 W_W S_{AC}}{R \cdot H \cdot g} \cdot \frac{\cosh\left[1.835 \left(\frac{H-y}{R}\right)\right]}{\cosh\left(1.835 \frac{H}{R}\right)} \quad P_C(0 \cdot ft) = 3.373 \cdot psi$$

$$P_C(H - X_C) = 1.581 \cdot psi$$

$$0.337 \cdot psi = 2.324 \cdot kPa$$

$$P_C(H - X_I) = 0.991 \cdot psi$$

$$P_C(H) = 0.726 \cdot psi$$

Note:  $P_C(y)$  is smaller at greater depth. The hydrodynamic convective pressures are generally negligible compared to the hydrodynamic impulsive pressure  $P_I$ , or the hydrostatic pressure  $P_{ST}$ , except at very shallow depths. The fundamental mode fluid slosh height  $h_s$  can be estimated to be,

$$h_s := 0.837 R \cdot \frac{S_{AC}}{g} = 7.768 \cdot ft \quad h_s = 2.368 \cdot m$$

Note that this sloshing height is more than half of the height of head.

### **H.2.3 Vertical Fluid Mode Response:**

The method to compute the natural frequency for the vertical fluid-tank system mode, which was used in the original CDFM method, is not applicable to this CST configuration. The example tank in the CDFM method has a  $t/R$  ratio of about 0.001, and the available data in the literature is only applicable to this  $t/R$  ratio. Note that the CST has a  $t/R$  ratio of 0.0021. As an alternative, also mentioned in the CDFM method, equation C3.5-13 in ASCE 4-98 is used instead in the following:

Water bulk modulus:  $K := 2.2 \times 10^9 Pa = 319.083 \cdot ksi$

$$f_v := \frac{1}{4H} \left[ \rho L \cdot \left( \frac{2 \cdot R}{t_S \cdot E_S} + \frac{1}{K} \right) \right]^{-0.5} = 11.824 \cdot Hz$$

The CDFM method recommends 5% of critical damping be used when estimating the vertical spectral acceleration. Using the Reg Guide 1.60 vertical acceleration spectra:

$$\begin{aligned} Ver\_Freq &:= (0.25 \ 3.5 \ 9.0 \ 33.)^T \cdot Hz & A_H &= 0.549 \cdot g \\ Ver\_SA\_50 &:= (0.3 \ 2.98 \ 2.61 \ 1)^T \cdot A_H \\ S_{AV} &:= \text{interp}(Ver\_Freq, Ver\_SA\_50, f_v) = 1.329 \cdot g \end{aligned}$$

The hydrodynamic vertical fluid response mode pressure:

$$\begin{aligned} P_V(y) &:= 0.8\rho_L \cdot H \cdot S_{AV} \cdot \cos\left(\frac{\pi}{2} \cdot \frac{H-y}{H}\right) & P_V(0ft) &= 0 \cdot psi \\ & & P_V(H) &= 13.936 \cdot psi \end{aligned}$$

#### H.2.4 Combined Responses:

Define a square root of sum of squares (SRSS) function for convenience ( $v$  must be a column vector):

$$SRSS(v) := \sqrt{v \cdot v}$$

The combined horizontal seismic responses for the base shear  $V_{SH}$ , base moment  $M_{SH}$ , and horizontal seismic hydrodynamic pressures  $P_{SH}$  can be obtained by the SRSS of the horizontal impulsive and convective responses.

$$\begin{aligned} V_{SH} &:= SRSS\left[\left(V_I \ V_C\right)^T\right] = 3.438 \times 10^3 \cdot kips & V_I &= 3.4 \times 10^3 \cdot kips \\ M_{SH} &:= SRSS\left[\left(M_I \ M_C\right)^T\right] = 4.374 \times 10^4 \cdot kips \cdot ft & M_I &= 4.261 \times 10^4 \cdot kips \cdot ft \\ P_{SH}(y) &:= SRSS\left[\left(P_I \ P_C(y)\right)^T\right] & P_{SH}(H) &= 7.91 \cdot psi \end{aligned}$$

Note that for this CST, the combined horizontal seismic responses are essentially equal to the impulsive mode responses and the influence of the convective mode is negligible.

**(1):** For the purpose of the membrane hoop stress capacity check, the maximum seismic hydrodynamic pressures  $P_{SM}$  can be obtained by SRSS of the horizontal

seismic pressures  $P_{SH}$  and the vertical fluid response hydrodynamic pressure  $P_V$ :

$$P_{SM}(y) := SRSS\left[\left(P_{SH}(y) \ P_V(y)\right)^T\right] \quad P_{SM}(H) = 16.024 \cdot psi$$

**(2):** For the purpose of estimating the buckling capacity of the tank shell, it is necessary to estimate the expected maximum and minimum of the fluid pressures acting against the tank shell near its base at the location of the maximum axial compression during the time of maximum base moment. The expected maximum and minimum compression zone pressure  $P_{C+}$  and  $P_{C-}$ , at the time of maximum base moment can be obtained as,

$$P_{C+} := P_{ST}(H) + P_{SH}(H) + 0.4P_V(H) = 26.592 \cdot psi$$

$$P_{C-} := P_{ST}(H) + P_{SH}(H) - 0.4P_V(H) = 15.444 \cdot psi$$

Where the factor of 0.4 on  $P_V$  is to account for the probable vertical mode hydrodynamic vertical pressure at the time of maximum base moment.

**(3):** Similarly, for the purpose of estimating the expected minimum fluid hold-down forces in the zone of maximum tank wall axial tension, it is required to estimate the minimum tension zone fluid pressure  $P_{T-}$  at the time of maximum moment:

$$P_{T-} := P_{ST}(H) - P_{SH}(H) - 0.4P_V(H) = -0.376 \cdot psi$$

**(4):** For the sliding capacity evaluation, the expected minimum average fluid pressure  $P_a$  on the base plate, at the time of the maximum base shear, can be estimated to be:

$$P_a := P_{ST}(H) - 0.4P_V(H) = 7.534 \cdot psi$$

**(5):** The expected minimum total effective weight  $W_{Te}$  of the tank shell acting on the base, at the time of maximum moment and base shear, can be estimated by (assuming the vertical stiffness of the tank shell and head system results in a frequency greater than 33 Hz):

$$W_{Te} := (W_H + W_S) \cdot \left[1 - 0.4 \left(\frac{A_H}{g}\right)\right] = 165.694 \cdot kips$$



## H.3 Capacity Assessment



The seismic overturning moment capacity of the CST at its base,  $M_{SC}$ , depends on the axial compressive buckling capacity of the tank shell  $C_m$ , the tensile hold-down capacity of the anchor bolts including their anchorage and attachment to the tank  $T_{BC}$ , and the hold-down capacity of the fluid pressure acting on the tank base plate  $T_e$ .

Although unlikely for larger radius tanks, the tank SME capacity is sometimes governed by the sliding shear capacity at the tank base,  $V_{SC}$ . Even though it does not appear that any butt welded steel tank has ever failed due to seismic induced membrane hoop stresses due to combined hydrostatic and hydrodynamic fluid pressures, the SME capacity of this failure mode,  $P_{CA}$ , should also be checked.

Additional assessment of the seismic capacity may include the possibility and consequence of the fluid sloshing against the tank roof, foundation failure for soil sites, and possibility of failure of piping or their attachment to the tank.

### H.3.1 Compressive Buckling Capacity of the Tank Shell:

The most likely buckling for tanks is the "elephant-foot" buckling near the base of the tank shell. The "elephant-foot" buckling is a combined effect of hoop tension, axial (vertical) compression, and restriction of radial deformation of the tank shell by the base plate. "Elephant-foot" buckling does not necessarily lead to failure of a tank (e.g., leakage). However, there is no simple capability evaluation method that can predict tank performance after the development of "elephant-foot" buckling. Therefore, for a CDFM SME capacity of tanks, the onset of "elephant-foot" buckling will be judged to represent the limit to the compressive buckling capacity of the tank shell. The onset of "elephant-foot" buckling can be estimated using elastic-plastic collapse theory as presented in the following:

The sidewall thickness near the shell base:  $t_s := t_S = 0.625 \cdot in$

The tank internal pressure near its base:  $P := P_{C+} = 1.833 \times 10^5 Pa$

Elastic modulus of the tank:  $E_S = 2.9 \times 10^4 \cdot ksi$

The CST shell is made of SA 204-type 304 stainless steel. This material does not have a flat yield plateau and as strain increases its stress can grow to a minimum

ultimate stress capacity of 75 ksi. In the CDFM method, an effective yield stress  $\sigma_{ye}$  is set to  $2.4S_M$  or 45 ksi, in line with the ASME seismic design limit for primary local membrane plus primary bending [ASME 1983, "ASME Boiler & Pressure Vessel Code"]. The potential uncertainty range for  $\sigma_{ye}$  is reported to be between 30 ksi and 60 ksi, according to the original CDFM method description.

$$\sigma_{ye} := 45 \text{ ksi}$$

$$\frac{R}{t_s} = 480.5$$

$$S_I := \frac{R}{t_s} \div 400 = 1.201$$

The "elephant-foot" buckling axial stress of the tank shell can be accurately predicted to be:

$$\sigma_p := \frac{0.6E_S}{R \div t_s} \left[ 1 - \left( \frac{P \cdot R}{\sigma_{ye} \cdot t_s} \right)^2 \right] \cdot \left( 1 - \frac{1}{1.12 + S_I^{1.5}} \right) \cdot \left( \frac{S_I + \frac{\sigma_{ye}}{36 \text{ ksi}}}{S_I + 1} \right) = 21.858 \cdot \text{ksi}$$

The compressive buckling capacity for HCLPF capacity computation utilizes a recommended 0.9 reduction factor of the buckling stress:

$$C_m := 0.9 \sigma_p \cdot t_s = 12.295 \cdot \frac{\text{kips}}{\text{in}}$$

Buckling capacity of the supported cylindrical shells under combined axial bending and internal pressure should also be checked although it is unlikely to govern for overall seismic response of fluid containing tanks. The axial bending induced buckling stress,  $\sigma_{CB}$ , for such a load case can be conservatively estimated (essentially lower bound) as follows.

A parameter  $\Delta\gamma$  to be used in the following procedure as an increase factor for internal pressure can be obtained from Figure 6 of "Buckling of Thin-walled Circular Cylinders," [NASA SP-8007].  $\Delta\gamma$  depends on the minimum compression zone pressure at the base of the tank shell,  $P_C$ , corresponding to the time of maximum moment.

Considering the potential range on  $\sigma_{ye}$  of 30 to 60 ksi, the resultant range on  $\sigma_p$  is 16.572 ksi to 26.702 ksi. Consequently,  $C_m$  has a range of 9.322 kips/in to 15.02 kips/in.

$$\frac{P_C}{E_S} \left( \frac{R}{t_S} \right)^2 = 0.123$$

From Figure 6 of NASA SP-8007:  $\Delta\gamma := 0.12$

$$\phi := \frac{1}{16} \cdot \sqrt{\frac{R}{t_S}} = 1.37$$

$$\gamma := 1 - 0.73(1 - e^{-\phi}) = 0.455$$

$$\sigma_{CB} := (0.6\gamma + \Delta\gamma) \frac{E_S}{R \div t_S} = 23.737 \cdot ksi$$

$$0.9\sigma_p = 19.672 \cdot ksi$$

$\sigma_{CB}$  exceeds  $0.9s_p$ , so it does not govern.

### H.3.2 Bolt Hold-down Capacity:

The bolt hold-down capacity should be determined as the smallest of the bolt tensile capacity, anchorage of bolt into concrete foundation, capacity of the top plate of bolt chairs to transfer bolt loads to the vertical chair gussets, attachment of the top plate and vertical chair gussets to the tank shell, and the capacity of tank shell to withstand concentrated loads imposed on it by the bolt chairs.

**Anchor bolt capacity:** the anchor bolt has a diameter of 2 1/2" and is made of A36 steel. The tensile capacity can be determined as:

$$d_{bolt} := 2.5in$$

$$A_{bolt} := \frac{\pi \cdot d_{bolt}^2}{4} = 4.909 \cdot in^2$$

Based on the AISC Code [9th edition, 1989] for threaded A36 bolts:

$$T_{BC} := 1.7A_{bolt} \cdot 19.1ksi = 159.387 \cdot kips \quad T_{BC} = 79.693 \cdot tonf$$

Note that  $T_{BC}$  is the capacity of one bolt and the capacity of the interacting multi-bolts will be considered later.

**Anchor bolt chair capacity check:** according to the drawing, the anchor bolt

chairs form a circumferentially continuous construction. Based on the continuous chair construction and the sizing of the plates and weld, it is judged that the anchor bolt chair and its attachment to the tank shell are adequate to transfer the bolt capacity load for the CST. The tank shell is also considered to be adequate in withstanding the concentrated loads imposed on it by bolt chairs, especially because the "elephant-foot" buckling capacity is also checked.

$$t_{chair} := \left(1 + \frac{3}{8}\right)in = 1.375 \cdot in$$

Weld width is 15 mm (5/8") according to the drawing.

**Capacity of bolt anchorage into concrete foundation:** the anchorage is constructed using non-shrinking grout. The tensile failure of bolt anchorage mainly consists of bolt failure, plug pull-out, and concrete cone failure, the last two of which typically are a combination of tensile failure of concrete in the upper portion of the anchorage that results in a partial depth cone-shaped spall and bond failure at the grout-concrete interface in the lower portion of the anchorage.

$$\text{Bolt spacing: } \Delta d := \pi \cdot \left[50ft + \left(9 + \frac{1}{16}\right)in\right] \div 78 = 2.044 \cdot ft$$

Lee, et al [2001] described an experimental and analytical work on the pull-out strength of large-sized anchor bolt, in a SMiRT 16 paper entitled "failure mechanism for large-sized grouted anchor bolt under tensile load." The test specimens were selected based on the real construction of a CST in the Yonggwang Nuclear Power Plant of Korea. The anchor bolt is 2-1/2 inches in diameter, and has an embedment length of 2 ft 2-3/8 inches. The anchor bolt material is ASTM A36. Non-shrinking grout was used in the post-installed anchorage construction. These construction variables are basically very similar to those of the subject CST for fragility analysis, except that the subject CST anchors have a slightly shorter embedment length of 2 ft 1 inch. The concrete strength of the subject CST foundation is not available, and is assumed to be the same as in this SMiRT 16 paper, which has a compressive strength of 4500 psi. The circumferential spacing is about 2 ft for both tanks. The test included 5 anchor bolt specimens.

As reported by Lee, et al [2001], the average 7 day and 28 day compressive strength of the concrete were 5419 psi and 7180 psi, respectively. The actual average compressive strength of non-shrinking grout at 7 days and 21 days were 7550 psi and 11100 psi, respectively. The non-shrinking grout has obviously larger compressive strength than the concrete, as expected for normal construction of anchorage. The reported bond strength of the non-shrinking grout (Masterflow 870) was 40 kgf/cm<sup>2</sup> (569 psi). The Young's modulus of A36 is 2.9\*10<sup>7</sup> psi and the Poisson's ratio is 0.3.

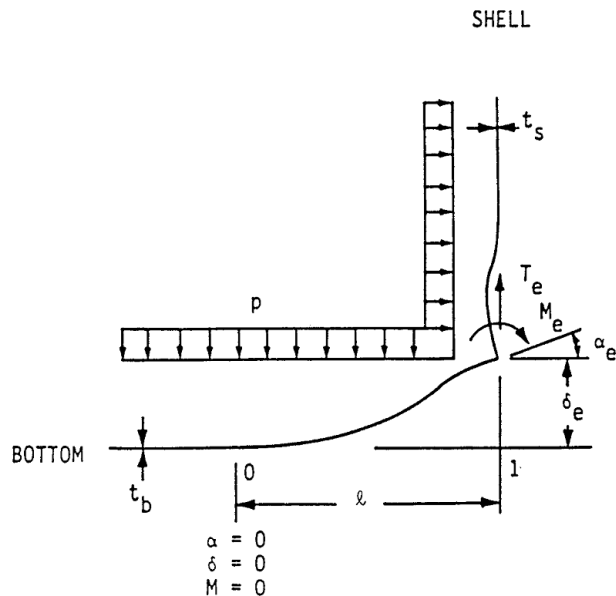
The test first confirmed a minimum required load of 50 tons (100 kips). Three of the

five grouted anchors were tested further until failure. Two specimens was judged to have failed by tensile failure of grout at the lower portion of the grout block, bonding failure between grout and the concrete, and tensile failure of concrete. The other specimen showed abrasion of anchor bolt thread. All specimens achieved at least 100 tons (200kips), after which the load-deformation curve became significantly flatter and the ultimate failure load scatters between 100 tons and 120 tons.

Based on the test, the anchorage capacity should be 200 kips, which is about 26% higher than the estimate based on tensile strength of the anchor bolt. It should be noted that in the test, one specimen had abrasion in its thread, suggesting the anchor bolt capacity should be also close to 200 kips. However, since the embedment in the test was about 1-3/8 inch longer than the subject CST case, the spacing of anchor bolts in the test is twice as long as in the subject CST case, and the lab test condition usually have a higher quality control, the estimate of 159.387 kips will be assumed as the anchorage capacity.

$$T_{BC} = 159.387 \cdot kips$$

### H.3.3 Fluid Hold-down Forces:



**Schematic Illustration of Tank Bottom Behavior Near Tensile Region of Tank Shell [NUREG/CR-5270]**

The hold-down force  $T_e$  increases with increasing fluid pressure  $P$ , which consequently assumes the minimum tension zone fluid press  $P_{T-}$ . A number of

other related parameters are also defined below.

$$P := P_{T_-} = -0.376 \cdot psi$$

$$\nu := 0.3$$

$$I_b := \frac{t_B^3}{12(1 - \nu^2)} = 1.917 \times 10^{-3} \cdot in^3$$

$$t_S = 0.625 \cdot in$$

$$t_B = 7 \cdot mm$$

$$K := \frac{E_S \cdot t_S^3}{12(1 - \nu^2)} = 7.325 \times 10^4 J$$

$$\kappa := \left[ \frac{R}{t_S} \cdot \sqrt{3(1 - \nu^2)} \right]^{0.5} = 28.177$$

$$MFP := \frac{R \cdot t_S}{\sqrt{12(1 - \nu^2)}} \left( 1 - \frac{R}{H \cdot \kappa} \right) = 0.036 m^2$$

MFP is a shortcut to  $M_F / P$

$$K_S := \frac{2 \cdot K \cdot \kappa}{R} = 5.412 \times 10^5 N$$

The uplift height  $\delta_e$ , the hold down tension  $T_e$ , moment  $M_e$ , rotation  $a_e$ , and maximum positive moment  $M_+$  can then be defined as functions of uplift length  $l$ :

$$F(l) := 1 + \frac{K_S \cdot l}{2E_S \cdot I_b}$$

$$\delta_e(l) := \left[ \frac{l^4}{24} - \frac{1}{F(l)} \left( \frac{K_S \cdot l^5}{72E_S \cdot I_b} + MFP \cdot \frac{l^2}{6} \right) \right] \cdot \left( \frac{P}{E_S \cdot I_b} \right)$$

$$T_e(l) := P \cdot \left[ \frac{l}{2} + \frac{1}{F(l)} \cdot \left( \frac{K_S \cdot l^2}{12E_S \cdot I_b} + \frac{MFP}{l} \right) \right]$$

Note: this equation as in the original CDFM method is singular at  $L = 0$  ft. The  $MFP/L$  term only has a minor effect on  $T_e$  when  $L$  is very small. The linear approximation in the original CDFM method can effectively avoid this singularity.

$$M_e(l) := P \cdot \left( \frac{1}{F(l)} \right) \cdot \left( \frac{K_S \cdot l^3}{12E_S \cdot I_b} + MFP \right)$$

$$M_+(l) := P \cdot \left( \frac{l^2}{8} - \frac{M_e(l)}{2P} + \frac{M_e(l)^2}{2P^2 \cdot l^2} \right)$$

The singularity in this equation can be similarly avoided by the linear approximation.

$$\alpha_e(l) := \frac{P \cdot l^3}{12E_S \cdot I_b} - \frac{M_e(l) \cdot l}{2E_S \cdot I_b}$$

Given

$$l := 0 \text{ in}$$

$$\frac{l^2}{24} - \frac{1}{F(l)} \left( \frac{K_S \cdot l^3}{72E_S \cdot I_b} + MFP \cdot \frac{1}{6} \right) = 0$$

$$l_{min} := \text{Find}(l) = 7.633 \cdot \text{in}$$

Given

$$l_{max} := 105 \text{ in}$$

$$\delta_e(l_{max}) = 0.165 \text{ in}$$

$$l_{max} := \text{Minerr}(l_{max}) = 4.907 \cdot \text{in}$$

$$l_{max} := \text{if}(l_{max} < l_{min}, 200 \text{ in}, l_{max})$$

$$l := l_{min}, l_{min} + 0.1 \text{ in} .. l_{max}$$

Linear Approximation:

$$i := 0 .. \frac{(l_{max} - l_{min})}{0.1 \text{ in}}$$

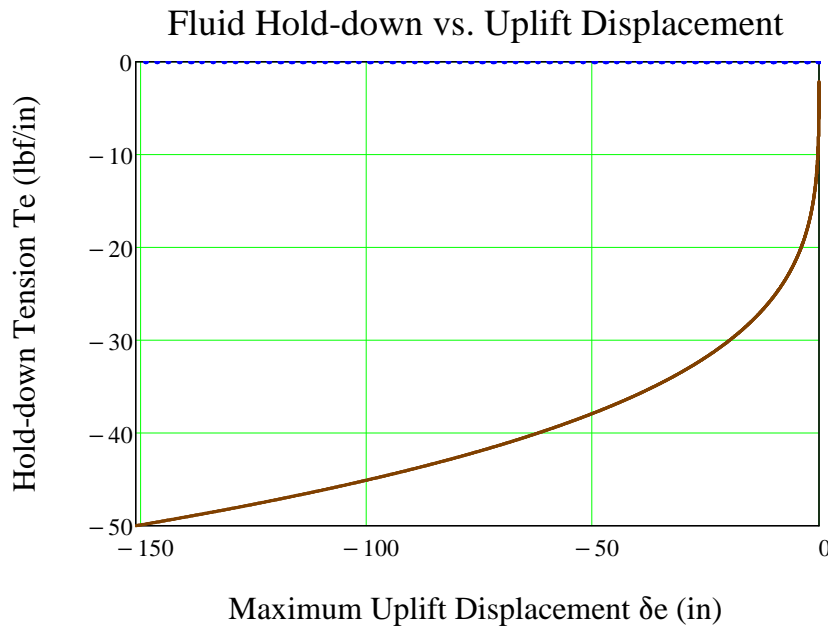
$$l_{vec_i} := l_{min} + i \cdot 0.1 \cdot \text{in}$$

$$\begin{pmatrix} T_{e0} \\ T_{e1} \end{pmatrix} := \text{line} \left[ \frac{\overrightarrow{\delta_e(l\_vec)}}{\text{in}}, \left( T_e(l\_vec) \cdot \frac{\text{in}}{\text{lbf}} \right) \right] = \begin{pmatrix} -16.512 \\ 0.299 \end{pmatrix}$$

$$T_{e0} := \text{if}(P_{T-} < 0\text{psi}, 0, T_{e0}) \frac{\text{lbf}}{\text{in}} = 0 \cdot \frac{\text{lbf}}{\text{in}}$$

$$T_{e1} := \text{if}(P_{T-} < 0\text{psi}, 0, T_{e1}) \cdot \frac{\text{lbf}}{\text{in}^2} = 0 \cdot \frac{\text{lbf}}{\text{in}^2}$$

$$T_{e\_lin}(\delta_e) := T_{e0} + T_{e1} \cdot \delta_e$$



It should be noted that these equations are derived based on small displacement theory, and are applicable to the following conditions:

1.  $L/R \leq 0.15$ . The solution does not consider the stiffening effect of hoop behavior on the base plate and consequently conservatively overpredicts the displace  $\delta_e$ , as the ratio of  $L/R$  becomes larger.
2.  $\delta_e/t_b \leq 0.6$ . As the solution is based on small displacement assumption, which ignores the beneficial influence of the membrane tension in the base

plate to reduce  $\delta_e$  for a given  $I_e$  as in large displacement theory. For

unanchored tanks, Manos (in "earthquake tank-wall stability of unanchored tanks," *Journal of Structural Engineering*, Vol 112, No. 8, ASCE, 1986) and Haroun and Badawi (in "nonlinear axisymmetric uplift of circular plates," *Dynamics of Structures*, ASCE, 1987) showed that large displacement membrane theory greatly increases the fluid hold-down force  $T_e$  and consequently the uplift  $\delta_e$ . Nevertheless, for anchored tanks like the subject CST, the uplift is not expected to be very large.

3.  $M_e/M_{pb} \leq 0.9$ ;  $M_e/M_{ps} \leq 0.9$ ; and  $M_+/M_{pb} \leq 0.9$ , where  $M_{pb}$  and  $M_{ps}$  are the plastic moment capacity of the base plate and shell sidewalls, respectively. These equations are derived from elastic solution, and these conditions prevent the potential unconservatism.

$$0.6t_B = 0.165 \cdot in$$

The second requirement leads to maximum  $\delta_e$  of 0.165 in, beyond which the small displacement theory becomes increasingly conservative. The original CDFM solved the problem by making a linear approximation of the  $\delta_e$ - $T_e$  curve in a range of  $\delta_e = 0$  to  $0.6t_B$ , and then use the linear equation to extrapolate beyond the  $0.6t_B$  to partially account for membrane tension effects. This approach will also be used in this study.

$$T_e := T_{e\_lin}$$

**Assessment of the upper limit on the fluid hold-down force:** based on a yield stress  $\sigma_y$  of 30 ksi, and an ultimate stress of 75 ksi, the fully plastic moment capacity  $M_{pb}$  of the 7 mm base plate is estimated to be 0.949 kips-inch/inch when the outer fiber reaches 75 ksi. It is also assumed that the effective hoop compressive yield stress  $\sigma_{ye}$  is equal to 45 ksi. The upper limit of the horizontal component of the membrane tension  $F_H$  can be found to be:

$$\sigma_{ye} = 45 \cdot ksi$$

$$M_{pb} := \frac{t_B^3}{12} \div \left( \frac{t_B}{2} \right) \cdot 75ksi = 0.949 \cdot \frac{kips \cdot in}{in}$$

$$F_H := \frac{\sigma_{ye} \cdot t_S}{2\kappa} + \frac{M_{pb} \cdot \kappa}{R} = 0.588 \cdot \frac{kips}{in}$$

$$(4M_{pb}P_{T-})^{0.5} = 37.763i \cdot \frac{lb_f}{in}$$

$$\frac{F_H}{2M_{pb}} = 0.31 \cdot \frac{1}{in}$$

Thus, the upper limit of the fluid hold-down force is estimated to be:

$$T_m(\delta_e) := 168.841 \frac{lb_f}{in} \left( 1 + \frac{0.31 \cdot \delta_e}{in} \right)^{0.5}$$

The maximum  $\delta_e$  can be found by equating  $T_e$  and  $T_m$ :

*Given*

$$\delta_{ee} := 0.15in$$

$$T_e(\delta_{ee}) = T_m(\delta_{ee})$$

$$\delta_{ee} := \text{Minerr}(\delta_{ee}) = -3.226 \cdot in$$

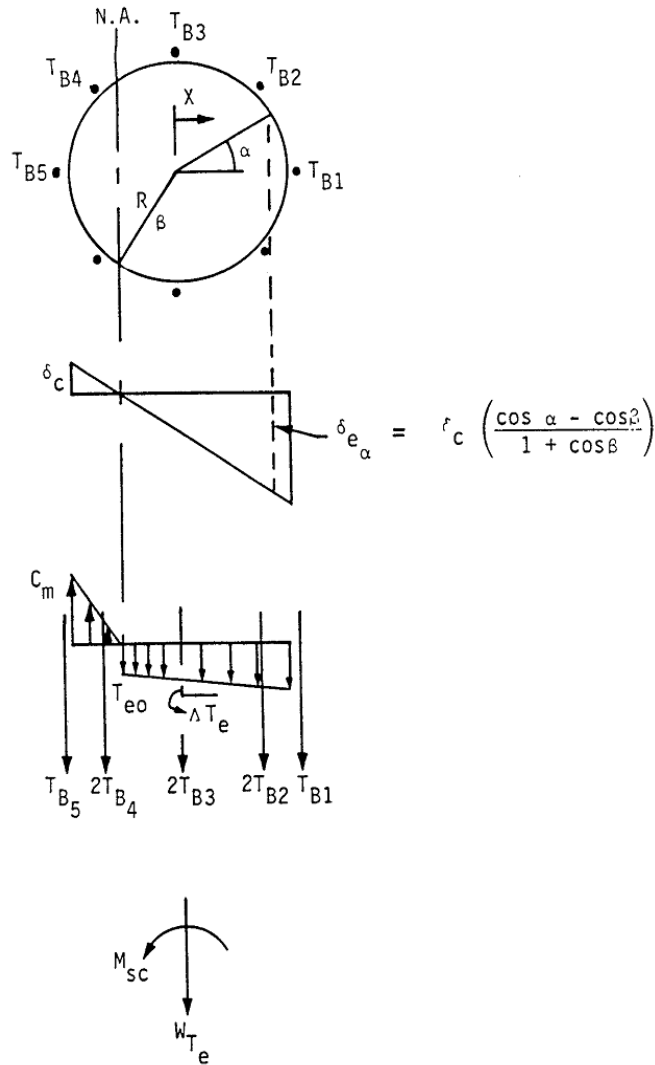
$$\delta_{ee} := \max(\delta_{ee}, 0in) = 0 \cdot in$$

Therefore, the linearized equation for  $T_e$  should not be extrapolated beyond  $\delta_e = 1.249$  inch.

Note that linearization is necessary later when developing overturning moment capacity.



### H.3.4 Overturning Moment Capacity:



#### Vertical Loading on Tank Shell at Base [NUREG/CR-5270]

The overturning moment capacity  $M_{SC}$  can be estimated using the compressive buckling capacity of the tank shell ( $C_B$ ), the anchor bolt hold-down capacity ( $T_{BC}$ ), and the relationship between fluid hold-down force and uplift displacement. The estimation approach in the CDFM method requires several conservative but reasonable assumptions as noted below:

1. The bottom of the tank shell is assumed to rotate rigidly about the neutral axis (plane sections remain plane).
2. The cross-section of the tank at the top of the top plate of the bolt chairs ( $h_c$  above the base) is assumed to remain horizontal so that all vertical tank distortions needed to result in base uplift and mobilization of the anchor bolts must be accommodated over the height  $h_c$ .
3. The compressive stress varies linearly from zero at the neutral axis ( $\alpha=\beta$  as in the figure above) to its maximum value  $C_m$  at  $\alpha=180^\circ$ ; as given by  $C_m = E_s t_s \delta_c / h_c \leq C_B$  (by converting eq. H-39), where  $\delta_c$  is the maximum compressive shortening.

Summary of parameters:

$$C_m = 12.295 \cdot \frac{\text{kips}}{\text{in}} \quad T_{BC} = 159.387 \cdot \text{kips}$$

$$T_{e0} = 0 \cdot \frac{\text{kips}}{\text{in}} \quad T_{e1} = 0 \cdot \frac{\text{kips}}{\text{in}^2}$$

$$W_{Te} = 165.694 \cdot \text{kips} \quad A_B := A_{bolt} \quad A_B = 4.909 \cdot \text{in}^2$$

$$E_B := 29 \times 10^3 \text{ ksi}$$

$$R = 25.026 \cdot \text{ft}$$

$$t_s = 0.625 \cdot \text{in} \quad E_s := E_S = 29 \times 10^3 \cdot \text{ksi}$$

$$h_c := 207 \text{ mm} = 8.15 \cdot \text{in}$$

$$h_a := 2 \text{ ft} + 1 \text{ in} = 25 \cdot \text{in}$$

Using the approach outlined in NUREG/CR-5270 instead of the EPRI NP-6041-SL appendix H in the following:

$$\delta_c := \frac{C_m \cdot h_c}{E_s \cdot t_s} = 5.528 \times 10^{-3} \cdot \text{in}$$

$$K_B := \frac{\delta_c \cdot A_B \cdot E_B}{h_a + h_c} = 23.74 \cdot \text{kips}$$

$$\Delta T_e := T_{eI} \cdot \delta_c = 0 \cdot \frac{\text{kips}}{\text{in}}$$

$$\delta_{ea}(a, b) := \delta_c \cdot \left( \frac{\cos(a) - \cos(b)}{1 + \cos(b)} \right)$$

Because the bolt pretension  $T_{BP}$  is unreliable after a number of years in service, it is conservatively assumed to be 0.

$$T_{BP} := 0 \text{ kips}$$

The neutral axis angle  $\beta$  can be determined iteratively using the following procedure.

Bolt locations:  $i := 0..77$

$$\alpha_i := \frac{2\pi}{78} i$$

$$T_{func}(\alpha, \beta) := \begin{cases} c \leftarrow T_{BP} + K_B \cdot \frac{\cos(\alpha) - \cos(\beta)}{1 + \cos(\beta)} \\ c \leftarrow T_{BC} \text{ if } c > T_{BC} \\ c \leftarrow 0 \text{ if } c < 0 \end{cases}$$

$$C_1(\beta) := \frac{1 + \cos(\beta)}{\sin(\beta) + (\pi - \beta)\cos(\beta)}$$

$$C_2(\beta) := \frac{\sin(\beta)\cos(\beta) + \pi - \beta}{1 + \cos(\beta)}$$

$$C_3(\beta) := \frac{\sin(\beta) - \beta \cdot \cos(\beta)}{\sin(\beta) + (\pi - \beta)\cos(\beta)}$$

$$C_4(\beta) := \frac{\beta - \sin(\beta)\cos(\beta)}{1 + \cos(\beta)}$$

$$T_B(\alpha, \beta) := \overrightarrow{T_{func}(\alpha, \beta)}$$

$$Cf'_m(\alpha, \beta) := \left( \frac{W_{Te} + \sum T_B(\alpha, \beta)}{2R} + T_{e0} \cdot \beta \right) \cdot C_1(\beta) + \Delta T_e \cdot C_3(\beta)$$

Equating  $Cf'_m$  and  $C_m$  to determine  $\beta$ :

$$func(\alpha, \beta) := Cf'_m(\alpha, \beta) - C_m$$

$$\beta := root(func(\alpha, \beta), \beta, 0, 3.1)$$

$$\beta = 2.2942 \quad \beta \cdot \frac{180}{\pi} = 131.448$$

$$C'_m := Cf'_m(\alpha, \beta) = 12.295 \cdot \frac{kips}{in} \quad C_m = 12.295 \cdot \frac{kips}{in}$$

Use  $C'_m$  and  $\beta$  to find the overturning moment capacity  $M_{SC}$ :

$$M_{SC} := C'_m \cdot C_2(\beta) \cdot R^2 + \sum \overline{(T_B(\alpha, \beta) \cdot R \cdot \cos(\alpha))} + T_{e0} \cdot R^2 \cdot 2 \cdot \sin(\beta) + \Delta T_e \cdot C_4(\beta) \cdot R^2$$

$$M_{SC} = 156879.129 \cdot kips \cdot ft$$

$$\sum T_B(\alpha, \beta) = 3.955 \times 10^3 \cdot kips$$

The largest bolt elongation (at  $\alpha=0$ ) should be checked to ensure that the anchorage has the capability:

$$\delta_{e0} := \delta_{ea}(\alpha_0, \beta) = 0.027 \cdot in$$

$$\text{Elongation ratio: } \frac{\delta_{e0}}{h_a + h_c} = 0.082 \cdot \%$$

The maximum elongation ratio is much smaller than 1%, which is recommended in the original CDFM method for the A307 bolt. One percent is also considered to be an appropriate percentage value for the A36 anchor bolt used in the subject CST construction.

The maximum tank shell uplift distortion  $\delta_{e0} = 0.026$  in, which is much less than the limit of 0.165 in for the small displacement theory to be applicable in developing the fluid hold-down capacity.

Because there are 78 anchor bolts (the example tank in the original CDFM method had only 8), the case where  $\alpha=0$  lies midway between bolts need not be checked.

The uncertainty in HCLPF buckling capacity of the tank shell due to the uncertain  $\sigma_{ye}$  can lead to an  $M_{SC}$  as low as 119133.414 kips-ft or as high as 192156.702 kips-ft. It should be noted that unlike in the original CDFM method,  $M_{SC}$  is sensitive to the estimate of  $C_m$ .

Inelastic energy absorption reduction factor  $k$  can be applied to linearly computed seismic response to obtain the actual overturning moment capacity. The combined bolt yielding and tank shell buckling failure mode for overturning moment is not brittle so that  $k$  can be less than unity. However, as stated in the original CDFM method, it is difficult to make an appropriate estimate of  $k$  for this failure mode. Therefore, it is conservatively assumed to be unity.

$$k := 1.0$$



$$SME_M := \frac{M_{SC}}{k \cdot M_{SH}} \cdot SME_e \qquad SME_M = 1.969 \cdot g$$

Since  $SME_M$  is substantially different from  $SME_e$ , the above procedure should be iterated to obtain the appropriate SME estimate. Since there are more capacities that need to be assessed, the iteration is conducted considering all capacities.

### H.3.5 Sliding Capacity:



The base plate of the CST has a slight cone ( with a slope of 1 to 96) so that the fluid will always drain away from the center of the tank. This cone is generally created by variable thickness of the oiled sand cushion between the tank bottom plate and its foundation. Therefore, the coefficient of friction between the tank base and its foundation is reasonably assumed to have a conservative value of 0.7 in the original CDFM method. For steel over concrete, the coefficient of friction is more reasonably set to 0.55, as suggested in BNL 52361 [Bandyopadhyay, et al., 1995]. For this study, the lower coefficient of friction of 0.55 is used.

$$COF := 0.55$$

The sliding shear capacity can then be calculated as,

$$V_{SC} := COF \cdot \left( W_{Te} + P_a \cdot \pi \cdot R^2 + \sum T_B(\alpha, \beta) \right) = 3.44 \times 10^3 \cdot kips$$

The shear capacity of the bolts should not be considered because (a) there is a large space between the concrete foundation and the anchor bolt chair, and (b) there is a 1/4" diametric clearance in the hole in the anchor bolt chair.



The sliding capacity with a unit inelastic absorption factor as suggested by the original CDFM method:

$$SME_V := \frac{V_{SC}}{k \cdot V_{SH}} \cdot SME_e \qquad SME_V = 0.549 \cdot g$$

By varying  $SME_e$ , the HCLPF shear capacity is found to be 0.549 g.

Unlike the example tank in the original CDFM method, the capacity of the CST appears to be governed by the sliding capacity. The sliding capacity considers only the friction between the bottom plate and the foundation.

### H.3.6 Fluid Pressure Capacity:

The inelastic energy absorption seismic response reduction factor  $k_u$  is suggested to be 0.8 for HCLPF capacity evaluation:

$$k_u := 0.8$$

For the CDFM hoop membrane stress capacity, it is recommended that the ASME seismic design limit of  $2 S_M$  for primary stress should be used, which is 37.5 ksi for SA240-type 304 stainless steel:

$$\sigma_a := 37.5 \text{ ksi}$$

The pressure capacity,  $P_{CA}$ , at the bottom of the tank shell (the CST has a uniform shell thickness), can be estimated to be:

$$P_{CA}(t) := \frac{\sigma_a \cdot t}{R}$$

$$P_{CA}(t_S) = 78.044 \cdot \text{psi}$$

The maximum seismic induced hydrodynamic pressures  $P_{SM}$  and the hydrostatic pressure  $P_{ST}$  at the bottom of the tank shell are:

$$P_{SM}(H) = 16.024 \cdot \text{psi}$$

$$P_{ST}(H) = 13.108 \cdot \text{psi}$$

The HCLPF fluid pressure capacity  $SME_p$  can be determined as:

$$SME_p := \frac{P_{CA}(t_S) - P_{ST}(H)}{k_u \cdot P_{SM}(H)} \cdot SME_e = 2.781 \cdot g$$

The HCLPF fluid pressure capacity does not govern. This agrees with seismic experience that the fluid pressure capacity seldom appears to govern the seismic

capacity for normal flat bottomed steel tanks with butt-welded side plates.

Summary of SME capacities:

$$SME_M = 1.969 \cdot g$$

$$SME_V = 0.549 \cdot g$$

$$SME_p = 2.781 \cdot g$$

$$SME_{cr} := \min(SME_M, SME_V, SME_p) = 0.549 \cdot g$$

$$SME_e = 0.549 \cdot g$$

It should be noted that the controlling SME capacity of 0.549 g based on the CDFM method is larger than 0.41 g as reported by Choun, et al [2008]. However, the SME capacity determined using the design water level was 0.426 g, very similar to the reported capacity of 0.41 g. All three capacities are associated with the sliding failure mode.

### **H.3.7 Consideration of Other Capacities:**

(1) Slosh height for roof damage: note that even with a  $SME_e = 0.334$  g (the initial guess), the slosh height is about 4.8 ft. With the HCLPF shear capacity of  $SME_e = 0.426$  g, the sloshing height can be about 6.1 ft, which is lower than the total height of the head (8.7', as approximated in the beginning part of this calculation).

$$h_s = 7.768 \cdot ft$$

$$SME_e = 0.549 \cdot g$$

The increase of sloshing height is not significant as  $SME_e$  increases from 0.334 g to 0.555 g. In addition, as pointed out in the original CDFM method, even if roof damage might be expected, such damage usually does not impair the ability of the tank to contain fluid.

(2) The CST is assumed to sit on rock/very stiff soil; therefore, soil-tank foundation interaction is not considered.

(3) Piping failure or failure of nozzles may lead to loss of fluid in the tank, and more importantly, may impair the normal function of the condensation system. As reported in the original CDFM method, a significant fraction of the cases of seismic induced loss of tank contents have been due to piping/nozzle failures because of poor detailing. The CDFM method also stated that a SME evaluation of piping/nozzle failure is necessary only when poor seismic detailing is found in the involved piping attached to the tank. This analysis assumes that the subject

CST is appropriately detailed, i.e. the piping and nozzle directly attached to the tank are properly designed and constructed so that sufficient piping flexibility can be achieved to accommodate large relative seismic anchor movements.

(4) The influence of the building in between the two CSTs on the SME is assessed in the following. The gap between the auxiliary building and the CSTs at the roof level is filled with elastomeric sealant.

The maximum tank shell uplift distortion is found to be 0.026 in, which corresponds to a neutral axis angle  $\beta$  of 2.29161 rad. Since the horizontal plane at the anchor bolt chair is assumed to remain plane and all distortion is assumed to occur below this level, the rotation angle around the neutral axis can be estimated to be:

$$\delta_{e0} = 0.027 \cdot \text{in}$$

$$\text{Rotation} := \frac{\delta_{e0}}{R \cdot (1 - \cos(\beta))} = 5.445 \times 10^{-5}$$

$$\beta = 2.294 \quad \cos(\beta) = -0.662$$

The maximum horizontal displacement at the roof of the auxiliary building, which is at an elevation of 114' 9" (Parapet elevation, compared to the tank floor elevation of 101' 9"), can be estimated to be:

$$\text{Rotation} \cdot 13\text{ft} = 8.495 \times 10^{-3} \cdot \text{in}$$

This horizontal displacement is much less than the width of the seismic separation joint at the roof elevation, which is 3 in. Therefore, the influence of the auxiliary building to the two CSTs is considered minimal.

## The Fragility of CST

$$SME_{HCLPF} := SME_e = 0.549 \cdot g$$

It should be emphasized that the HCLPF SME capacity assumes the Regulatory Guide 1.60 spectra anchored to the HCLPF SME PGA.

To determine the seismic fragility of the CST, one needs to convert the HCLPF SME PGA to median SME PGA. This conversion requires the estimate of both aleatory and epistemic uncertainties ( $\beta_R$  and  $\beta_U$ ). The Fragility Method, also presented along with the original CDFM method, estimates the aleatory and epistemic uncertainties to be 0.2 and 0.27, respectively. These uncertainties are nearly identical to those reported by Choun, et al [2008]. The SME median  $SME_m$  can then be estimated as well.

$$\beta_R := 0.2$$

$$\beta_U := 0.27$$

$$\beta_C := \sqrt{\beta_R^2 + \beta_U^2} = 0.336$$

$$SME_m := SME_{HCLPF} \cdot \exp[1.645(\beta_R + \beta_U)] = 1.189 \cdot g$$

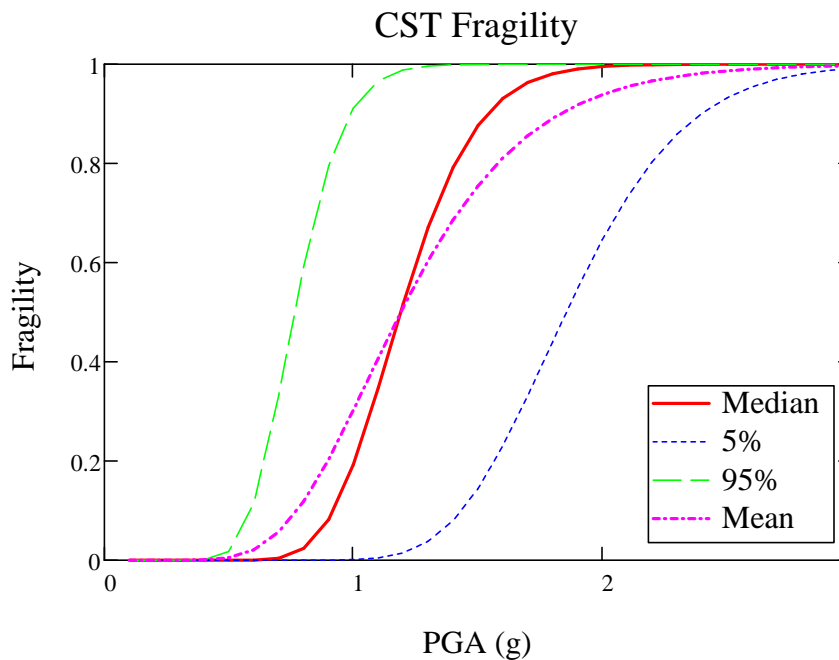
The fragility for the CST can now be calculated using the equations given below.

$$F(Q, a) := cnorm\left(\frac{\ln\left(\frac{a \cdot g}{SME_m}\right) + \beta_U \cdot qnorm(Q, 0, 1)}{\beta_R}\right)$$

$$F_{mean}(a) := cnorm\left(\frac{\ln\left(\frac{a \cdot g}{SME_m}\right)}{\beta_C}\right)$$

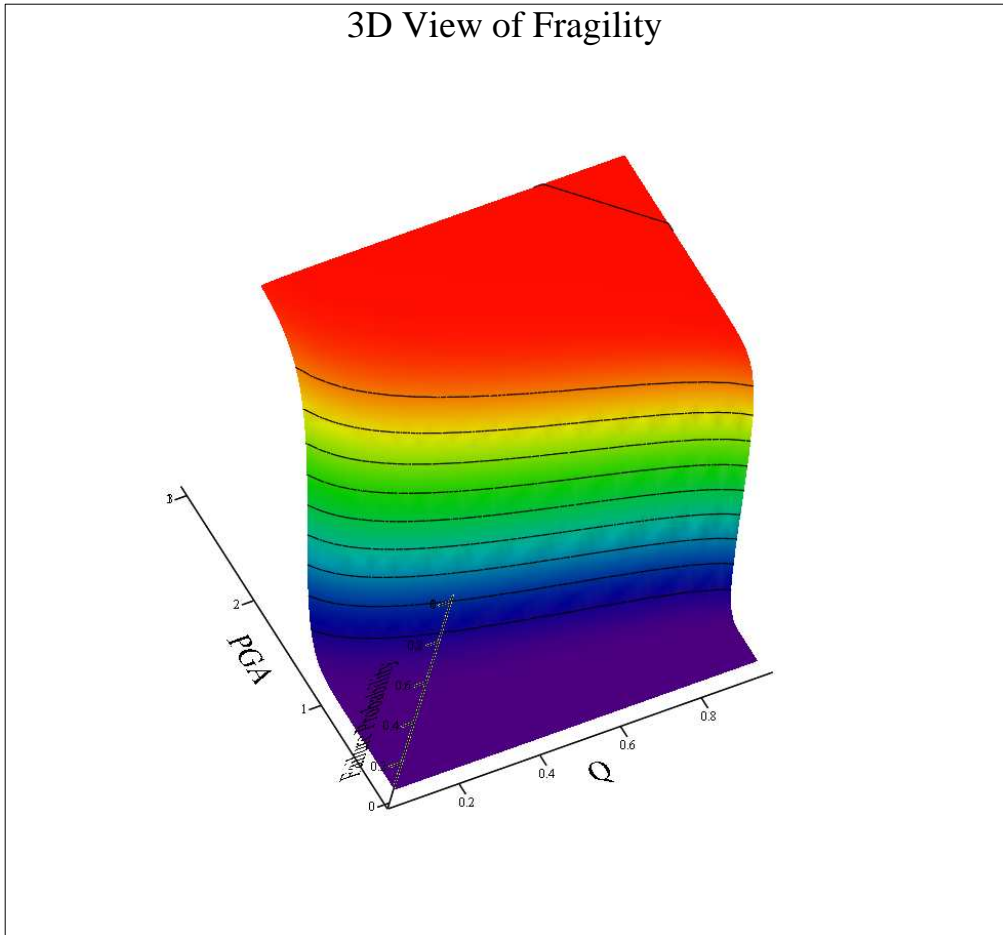
$$sa := 0.1, 0.2 \dots 3$$

The fragility curves for the median, 5% and 95% confidence levels, and the mean are shown in the figure below.



$Q := 0.05, 0.1 \dots 0.95$

A 3D surface plot of the fragility of the CST in terms of PGA and confidence level  $Q$  is shown below. The ordinate value is the probability of failure.



## **Appendix H   GENERATION OF OPTIMUM LATIN HYPER CUBE SAMPLES**



# KAERI Year 4 Task

## Generation of Correlated Factors for Degradation Cases A, B, and C

### Content of optimumLHS.txt

This file was generated using the optimumLHS function of the R package "lhs".

```
0.31658630 0.07205195 0.54324817
0.26743041 0.82646967 0.64185347
0.73532519 0.80586628 0.88003744
0.44882885 0.21346885 0.15957380
0.65661911 0.99634466 0.36644284
0.99309717 0.49822207 0.35577403
0.06610184 0.55519348 0.19868220
0.52925881 0.72711770 0.08904145
0.89262662 0.15844405 0.61828816
0.12228418 0.39575803 0.77377497
0.59774704 0.31844845 0.97906295
```

```
optimumLHS :=
    optimumLHS.txt
```

	0	1	2
0	0.317	0.072	0.543
1	0.267	0.826	0.642
2	0.735	0.806	0.88
3	0.449	0.213	0.16
4	0.657	0.996	0.366
5	0.993	0.498	0.356
6	0.066	0.555	0.199
7	0.529	0.727	0.089
8	0.893	0.158	0.618
9	0.122	0.396	0.774
10	0.598	0.318	0.979

### Check Sample Correlation Coefficient (Independence):

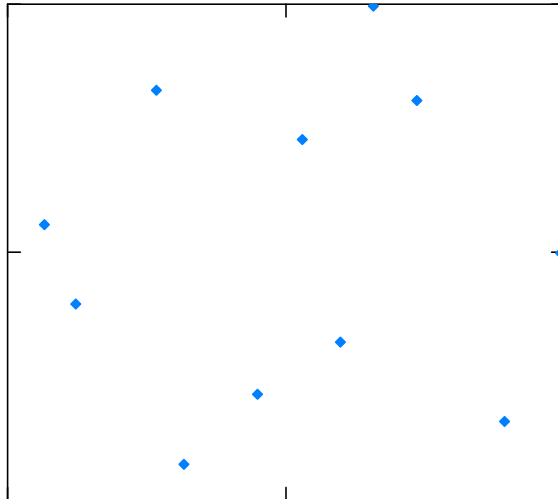
$$\text{corr}(\text{optimumLHS}^{\langle 0 \rangle}, \text{optimumLHS}^{\langle 1 \rangle}) = 0.039$$

$$\text{corr}(\text{optimumLHS}^{\langle 0 \rangle}, \text{optimumLHS}^{\langle 2 \rangle}) = 0.09$$

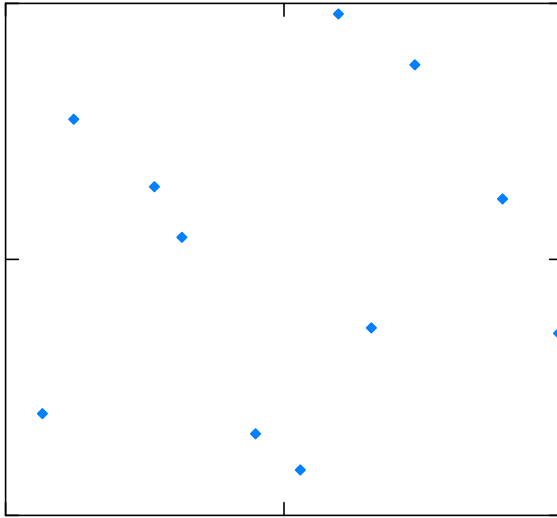
$$\text{corr}(\text{optimumLHS}^{\langle 1 \rangle}, \text{optimumLHS}^{\langle 2 \rangle}) = -0.1$$

### Visual Check of optimumLHS Samples in Three Planes:

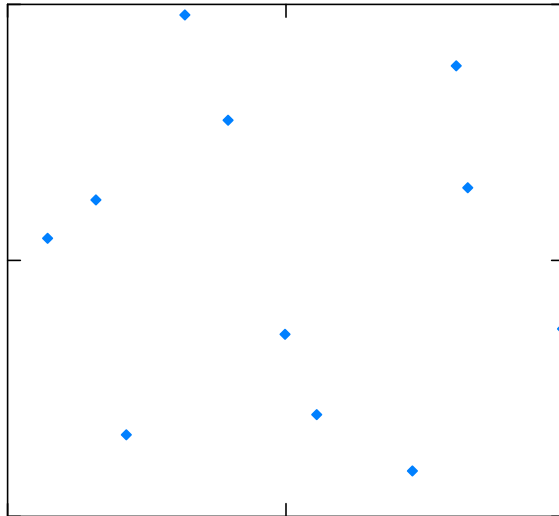
optimumLHS(0) - optimumLHS(1)



optimumLHS(0) - optimumLHS(2)



optimumLHS(0) - optimumLHS(2)



## Statistics of the Rate Factors:

$$\mu := \begin{pmatrix} 1 \\ 1 \\ 1 \end{pmatrix} \quad \rho := \begin{pmatrix} 1 & 0.4 & 0.4 \\ 0.4 & 1 & 0.7 \\ 0.4 & 0.7 & 1 \end{pmatrix}$$

$$\sigma := \begin{pmatrix} 0.2 \\ 0.25 \\ 0.3 \end{pmatrix}$$

$$i := 0..2 \quad j := 0..2$$

$$\Sigma_{i,j} := \rho_{i,j} \cdot \sigma_i \cdot \sigma_j$$

$$\Sigma = \begin{pmatrix} 0.04 & 0.02 & 0.024 \\ 0.02 & 0.063 & 0.053 \\ 0.024 & 0.053 & 0.09 \end{pmatrix}$$

## Statistics of the Corresponding Normal Variables

The generation of rate parameter samples follows a procedure as summarized by Nie, et al [2007].

$$\mu_{n_i} := \ln \left[ \frac{(\mu_i)^2}{\sqrt{(\mu_i)^2 + (\sigma_i)^2}} \right] \quad \mu_n = \begin{pmatrix} -0.02 \\ -0.03 \\ -0.043 \end{pmatrix}$$

$$\Sigma_{n_{i,j}} := \ln \left( 1 + \frac{\Sigma_{i,j}}{|\mu_i \cdot \mu_j|} \right) \quad \Sigma_n = \begin{pmatrix} 0.039 & 0.02 & 0.024 \\ 0.02 & 0.061 & 0.051 \\ 0.024 & 0.051 & 0.086 \end{pmatrix}$$

$$\underline{\underline{C}} := \text{cholesky}(\Sigma_n) = \begin{pmatrix} 0.198 & 0 & 0 \\ 0.1 & 0.225 & 0 \\ 0.12 & 0.174 & 0.204 \end{pmatrix}$$

$$C \cdot C^T = \begin{pmatrix} 0.039 & 0.02 & 0.024 \\ 0.02 & 0.061 & 0.051 \\ 0.024 & 0.051 & 0.086 \end{pmatrix}$$

## From Optimum LHS Points to Independent Standard Normal Variables Z

$n := 0..10$

$Z_{n,i} := \text{qnorm}(\text{optimumLHS}_{n,i}, 0, 1)$

	0	1	2
0	-0.477	-1.461	0.109
1	-0.621	0.94	0.363
2	0.629	0.863	1.175
3	-0.129	-0.794	-0.996
4	0.403	2.682	-0.341
5	2.462	$-4.457 \cdot 10^{-3}$	-0.37
6	-1.505	0.139	-0.846
7	0.073	0.604	-1.347
8	1.241	-1.001	0.301
9	-1.164	-0.264	0.751
10	0.248	-0.472	2.035

## From Z to Correlated Normal Vector Y

$$Y := C \cdot Z^T + \text{augment}(\mu_n, \mu_n, \mu_n, \mu_n, \mu_n, \mu_n, \mu_n, \mu_n, \mu_n, \mu_n, \mu_n)$$

$$Y^T =$$

	0	1	2
0	-0.114	-0.407	-0.333
1	-0.143	0.119	0.12
2	0.105	0.227	0.422
3	-0.045	-0.222	-0.4
4	0.06	0.614	0.403
5	0.468	0.215	0.176
6	-0.318	-0.15	-0.372
7	$-5.073 \cdot 10^{-3}$	0.113	-0.203
8	0.226	-0.131	$-7.552 \cdot 10^{-3}$
9	-0.25	-0.206	-0.075
10	0.029	-0.112	0.319

## From Y to Lognormal X

$$X_{i,n} := e^{Y_{i,n}}$$

$$X^T =$$

	0	1	2
0	0.892	0.666	0.717
1	0.867	1.127	1.128
2	1.111	1.254	1.525
3	0.956	0.801	0.67
4	1.062	1.847	1.496
5	1.597	1.24	1.192
6	0.728	0.861	0.69
7	0.995	1.12	0.816
8	1.254	0.877	0.992
9	0.779	0.814	0.927
10	1.03	0.894	1.375

$$X := X^T$$

X will be used as factors for the best estimate rates.

## Resulting Correlation in the 11 Samples

$$\text{corr}(X^{(0)}, X^{(1)}) = 0.36$$

$$\text{corr}(X^{(0)}, X^{(2)}) = 0.43$$

$$\text{corr}(X^{(1)}, X^{(2)}) = 0.71$$

$$\text{mean}(X^{(0)}) = 1.025$$

$$\text{mean}(X^{(1)}) = 1.045$$

$$\text{mean}(X^{(2)}) = 1.048$$

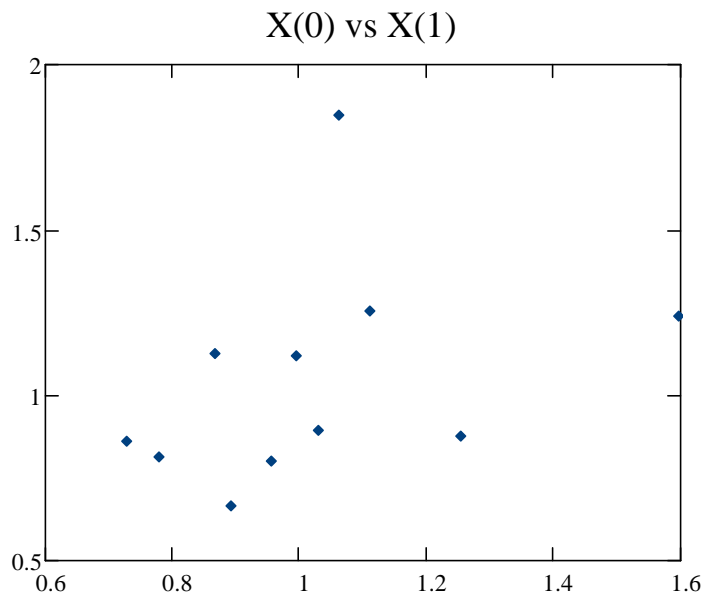
$$\text{Stdev}(X^{(0)}) = 0.242$$

$$\text{Stdev}(X^{(1)}) = 0.328$$

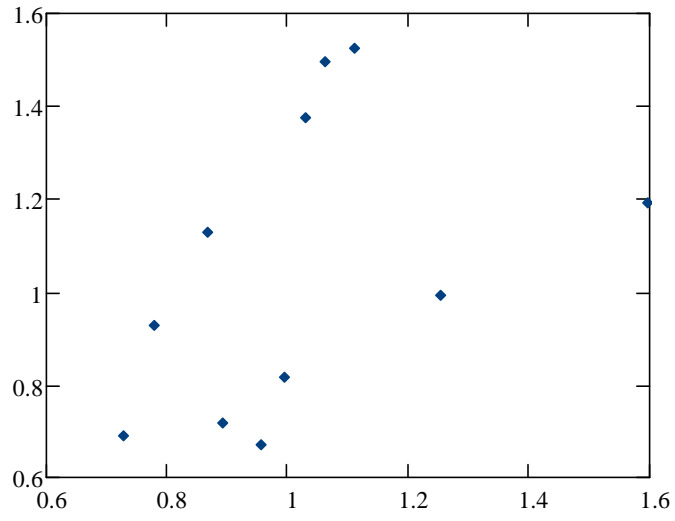
$$\text{Stdev}(X^{(2)}) = 0.319$$

The resulting correlations match the specified correlation very good.

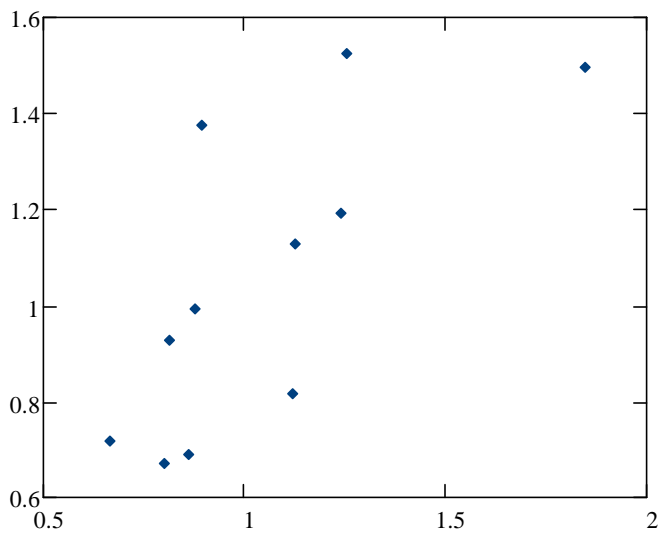
## Visual Check of Correlated Rate Parameters in Three Planes:



X(0) vs X(2)



X(1) vs X(2)



**Appendix I A SAMPLE RUN FOR FRAGILITY ANALYSIS OF THE CONDENSATE  
STORAGE TANK WITH REALISTIC DEGRADATION COMBINATION**



# KAERI Year 4 Task

## Fragility Analysis of Condensate Storage Tank

### - Realistically Correlated Degradation Cases A, B, and C - Using water level in normal operation

This calculation combines degradation cases (A) stainless steel tank shell, (B) anchor bolts, and (C-2) anchorage concrete cracking. The three degradations are combined using the sample rate factors that were generated using the Optimum Latin Hypercube samples. This appendix shows the first sample case.

$$year := 75$$

$$SME_e := 0.057g$$

---



Factor set 1:

$$abc := (0.892 \ 0.666 \ 0.717)^T$$

Degradation Case A: Stainless Steel Tank Shell

$$scc\_rate := 7.494 \times 10^{-3} \text{ in}$$

$$tshell\_degraded := \frac{5}{8} \text{ in} - scc\_rate \cdot year \cdot abc_0 = 0.124 \cdot \text{in}$$

Degradation Case B: Anchor Bolts

$$C_w := 70.6$$

$$\alpha := 0.79$$

$$X(t) := C \cdot t^\alpha \cdot \mu\text{m}$$

$$Dbolt\_degraded := 2.5 \text{ in} - 2 \cdot X(\text{year}) \cdot abc_1 = 2.38786 \cdot \text{in}$$

Degradation Case C: Anchorage concrete cracking - BNL model

$$crack := 0.0078 \cdot year \cdot mm \cdot abc_2 = 0.017 \cdot \text{in}$$

---



## H.1 Introduction

Same as Appendix F, Section H.1.

---



## H.2 Response Evaluation

Same as Appendix F, Section H.2, except for the use of the operational water level and the use of different equations for the effective horizontal impulsive weight calculation. These exceptions are documented in Appendix G.



## H.3 Capacity Assessment

Same as Appendix F, Section H.3, except for some programmatic conditions added to prevent numerical problems. These exceptions are described in Appendix G.



Summary of SME capacities:

$$SME_M = 0.057 \cdot g \quad SME_V = 0.33 \cdot g \quad SME_P = 0.1 \cdot g$$

$$SME_{cr} := \min(SME_M, SME_V, SME_P) = 0.057 \cdot g$$

$$SME_e = 0.057 \cdot g$$

$$if[SME_{cr} = SME_M, "Moment", (if(SME_{cr} = SME_V, "Shear", "Fluid Pressure"))] = "Moment"$$

$$year = 75 \quad t_g = 0.124 \cdot in \quad d_{bolt} = 2.388 \cdot in \quad crack = 0.419 \cdot mm$$

Summary of results:

Years:	0	5	10	15	20	25	30	35	40
ts (in):	0.625	0.592	0.558	0.525	0.491	0.458	0.424	0.391	0.358
dbolt(in):	2.5	2.487	2.477	2.469	2.461	2.453	2.446	2.439	2.432
cr(mm):	0	0.028	0.056	0.084	0.112	0.140	0.168	0.196	0.224
SME:	0.549	0.528	0.507	0.486	0.465	0.444	0.423	0.402	0.382
SMEM:	1.969	1.824	1.680	1.537	1.394	1.250	1.107	0.966	0.826
SMEV:	0.549	0.528	0.507	0.486	0.465	0.444	0.423	0.402	0.382
SMEP:	2.781	2.602	2.424	2.245	2.066	1.887	1.709	1.530	1.351
Mode:	Shear	Shear	Shear	Shear	Shear	Shear	Shear	Shear	Shear
Years:	45	50	55	60	65	70	75	80	
ts (in):	0.324	0.291	0.257	0.224	0.190	0.157	0.124		
dbolt(in):	2.425	2.419	2.412	2.406	2.400	2.394	2.388		
cr(mm):	0.252	0.280	0.308	0.336	0.364	0.391	0.419		
SME:	0.362	0.343	0.324	0.301	0.214	0.133	0.057	NA	
SMEM:	0.689	0.554	0.424	0.301	0.214	0.133	0.057		
SMEV:	0.362	0.343	0.324	0.308	0.314	0.321	0.330		
SMEP:	1.172	0.994	0.815	0.636	0.457	0.279	0.100		
Mode:	Shear	Shear	Shear	Moment	Moment	Moment	Moment		

### H.3.7 Consideration of Other Capacities:

Same as Appendix F, Section H.3.7.

